Polish Academy of Sciences

Institute of Physics

DOCTORAL DISSERTATION

Dynamics of Entanglement of Spin Qubits Based on Semiconductor Quantum Dots

Igor Bragar

Supervisor

dr. hab. Łukasz Cywiński, prof. IF PAN

Warszawa

2023

Igor Bragar's Open Researcher and Contributor ID (ORCID): 0000-0003-1321-2371

Contents

Abstract

The present doctoral dissertation entitled "Dynamics of Entanglement of Spin Qubits Based on Semiconductor Quantum Dots" is of triptych form: apart from a short presentation of the scientific knowledge about the spin qubits, entanglement and reasons of its decay contained in Chapter 1 "Introduction: Entanglement and Spin Qubits", and auxiliary chapters such as Chapter 5 "Concluding Part", and Appendix, it consists of three main parts: Chapter 2 "Dynamics of Decay of Two Electron-Spin Qubits Entanglement", Chapter 3 "Retardation of Entanglement Decay of Two Spin Qubits by Quantum Measurements", and Chapter 4 "Dynamical Generation of Entanglement of Two Singlet-Triplet Qubits". All three main parts have a common subject of study—the decay of entanglement of two qubits based on spins of electrons which are localized on quantum dots (QDs) in a semiconductor nanostructure (e.g. gated QDs created in AlGaAs/GaAs heterostructure or self-assembled InGaAs QDs). At the same time, these chapters contain research pieces which are independent of each other.

In Chapter 1, I summarize the most important, from the point of view of the subject of the dissertation, scientific knowledge about the formal description of complex systems in quantum mechanics, define the entangled states, discuss approaches to quantification of the level of entanglement of a given quantum state and give explicit definitions of measures of entanglement used in the following chapters. I also sum up the information about a few experimental realizations of spin qubits in semiconductor QDs. In particular, I describe the design of a few types of such devices and the possibilities of electron spin manipulations they provide. I end the chapter with an overview of physical mechanisms that lead to decoherence of quantum states of spin qubits.

In Chapter 2, I present the theoretical analysis of the time evolution of two electron spin QD qubits. It is shown there how entanglement decays due to the interaction of electron spins with nuclear spin environment of QDs. The impact of various states of the latter has been considered (e.g. a thermal state, narrowed states, correlated states). It has also been examined the efficiency of application of a two-qubit echo procedure in order to revert dephasing of qubits and obtain back the entangled state of qubits. The existence of a cut-off strength of magnetic field below which echo procedure gives no effect has been demonstrated. Additionally, it has been shown that the amount of entanglement of two-qubit state which is undergoing the hyperfine-induced decay can be detected and quantified without performing the two-qubit tomography. The amount of entanglement in such a case can be faithfully estimated by measuring a simple entanglement witness (projection on the initial two-qubit state). Moreover, this task can also be accomplished by measuring the averaged fidelity of quantum teleportation during which the analyzed state is consumed.

In Chapter 3, I develop further the study of the system of two electron spin QD qubits, namely, I investigate how one could counteract the decay of their entanglement. I show there that execution of a manipulation procedure based on joint evolution of qubits and their environments followed by quantum measurement of the qubits' subsystem may significantly retard the decay of qubits' entanglement. It turns out to be crucial to tune the parameters of the procedure (duration τ of free evolution of the system, number n of performed quantum measurements and their strength k) to maximize the effect of retardation of entanglement decay. It has been demonstrated that the effect can be achieved not only in the case of strong (projective) measurements but also for quantum measurements of moderate strength.

In Chapter 4, I concentrate on the dynamical creation of entangled states of two two-electron spin QD qubits. Motivated by the experimental realization of the procedure aimed at production of entangled states of two singlet-triplet (S-T_0) qubits, I analyze the impact of factors which limit the maximal possible amount of entanglement created in that system operated in a regime when energy associated with the magnetic field gradient ΔB_z is an order of magnitude smaller than the exchange energy J between singlet and triplet states. First, I study theoretically a single S-T_0 qubit in free induction (FID) and spin echo (SE) experiments. I have obtained the analytical expressions for averaged values of the components of S-T_0 qubit as functions of the procedure duration for quasistatical fluctuations of ΔB_z and quasistatical or $1/f^\beta$-type dynamical fluctuations of J. Next, I consider the impact of fluctuations of these parameters on the efficiency of the entangling procedure. In particular, I have obtained the analytical expressions for the density operator of two-qubit state which account for $1/f^\beta$-type fluctuations of J_1, J_2 and the degree of correlation of the noises. These expressions indicate the maximal possible level of entanglement that can be generated by performing the entangling procedure. The theoretical estimates deliver also an evidence that in the analyzed experiment, S-T_0 qubits were affected by uncorrelated $1/f^\beta$ charge noises.

Results presented in Chapter 2 are published in the scientific journal *Physical Review B* [1], while results contained in Chapters 3 and 4 have not been published yet.

Streszczenie [1]

Niniejsza rozprawa doktorska pt. „Dynamika splątania kubitów spinowych opartych na półprzewodnikowych kropkach kwantowych" posiada formę tryptyku: oprócz streszczenia wiedzy naukowej o kubitach spinowych, splątaniu i przyczynach jego zaniku, zawartego w rozdziale 1 „Wstęp: Splątanie i kubity spinowe", i rozdziałów pomocniczych, takich jak rozdział 5 „Wnioski" i dodatek, składa się ona z trzech głównych części: rozdziału 2 „Dynamika zaniku splątania dwóch kubitów, zrealizowanych na pojedynczych spinach elektronów", rozdziału 3 „Opóźnianie zaniku splątania dwóch kubitów spinowych pomiarami kwantowymi" i rozdziału 4 „Dynamiczne wytwarzanie splątania dwóch kubitów singletowo-trypletowych". Wszystkie trzy główne części mają wspólny przedmiot badań – zanik splątania dwóch kubitów opartych na spinach elektronów, które są zlokalizowane w kropkach kwantowych (KK) w półprzewodnikowej nanostrukturze (np. w bramkowanych KK wytworzonych w heterostrukturze AlGaAs/GaAs albo w samorosnących KK z InGaAs). Jednocześnie badania, przedstawione w tych rozdziałach, są od siebie niezależne.

W rozdziale 1 „Wstęp: Splątanie i kubity spinowe" streszczam najważniejszą, z punktu widzenia przedmiotu tej rozprawy, wiedzę naukową o formalnym opisie układów złożonych w mechanice kwantowej, podaję definicję stanów splątanych, omawiam podejścia do kwantyfikacji poziomu splątania stanu kwantowego i przytaczam jawne definicje miar splątania, wykorzystywanych w następnych rozdziałach. Reasumuję również wiedzę o kilku doświadczalnych realizacjach kubitów spinowych w półprzewodnikowych KK, zwłaszcza, opisuję konstrukcje kilku typów takich urządzeń oraz możliwości manipulacji spinem elektronu, które one dają. Rozdział ten kończę przeglądem mechanizmów fizycznych, które prowadzą do dekoherencji stanów kwantowych kubitów spinowych.

W rozdziale 2 przedstawiam analizę teoretyczną ewolucji czasowej dwóch kubitów, zrealizowanych na pojedynczych spinach elektronów w KK. Pokazano w nim, jak zanika splątanie na skutek oddziaływania kubitów z otoczeniem, składającym się ze spinów jądrowych w KK. Został rozważony wpływ rozmaitych stanów otoczenia (np. stan wysokotemperaturowy, stany zwężone, stany skorelowane). Zbadana została również wydajność stosowania procedury echa dwukubitowego, mającej na celu odwrócenie defazowania kubitów i przywrócenie stanu splątanego kubitów. Zostało zademonstrowane istnienie granicznej wartości natężenia pola magnetycznego, po-

[1] In accordance to art. 13, part 6 of the Act of 14 March 2003 on Scientific Degrees and Scientific Title as well as on Degrees and Title in Field of Art (*pol.* ustawa z dnia 14 marca 2003 r. o stopniach naukowych i tytule naukowym oraz stopniach i tytule w zakresie sztuki), which was in effect at the moment of initiation of the doctor degree awarding procedure as well as in accordance to art. 187, part 4 of the Act of 20 July 2018 The Law on Higher Education and Science (*pol.* ustawa z dnia 20 lipca 2018 r. Prawo o szkolnictwie wyższym i nauce), which has replaced the former and is currently in force, a dissertation written in a foreign language must containt an abstract in Polish.

niżej której procedura echa nie daje żadnego efektu. Dodatkowo zostało pokazane, że splątanie stanu dwukubitowego, który zanika na skutek oddziaływania nadsubtelnego, może być wykryte i określone ilościowo bez wykonywania tomografii stanu dwóch kubitów. Ilość splątania w takim przypadku może być wiernie oszacowana pomiarem prostych świadków splątania (rzut na początkowy stan dwukubitowy). Ponadto ten cel może również być osiągnięty pomiarem uśrednionej wierności teleportacji kwantowej, podczas której badany stan jest zużywany.

W rozdziale 3 rozwijam dalej badanie układu dwóch kubitów, zrealizowanych na pojedynczych spinach elektronów w KK, mianowicie, badam, jak można przeciwdziałać zanikowi ich splątania. Pokazuję, że wykonanie procedury manipulacji opartej na wspólnej ewolucji kubitów i ich otoczeń, po której następuje pomiar kwantowy podukładu kubitów, może znacząco opóźnić zanik splątania kubitów. Okazuje się, że istotne jest dobranie parametrów tej procedury (czasu trwania τ swobodnej ewolucji układu, liczby n wykonanych pomiarów kwantowych i ich siły k) w celu zwiększenia efektu opóźniania zaniku splątania. Zostało zademonstrowane, iż efekt może zostać osiągnięty nie tylko w przypadku silnych (rzutowych) pomiarów, ale również dla pomiarów kwantowych o umiarkowanej sile.

W rozdziale 4 skupiam się na dynamicznym wytwarzaniu stanów splątanych dwóch kubitów, każdy z których jest zrealizowany na stanach spinowych dwóch elektronów w podwójnej KK. Zmotywowany doświadczalną realizacją procedury, mającej na celu wytworzenie stanów splątanych kubitów singletowo-trypletowych (S-T_0), analizuję wpływ czynników, które ograniczają maksymalnie możliwą ilość splątania wytworzonego w tym układzie, działającym w trybie, gdy energia związana z gradientem pola magnetycznego ΔB_z jest o rząd wielkości mniejsza od energii wymiany J pomiędzy singletem a trypletem. Najpierw badam teoretycznie pojedynczy kubit S-T_0 w doświadczeniach swobodnego zaniku indukcji i echa spinowego. Otrzymałem wyrażenia analityczne, opisujące jego składowe jako funkcje czasu trwania procedur dla fluktuacji kwazistatycznych parametru ΔB_z oraz dla fluktuacji kwazistatycznych albo dynamicznych typu $1/f^\beta$ parametru J. Następnie rozpatrzyłem wpływ fluktuacji tych parametrów na wydajność procedury splątującej. Otrzymałem zwłaszcza wyrażenia analityczne operatora gęstości stanu dwukubitowego, które uwzględniają fluktuacje typu $1/f^\beta$ parametrów J_1, J_2 oraz stopień korelacji tych szumów. Te wyrażenia wyznaczają maksymalnie możliwy poziom splątania, wytwarzanego w wyniku wykonania rozważanej procedury splątującej. Teoretyczne oszacowania wskazują na to, że w analizowanym doświadczeniu kubity S-T_0 znajdowały się pod wpływem nieskorelowanych szumów ładunkowych typu $1/f^\beta$.

Wyniki przedstawione w rozdziale 2 są opublikowane w czasopiśmie naukowym *Physical Review B* [1], natomiast wyniki zawarte w rozdziałach 3 i 4 nie zostały jeszcze opublikowane.

Acknowledgements

I owe much to my supervisor, dr. hab. Łukasz Cywiński, prof. IF PAN. I am grateful to him for his guidance and support, without which this dissertation certainly would have never been appeared.

I am grateful to prof. dr. hab. Tomasz Dietl for his support he has given me at the early stage of my work at the institute.

I thank dr. Piotr Szańkowski for many lessons he gave me.

The research was supported in part by Polish National Science Centre (NCN), grant no. DEC-2012/07/B/ST3/03616.

I thank my current employer, Asseco Poland S.A., for a sabbatical, which was helpful for finishing the dissertation.

Chapter 1

Introduction: Entanglement and Spin Qubits

In this chapter, I discuss shortly the object of study of this dissertation (semiconductor quantum dots) as well as the subject of the dissertation (dynamics of entanglement of electron spins in semiconductor quantum dots) and formulate the main aims. In particular, I introduce here the notion of quantum states, discuss entangled quantum states and measures of entanglement. Next, I describe realizations of electron spin qubits in semiconductor quantum dots (QD) and discuss reasons of decoherence of their quantum states.

1.1 Entangled States and Measures of Entanglement

In quantum mechanics one obtains predictions about observables (i.e. physical quantities that can, in principle, be measured) by calculating their expectation values in a given state of a considered physical system using corresponding quantum operators. The state of the system in quantum framework is a purely theoretical tool that cannot be accessed directly in experiment. When the state of the system is known as precisely as the theory allows (i.e. the state is pure), it is described by a vector, say, $|\psi\rangle$, from the corresponding system's state space $\mathcal{H}$, which, technically, is a Hilbert space over the field of complex numbers $\mathbb{C}$, i.e. a complex linear vector space with inner product.

Vectors of a state space $\mathcal{H}$ form the closed set under commutative and associative addition:

- $|\alpha\rangle + |\beta\rangle \equiv |\beta\rangle + |\alpha\rangle \in \mathcal{H}$,
- $|\alpha\rangle + |\beta\rangle) + |\gamma\rangle \equiv |\alpha\rangle + (|\beta\rangle + |\gamma\rangle) \in \mathcal{H}$,

where $|\alpha\rangle$, $|\beta\rangle$, $|\gamma\rangle \in \mathcal{H}$;
as well as under multiplication by a scalar, being any complex number, with the following properties:

- $a(|\alpha\rangle + |\beta\rangle) \equiv a|\alpha\rangle + a|\beta\rangle \in \mathcal{H}$
- $(a+b)|\alpha\rangle \equiv a|\alpha\rangle + b|\alpha\rangle \in \mathcal{H}$,
- $a(b|\alpha\rangle) \equiv (ab)|\alpha\rangle \in \mathcal{H}$,

where a, $b \in \mathbb{C}$.

There exists in a state space $\mathcal{H}$ a null (or zero) vector, $|\mathtt{0}\rangle \in \mathcal{H} : \forall\, |\alpha\rangle, |\alpha\rangle + |\mathtt{0}\rangle \equiv |\alpha\rangle$. Multiplication by the identity vector $\mathbb{1}$ or a scalar unity does not change any vector, $\forall\, |\alpha\rangle, \mathbb{1}|\alpha\rangle \equiv |\alpha\rangle$ and $1|\alpha\rangle \equiv |\alpha\rangle$. Moreover, each vector has a corresponding negative vector (also called an inverse element), $\forall\, |\alpha\rangle\, \exists\, |\beta\rangle$: $|\alpha\rangle + |\beta\rangle = |\mathtt{0}\rangle$, $|\beta\rangle \equiv (-1)|\alpha\rangle$.

Inner product, defined as a mapping of two elements of a state space $\mathcal{H}$ onto $\mathbb{C}$, possesses the following properties:

- conjugate symmetric property, $\langle\alpha|\beta\rangle \equiv (\langle\beta|\alpha\rangle)^*$;
- linearity in the second argument, $\langle\alpha|(a|\beta\rangle + b|\gamma\rangle) \equiv a\langle\alpha|\beta\rangle + b\langle\alpha|\gamma\rangle$;
- positive definite property $\langle a|a\rangle > 0$,
- only one specific zero vector $|\mathtt{0}\rangle$ has zero norm $||\,|\mathtt{0}\rangle\,|| = \sqrt{\langle\mathtt{0}|\mathtt{0}\rangle} = 0$, and the vector's norm is defined as $||\,|\alpha\rangle\,|| \coloneqq \sqrt{\langle\alpha|\alpha\rangle}$, where Dirac's notation $|...\rangle$ for vectors is used, $\langle\alpha|$ is a dual vector for the vector $|\alpha\rangle$, $\langle\alpha| \equiv |\alpha\rangle^\dagger \equiv (|\alpha\rangle^T)^*$.

As an example, let us consider a physical system that has a countable state space $\mathcal{H}$ of finite dimension, $\dim \mathcal{H} = D < \infty$ (such spaces are important for this dissertation). In that space one can choose an orthonormal basis (one from infinitely many bases existing in that space), i.e. such a set of vectors $\{|\varphi_i\rangle, i = 1, 2, ..., D\}$ that: all vectors from the set are linearly independent, i.e. $\sum_{i=1}^{D} a_i|\varphi_i\rangle = 0$ only when all coefficients $a_i = 0$; all vectors from the set are normalized and orthogonal to each other, $\forall i, j\ \langle\varphi_i|\varphi_j\rangle = \delta_{ij}$; and the completeness relation is satisfied, $\sum_{i=1}^{D} |\varphi_i\rangle\langle\varphi_i| = \mathbb{1}$. Any vector $|\psi\rangle$ of that space can be represented as a combination of the basis vectors:

$$|\psi\rangle \equiv \mathbb{1}|\psi\rangle = \sum_{i=1}^{D} |\varphi_i\rangle\langle\varphi_i|\psi\rangle = \sum_{i=1}^{D} c_i|\varphi_i\rangle,$$

where $c_i \coloneqq \langle\varphi_i|\psi\rangle \in \mathbb{C}$. State vectors are normalized, so $||\,|\psi\rangle\,||^2 = \langle\psi|\psi\rangle = \sum_{i=1}^{D} |c_i|^2 = 1$.

The state of a physical system can also be represented by a density operator (or state operator, or density matrix) $\hat{\rho}$. Description of a system state with the help of a state vector $|\psi\rangle$ is equivalent to using a density operator $\hat{\rho} = |\psi\rangle\langle\psi|$, but when knowledge about the system's state is not complete[1], then a density operator

[1] The incompleteness of knowledge about the system state may originate, for example, from the method of system preparation/initialization (e.g. at nonzero temperature the state of a single confined particle being in a thermodynamic equilibrium is a mixture of energy eigenstates according to its thermal distribution) or from the fact that system of interest is actually entangled with another one while the state of the joint system is pure, so no pure state can be ascribed to the system of interest alone.

formalism is the only possible description of a system, i.e.

$$\hat{\rho} = \sum_i w_i |\psi_i\rangle\langle\psi_i|, \tag{1.1}$$

where $\{|\psi_i\rangle\}$ is a nonunique set (or ensemble) of system's pure states (not necessarily orthogonal to each other) and $w_i \in (0,1]$ is a weight of the state $|\psi_i\rangle$ in the mixed state $\hat{\rho}$, which can be interpreted as a probability that system is in the state $|\psi_i\rangle$, so $\sum_i w_i = 1$. Such a state $\hat{\rho}$ is called a mixed state or ensemble of pure states $|\psi_i\rangle$. Every density operator $\hat{\rho}$ has a spectral decomposition (or eigendecomposition),

$$\hat{\rho} = \sum_{i=1}^{D} p_i |\phi_i\rangle\langle\phi_i|,$$

where $|\phi_i\rangle$ are its eigenvectors and $p_i \in [0,1]$ are its eigenvalues, which, as probabilities, add up to unity, $\sum_{i=1}^{D} p_i = 1$. Density operator has two important properties: its trace is equal to one, $\mathrm{Tr}\,(\hat{\rho}) = \sum_{i=1}^{D} p_i \mathrm{Tr}\,(|\phi_i\rangle\langle\phi_i|) = \sum_{i=1}^{D} p_i = 1$, and density operator is a nonnegative operator, i.e. for any vector $|\chi\rangle \in \mathcal{H}$, the following inequality holds

$$\langle\chi|\hat{\rho}|\chi\rangle = \langle\chi| \left(\sum_{i=1}^{D} p_i |\phi_i\rangle\langle\phi_i| \right) |\chi\rangle = \sum_{i=1}^{D} p_i \langle\chi|\phi_i\rangle\langle\phi_i|\chi\rangle = \sum_{i=1}^{D} p_i |\langle\chi|\phi_i\rangle|^2 \geqslant 0.$$

The density operators representing pure states are idempotent, i.e. such a density operator fulfills the relation $\hat{\rho}^2 = (|\psi\rangle\langle\psi|)(|\psi\rangle\langle\psi|) = |\psi\rangle\langle\psi| = \hat{\rho}$. The purity of $\hat{\rho}$, which is defined as a trace of $\hat{\rho}^2$, indicates if the state $\hat{\rho}$ is pure:

$$\begin{aligned}\mathrm{Tr}\left(\hat{\rho}^2\right) &= \mathrm{Tr}\left(\Big(\sum_{i=1}^{D} p_i |\phi_i\rangle\langle\phi_i| \Big) \Big(\sum_{j=1}^{D} p_j |\phi_j\rangle\langle\phi_j| \Big) \right) = \mathrm{Tr}\left(\sum_{i,j=1}^{D} p_i p_j |\phi_i\rangle\langle\phi_j| \delta_{ij} \right) \\ &= \mathrm{Tr}\left(\sum_{i=1}^{D} p_i^2 |\phi_i\rangle\langle\phi_i| \right) = \sum_{i=1}^{D} p_i^2 \leqslant 1,\end{aligned}$$

where equality is possible only when all but one weights are zero, $p_i = 1$, i.e. in the case of a pure state $\hat{\rho} = |\phi_i\rangle\langle\phi_i|$. From the definition of density operator (Eq. (1.1)) it directly follows that $\hat{\rho}$ is a Hermitian operator, $\hat{\rho}^\dagger = \hat{\rho}$.

Often when dealing with a complex physical system we are interested in the state of a particular subsystem (i.e. specified part of a system), called A, whereas the rest of a system will be denoted by B (for the sake of simplicity of notation a bipartite system will be considered). The state space of such a system is a tensor product of state spaces of A and B, $\mathcal{H}^{AB} = \mathcal{H}^A \otimes \mathcal{H}^B$. It is worth noting that spaces that correspond to the subsystems are themselves legitimate state spaces with all the properties mentioned above retained. With such a decomposition of a system space, spaces corresponding to the subsystems are disjoint, so e.g. any combination of vectors from a given space is a vector that belongs to the same space, $\forall\ |\psi_1^X\rangle, |\psi_2^X\rangle \in \mathcal{H}^X$ and $\forall\ a, b \in \mathbb{C}$, $a|\psi_1^X\rangle + b|\psi_2^X\rangle = |\psi_3^X\rangle \in \mathcal{H}^X$, $X = A, B$. Taking into account the structure of a physical system, the system's density operator

can be rewritten as follows

$$\begin{aligned}
\hat{\rho}^{AB} &= \sum_i p_i |\psi_i^{AB}\rangle\langle\psi_i^{AB}| = \sum_i p_i \mathbb{1}^{AB} |\psi_i^{AB}\rangle\langle\psi_i^{AB}| \mathbb{1}^{AB} \\
&= \sum_i p_i \mathbb{1}^A \otimes \mathbb{1}^B |\psi_i^{AB}\rangle\langle\psi_i^{AB}| \mathbb{1}^A \otimes \mathbb{1}^B \\
&= \sum_i p_i \Big(\sum_{a=1}^{\dim \mathcal{H}_A} |\varphi_a^A\rangle\langle\varphi_a^A| \Big) \otimes \Big(\sum_{b=1}^{\dim \mathcal{H}_B} |\chi_b^B\rangle\langle\chi_b^B| \Big) |\psi_i^{AB}\rangle \\
&\times \langle\psi_i^{AB}| \Big(\sum_{c=1}^{\dim \mathcal{H}_A} |\varphi_c^A\rangle\langle\varphi_c^A| \Big) \otimes \Big(\sum_{d=1}^{\dim \mathcal{H}_B} |\chi_d^B\rangle\langle\chi_d^B| \Big) \\
&= \sum_i p_i \sum_{abcd} g_{abi}\, g_{cdi}^* |\varphi_a^A\rangle \otimes |\chi_b^B\rangle\langle\varphi_c^A| \otimes \langle\chi_d^B| \\
&= \sum_i p_i \sum_{abcd} g_{abi}\, g_{cdi}^* |\varphi_a^A\rangle\langle\varphi_c^A| \otimes |\chi_b^B\rangle\langle\chi_d^B|,
\end{aligned}$$

where $g_{abi} \coloneqq \left(\langle\varphi_a^A| \otimes \langle\chi_b^B|\right) |\psi_i^{AB}\rangle$ and $\{|\varphi_a^A\rangle\},\ \{|\chi_b^B\rangle\}$ are some bases in the corresponding subspaces.

The density operator of the subsystem is obtained from the density operator of the system by tracing out all other subsystems, e.g. the state of subsystem A of the bipartite system AB is obtained by tracing out the subsystem B as follows

$$\begin{aligned}
\hat{\rho}^A &= \mathrm{Tr}_B\left(\hat{\rho}^{AB}\right) = \sum_l \langle\chi_l^B|\hat{\rho}^{AB}|\chi_l^B\rangle \\
&= \sum_i p_i \sum_{abcdl} g_{abi}\, g_{cdi}^* |\varphi_a^A\rangle\langle\varphi_c^A| \langle\chi_l^B|\chi_b^B\rangle\langle\chi_d^B|\chi_l^B\rangle \\
&= \sum_i p_i \sum_{abcd} g_{abi}\, g_{cdi}^* |\varphi_a^A\rangle\langle\varphi_c^A| \delta_{bd} \\
&= \sum_i p_i \sum_{abc} g_{abi}\, g_{cbi}^* |\varphi_a^A\rangle\langle\varphi_c^A|.
\end{aligned}$$

Obviously, a physical system may consist of a larger number n of subsystems and correspondingly its state space is equivalent to the tensor (or direct) product of n subsystems' spaces.

While considering pure states of a composite system (in other words, such states that can be expressed as a vector, or a density operator with a single term in its decomposition with $w_1 = 1$) one can notice that there exist states of separable form (i.e. the system's state can be expressed as a tensor product of subsystems' states, $|\psi^{AB}\rangle = |\psi^A\rangle \otimes |\psi^B\rangle$) and there are also pure states that cannot be expressed in such a form. A pure state that is not separable one is called an *entangled pure state*. Schmidt decomposition of a given pure state helps to determine if that state is entangled or not. To illustrate this, let us consider a pure state of bipartite system AB, $|\psi^{AB}\rangle \in \mathcal{H}^{AB} = \mathcal{H}^A \otimes \mathcal{H}^B$, $\dim \mathcal{H}^A = \dim \mathcal{H}^B = D$. There exist orthonormal (Schmidt) bases $\{|\chi_i^A\rangle\},\ \{|\chi_i^B\rangle\}$ in state spaces $\mathcal{H}^A$, $\mathcal{H}^B$ such that allow the following decomposition of any pure state $|\psi^{AB}\rangle$:

$$|\psi^{AB}\rangle = \sum_{i=1}^{D} c_i |\chi_i^A\rangle \otimes |\chi_i^B\rangle,$$

where $0 \leqslant c_i \in \mathbb{R}$ are called Schmidt coefficients and $\sum_{i=1}^{D} c_i^2 = 1$. Schmidt bases and coefficients are obtained as follows. The vector $|\psi^{AB}\rangle$ can be represented in a standard way $|\psi^{AB}\rangle = \sum_{a,b=1}^{D} g_{ab}|\varphi_a^A\rangle \otimes |\varphi_b^B\rangle$. The matrix $g = (g_{ab})$ can be represented using singular value decomposition as $g = udv$, where d is a diagonal matrix with nonnegative elements, whereas u and v are unitary matrices, so $|\psi^{AB}\rangle = \sum_{a,i,b=1}^{D} = u_{ai}d_{ii}v_{ib}|\varphi_a^A\rangle \otimes |\varphi_b^B\rangle$, and hence, one can rewrite the vector $|\psi^{AB}\rangle$ in Schmidt bases that are defined as follows: $|\chi_i^A\rangle \coloneqq \sum_{a=1}^{D} u_{ai}|\varphi_a^A\rangle$, $|\chi_i^B\rangle \coloneqq \sum_{b=1}^{D} v_{ib}|\varphi_b^B\rangle$, using Schmidt coefficients that are elements of the diagonal matrix d: $c_i \coloneqq d_{ii}$, $|\psi^{AB}\rangle = \sum_{i=1}^{D} c_i|\chi_i^A\rangle \otimes |\chi_i^B\rangle$. The Schmidt bases $\{|\chi_i^A\rangle\}$, $\{|\chi_i^B\rangle\}$ are orthonormal as a consequence of orthonormality of the original bases $\{|\varphi_i^A\rangle\}$, $\{|\varphi_i^B\rangle\}$ and unitarity of matrices u and v, $u^\dagger u = uu^\dagger = \mathbb{1}$, $v^\dagger v = vv^\dagger = \mathbb{1}$, e.g. $\langle\chi_i^A|\chi_j^A\rangle = (\sum_{a=1}^{D} u_{ai}^*\langle\varphi_a^A|)(\sum_{b=1}^{D} u_{bj}|\varphi_b^A\rangle) = \sum_{a,b=1}^{D} u_{ai}^* u_{bj}\langle\varphi_a^A|\varphi_b^A\rangle = \sum_{a=1}^{D} u_{ai}^* u_{aj} = \delta_{ij}$.

The number of nonzero coefficients c_i in Schmidt decomposition of $|\psi^{AB}\rangle$ is called the Schmidt number for the state $|\psi^{AB}\rangle$. Schmidt number is invariant under unitary transformations of any subsystem, e.g. $\hat{U}^A \otimes \hat{U}^B|\psi^{AB}\rangle = \sum_{i=1}^{D} c_i(\hat{U}^A|\chi_i^A\rangle) \otimes (\hat{U}^B|\chi_i^B\rangle)$, where $\hat{U}^A$, $\hat{U}^B$ are unitary operators in state spaces $\mathcal{H}^A$, $\mathcal{H}^B$, respectively, and because of that it is a reliable indicator of entanglement of the state: $|\psi^{AB}\rangle$ is a product state if and only if its Schmidt number is equal to one, and, correspondingly, the state $|\psi^{AB}\rangle$ is entangled if and only if its Schmidt number is greater that one. It is worth stressing that state $|\psi^{AB}\rangle$ is maximally entangled when moduli of all nonvanishing Schmidt coefficients are equal to each other.

A few important observations can be made using Schmidt decomposition, namely: if the system is in a pure state $|\psi^{AB}\rangle$, then the reduced density operators of subsystems, $\hat{\rho}^A$ and $\hat{\rho}^B$, have the same eigenvalues, which follows from direct calculation of the reduced density operators

$$\begin{aligned}\hat{\rho}^A &= \mathrm{Tr}_B\left(|\psi^{AB}\rangle\langle\psi^{AB}|\right) \\ &= \mathrm{Tr}_B\left(\left(\sum_{i=1}^{D} c_i|\chi_i^A\rangle \otimes |\chi_i^B\rangle\right)\left(\sum_{j=1}^{D} c_j^*\langle\chi_j^A| \otimes \langle\chi_j^B|\right)\right) \\ &= \sum_{i=1}^{D} c_i^2|\chi_i^A\rangle\langle\chi_i^A|,\end{aligned}$$

and similarly $\hat{\rho}^B = \mathrm{Tr}_A\left(|\psi^{AB}\rangle\langle\psi^{AB}|\right) = \sum_{i=1}^{D} c_i^2|\chi_i^B\rangle\langle\chi_i^B|$; the system state $|\psi^{AB}\rangle$ is a pure product state if and only if the reduced density operators, $\hat{\rho}^A$ and $\hat{\rho}^B$, are pure states; if the system state $|\psi^{AB}\rangle$ is a maximally entangled state, then reduced density matrices are proportional to the identity matrices in the subspaces spanned by the Schmidt basis vectors belonging to the nonvanishing Schmidt coefficients [2, 3].

Here it is worth to mention the possibility to theoretically purify a quantum state: when state of the system is mixed, $\hat{\rho}^A \in \mathsf{H}^A$ (a space of density operators associated with $\mathcal{H}^A$), one can suppose that considered system is a part of a larger hypothetical system which has the second part of the same state space $\mathcal{H}^B \sim \mathcal{H}^A$, and in the joint system space $\mathcal{H}^{AB} = \mathcal{H}^A \otimes \mathcal{H}^B$ there exists a pure state $|\psi^{AB}\rangle$ such that $\hat{\rho}^A \equiv \mathrm{Tr}_B(|\psi^{AB}\rangle\langle\psi^{AB}|)$. Pure state $|\psi^{AB}\rangle$ has the form of Schmidt decomposition:

$$|\psi^{AB}\rangle \coloneqq \sum_{i=1}^{D} \sqrt{p_i}|\phi_i^A\rangle \otimes |\phi_i^B\rangle,$$

where p_i are the coefficients from ensemble representation of the density operator $\hat{\rho}^A = \sum_{i=1}^{D} p_i |\phi_i^A\rangle\langle\phi_i^A|$ and $\{|\phi_i^A\rangle\}$ is an orthonormal basis in state spaces $\mathcal{H}^A$, $\mathcal{H}^B$.

In general case, a separable mixed state is defined as a convex combination of product states [4]

$$\hat{\rho}^{AB} = \sum_i p_i \hat{\rho}_i^A \otimes \hat{\rho}_i^B. \tag{1.2}$$

Any state described by Eq. (1.2) is also called a classically correlated state, because, in contrast to an explicitly separable state $\hat{\rho}_{\text{sep}}^{AB} = \hat{\rho}^A \otimes \hat{\rho}^B$, the expectation values of observables measured at the same instant on both subsystems do not factorize, $\text{Tr}\left(\hat{\rho}^{AB}\,\hat{O}^A \otimes \hat{O}^B\right) \neq \text{Tr}\left(\hat{\rho}^A\,\hat{O}^A\right)\text{Tr}\left(\hat{\rho}^B\,\hat{O}^B\right)$, but these correlations of expectation values are of classical nature, since they can be created by simultaneous local manipulations on each subsystem applied with taking into account possibility of classical communication of information about each subsystem [5, 6, 7]. Any state that cannot be described by Eq. (1.2) is an *entangled state*.

The simplest physical system that can be in an entangled state is that consisting of two qubits. A qubit (or quantum bit), in turn, is the simplest physical system that can carry quantum information. It is a two-level system, i.e. its pure state $|\psi_{\text{q}}\rangle$ is a superposition of two states which are supposed to constitute an orthonormal basis of qubit's state space and usually are denoted as $|\uparrow\rangle$, $|\downarrow\rangle$:

$$|\psi_{\text{q}}\rangle = a|\uparrow\rangle + b|\downarrow\rangle,$$

where coefficients $a,\ b \in \mathbb{C}$ are tied by the normalization condition $|a|^2 + |b|^2 = 1$. Qubit is recognized as a unit of quantum information [8], whereas a maximally entangled two-qubit state is a unit of bipartite entanglement (ebit) [9].

It is worth to mention that qubit state space has a geometrical interpretation called the Bloch sphere (in fact, it is a unit ball) that arises from the representation of qubit density operator $\hat{\rho}_{\text{q}}$ in the basis of four orthogonal matrices $\{\hat{\zeta}_m \coloneqq \frac{1}{\sqrt{2}}\hat{\sigma}_m\}$, $\text{Tr}\left(\hat{\zeta}_m\hat{\zeta}_n\right) = \delta_{mn}$, where $\hat{\sigma}_0 \coloneqq \mathbb{1} = |\uparrow\rangle\langle\uparrow| + |\downarrow\rangle\langle\downarrow|$ and the remaining $\hat{\sigma}_1 \coloneqq |\uparrow\rangle\langle\downarrow| + |\downarrow\rangle\langle\uparrow|$, $\hat{\sigma}_2 \coloneqq i(|\downarrow\rangle\langle\uparrow| - |\uparrow\rangle\langle\downarrow|)$, $\hat{\sigma}_3 \coloneqq |\uparrow\rangle\langle\uparrow| - |\downarrow\rangle\langle\downarrow|$ are the Pauli matrices:

$$\hat{\rho}_{\text{q}} = \sum_{m=0}^{3} c_m \hat{\zeta}_m,$$

where $c_m \coloneqq \text{Tr}\left(\hat{\rho}_{\text{q}}\hat{\zeta}_m\right) \in \mathbb{R}$, coefficient c_0 is constant as a consequence of unity trace of the density operator, $c_0 = \text{Tr}\left(\hat{\rho}_{\text{q}}\frac{1}{\sqrt{2}}\mathbb{1}\right) \equiv \frac{1}{\sqrt{2}}$. It is convenient to rewrite the representation as

$$\hat{\rho}_{\text{q}} = \frac{1}{2}(\mathbb{1} + r_1\hat{\sigma}_1 + r_2\hat{\sigma}_2 + r_3\hat{\sigma}_3) \equiv \frac{1}{2}(\mathbb{1} + \boldsymbol{r}\cdot\boldsymbol{\sigma}) \equiv \frac{1}{2}\begin{pmatrix} 1+r_3 & r_1 - ir_2 \\ r_1 + ir_2 & 1-r_3 \end{pmatrix}, \tag{1.3}$$

where $r_m \coloneqq \text{Tr}\,(\hat{\rho}_{\text{q}}\hat{\sigma}_m) \equiv \sqrt{2}c_m$, $r_0 \equiv 1$, $r_1 = \rho_{12}+\rho_{21}$, $r_2 = i(\rho_{12}-\rho_{21})$, $r_3 = \rho_{11}-\rho_{22}$, and $\boldsymbol{r} \coloneqq (r_1, r_2, r_3)$ is the Bloch vector, $\boldsymbol{\sigma} \coloneqq (\hat{\sigma}_1, \hat{\sigma}_2, \hat{\sigma}_3)$. Equation (1.3) shows that any state of the two-level system, $\hat{\rho}_{\text{q}} = \begin{pmatrix} \rho_{11} & \rho_{12} \\ \rho_{21} & \rho_{22} \end{pmatrix}$ can be represented as a point in

three-dimensional (3D) space specified by the vector $\boldsymbol{r}$ using the relations:

$$\begin{aligned}
\rho_{11} = 1 - \rho_{22} &= \frac{1}{2}(1 + r_3), \\
\rho_{12} = \rho_{21}^* \qquad &= \frac{1}{2}(r_1 - ir_2), \\
\rho_{21} = \rho_{12}^* \qquad &= \frac{1}{2}(r_1 + ir_2), \\
\rho_{22} = 1 - \rho_{11} &= \frac{1}{2}(1 - r_3).
\end{aligned}$$

The components r_m of a Bloch vector are bounded, $r_m \in [-1, 1]$, since the density operator is nonnegative, $\det(\hat{\rho}_\mathrm{q}) = \frac{1}{4}(1 - \boldsymbol{r}^{\,2}) \geqslant 0 \Rightarrow |\boldsymbol{r}| \leqslant 1$, so a point defined by $\boldsymbol{r}$ falls into a 3D unit ball. Qubit, the two-level quantum system, is isomorphic to a spin $\frac{1}{2}$, so, in such a light, components r_1, r_2, r_3 may be interpreted as projections (or expectation values) of spin (qubit state) on particular 3D space directions, x, y, z. The limiting case $\det(\hat{\rho}_\mathrm{q}) = 0 \Rightarrow |\boldsymbol{r}| = 1$ (a unit sphere), i.e. when the density operator $\hat{\rho}_\mathrm{q}$ has the eigenvalues[2] of 0 and 1, corresponds to a pure state $\hat{\rho}_\mathrm{q} = |\psi\rangle\langle\psi|$. As a point on a unit sphere, a pure qubit state $|\psi\rangle$ can be parameterized with angles of the spherical coordinate system:

$$|\psi\rangle = |\psi(\theta, \varphi)\rangle = \mathrm{e}^{-i\varphi/2} \cos\frac{\theta}{2}|\uparrow\rangle + \mathrm{e}^{i\varphi/2} \sin\frac{\theta}{2}|\downarrow\rangle = \begin{pmatrix} \mathrm{e}^{-i\varphi/2} \cos\frac{\theta}{2} \\ \mathrm{e}^{i\varphi/2} \sin\frac{\theta}{2} \end{pmatrix},$$

where $\theta \in [0, \pi]$ is the polar (or inclination) angle and $\varphi \in [-\pi, \pi)$ is the azimuthal angle of a given point. These angles,

$$\begin{aligned}
\theta &= 2 \arccos\left(|a|\right), \\
\varphi &= \arccos\left(\mathrm{Re}\, q\right) \mathrm{sgn}\left(\mathrm{Im}\, q\right), \quad \text{where } q \coloneqq \frac{b}{|b|} \Big/ \frac{a}{|a|},
\end{aligned}$$

are related uniquely to the components of Bloch vector $\boldsymbol{r}$ of a pure qubit state: $r_m = \langle\psi|\hat{\sigma}_m|\psi\rangle$,

$$\begin{aligned}
r_1 &= \cos\varphi \sin\theta, \\
r_2 &= \sin\varphi \sin\theta, \\
r_3 &= \cos\theta.
\end{aligned}$$

The analysis of single-qubit and two-qubit states and their evolutions under unitary transformations induced by a given Hamiltonian is of particular importance due to the fact proved in theory of quantum circuits that any unitary transformation (i.e. a quantum gate) of a high-dimensional quantum state can be decomposed into a product of single-qubit and two-qubit quantum gates, and that any quantum circuit (i.e. a sequence of quantum gates followed by quantum measurements) can be approximated using the standard set of single-qubit and two-qubit gates (e.g. Hadamard, phase, $\pi/8$ and CNOT gates) [3, 10].

[2] The characteristic equation $\lambda^2 - \lambda + \rho_{11}\rho_{22} - \rho_{12}\rho_{21} = 0$ has roots $\lambda_{1,2} = \frac{1 \pm \sqrt{1 - 4(\rho_{11}\rho_{22} - \rho_{12}\rho_{21})}}{2} = \frac{1 \pm 1}{2}$, when $\rho_{11}\rho_{22} - \rho_{12}\rho_{21} = 1 - \boldsymbol{r}^{\,2} = 0$.

The simplest examples of maximally entangled states are states of a system of two qubits, such as Bell states,

$$|\Phi_\pm\rangle \coloneqq \frac{1}{\sqrt{2}}\left(|\uparrow\uparrow\rangle \pm |\downarrow\downarrow\rangle\right),$$
$$|\Psi_\pm\rangle \coloneqq \frac{1}{\sqrt{2}}\left(|\uparrow\downarrow\rangle \pm |\downarrow\uparrow\rangle\right),$$

whereas Werner state [4, 11, 12, 6, 7] is an example of partially entangled state for $p \in [\frac{1}{3}, 1)$

$$\hat{\rho}_{\mathrm{W}} \coloneqq \frac{1-p}{4}\mathbb{1} + p|\Psi_-\rangle\langle\Psi_-|.$$

Entangled states possess a counter-intuitive property, which is best seen in the case of pure maximally entangled states of multiqubit system of the form $\frac{1}{\sqrt{2}}(|\uparrow\rangle^{\otimes D} + \mathrm{e}^{i\xi}|\downarrow\rangle^{\otimes D})$, where ξ is some relative phase between components of the state: while the system state is precisely known, the states of individual qubits are maximally mixed (i.e. of the least information content about particular subsystem) and at the same time subsystems are strongly correlated, even when they do not interact directly with each other. This property has been explicitly pointed out in Ref. [13] and has been well formulated by E. Schrödinger [14, 15, 16, 17]: "Maximal knowledge of a total system does not necessarily include total knowledge of all its parts, not even when these are fully separated from each other and at the moment are not influencing each other at all."

During time evolution of a complex physical system, its parts become correlated due to interactions between them. If one is interested in the state of the specific subsystem (denoted by A), then one should trace the system's state over the rest of the system (denoted by B), which in such a case is often called an environment of a considered subsystem (usually environment is large compared to the system of interest, i.e. it has a large number of degrees of freedom and is beyond of direct control of experimentalists). In the course of time evolution of the complex system the interaction between subsystem A and its environment B leads to singling out of the pointer basis in the state space of A (which usually is the basis of energy eigenstates, but not in every system [18]) and to reduction of coherences between these basis states [19].

The effect of decoherence is clearly seen in the canonical example [2, 20], when interaction is of the form $\hat{H}_{\mathrm{int}} = \sum_n |n\rangle\langle n| \otimes \hat{B}_n$, where $\hat{B}_n$ are some environment's operators, as every observable they are Hermitian, $\hat{B}_n = \hat{B}_n^\dagger$. Such an interaction Hamiltonian causes a pure dephasing of the subsystem's A state $\hat{\rho}^A$. The Hamiltonian of a complex system AB has the form

$$\hat{H}^{AB} = \hat{H}^A \otimes \mathbb{1}^B + \mathbb{1}^A \otimes \hat{H}^B + \hat{H}_{\mathrm{int}} = \hat{H}_0 + \hat{H}_{\mathrm{int}}, \tag{1.4}$$

where $\hat{H}^A$ and $\hat{H}^B$ are Hamiltonians describing subsystems A and B, respectively. The interaction Hamiltonian singles out a certain basis in state spaces of subsystem A, $\{|n\rangle\}$. Additionally, here it is assumed that $\hat{H}^A$ commutes with $\hat{A}_n = |n\rangle\langle n|$, which also means that $[\hat{H}^{AB}, \hat{A}_n] = 0$, so the mean energy of the subsystem A is constant, $\frac{\mathrm{d}}{\mathrm{d}t}\langle\hat{H}^A(t)\rangle = 0$.

In the interaction picture, the interaction part of the Hamiltonian Eq. (1.4) reads

$$\hat{H}_{\mathrm{int}}(t) = \exp\left(i\hat{H}_0 t\right)\hat{H}_{\mathrm{int}}\exp\left(-i\hat{H}_0 t\right) = \sum_n |n\rangle\langle n| \otimes \hat{B}_n(t),$$

where $\hat{B}_n(t) \coloneqq \exp\left(i\hat{H}_0 t\right)\hat{B}_n \exp\left(-i\hat{H}_0 t\right)$. The operator of time evolution is given by

$$\hat{U}(t) \coloneqq \mathcal{T}\exp\left(-i\int_0^t \mathrm{d}\tau \hat{H}_{\mathrm{int}}(\tau)\right) = \mathcal{T}\exp\left(-i\int_0^t \mathrm{d}\tau \sum_n |n\rangle\langle n| \otimes \hat{B}_n(\tau)\right),$$

where symbol $\mathcal{T}$ denotes the time ordering of operators $\hat{H}_{\mathrm{int}}(\tau)$ in the series hidden under the symbol of exp(...). Therefore, the initial state, which at $t = 0$ is supposed to be a tensor product of superposed pure state of subsystem A and some pure state of subsystem B, $|\psi^{AB}(0)\rangle = \sum_n c_n|n\rangle \otimes |\phi\rangle$, becomes at further instance t

$$|\psi^{AB}(t)\rangle = \hat{U}(t)|\psi^{AB}(0)\rangle = \sum_n c_n|n\rangle \otimes |\phi_n(t)\rangle,$$

where

$$|\phi_n(t)\rangle = \mathcal{T}\exp\left(-i\int_0^t \mathrm{d}\tau \hat{B}_n(\tau)\right)|\phi\rangle = \hat{V}_n(t)|\phi\rangle,$$

$$\hat{V}_n(t) \coloneqq \mathcal{T}\exp\left(-i\int_0^t \mathrm{d}\tau \hat{B}_n(\tau)\right),$$

due to the fact that basis states $|n\rangle$ are not affected by the dynamics governed by the interaction Hamiltonian. As can explicitly be seen, $|\psi^{AB}(t)\rangle$ is a superposition of product states of subsystems, i.e. the system's state becomes an entangled one with respect to subsystems A and B. The evolved state of subsystem A is

$$\begin{aligned}
\hat{\rho}^A(t) &= \mathrm{Tr}_B\left(\hat{\rho}^{AB}\right) = \mathrm{Tr}_B\left(|\psi^{AB}\rangle\langle\psi^{AB}|\right) \\
&= \mathrm{Tr}_B\Big(\sum_n c_n|n\rangle \otimes |\phi_n(t)\rangle \sum_m c_m^*\langle m| \otimes \langle\phi_m(t)|\Big) \\
&= \mathrm{Tr}_B\Big(\sum_n c_n|n\rangle \otimes \hat{V}_n(t)|\phi\rangle \sum_m c_m^*\langle m| \otimes \hat{V}_m^*(t)\langle\phi|\Big) \\
&= \sum_{n,m} c_n c_m^*|n\rangle\langle m|\hat{V}_n(t)\hat{V}_m^*(t) = \sum_{n,m} c_n c_m^*|n\rangle\langle m|\langle\phi_m(t)|\phi_n(t)\rangle.
\end{aligned}$$

The diagonal elements of $\hat{\rho}^A(t)$ are time-independent ($\langle\phi_n(t)|\phi_n(t)\rangle = 1$), while the off-diagonal elements evolve in time: their moduli decrease as overlap between evolved states of environment $|\langle\phi_m(t)|\phi_n(t)\rangle|$, which depends on the exact form of interaction Hamiltonian and its parameters as well as on the chosen initial state. In most cases, interaction between subsystems leads to irreversible dynamics of $\hat{\rho}^A(t)$ and to a fast decay of the overlap between distinct environmental states, $|\langle\phi_m(t)|\phi_n(t)\rangle|$, $n \neq m$. At long times, i.e. $t \gg t_{\mathrm{decoh}}$, where t_{decoh} is a time scale of decoherence, $\langle\phi_m(t)|\phi_n(t)\rangle \approx \delta_{nm}$, and thus the subsystem A is in an incoherent state in basis $\{|n\rangle\}$, $\hat{\rho}^A(t \gg t_{\mathrm{decoh}}) \approx \sum_n |c_n|^2|n\rangle\langle n|$.

The same reasoning applies in the case when initial state of environment is mixed, i.e. when the system's initial state is of the form $\hat{\rho}^{AB}(0) = |\psi^A(0)\rangle\langle\psi^A(0)| \otimes \hat{\rho}^B(0)$, where $|\psi^A(0)\rangle = \sum_n c_n|n\rangle$ is an initial state of subsystem A and $\hat{\rho}^B(0)$ is an initial state of environment. The system state evolves as follows $\hat{\rho}^{AB}(t) =$

$\hat{U}(t)\hat{\rho}^{AB}(0)\hat{U}^{\dagger}(t) = \sum_{n,m} c_n c_m^* |n\rangle\langle m| \otimes \hat{V}_n(t)\hat{\rho}^B(0)\hat{V}_m^{\dagger}(t)$, and the reduced state of the subsystem A is

$$\begin{aligned}\hat{\rho}^A(t) &= \mathrm{Tr}_B(\hat{\rho}^{AB}(t)) = \sum_{n,m} c_n c_m^* |n\rangle\langle m| \ \mathrm{Tr}(\hat{V}_n(t)\hat{\rho}^B(0)\hat{V}_m^{\dagger}(t)) \\ &= \sum_{n,m} c_n c_m^* |n\rangle\langle m| \ \mathrm{Tr}(\hat{V}_m^{-1}(t)\hat{V}_n(t)\hat{\rho}^B(0)),\end{aligned}$$

from which one can see that coherence moduli decay as $\mathrm{Tr}(\hat{V}_m^{-1}(t)\hat{V}_n(t)\hat{\rho}^B(0))$.

While considering entanglement of quantum states as a resource, one naturally needs to quantify the amount of entanglement contained in a given quantum state. It turned out that the problem of quantifying of entanglement of mixed states is quite complex (in fact, even checking if a given mixed quantum state is entangled is a nontrivial task itself) [6, 7]. There exist a few different approaches to this problem [6, 7]: one can use operational measures of entanglement that make use of the fact that entanglement is a physical resource which can be spent during execution of a certain task the efficiency of which depends on the amount of entanglement contained in the state (e.g. fidelity of teleportation during which analyzed state has been spent is a function of entanglement amount of that state); it is also possible to define axiomatic measures of entanglement, which must satisfy some reasonable conditions that are in accordance with the essence of entanglement, like monotonicity under local operations and classical communication, which originates from the fact that entanglement cannot be produced by local operations possibly backed by classical communication (concurrence is an example of measure of that kind) [5]; besides this, one can also adopt a geometrical approach to entanglement quantification, in which entanglement is estimated through the distance between the considered state and the closest separable state, i.e. the estimate of entanglement amount is derived from the geometrical structure of the space of density operators (e.g. relative entropy of entanglement).

Since the dissertation is focused on the two-qubit states, their entanglement will be quantified by one of the most commonly used measures for two-qubit states, which is concurrence [21], $C(\hat{\rho}) \in [0, 1]$ (where $C = 0$ means that the state is separable, and $C = 1$ means that the state is maximally entangled). Concurrence is given by

$$C(\hat{\rho}) \coloneqq \max(0, \sqrt{\lambda_1} - \sqrt{\lambda_2} - \sqrt{\lambda_3} - \sqrt{\lambda_4}),$$

where $\lambda_1 \geqslant \lambda_2 \geqslant \lambda_3 \geqslant \lambda_4$ are eigenvalues of the matrix $\hat{\rho}\,(\hat{\sigma}_y \otimes \hat{\sigma}_y)\,\hat{\rho}^*\,(\hat{\sigma}_y \otimes \hat{\sigma}_y)$, $\hat{\sigma}_y$ is the Pauli matrix, and $\hat{\rho}^*$ is the complex conjugate of $\hat{\rho}$. For the two-qubit states of X form (e.g. the Bell states or the Werner state), there exists a simplified way to calculate the concurrence [22]

$$C(\hat{\rho}) = 2\max(0, |\rho_{14}| - \sqrt{\rho_{22}\rho_{33}}, |\rho_{23}| - \sqrt{\rho_{11}\rho_{44}}), \tag{1.5}$$

where ρ_{ij} are the density operator elements (in the standard $|\sigma_A\sigma_B\rangle$ basis) of $\hat{\rho}(t)$. Concurrence can be easily calculated for a pure two-qubit state $|\psi\rangle$,

$$C(|\psi\rangle) = |\langle\psi|\hat{\sigma}_y \otimes \hat{\sigma}_y|\psi^*\rangle|,$$

where the vector $|\psi^*\rangle$ is the complex conjugate of $|\psi\rangle$.

Another convenient measure of bipartite entanglement is negativity [23], which is based on the Peres-Horodecki criterion [24, 25]: if a density operator partially transposed with respect to some subsystem is negative, then such a state necessarily possesses entanglement between the subsystem and the rest of the system. Negativity is defined as

$$N(\hat{\rho}_{AB}) \coloneqq \frac{1}{2}\left(||\hat{\rho}_{AB}^{\mathrm{T}_A}|| - 1\right),$$

where

$$\hat{\rho}_{AB}^{\mathrm{T}_A} \coloneqq \Big(\sum_{\alpha\beta\gamma\delta} \rho_{\alpha\beta,\gamma\delta}|\alpha\rangle_A \otimes |\beta\rangle_{BA}\langle\gamma| \otimes {}_B\langle\delta|\Big)^{\mathrm{T}_A} = \sum_{\alpha\beta\gamma\delta} \rho_{\alpha\beta,\gamma\delta}|\gamma\beta\rangle\langle\alpha\delta|$$

is a partially transposed density operator with respect to the subsystem A, and the norm of a matrix M is defined as $||M|| = \mathrm{Tr}\left(\sqrt{M^\dagger M}\right)$ (in the case of a density operator this norm is equal to the sum of moduli of its eigenvalues). Although negativity fails to detect entanglement for some states when the dimension of the state space is greater than 2×3, it is widely used because it is applicable to systems of any size and is relatively easy to calculate, unlike most of the entanglement measures for mixed states (e.g. entanglement of formation), which usually involve optimization over a set of density operators (that is impossible to perform in practice even for systems of moderate size due to exponential growth of size of system's state space).

Lastly, it is worth noting that in the framework of quantum mechanics, entangled state can be created in two fundamentally different ways. One way is deterministic creation of an entangled state starting from the separable one in course of joint evolution of a few subsystems that appropriately interact with each other. For example, an entangled state of two qubits is generated when their interaction is described by Ising-like Hamiltonian $\hat{H}_{\mathrm{int}} = \frac{\hbar}{4}J(\hat{\sigma}_z + \hat{\mathbb{1}}) \otimes (\hat{\sigma}_z + \hat{\mathbb{1}})$ (see Chapter 4). Another way of entanglement production is execution of the projective measurement in a basis of the system's entangled states[3]. The outcome of such a measurement will necessarily be one of the basis states. As long as measurement problem in quantum mechanics is not solved this method of entanglement production has its formal foundation in the measurement postulate (post-measurement state-update rule and Born's rule) [26, 27], which skips the physical mechanism of that process as well as its dynamics and only assigns probabilities to the particular outcomes. Certainly, during execution of the projective measurement that is aimed at entanglement production, all subsystems of a measured quantum system must interact simultaneously with the measuring apparatus, so it can be reasonably presumed that such a measurement induces a strong interaction through the apparatus between the subsystems. Thus, in one way or another both methods of entanglement production are based on forcing subsystems to interact with each other, with the only difference whether the final desired entangled state is obtained in a deterministic way or randomly with some probability.

It is interesting enough that, although some counter-intuitive features of quantum states have been noticed and discussed shortly after the formulation of quantum mechanics [13, 28, 14, 15, 16, 17], conceptualization of quantum information and understanding the fact that quantum correlations contained in quantum states are a

[3] A certain role of the quantum measurement checking if two-qubit state is the entangled one is studied in Chapter 3.

unique resource, which can be used for useful applications otherwise impossible, took decades, resulting in forming of a wide branch of quantum science. Several milestones on that path are worth mentioning such as derivation of Bell's inequalities [29], establishing a limit on a conversion of information from quantum representation to the classical one (Holevo's theorem) [30], first suggestions for using quantum systems for computing [31, 32], discovery of the principle of superdense coding [33] and quantum teleportation [34], and invention of quantum algorithms [35, 36] which show explicitly advantages of quantum computations over classical counterparts. In contrast to difficulties which one encounters in any attempt to define classical information, the definition of quantum information is strikingly simple and sharp: it is the state of a quantum system of interest, which can be described in terms of classical information by a state vector (if the state is pure) or a density operator in a chosen basis of the system's state space (i.e. the set of corresponding coefficients or the set of density operator elements). To be useful for potential applications, quantum information should be contained in a physical system that is clearly defined and is suited for performing desired manipulations with it (quantum logic gates, quantum measurements, etc.). Unlike classical information, that can be written in different substrates without any loss or change of its content, quantum information cannot be considered without explicit description of the state space of the system which is chosen to carry that information. The nature of quantum information determines a fundamentally different approach to its processing. A series of no-go theorems, which stress the peculiarities of quantum information in comparison to classical information, has been discovered: no-cloning theorem (impossibility to create identical copy of an arbitrary unknown quantum state) [37, 38, 39, 40], no-deleting theorem (impossibility to delete one of the identical copies of some arbitrary quantum state, a time-reversed partner of the no-cloning theorem) [41], no-broadcast theorem (impossibility to create two copies of an unknown quantum state, a corollary of the no-cloning theorem) [42], no-hiding theorem (loss of quantum information of the system is always accompanied by transfer of that information to the environment, quantum information cannot disappear from a closed quantum system, and no information is contained in the correlations between the decohered system and its environment) [43], no-teleportation theorem (impossibility to convert a quantum state to classical information that fully describes it by performing a quantum measurement[4] on a single copy of that state) [44], no-communication (impossibility to communicate instantly the information by measuring entangled states) [45], no-programming theorem (impossibility of existence of a universal programmable quantum processor) [46].

[4] One can deduce the quantum state of the system only by performing a number of quantum measurements executed on a physical system being each time in the same quantum state and estimating the probabilities of outcomes. The result of a single quantum measurement gives, in fact, no information about the quantum state in which the system was just before the measurement—it only informs us in what state the system happened to be right after the execution of that measurement and that the measured state certainly has been a component of the ensemble representation of the state in which system was just before the measurement.

1.2 Quantum Dot Spin Qubits

In the last few decades, various physical systems have been considered as a physical realization of quantum-information concepts. Among others, qubits based on localized electron spins in semiconductor nanostructures have been investigated in depth, both theoretically and experimentally, for their possible use as building blocks of a quantum computer. Several different types of such qubits have been mastered, such as spin qubits based on gated quantum dots (QDs) in AlGaAs/GaAs [47, 48, 49] or Si nanostructure [50, 51, 52, 53], self-assembled QDs [54, 55], nitrogen-vacancy (NV) centers in diamond [56], and electrons bound to phosphorous donors in silicon [57]. In particular, advances in controlling the coupling between two spin qubits [58, 59, 60, 61, 62, 63, 64, 65] have led to demonstration of creation and manipulation of entangled states of two electron spin-based qubits [66, 67].

By the end of 1990s several kinds of semiconductor QD devices which are able to fully confine (i.e. in all three spatial dimensions) a single electron [68] and allow to perform some manipulations with it as well as measurements of its state were mastered. The following types of QDs deserve a mention here, since such systems are the object of studies presented in the following chapters.

1.2.1 Gated lateral quantum dots

Electrically defined *gated lateral QDs* [47] are created in AlGaAs/GaAs heterostructure grown by molecular-beam epitaxy. By doping AlGaAs layer with Si one introduces additional conduction band electrons to the heterostructure. Due to the conduction band mismatch at the interface between GaAs and AlGaAs a triangular quantum well[5] is formed there, which confines electrons in a plane perpendicular to the growth direction (usually called z direction) of the heterostructure. As a result, two-dimensional electron gas (2DEG) appears inside the structure at the interface, which is circa $50 \div 100$ nm below the surface of AlGaAs layer. The width of that 2DEG is[6] about $10 \div 20$ nm. The confinement of electrons from 2DEG in lateral QDs is completed in the xy plane by electrostatic potential produced by negatively charged metallic electrodes fabricated on the surface of AlGaAs layer. Typically, electrodes which form a QD have a rounded shape and circle an area about a hundred nm in diameter. Inside this area, a small number of electrons from 2DEG can be localized, as a potential barrier in the xy plane is created by electric field originated from the electrodes. Fine tuning of the electrostatic potential inside the QD is performed with the help of the gate electrode: by varying the voltage on the gate, one can control the number of electrons in the QD in a precise way. The device is usually equipped with a quantum point contact (QPC) nearby the QD, which is used to determine the number of electrons in the QD. The conductance of QPC is sensitive to charges in its surroundings, so it can clearly detect a transition of a

[5] The depth of the triangular quantum well of a $Al_xGa_{1-x}As/GaAs$ heterostructure is limited from above by the discontinuity of the bottom of conduction band on the interface ΔE_c, which is determined by Al mole fraction x and is about 365 meV at most for $x = 0.45$ [69]. Typically, for gated lateral QDs one uses a heterostructure with $x = 0.3$ [61], which has $\Delta E_c \approx 243$ meV.

[6] Width W_z of the quantum well formed on the interface between AlGaAs and GaAs can be estimated using the formula [70, 71, 72]: $W_z = 2\sqrt[3]{\frac{10^{12}\ \mathrm{cm}^{-2}}{n}} \cdot 5.5\,\mathrm{nm}$, where n is 2D electron density at AlGaAs/GaAs interface, which typically is about $n \approx (1 \div 5) \cdot 10^{11}\ \mathrm{cm}^{-2}$ [47], so it gives $W_z \approx 10 \div 20$ nm.

single electron into or out of the QD. To make the described device operational, it is required to cool it down to low enough temperature, typically about tens mK. This requirement is dictated by the need to keep the confined electrons in their ground state orbitals: at typical operating temperature $T = 20$ mK the thermal energy $k_{\mathrm{B}}T \approx 2$ μeV, which is much less than the energy difference between the ground orbital and the lowest excited one[7], ΔE_{orb}. Low temperatures also help to suppress one of the mechanisms of decoherence of electron spin state, namely, that one which is induced by interaction with phonons.

1.2.2 Single electron spin qubit in a gated quantum dot

The idea to use spin of an electron confined in a semiconductor QD as a qubit was explicitly formulated in Ref. [73] (the Loss–DiVincenzo proposal) bearing in mind a gated lateral QD device. Electron spin, which magnitude is $\frac{\hbar}{2}$, has two basis states, therefore, it is a natural qubit. Electron spin states becomes distinguishable in a magnetic field by their energies: $E_{0\downarrow}$, $E_{0\uparrow} = E_{0\downarrow} + E_{\mathrm{Z}}$, where $E_{0\downarrow}$, $E_{0\uparrow}$ are the energies of electron in ground orbital states, $E_{\mathrm{Z}} = g\mu_{\mathrm{B}}B_z$ is the Zeeman energy (i.e. the energy splitting between electron spin states $|\uparrow\rangle$ and $|\downarrow\rangle$), where g is the effective electron spin g-factor[8], μ_{B} is the Bohr magneton, and B_z is the z-component of magnetic field. The first excited orbital is separated from the ground one by the energy gap ΔE_{orb}, which is much higher than energies of thermally populated (at mK temperatures) phonon modes in the QD, so thermal excitations of electron to higher orbital states can be safely neglected that makes its spin states reliable qubit states.

Such a qubit can be easily initialized by putting it into a strong magnetic field and waiting a while until it equilibrates to its ground state [73]. This occurs at time scales of milliseconds and longer [74] and is caused by phonon emission accompanied by spin flip made possible by finite spin–orbit coupling for conduction band electrons in a given semiconductor. A couple of faster ways of electron state initialization have been proposed, e.g. spin injection from a ferromagnet [73], by spin-polarized current from a spin filter [73], or simply by gradual deepening of the confining potential which results in populating an empty QD with a single electron: in a strong magnetic field in such system configuration only electron in spin up state can tunnel into a QD from 2DEG while energy of spin down state is kept higher than electrochemical potential of 2DEG [47]. In the Loss–DiVincenzo proposal [73], it has been suggested that single-qubit gates can be realized by applying locally appropriate magnetic fields to individual electrons for a specific period during which a desired rotation of an electron spin state is completed. These magnetic fields could be external ones (e.g. produced by a magnetic material on the probe tip of a scanning microscope interacting with the device) as well as could originate from the nuclear spins of atoms of the QDs (Overhauser field) or even could be effective

[7] Apart from the fact that energy difference between the ground state and first excited one can be measured in experiment, the order of its magnitude can be roughly estimated in advance from the size of confining potential, which can be evaluated from the geometrical size of QD for that purpose: assuming an electron in a rectangular potential box, the energy levels are given by well-known formula $E_{n_x,n_y,n_z} = \frac{\hbar^2\pi^2}{2m_{\mathrm{e}}^*}\left(\left(\frac{n_x}{L_x}\right)^2 + \left(\frac{n_y}{L_y}\right)^2 + \left(\frac{n_z}{L_z}\right)^2\right)$, and for $L \approx 20$ nm the energy difference ΔE_{orb} is of the order of 1 meV for a gated AlGaAs/GaAs QD.

[8] Electron in a AlGaAs/GaAs heterostructure has $g \approx -0.4 < 0$, so $E_{\mathrm{Z}} < 0$ and $E_\uparrow < E_\downarrow$.

ones due to interaction of the electron through tunnel coupling with an adjacent ferromagnetic QD, etc. It has been shown in experiment that state of a single electron can be coherently manipulated with a high precision using electron spin resonance (ESR) technique [75, 76, 77, 47], which requires to invest an additional effort in designing and production of an appropriate device, since to execute ESR manipulations one needs to generate ac magnetic field in that device and to apply it perpendicularly to the constant magnetic field already present in the QD. In such a case, the electron spin Hamiltonian acquires a time-dependent term: $\hat{H}_{\mathrm{q}}(t) = \frac{1}{2} g\mu_{\mathrm{B}} \left(B_z \hat{\sigma}_z + B_x \cos(\omega t + \theta)\hat{\sigma}_x\right)$, where ω is the frequency of the ac magnetic field and θ is its initial phase. To have an effect, the ac magnetic field frequency ω used in ESR should be close to that associated with the spin splitting energy, $\frac{g\mu_{\mathrm{B}} B_z}{\hbar}$. Clear evidence of coherent rotations (Rabi oscillations) of a single electron spin done by ESR was reported for the first time in Ref. [77], although amplitude of Rabi oscillations decreases with time $\propto \frac{1}{\sqrt{t}}$ due to decoherence caused by electron's environment consisting of nuclear spins.

Since in the Loss–DiVincenzo proposal [73] the electrically gated lateral QD was chosen as a prototype system, it was shown there that two-qubit gates can be realized for such qubits by pulsing the exchange coupling between neighboring confined electron spins that can effectively be described by the two-spin Hamiltonian of an isotropic Heisenberg form, $\hat{H}_{2\mathrm{q}}(t) = J(t)\, \hat{\mathbf{S}}_L \otimes \hat{\mathbf{S}}_R$, where $\hat{\mathbf{S}}$ is the electron spin operator of left or right QD, and $J(t)$ is the coupling between the spins. In the considered QD system, exchange coupling could be produced by varying the voltage on the interdot gate electrode that leads to lowering the potential barrier between the QDs, so exchange coupling increases with growing overlap of electron wave functions localized in the two QDs. The same effect can be achieved with a constant voltage on the interdot gate electrode when QD potential minima are elevated by applying a proper voltage to the back gates of the device [58], so electrons get less localized and because of that overlapping of wave functions increases. Assuming in the simplest case a stepwise change of $J(t)$, after a time period $\tau_s = \frac{\pi}{J_0}$, where J_0 is a constant value of the coupling $J(t)$ when it is switched on, two qubits exchange their states, which means that SWAP gate is completed. In half of that time period, $\tau_s/2$, $\sqrt{\mathrm{SWAP}}$ gate is performed, which together with single-qubit operations forms a complete set of quantum gates for quantum computation [73, 78, 79].

A few ways of a single-shot measurement of such a qubit were initially proposed [73], e.g. the inference of a spin states of electron by making use of a supercooled paramagnetic dot to which electron tunnels from the QD. Electron stimulates the transition of such a paramagnetic dot to the ferromagnetic phase. The direction of magnetization of a created ferromagnetic domain will agree with the measured electron spin state, and it could be measured by conventional means. Another possible way to measure electron spin state is to use a spin valve connected to the QD. The spin valve would allow to tunnel through it only electron being in one certain spin orientation. In such an arrangement, an electron being in allowed spin state tunnels to the next QD, where it will be detected due to its charge by a sensitive electrometer. Finally, it turned out that in practice the most convenient way to measure a spin state of an electron is to make use of spin-to-charge conversion and observe the electric current through a QPC which is located near the QD [47]. A spin-to-charge conversion is based on the simple fact that if the QD ground spin state (say, state $|\uparrow\rangle$) is below the electrochemical potential of the 2DEG outside the

QD, and another spin state is above that potential, then only the electron in state $|\downarrow\rangle$ can tunnel off the QD (energy-selective readout) [47]. A spin-to-charge conversion can also take place in a system configuration where both states are above the 2DEG electrochemical potential but have different tunnel rates, $\Gamma_\uparrow$ and $\Gamma_\downarrow$. When difference in tunnel rates of different spin states is high enough, e.g. $\Gamma_\downarrow \gg \Gamma_\uparrow$, electron will tunnel off the QD mostly from the spin state $|\downarrow\rangle$ during measurement time $\Gamma_\uparrow^{-1} \gg \tau \gg \Gamma_\downarrow^{-1}$ (tunnel-rate-selective readout) [80, 47].

1.2.3 Double quantum dots and singlet-triplet qubits

A double gated lateral QD (DQD) is of special interest because it also offers a possibility to use two-electron spin states as a qubit that can be fully controlled by gate voltages, with no need for time-dependent magnetic fields. Since the confining potential of each QD can be controlled independently, the QDs may be differently populated with electrons, which can be seen on charge stability diagram or experimentally measured charge sensing data. Charge stability diagram of a DQD is derived within the constant interaction (or capacitive charging) model [81, 82, 47]. In that model, couplings of QDs to each other as well as to the exterior or gates are represented as capacitors and the position of confining potential bottom directly depends on the voltage on the corresponding gate electrode. Two simplifying assumptions are used in this model: Coulomb interaction between electrons inside the QD as well as with the QD exterior is parameterized by a constant capacitance C, and the QD single-particle energy spectrum is obtained for non-interacting electrons, so the total energy of the QD system is a sum of energies of the populated energy levels and corresponding multiplicity of charging energy (a term proportional to square of the number of electrons in the QD, N^2, and the charging energy $E_\mathrm{C} = \frac{e^2}{C}$, where e is electron charge and C is a capacitance of the QD) along with the energies associated with the QD electrodes due to supplied voltages on them. Therefore, within the model, the addition of an electron to the QD requires energy $E_\mathrm{add} = E_\mathrm{C} + \Delta E$, where ΔE is the energy difference between the highest already occupied state and the next one. The main finding which came out from that model and has been confirmed in experiment is the fact that charge configurations form a hexagonal (honeycomb) lattice which fills the plane parameterized in orthogonal directions by gates' voltages [83, 47, 82].

When a DQD is in a two-electron configuration, e.g. $(1,1)$ or $(0,2)$, where the symbol (n,m) denotes the electron populations of individual QDs comprising the DQD, the possible spin states of electrons are a singlet and three triplets:

$$
\begin{aligned}
|S\rangle &= \frac{1}{\sqrt{2}}\left(|\uparrow\downarrow\rangle - |\downarrow\uparrow\rangle\right), \\
|T_0\rangle &= \frac{1}{\sqrt{2}}\left(|\uparrow\downarrow\rangle + |\downarrow\uparrow\rangle\right), \\
|T_+\rangle &= |\uparrow\uparrow\rangle, \\
|T_-\rangle &= |\downarrow\downarrow\rangle.
\end{aligned}
$$

In experiment, during manipulation of two-electron states, typically one keeps the average energy of electron ground states in two QDs constant, or in other words, the sum of QD electrochemical potentials is fixed. For description of the shape of

confining potential of a DQD staying in a two-electron configuration, and, as a consequence, relative positions of electron energy levels, a parameter called detuning is used. This parameter is defined by different authors in one of two ways: either as a difference ε between energies of singlet states $|S(1,1)\rangle$ and $|S(0,2)\rangle$ (so, $\varepsilon = 0$ at anticrossing of states $|S(1,1)\rangle$ and $|S(0,2)\rangle$, which takes place when a confining potential of the second QD is deeper) [47], or as a difference ϵ between the electrochemical potentials of QDs (and then $\epsilon = 0$ corresponds to symmetric confining potential of DQD) [48]. In a configuration in which both electrons are in the same QD, e.g. $(0,2)$ when $\varepsilon > 0$, singlet and triplet states are naturally split by energy approximately equal to the difference of energies between the first excited orbital and the ground orbital[9], whereas for slightly negative ε that corresponds to the configuration $(1,1)$, in which electrons are localized in different QDs, the energy difference between singlet and triplet states, denoted by J, is a function of the tunnel coupling t_c between the QDs and the energy E_C of charging of a single QD (energy of Coulomb interaction between two electrons in the QD). The magnitude of J strongly depends on tunnel coupling t_c between the QDs, which can be seen from an estimate derived using a Hubbard approximation for a DQD [48],

$$\begin{aligned}\hat{H} = {} & (E_\mathrm{C} - \epsilon)|S(0,2)\rangle\langle S(0,2)| + (E_\mathrm{C} + \epsilon)|S(2,0)\rangle\langle S(2,0)| \\ & + \sqrt{t_\mathrm{c}}(|S(2,0)\rangle\langle S(1,1)| + |S(0,2)\rangle\langle S(1,1)| + \mathrm{h.c.}),\end{aligned}$$

that is written using a particular choice of zero energy – it is set at the level of sum of electrochemical potentials of the QDs[10]. From this Hamiltonian one can obtain $J \approx 4t_\mathrm{c}^2 \frac{E_\mathrm{C}}{E_\mathrm{C}^2 - \epsilon^2}$ [78, 48], so J can be varied in a wide range, practically from 0 to some J_max, either by varying the detuning ϵ while keeping constant t_c of tunnel coupling [47], or by varying the interdot barrier height at fixed detuning ϵ which leads to changes of constant tunnel coupling t_c [84]. It is worth stressing that singlet state in a DQD is a mixture of spatially distributed state $|S(1,1)\rangle$ with spatially concentrated states $|S(2,0)\rangle$ and $|S(0,2)\rangle$, which can be sketched from the Hubbard approximation as $|S\rangle \approx |S(1,1)\rangle - \frac{\sqrt{2}t_\mathrm{c}}{E_C - \epsilon}|S(0,2)\rangle - \frac{\sqrt{2}t_\mathrm{c}}{E_C + \epsilon}|S(2,0)\rangle$, whereas triplet state is always a spatially distributed state $|T(1,1)\rangle$, because entering an excited orbital is energetically inaccessible for electrons in typical experimental conditions [47, 48].

Exchange interaction between electron spins conserves the total spin ($S = 0$ for singlet and $S = 1$ for triplet) as well as its z projection, so two-electron states with different values of z projection hardly mix with each other, and hence, it is possible to use singlet $|S\rangle$ and unpolarized triplet $|T_0\rangle$ as a qubit (called S-T_0 qubit) when constant external magnetic field (typically, $B = 0.1 \div 1$ T) is applied in the plane of 2DEG that splits off polarized triplets $|T_+\rangle$ and $|T_-\rangle$ from the states $|S\rangle$ and $|T_0\rangle$. Naturally, splitting energy J between singlet $|S\rangle$ and triplet $|T_0\rangle$ becomes the key parameter of S-T_0 qubit. The other possibility to affect the state of S-T_0 qubit arises

[9] Antisymmetry of singlet two-electron wave function under particle exchange is secured by wave function's spin part, so two electrons being in singlet state may stay in the same orbital. In contrast to this, antisymmetry of triplet wave function is due to spatial part of the wave function, so at least two different orbitals must be occupied by electrons.

[10] Term $|S(1,1)\rangle\langle S(1,1)|$ and all three triplet terms $|T_i(1,1)\rangle\langle T_i(1,1)|$ with $i = 0, +, -$ are not explicitly seen in the Hamiltonian because they are multiplied by zero energy, whereas triplet terms $|T_i(0,2)\rangle\langle T_i(0,2)|$, $|T_i(2,0)\rangle\langle T_i(2,0)|$ with $i = 0, +, -$ are not included in the Hamiltonian because of their too high energies.

when magnetic field in QDs is different, i.e. a gradient of magnetic field ΔB_z in the DQD is present, which leads to mixing of singlet $|S\rangle$ and triplet $|T_0\rangle$ as a result of oscillating relative phase between the states $|\uparrow\downarrow\rangle$ and $|\downarrow\uparrow\rangle$: $|S\rangle = \frac{1}{\sqrt{2}}\left(|\uparrow\downarrow\rangle - |\downarrow\uparrow\rangle\right) \xrightarrow{t} \frac{1}{\sqrt{2}}\left(|\uparrow\downarrow\rangle - \mathrm{e}^{it\Delta B_z}|\downarrow\uparrow\rangle\right)$. Therefore, the Hamiltonian of S-T_0 qubit written in basis of states $|S\rangle$ and $|T_0\rangle$ reads as follows

$$\hat{H}_{\mathrm{q}} = \frac{J(t)}{2}\left(|T_0\rangle\langle T_0| - |S\rangle\langle S|\right) + \frac{\Delta B_z}{2}\left(|T_0\rangle\langle S| + |S\rangle\langle T_0|\right) = \frac{1}{2}\Big(J(t)\hat{\sigma}_z + \Delta B_z\hat{\sigma}_x\Big), \tag{1.6}$$

where parameter ΔB_z denotes the energy associated with magnetic field gradient between the QDs (in fact, this energy may be also due to difference of electron g-factors between the QDs).

It is worth to note that S-T_0 qubit uses a two-electron states that are insensitive to global magnetic field, since both $|S\rangle$ and $|T_0\rangle$ have zero z projection, i.e. these states are from the decoherence free subspace of two-electron state space. Nevertheless, S-T_0 qubit still remains sensitive to fluctuations of local magnetic field (external one or the Overhauser field generated by the nuclei of the atoms of the nanostructure) or local value of g-factor that result in fluctuating ΔB_z term of the qubit's Hamiltonian. Moreover, due to the fact that J depends on the confining potential, which is controlled electrically, the splitting energy J is, hence, susceptible to fluctuations of local electric field in the DQD.

Initialization of S-T_0 qubit starts from the empty DQD configuration (0,0) and is executed by gradual deepening the confining potential of one of QDs. That QD traps two electrons from 2DEG in a sequence, the final state of which is singlet, since the confining potential is never made too deep to bind the triplet state in a single QD. Next, DQD configuration is changed to the basic operational configuration (1,1) by smooth reducing the detuning ε making DQD confining potential almost symmetric.

Once the DQD is in (1,1) configuration, an attempt to bring two electrons into the same QD by gradual tilting the confining potential which pushes one of the electrons into the other dot discriminates singlet (electron has tunnelled to the neighboring QD) and triplet (electron stays in its QD) states, hence, acts as a measurement from which one can infer what was the two-electron spin state by observing the charge distribution in the DQD. This phenomenon is called the Pauli spin blockade. As long as the total spin of two electrons confined in a DQD is conserved (which is true up to, at least, millisecond time scale [74]), the spatial parts of their wave function are uniquely correlated with their spin states, and for moderate detunings $|\epsilon| \approx E_{\mathrm{C}}$ the transitions between charge configurations $(1,1) \to (0,2)$ and $(1,1) \to (2,0)$ are possible only from singlet state $|S\rangle$.

As can be seen from the Hamiltonian of S-T_0 qubit (Eq. (1.6)), such a qubit has two naturally predefined axes of rotations, x and z, therefore, to rotate a qubit state about one of these axes, its rotations about another one must be suppressed (by vanishing the corresponding factor in Eq. (1.6)). It is possible in experiment to change rapidly the value of J in a wide range, starting practically from 0, but ΔB_z cannot be tuned at a necessarily high rate. This causes some difficulties in its operation that, however, can be overcome by designing advanced control sequences which are based solely on control of $J(t)$ and overshadowing of ΔB_z by high enough value of J when needed (see Chapter 4 for more details).

The fact that the asymmetric charge distribution in DQD is characteristic only for singlet state has one more important implication. When two closely located S-T_0

qubits both are in singlet states they become coupled through the electric dipole-dipole interaction, which slightly changes charge distributions in both DQDs and, as a result, impacts the actual values of energy splittings, J_1 and J_2, of these qubits, so two-qubit interaction Hamiltonian is of Ising form $\hat{H}_{\text{int}} \propto |SS\rangle\langle SS|$ or, in matrix representation, $\propto (\hat{\sigma}_z + \mathbb{1})^{\otimes 2}$, which allows to perform the two-qubit CPHASE gate on a pair of S-T_0 qubits.

A number of other physical realizations of a qubit in gated lateral QDs has been proposed [48]. For example, the concept to use states $|S\rangle$ and $|T_+\rangle$ of two electrons in a DQD as a qubit has been reported [85], although no experimental demonstration of such a working device is available [48]. A desire to have electrical-only control over qubits has led to elaboration of several concepts of a-few-electron qubits, all single- and two-qubit operations on which can be performed using the exchange interaction between electrons that is ultimately controlled by voltages on the device's gates [48].

1.2.4 Other kinds of quantum dots

Gated vertical QDs are similar to gated lateral QDs. Vertical QD is formed by etching a pillar in GaAs/AlGaAs/InGaAs/AlGaAs/GaAs heterostructure, so electrons can be confined in InGaAs layer, since conductance band bottom of InGaAs is lower than that of adjacent layers. The shape of vertical QD confining potential is mainly defined by the geometry of the QD, which typically is about a few hundred nm in diameter and its thickness is approximately 10 nm. The side metallic gate, which wraps the pillar, provides a possibility to squeeze the lateral binding potential of the QD that allows to control the number of electrons in the QD in a precise way via voltage on the gate. A constant interaction model helps greatly to understand the properties of gated vertical QDs, e.g. such as charge stability diagram with characteristic Coulomb diamonds. A DQD has also been realized using vertical arrangement [81].

Self-assembled QDs are obtained by the Stranski-Krastanov growth in the process of molecular-beam epitaxy, in which due to the mismatch of lattice constants of substrate (e.g. GaAs) and QD material (e.g. InAs) the resulting strain forms small islands of QD material embedded in the host material. The obtained QDs have a lens shape with typical size of a few tens nm in diameter at most and a few nm in width in growth direction. By repeating that process, one can fabricate a device with several layers of QDs. In such nanostructures, strains that arise near the QDs in the lower layer predetermine to great extent the positions of the QDs in the subsequent layers, so the chains of QDs tend to form in a multilayer structure. In particular, this is helpful for the fabrication of DQDs, i.e. systems of two nearly situated QDs separated by a thin barrier layer (about 9 nm [62, 86]), so tunneling of the electron from one QD to another is possible. In self-assembled QDs, charge carriers are usually tightly confined in the QDs (compared to gated lateral ones) because potential 3D well is deep enough, e.g. in a InAs/GaAs QD the discontinuities of the bottom of conduction band as well as the top of valence band for heavy holes are about 0.4 eV, so excitons, produced by optical pulses stimulating electron interband transitions, do not escape from the QDs. Therefore, transitions from single-electron states in the QD to some optically excited ones and back can be utilized as a means of initialization, manipulation and read out of a spin state of electron [55]. The QDs constituting a DQD are intentionally made of slightly

different sizes that imply they have different optical transition energies, and hence, this enables optical access to each of the QDs independently by using appropriate laser frequency while the device is operated at liquid helium temperatures. The QDs are enclosed in a Schottky diode. This enables for applying a proper voltage to the device, which translates into an electric field bias inside the structure along the growth direction, and, as a result, allows to populate each of QDs with one electron and to tune their energy levels.

Initialization of spin states as well as single-spin and two-spin manipulations are possible due to optical transitions between electron states and some optically excited states (e.g. trion states). Depending on a system configuration[11] realized in experiment, certain selection rules for optical transitions applies, according to which one can choose a Λ-system consisting of electron spin states and some excited one and use it for electron spin manipulations [54, 55]. For example, when QD is populated with a single electron its spin may be faithfully initialized by optical pumping the frequency and the polarization of which is tuned to the transition between the higher single electron spin level (say, $|\downarrow\rangle$) and the corresponding trion level ($|\uparrow\downarrow\Downarrow\rangle$, a pair of electrons and a heavy hole). After a few cycles, the electron spin state $|\uparrow\rangle$ is initialized, since the end state after electron-hole recombination can be both $|\uparrow\rangle$ and $|\downarrow\rangle$, but the state $|\downarrow\rangle$ is continuously emptied by the pumping [87]. Similarly, a DQD can be initialized in singlet state by optical pumping when Λ-system consists of singlet, triplet and corresponding exciton state [62]. The complete control of a single electron qubit is based on use of ultrafast optical broadband rotation pulses, which are tuned in such a way that they do not directly excite any trion in the QD but give a raise to an effective coupling between the single electron spin states (i.e. rotation about qubit's x axis) through stimulated Raman transitions [87]. On the other hand, every superposition of the basis states precesses about the direction of the external magnetic field[12] (i.e. rotation about qubit's z axis), so by combining together the two kinds of rotations any transformation of the qubit state becomes achievable. In has been demonstrated in the experiment [62] that applying a narrowband laser pulse tuned to singlet (or triplet) state results in the effective two-qubit interaction due to coherent driving the system to an excited state, which adds a phase ϕ to that component of a two-qubit state: $|S\rangle \xrightarrow{\text{control pulse}} \mathrm{e}^{i\phi}|S\rangle$ (or $|T_0\rangle \xrightarrow{\text{control pulse}} \mathrm{e}^{i\phi}|T_0\rangle$). The electron spin state can also be measured with the help of optical pumping. In a single QD the frequency of optical pumping should be tuned to the state $|\downarrow\rangle$: when the electron is in the state $|\downarrow\rangle$, the QD system can be driven to the trion state to transit subsequently from the trion state to the state[13] $|\uparrow\rangle$ emitting a photon, which will be registered by a single-photon counter with a proper optical filter [87]; whereas in a DQD the probe laser should be tuned to the triplet transition, and similar scheme of utilization of a Λ-system is used, which reveals the electron spin state in the measured differential optical transmission of the device [62].

Self-assembled QDs have a disadvantage: the shape of the confining potential of the self-assembled QD is mainly determined by its geometry and chemical com-

[11] Mutual orientation of the optical axis and the direction of the external magnetic field is called Voigt geometry when they are perpendicular and Faraday geometry when parallel.

[12] In the experiment [87], a quite strong magnetic field $B_{\text{ext}} = 7\,\text{T}$ was used.

[13] Transitions from the trion state back to the state $|\downarrow\rangle$ are allowed as well, but there is obvious difficulty to count photons created in such transitions while photons of pumping laser are of the same energy, so that part of transitions from the trion state is not taken into account.

position. As one cannot have full control over the growth process, not all grown QDs have the desired properties. Moreover, the properties of self-assembled QDs are harder to adjust by external electric field, in contrast to electrically defined QDs, which are easier to tune the shapes of their confining potentials and to change them dynamically when needed.

1.3 Decoherence of Quantum Dot Spin Qubits

Before the discussion of the decoherence of QD spin qubits, it is instructive to recall the definitions of the key parameters used for description of the decay of qubit's states, namely, time constants T_1, T_2, and T_2^*. These parameters have first been introduced in a phenomenological model (Bloch equations) for description of dynamics of magnetic moments of nuclei [88]. Bloch equations are applicable to a qubit as well and provide an effective description of the dynamics of the state of a qubit that dissipatively interacts with its memoryless environment:

$$\frac{\mathrm{d}\boldsymbol{r}(t)}{\mathrm{d}t} = \mathfrak{g}\boldsymbol{r}(t) \times \boldsymbol{B} - \frac{r_1(t)}{T_2}\boldsymbol{i} - \frac{r_2(t)}{T_2}\boldsymbol{j} - \frac{r_3(t) - r_3^{\mathrm{equil}}}{T_1}\boldsymbol{k},$$

where a Cartesian coordinate system with a standard basis $\{\boldsymbol{i}, \boldsymbol{j}, \boldsymbol{k}\}$ set by the direction of a constant external magnetic field $\boldsymbol{B}$ is used in which z direction is along the field $\boldsymbol{B}$, so $\boldsymbol{B} \equiv (0, 0, B_z) \equiv (0, 0, B_3)$, $\mathfrak{g}$ is the gyromagnetic ratio, and r_3^{equil} is a state of equilibrium between the qubit and its environment in the constant external magnetic field $\boldsymbol{B}$. The two limiting cases should be noted: qubit at zero temperature, leading to $r_3^{\mathrm{equil}} = -1$ (the ground state of the qubit, i.e. $|\psi_{\mathrm{q}}\rangle = |{\downarrow}\rangle$); and qubit at infinite temperature (in practice at temperature for which $k_B T$ is much larger than the energy splitting of the qubit, $\mathfrak{g}B_z$), leading to $r_3^{\mathrm{equil}} = 0$ (completely mixed state of the qubit, i.e. $\hat{\rho}_{\mathrm{q}} = \frac{1}{2}\mathbb{1}$). The Bloch equations for a qubit are derived starting from the generalized master equation $\frac{\mathrm{d}}{\mathrm{d}t}\hat{\rho}(t) = -i\mathcal{L}\big(\hat{\rho}(t)\big)$ with $\mathcal{L} \equiv [\hat{H}(t), \hat{\rho}(t)]$, which describes evolution of the density operator $\hat{\rho}(t)$ of the system consisting of a qubit interacting with its environment (the Hamiltonian of the system contains Hamiltonians of the qubit, its environment and their interaction: $\hat{H}(t) = \hat{H}_{\mathrm{q}}(t) \otimes \mathbb{1}_{\mathrm{E}} + \mathbb{1}_{\mathrm{q}} \otimes \hat{H}_{\mathrm{E}}(t) + \hat{H}_{\mathrm{int}}(t)$) by making use of Born's approximation (when coupling between the qubit and its environment is weak) in tandem with Markov's approximation (when temporal correlations of qubit's environment are vanishing on time scales much shorter than the time scales on which the qubit dynamics happens, so qubit's evolution depends solely on the present state of its environment), so one can rewrite the master equation in form of so-called Redfield equation (i.e. the Born-Markov master equation written in the eigenstate basis of $\hat{H}_{\mathrm{q}}$), which contains the Redfield tensor [89, 90, 91]. Redfield equation can be next transformed into the set of equations for expectation values of qubit's components, and when magnetic field is strong enough, the secular approximation of the Redfield tensor R is justified, which results in $R \approx \mathrm{diag}\left(\frac{1}{T_2}, \frac{1}{T_2}, \frac{1}{T_1}\right)$. The solutions of the

Bloch equations indicate the exponential decay of a qubit state with time:

$$r_1(t) = \Big(r_1(0)\cos(\mathfrak{g}B_3 t) + r_2(0)\sin(\mathfrak{g}B_3 t)\Big)\exp\left(-\frac{t}{T_2}\right),$$
$$r_2(t) = \Big(-r_1(0)\sin(\mathfrak{g}B_3 t) + r_2(0)\cos(\mathfrak{g}B_3 t)\Big)\exp\left(-\frac{t}{T_2}\right),$$
$$r_3(t) = r_3^{\text{equil}} + \Big(r_3(0) - r_3^{\text{equil}}\Big)\exp\left(-\frac{t}{T_1}\right).$$

It is clear that the qubit's coherence decays exponentially as well, $\rho_{12} = \rho_{12}^* = \frac{1}{2}(r_1 + ir_2) \propto \exp\left(-\frac{t}{T_2}\right) \xrightarrow{t\to\infty} 0$.

Change of populations occurs on a time scale which is described by the longitudinal relaxation time constant T_1, whereas coherence decay is characterized by the transversal relaxation time constant T_2. The parameter T_1 is also called a decay time, since it indicates a time scale on which qubit's excited state will be gone, while the parameter T_2 is also called a dephasing time, as it specifies a time scale on which a superposition of qubit's basis states turns into a statistical mixture of them. When a qubit's observable is derived from an ensemble measurement[14] of a number of qubits, which are in a spatially inhomogeneous magnetic field, the transversal relaxation is described by the effective time constant T_2^* (instead of T_2), which accounts for the ensemble averaging. The normal distribution of external magnetic field over the ensemble, which is the most common case, leads to the Gaussian decay of qubit's coherence $\propto \exp\left(-\left(\frac{t}{T_2^*}\right)^2\right)$.

One can catch the relation between T_1 and T_2 using the simplest example of a qubit interacting dissipatively with its environment at zero temperature expressed in terms of the quantum master equation [92, 93, 2]: $\frac{\mathrm{d}}{\mathrm{d}t}\hat{\rho}_{\mathrm{q}}(t) = \mathcal{L}\big(\hat{\rho}_{\mathrm{q}}(t)\big)$, where $\mathcal{L}\big(\hat{\rho}_{\mathrm{q}}(t)\big) = -i[\hat{H}_{\mathrm{q}}, \hat{\rho}_{\mathrm{q}}(t)] + \sum_j \gamma_j \left(\hat{A}_j\hat{\rho}_{\mathrm{q}}(t)\hat{A}_j^\dagger - \frac{1}{2}\hat{A}_j^\dagger\hat{A}_j\hat{\rho}_{\mathrm{q}}(t) - \frac{1}{2}\hat{\rho}_{\mathrm{q}}(t)\hat{A}_j^\dagger\hat{A}_j\right)$ with the Hamiltonian $\hat{H}_{\mathrm{q}} = \frac{1}{2}g\mu_{\mathrm{B}}B_3\hat{\sigma}_3$ and a single operator $\hat{A} = \frac{1}{2}(\hat{\sigma}_1 - i\hat{\sigma}_2)$ describing the relaxation with a rate γ from the excited state to the ground state. The time evolutions of the density operator elements are given by the following expressions:

$$\rho_{11}(t) = \rho_{11}(0)\exp(-\gamma t),$$
$$\rho_{22}(t) = 1 - \rho_{11}(t) = 1 - \rho_{11}(0)\exp(-\gamma t),$$
$$\rho_{12}(t) = \rho_{21}^*(t) = \rho_{12}(0)\exp\left(-\frac{i}{2}g\mu_{\mathrm{B}}B_3 t\right)\exp\left(-\frac{1}{2}\gamma t\right),$$

from which one can see that $T_1 = \frac{1}{\gamma}$ is twice shorter than $T_2 = \frac{2}{\gamma}$. In fact, this is the fundamental upper bound for the dephasing time T_2, which cannot be grater than $2T_1$.

In a semiconductor QD, electron spin interacts with external magnetic field, with electric field through spin–orbit interaction, with other spins in its surroundings, and with electrons from the 2DEG through virtual exchange processes. The latter processes can be safely neglected, as they strongly depend on the tunnel coupling with the exterior of a QD [94, 47], which in typical operation of electron spin qubits is

[14] Ensemble can be spatial, when qubits are placed in different positions in space and are measured together at once, or temporal, when it is obtained by repeating the same manipulations on the same qubit.

low enough. The external magnetic field is precisely controlled by experimentalists, so it does not lead to an unintentional dephasing of electron spin qubits. Thus, we are left to look closely at the impact of spin–orbit interaction and interaction with nuclear spins on a state of electron spin in a QD.

1.3.1 Decoherence due to spin-orbit interaction

In a crystal possessing the bulk inversion asymmetry (e.g. GaAs, which has the zinc-blende structure), the Dresselhaus contribution to the spin–orbit interaction takes place [95, 96, 47] (although a crystal is electrically neutral, lack of spatial inversion symmetry of local charges leads to emergence a momentum-dependent effective magnetic field for an electron inside such a crystal [97], and results in a nonzero net contribution to spin–orbit interaction). Moreover, an asymmetric confining potential causes another kind of spin–orbit interaction due to the structural inversion asymmetry, called the Rashba contribution [98, 99]. In gated lateral QDs, the origin of that contribution is the asymmetry of the confining potential of 2DEG at the interface of AlGaAs and GaAs [70] causing a mixing of states of electrons from different bands (conduction and valence ones) that produces an effect, which can be interpreted as an effective electric field acting on a confined electron [100, 47]. Ultimately, for an electron from 2DEG which is formed in the plane perpendicular to (001) crystallographic direction (z direction) of a zinc-blende crystal the reduced Dresselhaus Hamiltonian reads as [95, 47]

$$\hat{H}_{\mathrm{D}}^{\mathrm{2D},(001)} = \beta(-\hat{p}_x \otimes \hat{\sigma}_x + \hat{p}_y \otimes \hat{\sigma}_y),$$

where $\hat{p}_x$, $\hat{p}_y$ are the components of the electron's momentum operator, and β is the parameter of the Dresselhaus contribution, which depends on the material properties and on the degree of electron confinement in z direction, $\langle \hat{p}_z^2 \rangle$, while the Rashba Hamiltonian when the confining electric field is along z direction reads as [47]

$$\hat{H}_{\mathrm{R}} = \alpha(-\hat{p}_y \otimes \hat{\sigma}_x + \hat{p}_x \otimes \hat{\sigma}_y),$$

where α is the parameter of Rashba contribution, which also depends on the material as well as on the confining potential.

Although the spin–orbit Hamiltonian, $\hat{H}_{\mathrm{SO}} = \hat{H}_{\mathrm{D}}^{\mathrm{2D},(001)} + \hat{H}_{\mathrm{R}}$, does not directly couple different electron spin states of the same orbital [47],

$$\langle nl\bar{\sigma}|\hat{H}_{\mathrm{SO}}|nl\sigma\rangle \propto \langle nl|\hat{p}_{x,y}|nl\rangle\langle\bar{\sigma}|\hat{\sigma}_{x,y}|\sigma\rangle = 0$$

(where $|nl\sigma\rangle$ is an electron state obtained in the 2D harmonic oscillator approximation [81] having the radial quantum number $n = 0, 1, 2, ...$, the angular momentum quantum number $l = 0, \pm 1, ...$, and the spin quantum number σ, $|\uparrow\rangle$ or $|\downarrow\rangle$, while $\bar{\sigma}$ denotes the opposite of σ), because $\langle \hat{p}_i \rangle = 0$ for a confined electron, this Hamiltonian mixes electron states of both different spatial and spin parts. In the case when the unperturbed Zeeman energy $|E_{\mathrm{Z}}|$ is much less than differences between energies of subsequent orbitals ΔE_{orb} (which is true for typical experiments), the eigenstates of an electron in a gated lateral QD can be approximated in first order perturbation theory as [47]

$$|nl\sigma\rangle^{(1)} = |nl\sigma\rangle + \sum_{(n',\,l')\neq(n,\,l)} \frac{\langle n'l'\bar{\sigma}|\hat{H}_{\mathrm{SO}}|nl\sigma\rangle}{E_{nl} - E_{n'l'} + E_{\mathrm{Z}}\langle\sigma|\hat{\sigma}_3|\sigma\rangle}|n'l'\bar{\sigma}\rangle. \tag{1.7}$$

One can see from the above formula that actual electron states, despite a heuristic argument that electron state (or wave function) can be decomposed into separate spatial and spin parts because of energetic inaccessibility of higher orbitals, are in fact the mixtures of different orbitals and spin states. Nevertheless, the two lowest perturbed states differ only by the spin quantum number, $|00\downarrow\rangle^{(1)}$ and $|00\uparrow\rangle^{(1)}$, so after the renormalization of the Zeeman energy, $E_{\mathrm{Z}}^{(1)} = E_{\uparrow}^{(1)} - E_{\downarrow}^{(1)}$, one can refer to these states as spin up and down states of an electron confined in a QD. Complex structure of the electron states (Eq. (1.7)) enables an indirect mechanism of influence of electric field on an electron spin state, leading to electron spin relaxation due to fluctuations of electric field. The electric field inside a QD can fluctuate due to a number of reasons, such as fluctuations of gate potentials, charge fluctuations in the nanostructure, electric noise in the device, etc. Besides this, the phonon bath can produce noticeable fluctuations of local electric field: deformation potential phonons cause a spatial modulation of the band gap as they inhomogeneously deform the crystal lattice, while in a polar crystal (e.g. GaAs) homogeneous strains caused by piezoelectric phonons create an additional contribution to the local electric field due to piezoelectric effect. As it turned out in experiment, the decohering impact of electric-field fluctuations created due to phonons prevails that of other sources, so the interaction of a confined electron with phonons should be accounted first. From the general consideration, it is obvious that to relax an electron from a higher spin state to a lower one its energy should be transferred to a phonon simultaneously with accomplishment of a spin flip, which is also performed by a phonon through the coupling between different electron states perturbed by the electron–phonon interaction. The efficiency of spin-flip process due to phonons depends on several factors, such as the degree of coupling between orbital and spin parts of electron states, the strength of electric field produced by a single phonon, the strength of phonon coupling to particular electron orbitals, the phonon occupation, the strength of external magnetic field. Detailed analysis of mentioned factors predicts that the relaxation rate due to phonons at low temperatures $T \ll \frac{|E_{\mathrm{Z}}|}{k_{\mathrm{B}}}$ scales with magnetic field as follows [101, 47]: $\frac{1}{T_1} \propto \frac{|E_{\mathrm{Z}}|^5}{\Delta E_{\mathrm{orb}}^4} \propto B^5$, which was confirmed in experiment [74, 47], while at high temperature $T \gg \frac{|E_{\mathrm{Z}}|}{k_{\mathrm{B}}}$ the relation is [47]: $\frac{1}{T_1} \propto \frac{E_{\mathrm{Z}}^4 k_{\mathrm{B}} T}{\Delta E_{\mathrm{orb}}^4}$. It has been theoretically shown that spin–orbit interaction induces no pure dephasing of electron spin [102], so the upper bound on the dephasing time would be its actual limit for spin of an electron confined in a QD, $T_2 = 2T_1$, if interaction with phonons was the only reason of electron spin dephasing. It has been experimentally established that in gated lateral AlGaAs/GaAs QDs at moderate magnetic fields ($B \approx 1$ T) the spin relaxation time T_1 can be as long as 1 s [74].

1.3.2 Hyperfine interaction

Magnetic interaction of an electron confined in a QD with atoms' nuclei can be described analogously as the same interaction of an electron in an atom [90, 103]. The description of the magnetic interaction in an atom, which is referred below after Ref. [104], is based on a few assumptions consistent with actual atom's physics. Firstly, magnetic properties of a nucleus are described by its magnetic dipole $\boldsymbol{\mu}_{\mathrm{J}} = \gamma_{\mathrm{J}} \hbar \boldsymbol{J}$, where $\gamma_{\mathrm{J}} = g_{\mathrm{J}} \frac{e_{\mathrm{p}}}{2m_{\mathrm{p}}}$ is the nucleus' gyromagnetic ratio (g_{J} is the g-factor of the nucleus, e_{p} is the proton's charge, m_{p} is the proton's mass), and $\boldsymbol{J}$ is the nu-

cleus' spin[15]. Secondly, the interaction of the nucleus (nuclear magnetic dipole) with the electron being in some stationary orbital is derived ab initio from the basic nonrelativistic Hamiltonian of Pauli equation using a perturbation method. In particular, the electron's momentum $\boldsymbol{p}$ is replaced by the generalized momentum $\boldsymbol{p}+e\boldsymbol{A}$, where $\boldsymbol{A}$ is the magnetic vector potential possessing the following properties: $\operatorname{div}\boldsymbol{A} = \boldsymbol{\nabla}\cdot\boldsymbol{A} = 0$, and $\operatorname{curl}\boldsymbol{A} = \boldsymbol{\nabla}\times\boldsymbol{A} = \boldsymbol{B}$, where $\boldsymbol{B}$ is the magnetic field. At a point in space specified by the position vector (or radius vector)[16] $\boldsymbol{r}$, a magnetic dipole[17] creates a magnetic field, which according to the classical electromagnetic theory quantitatively is[18] $\boldsymbol{A} = \frac{\mu_0}{4\pi}\cdot\frac{\boldsymbol{\mu}\times\boldsymbol{r}}{r^3} = \frac{\mu_0}{4\pi}\cdot\operatorname{curl}\left(\frac{\boldsymbol{\mu}}{r}\right) = \frac{\mu_0}{4\pi}\cdot\boldsymbol{\nabla}\times\left(\frac{\boldsymbol{\mu}}{r}\right) = \frac{\mu_0}{4\pi}\cdot\boldsymbol{\nabla}\left(\frac{1}{r}\right)\times\boldsymbol{\mu}$, where μ_0 is the permeability of vacuum, $\boldsymbol{r}$ is the position vector and r is its length. The Hamiltonian of an electron in a magnetic field reads

$$H = \frac{1}{2m_\mathrm{e}}\left(\boldsymbol{p}+e\boldsymbol{A}\right)^2 + g_\mathrm{e}\mu_\mathrm{B}\boldsymbol{S}\cdot\operatorname{curl}\boldsymbol{A} \tag{1.8}$$

$$= \frac{\boldsymbol{p}^2}{2m_\mathrm{e}} + \frac{e}{2m_\mathrm{e}}\left(\boldsymbol{p}\cdot\boldsymbol{A}+\boldsymbol{A}\cdot\boldsymbol{p}\right) + g_\mathrm{e}\mu_\mathrm{B}\boldsymbol{S}\cdot\operatorname{curl}\boldsymbol{A} + \frac{1}{2m_\mathrm{e}}\left(e\boldsymbol{A}\right)^2$$

$$= H_0 + H_1 + H_2, \tag{1.9}$$

where m_e is the electron's mass, e is the electron's charge, g_e is the electron's g-factor, $\mu_\mathrm{B} = \frac{e\hbar}{2m_\mathrm{e}}$ is the Bohr magneton, and $\boldsymbol{S}$ is the electron spin quantum operator, consisting of Pauli matrices. The introduced symbols H_i contain the terms of ith order in magnetic vector potential $\boldsymbol{A}$ from Eq. (1.8). Equation (1.9) can be considered as an expansion of H in a series with expansion parameter $\boldsymbol{A}$. In the present case, it is expected that the first order correction will provide good enough description of the interaction between nucleus (magnetic dipole) and electron residing in atom's orbital, so we neglect H_2, which does not contain the electron spin operator, and concentrate on the Hamiltonian H_1:

$$H_1 = \frac{e}{2m_\mathrm{e}}\big(\boldsymbol{p}\cdot\boldsymbol{A}(\boldsymbol{\mu},r)+\boldsymbol{A}(\boldsymbol{\mu},r)\cdot\boldsymbol{p}\big) + g_\mathrm{e}\mu_\mathrm{B}\boldsymbol{S}\cdot\operatorname{curl}\boldsymbol{A}(\boldsymbol{\mu},r). \tag{1.10}$$

The Hamiltonian H_1 (Eq. (1.10)) can be written in the following form using abovementioned relation between the magnetic vector potential $\boldsymbol{A}$ and the magnetic dipole $\boldsymbol{\mu}$, which creates it:

$$H_1 = \frac{\mu_0}{4\pi}g_\mathrm{e}\mu_\mathrm{B}\left(\frac{\boldsymbol{l}\cdot\boldsymbol{\mu}}{r^3} + \boldsymbol{S}\cdot\operatorname{curl}\operatorname{curl}\left(\frac{\boldsymbol{\mu}}{r}\right)\right), \tag{1.11}$$

where $\boldsymbol{l}$ related to the quantized orbital momentum of the electron $\boldsymbol{L} = \hbar\boldsymbol{l} = \boldsymbol{r}\times\boldsymbol{p}$ is used. The second term of the Hamiltonian H_1 (Eq. (1.10)), which is spin-dependent,

[15] In the consideration spins are treated unequally: the spin of a nucleus is treated as a source of a magnetic field, whereas the spin of an electron is described quantum-mechanically after W. Pauli [105].

[16] The origin of the coordinate system is set at the location of the nucleus (magnetic dipole).

[17] From now on the label J in the subscript of μ and γ is dropped.

[18] Here, the physical quantities appearing in the equations are expressed in units of the International System of Units (SI).

can be written as

$$H_1^{\mathrm{s}} = \frac{\mu_0}{4\pi} g_{\mathrm{e}} \mu_{\mathrm{B}} \boldsymbol{S} \cdot \left[\boldsymbol{\nabla} \times \left(\boldsymbol{\nabla} \times \left(\frac{\boldsymbol{\mu}}{r} \right) \right) \right] \tag{1.12}$$

$$= \frac{\mu_0}{4\pi} g_{\mathrm{e}} \mu_{\mathrm{B}} \left[(\boldsymbol{S} \cdot \boldsymbol{\nabla})(\boldsymbol{\mu} \cdot \boldsymbol{\nabla}) - (\boldsymbol{S} \cdot \boldsymbol{\mu}) \boldsymbol{\nabla}^2 \right] \frac{1}{r} \tag{1.13}$$

$$= \frac{\mu_0}{4\pi} g_{\mathrm{e}} \mu_{\mathrm{B}} \left[(\boldsymbol{S} \cdot \boldsymbol{\nabla})(\boldsymbol{\mu} \cdot \boldsymbol{\nabla}) - \frac{1}{3} (\boldsymbol{S} \cdot \boldsymbol{\mu}) \boldsymbol{\nabla}^2 \right] \left(\frac{1}{r} \right) - \frac{\mu_0}{4\pi} \frac{2}{3} g_{\mathrm{e}} \mu_{\mathrm{B}} (\boldsymbol{S} \cdot \boldsymbol{\mu}) \boldsymbol{\nabla}^2 \left(\frac{1}{r} \right), \tag{1.14}$$

where identity $\boldsymbol{\nabla} \times (\boldsymbol{\nabla} \times \boldsymbol{v}) \equiv \boldsymbol{\nabla}(\boldsymbol{\nabla} \cdot \boldsymbol{v}) - \boldsymbol{\nabla}^2 \boldsymbol{v}$, which is true for any arbitrary vector $\boldsymbol{v}$, was used to transform Eq. (1.12) into Eq. (1.13). The term of Eq. (1.13) $-(\boldsymbol{S} \cdot \boldsymbol{\mu}) \boldsymbol{\nabla}^2 \left(\frac{1}{r} \right) \equiv (-\frac{1}{3} - \frac{2}{3}) (\boldsymbol{S} \cdot \boldsymbol{\mu}) \boldsymbol{\nabla}^2 \left(\frac{1}{r} \right)$ has been split in two terms in Eq. (1.14). Such a representation of that term is justified [104, 103], as it helps in calculation of matrix elements of that Hamiltonian, $\langle \psi_{\mathrm{e}} | H_1^{\mathrm{s}} | \psi_{\mathrm{e}} \rangle$, where ψ_{e} is the electron's wave function, which is performed as follows. Integration over the electron's spatial coordinates can be performed in spherical coordinates with two steps in r: from 0 to some infinitesimal number $\eta > 0$ and from η to infinity. Integral over r from η to infinity is obviously calculable, whereas integration over r in the vicinity of 0, i.e. from 0 to η, requires an inspection due to singularity of the Hamiltonian (cf. Eq. (1.14)) at $r = 0$. Integration of the first term of Eq. (1.14), denoted by $H_1^{\mathrm{s}'}$, results in a finite value because $H_1^{\mathrm{s}'}$ possesses a property that under a rotation of the coordinate system it transforms as a spherical harmonic of the second order, which leads to a simplification of the calculation of matrix element $\langle \psi_{\mathrm{e}} | H_1^{\mathrm{s}'} | \psi_{\mathrm{e}} \rangle$: electron's wave function can be expressed as a series of spherical harmonics, $\psi_{\mathrm{e}} = \sum_l a_l \psi_l$, and the only nonzero terms of the matrix element are those satisfying the relation $l + l' \geqslant 2$, $\langle \psi_l | H_1^{\mathrm{s}'} | \psi_{l'} \rangle \neq 0$. Noting that $\psi_l \propto r^l$ for $r \to 0$, one can conclude $|\langle \psi_l | H_1^{\mathrm{s}'} | \psi_{l'} \rangle| = |\int_{r=0}^{\eta} \int_{\theta=0}^{\pi} \int_{\phi=0}^{2\pi} \psi_l^* H_1^{\mathrm{s}'} \psi_{l'} r^2 \mathrm{d}r \mathrm{d}\Omega| < \infty$, where $\mathrm{d}\Omega = \sin\theta \mathrm{d}\theta \mathrm{d}\phi$, as the integrand $\psi_l^* H_1^{\mathrm{s}'} \psi_{l'} r^2 \propto r^{l-3+l'+2}$ with $l + l' \geqslant 2$ (so at $r = 0$ the integrand has a well-defined value of 0).

The second term of Eq. (1.14) can be expressed as follows

$$-\frac{\mu_0}{4\pi} \frac{2}{3} g_{\mathrm{e}} \mu_{\mathrm{B}} (\boldsymbol{S} \cdot \boldsymbol{\mu}) \boldsymbol{\nabla}^2 \left(\frac{1}{r} \right) = \frac{2}{3} \mu_0 g_{\mathrm{e}} \mu_{\mathrm{B}} (\boldsymbol{S} \cdot \boldsymbol{\mu}) \delta(\boldsymbol{r})$$

due to the relation[19] [107]: $\boldsymbol{\nabla}^2 \left(\frac{1}{r} \right) = -4\pi\delta(\boldsymbol{r})$. After integration over the electron's spatial coordinates, this term becomes $\frac{2}{3} \mu_0 g_{\mathrm{e}} \mu_{\mathrm{B}} (\boldsymbol{S} \cdot \boldsymbol{\mu}) |\psi_{\mathrm{e}}(0)|^2$, which has nonzero (but finite) value only for s electron ($l = 0$).

After evaluating of nabla's actions, $(\boldsymbol{S} \cdot \boldsymbol{\nabla})(\boldsymbol{\mu} \cdot \boldsymbol{\nabla}) \left(\frac{1}{r} \right) = 3 \frac{(\boldsymbol{S} \cdot \boldsymbol{r})(\boldsymbol{\mu} \cdot \boldsymbol{r})}{r^5} - \frac{\boldsymbol{S} \cdot \boldsymbol{\mu}}{r^3}$, the Hamiltonian H_1 of the magnetic interaction of the electron with the nucleus can be written as

$$H_1 = \frac{\mu_0}{4\pi} g_{\mathrm{e}} \mu_{\mathrm{B}} g_{\mathrm{J}} \mu_{\mathrm{J}} \boldsymbol{J} \cdot \left(\frac{\boldsymbol{l}}{r^3} - \frac{\boldsymbol{S}}{r^3} + 3 \frac{\boldsymbol{r} (\boldsymbol{S} \cdot \boldsymbol{r})}{r^5} + \frac{8\pi}{3} \boldsymbol{S} \delta(\boldsymbol{r}) \right). \tag{1.15}$$

It is worth noting that the first term in the above Hamiltonian is absent for s electron (when $l = 0$), whereas the last term produces no effect for an electron residing in any higher orbital (when $l > 0$).

[19] This relation can also be obtained from the Poisson's equation for a point electric charge q: $\boldsymbol{\nabla}^2 \varphi = -\frac{\rho}{\varepsilon_0}$, where $\varphi = \frac{1}{4\pi\varepsilon_0} \cdot \frac{q}{r}$ is the electric potential of a point electric charge, ε_0 is the permittivity of vacuum, $\rho = q\delta(\boldsymbol{r})$ is the electric charge density; $\boldsymbol{\nabla}^2 \left(\frac{1}{4\pi\varepsilon_0} \cdot \frac{q}{r} \right) = -\frac{q}{\varepsilon_0} \delta(\boldsymbol{r}) \Rightarrow \boldsymbol{\nabla}^2 \left(\frac{1}{r} \right) = -4\pi\delta(\boldsymbol{r})$ [106].

Hamiltonian of the same form as Eq. (1.15) is used to describe hyperfine interaction between nuclear spins and spins of charge carriers in a semiconductor nanostructure [90, 103], in particular, in a QD. Since a confined electron in a QD belongs to conduction band, the Bloch part of its wave function, which describes properties of the electron on the scale of a lattice cell, is of s type (i.e. maximized at the position of the nucleus), the main contribution comes from the last δ-term of the Hamiltonian. In contrast to electron in an atom, electron in a III-V semiconductor QD interacts with many nuclear spins, as it wave function extends over an area $\sim (10\text{ nm})^3$ of a crystal built of atoms having spinful nuclei, which effectively couples the electron to about a million of nuclear spins.

The orbital part of the wave function of the conduction band electron in a bulk semiconductor (e.g. GaAs) can be written as [108] $\psi_{\rm e}(\boldsymbol{r}) = \varphi_{\rm c}(\boldsymbol{r})u(\boldsymbol{r})$, where $\varphi_{\rm c}(\boldsymbol{r})$ is the conduction band electron envelope function with the normalization $\int_V {\rm d}\boldsymbol{r}|\varphi_{\rm c}(\boldsymbol{r})|^2 = v_0$, where v_0 is the primitive cell volume ($v_0 = \frac{a_0^3}{4}$ for a zinc-blende crystal lattice with lattice constant a_0), and $u(\boldsymbol{r})$ is the Bloch amplitude with the normalization[20] $\int_{v_0} |u(\boldsymbol{r})|^2 {\rm d}\boldsymbol{r} = 1$. Therefore, the effective Hamiltonian of hyperfine interaction (Fermi contact interaction) for an electron in a QD can be written as

$$\hat{H}'_{\rm hf} = \mathfrak{A}\sum_{i=1}^{N} \hat{\mathbf{S}}\cdot\hat{\mathbf{J}}_i\delta(\boldsymbol{r}_i) \tag{1.16}$$

or

$$\hat{H}_{\rm hf} = \int\limits_V \psi^*_{\rm e}(\boldsymbol{r})\hat{H}'_{\rm hf}\psi_{\rm e}(\boldsymbol{r}){\rm d}\boldsymbol{r} = \mathcal{A}\sum_{i=1}^{N}\hat{\mathbf{S}}\cdot\hat{\mathbf{J}}_i|\varphi_{\rm c}(\boldsymbol{r}_i)|^2 = \sum_{i=1}^{N} A_i\hat{\mathbf{S}}\cdot\hat{\mathbf{J}}_i, \tag{1.17}$$

where $\mathfrak{A} = \frac{2}{3}\mu_0 g_{\rm e}\mu_{\rm B} g_{\rm J}\mu_{\rm J}$ is the factor of hyperfine interaction, $\mathcal{A} = \mathfrak{A}|u(\boldsymbol{r}_{\rm J})|^2 = \frac{2}{3}\mu_0 g_{\rm e}\mu_{\rm B} g_{\rm J}\mu_{\rm J}|u(\boldsymbol{r}_{\rm J})|^2$, is the energy constant of hyperfine interaction, where Bloch amplitude is evaluated at $\boldsymbol{r}_{\rm J}$, which is the position of the nucleus, $\varphi_{\rm c}(\boldsymbol{r}_i)$ is the conduction band electron's envelope function at position $\boldsymbol{r}_i$ of the ith nucleus, $A_i = \mathcal{A}|\varphi_{\rm c}(\boldsymbol{r}_i)|^2 = \mathfrak{A}|u(\boldsymbol{r}_{\rm J})|^2|\varphi_{\rm c}(\boldsymbol{r}_i)|^2 = \frac{2}{3}\mu_0 g_{\rm e}\mu_{\rm B} g_{\rm J}\mu_{\rm J}|\psi_{\rm e}(\boldsymbol{r})|^2$ is the coupling between electron spin and the ith nuclear spin, and N is the number of nuclear spins interacting with the electron. The Hamiltonian in Eq. (1.17) is the result of integration of the Hamiltonian in Eq. (1.16) over the electron's orbital $\psi_{\rm e}(\boldsymbol{r})$. The values of energy constant of hyperfine interaction $\mathcal{A}$ in GaAs and similar semiconductors are of the order of tens of μeV [109]. The Hamiltonian of Eq. (1.17) can be written as

$$\sum_i A_i\hat{\mathbf{S}}\cdot\hat{\mathbf{J}}_i \equiv \sum_{k=x,y,z}\hat{h}^k\hat{S}^k \equiv \hat{h}^z\hat{S}^z + \hat{V}_{\rm ff}, \tag{1.18}$$

where the three components of the Overhauser field operator are introduced, $\hat{h}^k \coloneqq \sum_i A_i\hat{J}^k_i$, and in the third expression the term related to the longitudinal component

[20] With such a choice of normalizations the envelope function $\varphi_{\rm c}(\boldsymbol{r})$ is dimensionless, so $|\varphi_{\rm c}(\boldsymbol{r})|^2$ is dimensionless as well, whereas the Bloch amplitude $u(\boldsymbol{r})$ is of dimension $[\text{length}]^{-\frac{3}{2}}$, hence, $|u(\boldsymbol{r})|^2$ is of dimension $[\text{length}]^{-3}$. The wave function $\psi_{\rm e}(\boldsymbol{r})$ is then of dimension $[\text{length}]^{-\frac{3}{2}}$ and is normalized to 1: $\int_V |\psi_{\rm e}(\boldsymbol{r})|^2{\rm d}\boldsymbol{r} = \int_V |\varphi_{\rm c}(\boldsymbol{r})|^2|u(\boldsymbol{r})|^2{\rm d}\boldsymbol{r} = \sum_{i=1}^N \int_{v_0^{(i)}} |\varphi_{\rm c}(\boldsymbol{r})|^2|u(\boldsymbol{r})|^2{\rm d}\boldsymbol{r} = \sum_{i=1}^N |\varphi_{\rm c}(\boldsymbol{r}_i)|^2 \int_{v_0^{(i)}} |u(\boldsymbol{r})|^2{\rm d}\boldsymbol{r} = \sum_{i=1}^N |\varphi_{\rm c}(\boldsymbol{r}_i)|^2 = \sum_{i=1}^N |\varphi_{\rm c}(\boldsymbol{r}_i)|^2 \frac{1}{v_0}\int_{v_0^{(i)}}{\rm d}\boldsymbol{r} = \frac{1}{v_0}\int_V |\varphi_{\rm c}(\boldsymbol{r})|^2{\rm d}\boldsymbol{r} = \frac{1}{v_0}v_0 = 1$, where $N = \frac{V}{v_0}$ is the number of primitive cells in a sample of the volume V, $v_0^{(i)}$ is a volume of the ith primitive cell (all $v_0^{(i)}$ are equal to each other), and $\boldsymbol{r}_i$ is a position inside the ith primitive cell.

$\hat{h}^z$ is separated from the transverse components appearing in the electron-nucleus flip-flop operator $\hat{V}_{\rm ff} \coloneqq \frac{1}{2}\sum_i A_i(\hat{S}^+\hat{J}_i^- + \hat{S}^-\hat{J}_i^+)$, in which the spin ladder operators have been used, $\hat{S}^\pm \coloneqq \hat{S}^x \pm i\hat{S}^y$, $\hat{J}_i^\pm \coloneqq \hat{J}_i^x i \pm \hat{J}_i^y$.

1.3.3 Decoherence due to hyperfine interaction with nuclear spins

Since couplings A_i are derived from the spatial part of the wave function of an electron which is quite strongly localized in a QD, they are inevitably different, beginning from the strongest ones in the center of a QD through weaker ones at the edges of a QD to negligibly small ones far out of a QD, so in the interaction of the electron spin with the nuclear spins is a many-body problem (so-called central spin problem), which can have a complex dynamics (with no hope for an exact analytical description in general case).

Complex dynamics of the system is partially due to the fact the time scale of internal dynamics of nuclear spin bath is much longer than the time scale of dynamics of the electron spin. Besides this, in a low or moderate external magnetic field, the coupling between the electron spins and nuclear spin bath cannot be considered as a weak one: the time scale of electron spin dynamics due to hyperfine interaction turns out to be much shorter than the time scales of internal dynamics of the nuclear bath (see the discussion below). Therefore, neither Born's, no Markov's approximation is applicable to the problem of an electron confined in a QD that interacts with a nuclear spin bath, and as a consequence the Bloch equations cannot be used as a description of time evolution of the state of electron spin in a QD.

The nuclear spin bath Hamiltonian reads

$$\hat{H}_{\rm bath} = \sum_k \omega_k \hat{J}_k^z + \hat{H}_{\rm dip}, \tag{1.19}$$

where ω_k is the Zeeman splitting of the k-th nuclear spin, it is equal to one of ω_α values depending on the kind of nucleus present at site k, $\hat{H}_{\rm dip}$ is the internuclear dipolar interaction, which for typically used in experiment magnetic fields can be approximated by its secular form:

$$\hat{H}_{\rm dip} = \sum_{i\neq j} b_{ij}(\hat{J}_i^+\hat{J}_j^- - 2\hat{J}_i^z\hat{J}_j^z), \tag{1.20}$$

where b_{kl} are the dipolar couplings between the nuclei. For the present consideration, their exact form does not matter, since they decay quickly with the distance between nuclei k and l, r_{kl} (as $b_{kl} \propto 1/r_{kl}^3$), and they are small compared to all the other interaction energies in the Hamiltonian (i.e. hyperfine couplings). In experiments on spin qubits, $b_{kl} \ll k_B T$, and also $\omega_\alpha \ll k_B T$, unless very high magnetic fields ($B > 10$ T) are used. Hence, the equilibrium density operator of the nuclear spin bath is

$$\hat{\rho}_J^{\rm eq} = \frac{1}{Z}\mathbb{1}, \tag{1.21}$$

where Z is the statistical sum of a bath, in the case of homonuclear spin bath consisting of N nuclei of spin J it is given by $Z = (2J+1)^N$.

The next key fact about the system of the electron spin coupled to the nuclear bath is that the electron's Zeeman energy in the presence of external magnetic

field B is much higher than that of a nuclear spin, so processes of simultaneous correlated spin flips of electron and nucleus described by $\hat{V}_{\rm ff}$, possible at zero or low B, become suppressed with increasing external magnetic field. Presence of electron in the system brings an alternative channel of intrabath interaction: virtual processes of electron spin flip provide an effective coupling between two different nuclear spins, i.e. electron and the first nuclear spin perform spin flip due to $\hat{V}_{\rm ff}$, and right after that the electron performs similar spin flip in a pair with another nucleus, so finally electron spin is in its initial state, and spin flips are performed between two nuclear spins [110, 111]. The energy scale of these interactions is also much less than k_BT [111], so the form of the equilibrium nuclear density matrix given above still holds.

The weakness of the internuclear interactions manifests also in the slowness of the intrinsic dynamics of nuclear spin bath. In the presence of magnetic field B larger than the magnetic resonance linewidth of nuclei [104] (caused by $\hat{J}_i^z\hat{J}_j^z$ interactions in Eq. (1.20)), i.e. for $B\gg 0.1$ mT, the dynamics of the longitudinal component of the Overhauser field, h^z, is much slower than that of the transverse components $h^\perp = h^x$, h^y. This is because the latter are proportional to the sum over $J_k^{x,y}$ nuclear spin components, which are undergoing precession with their Larmor frequencies, and also the total $h^{x,y}$ fields decorrelate on time scale given by the inverse of the above-mentioned linewidth. The resulting characteristic time scale of randomization of $h^\perp$ fields is $\tau_\perp \sim 100$ μs. On the other hand, the dynamics of h^z is governed by diffusion of nuclear polarization (via nearest-neighbor flip-flops caused by $\hat{J}_k^+\hat{J}_l^-$ interactions in Eq. (1.20)) out of the volume of the QD [112]. The flip-flops can occur only between nuclear spins that are approximately resonant (i.e. they have the same splittings due to the external B field and local fields generated by $\sum b_{ij}\hat{J}_i^z\hat{J}_j^z$ terms) The characteristic time scale $\tau_{||}\sim L^2/D$, where L is the size of the QD and D is the nuclear diffusion constant. It is known from experiments that $\tau_{||}\sim 10$ s in GaAs QDs [113, 114], which is in qualitative agreement with theory [112].

The relation between $\tau_{||}$ and $\tau_\perp$ and the time scale on which the electron spin qubit coherence is measured has a nontrivial effect in the nuclear state $\hat{\rho}_J$ that should be used in calculation of electron spin dynamics. To reconstruct the electron spin density operator, experimentalists gather data from multiple runs of manipulation cycle containing initialization, manipulations and measurements of qubits' states, therefore, the whole process of data acquisition takes time T_M. The seemingly obvious choice of the thermal equilibrium state in the form of Eq. (1.21) is correct if $T_M > \tau_{||}$ (while $\tau_{||}\gg\tau_\perp$ according to the above considerations). This is because when this condition is fulfilled, the dynamics of the nuclear bath is ergodic, i.e. the time average over many instances of the same electron spin interacting with the same bath can be replaced by an ensemble average, with the ensemble described by $\hat{\rho}_J^{\rm eq}$. On the other hand, employing the single-shot readout methods [115], one can measure the electron spin precession dynamics on a time scale fulfilling $T_M \ll \tau_{||}$ (i.e. a few tens or a hundred milliseconds), but still much longer than $\tau_\perp$. Such a fast measurement of spin precession detects the full spin splitting, $E_{\rm Z}+h^z$, and hence, allows to gather some information about the state of nuclear spin bath. The correct nuclear bath state to be used in calculations aimed at reproducing the results of such experiments is called the *narrowed state* [116, 117, 118, 119]. Such states of QD nuclear spin baths were obtained in experiment [120, 121, 122]. In the theoretical description of narrowed state free induction decay (NFID) experiments [116, 110, 123, 111, 124, 125, 126], such states are described by a nuclear spin bath

density operator that has a fixed value of h^z or by a distribution of h^z values which is narrowed compared to that of the completely mixed nuclear bath state.

To build an intuition about the nuclear spin bath, one can attempt to treat the Overhauser field classically. The distribution of the classical magnetic field $\mathbf{h}$ corresponding to the above density operator from Eq. (1.21) is given by [127]

$$P(\mathbf{h}) = \frac{1}{(2\pi)^{3/2}\sigma_{\mathrm{h}}^3} \exp\left(-\frac{h^2}{2\sigma_{\mathrm{h}}^2}\right), \tag{1.22}$$

where

$$\sigma_{\mathrm{h}}^2 = \sum_k A_k^2 \langle (\hat{J}_k^z)^2 \rangle_{\mathrm{eq}} = \frac{1}{3}\sum_\alpha J_\alpha (J_\alpha + 1) n_\alpha \frac{\mathcal{A}_\alpha^2}{N}, \tag{1.23}$$

where the angle brackets $\langle ... \rangle_{\mathrm{eq}}$ denote averaging with respect to the nuclear density operator from Eq. (1.21), and J_α is the magnitude of spin of α species. The standard deviation σ_{h} gives the value of the typical Overhauser field, which affects the electron spin interacting with a high-temperature nuclear bath.

Let us put all the above together. Experimentally established coherence time T_2^* (measured in the free induction decay experiment) of an electron spin in GaAs QD is about 10 ns [128, 129, 130, 131]. This is much shorter time compared to all the above-mentioned characteristic time scales of nuclear spin bath dynamics.This allows one to apply the so-called quasistatic bath approximation (QSBA) as a starting point [132, 133, 108]: the state of the bath is treated as static on the time scale of electron spin dynamics, sum of nuclear spin operator $\sum_{i=1}^N A_i \hat{\mathbf{J}}$ is substituted by a classical vector of Overhauser field $\mathbf{h}$, and nuclear Zeeman energies are neglected, dipolar interaction between the nuclear spins are ignored as well, i.e. the Hamiltonian becomes $\hat{H}_{\mathrm{QD}}^{\mathrm{QSBA}} = \hat{H}_{\mathrm{Z}} + \mathbf{h}\cdot\hat{\mathbf{S}}$. The dynamics of electron spin is next averaged over various states of the nuclear spin bath, which account for changes of its state in different runs of the experiment. In the limit of large number nuclear spins, unpolarized nuclear spin bath (consisting, in general, of nuclear spins of a few species) can be described by Overhauser field, the magnitude of which is distributed according to normal distribution around zero mean, given above in Eq. (1.22).

In a high external magnetic field, $\mathbf{B} \gg \sigma_{\mathrm{h}}$, when z axis is explicitly set by the external field, the Hamiltonian can be further simplified: $H_{\mathrm{QD}}^{\mathrm{QSBA}} \approx \hat{H}_{\mathrm{Z}} + h^z \hat{S}^z$, which allows to derive analytically the evolution of electron spin, e.g. the mean value of x-component of electron spin initially oriented in x direction is given by $\langle S_x(t)\rangle = \frac{1}{2}\int_V P(\mathbf{h})\cos((E_{\mathrm{Z}} + h^z t)\mathrm{d}\mathbf{h} = \frac{1}{2}\cos(E_{\mathrm{Z}}t)\exp\left(-\left(\frac{t}{T_2^*}\right)^2\right)$, where $T_2^* = \frac{\sqrt{2}}{\sigma_{\mathrm{h}}} \propto \frac{\sqrt{N}}{\mathcal{A}}$. It has been is argued that results obtained within quasistatic bath approximation are trustworthy up to time $t \ll \frac{N}{\mathcal{A}}$ [108].

In the above-introduced case of narrowed state FID (NFID), one can attempt a similar calculation, but with an anisotropic normal distribution $P_{\mathrm{n}}(\mathbf{h})$ in which the rms of the h^z component (the slowest component of the Overhauser field), $\sigma_{\mathbf{h}}^{z,n}$ is smaller than its "natural" value σ_{h} from Eq. (1.23). The rms of distributions of h^x and h^y components should remain the same as before. An example of such calculation for NFID is given in Ref. [108].

It should be noted that QSBA gives unphysical predictions in low magnetic fields, $\mathbf{B} \ll \sigma_{\mathrm{h}}$, at which decay of averaged electron spin component is incomplete, but taking into account a realistic shape of electron's wave function the predictions of

QSBA can be improved [134, 135, 136, 137, 138]. It has been shown that predictions of QSBA at low fields are correct on a time scale of T_2^* at least [134].

A few approaches other than the nuclear state narrowing (which is quite non-trivial as one has to perform single-shot measurements and quickly analyze the data obtained from them) have been proposed in order to extend electron spin coherence time, such as dynamical decoupling of electron spin from nuclear spin bath or making use of fully polarized nuclear spin bath. The former proposition [139, 140] is based on the manipulation technique developed in the nuclear magnetic resonance (NMR), which suggests to perform sequences of electron spin rotations (e.g. Carr–Purcell–Meiboom–Gill sequence, consisting of so-called π pulses, i.e. rotations of spin state by π around chosen axis separated by periods of free evolution), which remove the quasistatic influence of interaction of electron spin with nuclear spin bath and as a result help to preserve the electron spin coherence for a longer time. The simplest example of an experiment using π pulses is the spin-echo experiment, in which a single pulse is applied at the mid-point of evolution. The latter method is based on the observation that when nuclear spin bath is fully polarized the nuclear flip-flop process are effectively blocked, since total spin must be conserved, hence, nuclear spin bath is practically locked in that state and dephases the electron spin much slower (flip-flop processes between electron spin and nuclear spins are still possible, but they produce a small effect) [141, 142, 143].

Finally, it should be noted that when spin echo or dynamical decoupling is applied to the electron spin, one has to consider the dynamics of the nuclear bath that occurs on the time scale of electron spin coherence dynamics, which in such a case is lengthened compared to T_2^*, i.e. take into account the nuclear evolution caused by dipolar interactions, or electron-mediated interactions. This dynamics causes that the energy splitting of the electron spin undergoes the so-called spectral diffusion due to fluctuations of the Overhauser field. For example, the dipolar interaction enables a flip-flop process between any pair of nuclear spins (term $b_{ij}\hat{J}_i^+\hat{J}_j^-$), which changes the expectation value of the Overhauser operator $\hat{h}^z$ by the amount $A_i - A_j$, since the hyperfine couplings are different, $A_i \neq A_j$, and consequently the electron spin precesses in a slowly varying magnetic field (see Ref. [144] and references therein on many-body methods used to calculate the echo signal in this regime). From experimentalist's point of view, it looks as electron precession frequency fluctuates in a constant external magnetic field. For the echo procedure applied to electron spins dephased by nuclear baths at rather low magnetic field, which is considered in Chapter 2, this dynamics can be neglected, since the direct flip-flop processes between an electron spin and nuclear spins are a much stronger source of electron's decoherence.

1.3.4 $1/f$ noise affecting spin qubits

Qubits which are controlled electrically through voltages applied to the gates of semiconductor devices (e.g. S-T_0 qubits) are susceptible to the fluctuations of electric field in the vicinity of the QDs. Fluctuations of electric field (so-called charge noise) may be produced by several kinds of sources (impurities, fluctuating background charges, etc.). In many devices, a noise whose spectral density (i.e. the Fourier transform of noise autocorrelation function) is of $1/f$-type has been detected [145]. Although there is still lack of the complete clarity about the origin of the $1/f$ noise,

and moreover there are numerous evidences that in different physical systems, its physical origins are essentially unlike, the $1/f$ noise is viewed as an effect of a large number of two-level fluctuators which switching times are distributed over a broad range [145]. For example, when there are two-level fluctuating background charges in the system, which are switching randomly between two states (i.e. they are sources of so-called Random Telegraph Noise, the autocorrelation function has an exponential form), one can assume that their spectral density functions are given by Lorenzians, and their total power spectrum is therefore [146]

$$S_{\mathrm{BC}}(\omega) = \frac{1}{2\hbar^2} \sum_i v_i^2 \frac{2\gamma_i}{\omega^2 + \gamma_i},$$

where v_i is the coupling strength of the fluctuator i, γ_i is the switching rate of the fluctuator i. Due to the fact that the number of fluctuators in the system is rather large, one should average the power spectrum $S_{\mathrm{BC}}(\omega)$ over the distribution $P(v, \gamma)$ of coupling strengths v_i and switching rates γ_i,

$$S_{\mathrm{BC}}(\omega) \propto \iint \mathrm{d}v \mathrm{d}\gamma P(v, \gamma) v^2 \frac{2\gamma}{\omega^2 + \gamma^2}.$$

Models of microscopic origins of $1/f$ noise have been presented in Refs. [147, 148], where several different fluctuator distribution functions have been studied. In the simplest case, when the switching rates have a log-uniform distribution, i.e. assuming $\gamma \propto \exp\left(-\frac{l}{l_0}\right)$, where l can be interpreted as a tunneling distance for charges and supposing that the distribution of l is uniform in a range much wider than the characteristic distance l_0, one obtains [146]

$$S_{\mathrm{BC}}(\omega) \propto \overline{v^2} \int_{-\infty}^{\infty} \mathrm{d}l \frac{2\gamma(l)}{\omega^2 + \gamma^2(l)} \propto \overline{v^2} \int_{-\infty}^{\infty} \frac{\mathrm{d}\gamma}{\gamma} \frac{2\gamma}{\omega^2 + \gamma^2} \propto \frac{\overline{v^2}}{|\omega|},$$

where $\overline{v^2}$ is the averaged squared coupling. Similar power spectrum can be obtained as a low-frequency limit of interaction with an oscillator bath [146]. It has also been shown that $1/f$ noise can be produced by a set of coherent two-level systems [146].

Stochastic (or random) process corresponding to the $1/f$ noise is generally non-Gaussian [149], i.e. its higher-order moments cannot be reduced exclusively to its second-order moment (pair correlations) [145]. However, when coupling to noise is weak, the Gaussian approximation gives satisfactory predictions (even for a single two-state fluctuator the Gaussian approximation is acceptable in the weak coupling limit [150]). It is worth to note that a stochastic process of $1/f$ type cannot be considered as a Markovian random process [145]. The next issue about $1/f$ noise remaining unsettled is the resolution if $1/f$ noise is a stationary stochastic process, i.e. if the translated in time process produces the same effect on the physical system it is affecting [145]. Of particular interest is establishing the lower frequency limit of $1/f$ noise and estimation of noise power in the vicinity of zero frequency, which need to be done for each device individually as they vary in different physical systems and are even sample-dependent. It turns out that deviations of the functional form of the spectral density are frequent, i.e. it is not exactly $1/f$ but rather $1/f^\beta$ with $0 < \beta \lesssim 2$ (e.g. $\beta \approx 0.7$ has been reported for S-T_0 qubits [151]).

1.4 Motivation and Aims

Due to the fact that quantum features manifest to the greatest extent in entangled quantum states, such states are the most interesting ones for theoretical considerations [6] as well as for experimental verifications of quantum supremacy [152] and practical applications in quantum technologies. Therefore, a resolution of the issue of creation of entangled states as well as keeping the system in an entangled state as long as needed for execution of the intended operations is a basic requirement.

To be specific, the aims of this dissertation were:

- to investigate theoretically the decay of entanglement in the system of two electron spin QD qubits taking into account various experimentally accessible states of nuclear spin baths (see Chapter 2);
- to explore the way of inhibition of entanglement decay of two electron spins interacting with the nuclear spin bath by execution of an experimentally undemanding manipulation sequence with electrons subsystem only (see Chapter 3);
- to estimate the amount of entanglement that can be obtained in the system of two singlet-triplet qubits taking into account fluctuations of key system parameters observed in the experiment (see Chapter 4).

Chapter 2

Dynamics of Decay of Two Electron-Spin Qubits Entanglement

This chapter is devoted to the analysis of the dynamics of entanglement of two electron spins in two QDs, in which each electron is interacting with its nuclear spin environment. The decay of entanglement due to the hyperfine interaction with the nuclei is calculated for uncoupled dots, in which electron spins are initialized in either Bell or Werner state. The study is focused on the regime of magnetic fields in which the bath-induced electron spin flips play a role, for example, their presence leads to the appearance of entanglement sudden death at finite time for two qubits initialized in a Bell state. In such fields, the intrabath dipolar interactions and spatial inhomogeneity of hyperfine couplings are irrelevant on the time scale of coherence (and entanglement) decay, so the presented results are obtained using the uniform-coupling approximation to the exact hyperfine Hamiltonian. The entanglement decay is analyzed in the case of free evolution of the qubits as well as in two-qubit spin echo procedure. The experimentally relevant bath states are considered: the thermal state, narrowed states (characterized by diminished uncertainty of one of the components of the Overhauser field) of two uncorrelated baths, and a correlated narrowed state with a well-defined value of the z component of the Overhauser field interdot gradient. In most cases the concurrence is used to quantify the amount of entanglement in a mixed state of the two electron spins, but it is also shown that their entanglement dynamics can be reconstructed from entanglement witnesses that are easy to measure or from the fidelity of quantum teleportation in which a partially disentangled state is used as an entanglement resource. The results contained in this chapter have been presented at a few conferences (see List of Conference Presentations on p. 129) and have been published in Phys. Rev. B [1].

2.1 Introduction

In this chapter, section 2.2 contains the description of a system of electron spin in a semiconductor QD. The relevant for experiment states of the nuclear spin bath are discussed there. The general formalism used for description of the time evolution of two-qubit state is presented in section 2.3. Next, the approximation schemes used for the calculation of two-qubit state evolution are introduced is section 2.4. Finally, the results are shown in section 2.5, where decay of entanglement of two electron spins interacting either with two uncorrelated nuclear spin baths in the state of thermal equilibrium (Sec. 2.5.2), in narrowed states (Sec. 2.5.3.1), or with baths in the correlated narrowed state (Sec. 2.5.3.2). The qubits are supposed to be initially in a state from the family of Bell-diagonal states (one of the pure Bell states or the Werner state). To quantify the amount of entanglement of possibly mixed two-qubit state, the concurrence [21] is used. The signal of two-qubit spin echo procedure is shown in section 2.5.4. After noting the general features of the disentanglement of considered electron spin qubits, another ways for entanglement quantification are discussed in section 2.5.5, such as expectation values of easy-to-implement (for certain spin qubit systems) entanglement witnesses [153, 154] and the fidelity of a teleported qubit state obtained after execution of the quantum teleportation protocol [155, 156, 157, 158], in which a partially disentangled two-qubit state is used as a resource. The conclusions of the study presented in this chapter are given is section 2.6.

2.2 The Physical System and the Model

2.2.1 Hamiltonian of electron spin in a QD

The system consisting of an electron spin interacting with nuclear spins in a QD via contact hyperfine coupling (see Sec. 1.3.2) is described by the Hamiltonian

$$\hat{H} = \Omega \hat{S}^z + \sum_k A_k \hat{\mathbf{S}} \cdot \hat{\mathbf{J}}_k, \tag{2.1}$$

where $\hat{\mathbf{S}}$ and $\hat{\mathbf{J}}_k$ are the spin operators of the electron and the kth nuclear spin, respectively, A_k is the hyperfine coupling to the spin of the kth nucleus, and $\Omega = g\mu_\mathrm{B}B$ is the electron spin Zeeman splitting, where g is the effective g-factor of the electron in a QD, μ_B is the Bohr's magneton, B is the external magnetic field. In III-V semiconductor QDs, atoms' nuclei possess spin (nuclei of various isotopes of Ga, As, In, etc., are spinful). The hyperfine coupling for the nuclear spin of species α located at site k is $A_k = \mathcal{A}_\alpha |F(\mathbf{r}_k)|^2$, where α labels different species of nuclear spins, $F(\mathbf{r}_k)$ is the envelope function of the localized electron state, and $\mathcal{A}_\alpha$ is the energy of hyperfine interaction characteristic for a nuclear spin of kind α of an atom in a

crystal lattice. As mentioned in Sec. 1.3.2 (Eq. (1.18)), the interaction term of the Hamiltonian Eq. (2.1) can be written using the Overhauser field operator $\hat{\mathbf{h}}$.

The effective number N of nuclear spins coupled to the electron spin is defined as

$$\frac{1}{N} \coloneqq \sum_u |F(\mathbf{r}_u)|^4, \tag{2.2}$$

where u labels the primitive unit cells, and the envelope function $F(\mathbf{r})$ is approximately constant inside each cell.

2.2.2 Possible states of the nuclear spin bath

As discussed in Sec. 1.3.3, depending on details of procedure of measurement of coherence of an electron spin interacting with the nuclei, various states of nuclei should be used. In some cases, using the completely mixed state of the nuclear system is justified. In others, one should employ the narrowed states, with diminished variance of the z component of the Overhauser operator, and possibly with finite polarization along this axis. To describe these bath states, one can use the basis of product J^z eigenstates of individual nuclear spins, where $\hat{J}^z_k |\chi\rangle = J^z_k |\chi\rangle$, and $|\chi(h^z)\rangle$ is defined as a state corresponding to a given eigenvalue h^z of $\hat{h}^z$. Due to the finiteness of the nuclear spin environment, values h^z are from a discrete spectrum. The number $M(h^z)$ of states $|\chi(h^z)\rangle$, which realize the same value h^z, is finite, so these states $|\chi_i(h^z)\rangle$ can be labelled with index $i \in [1, M(h^z)]$. Using such a notation, one can express a partially narrowed state of the nuclear spin bath as

$$\hat{\rho}_J(\bar{h}^z, \sigma_\mathrm{n}) = \frac{1}{Z} \sum_{h^z} p_{\bar{h}^z,\sigma_\mathrm{n}}(h^z) \sum_i |\chi_i(h^z)\rangle \langle\chi_i(h^z)| \,, \tag{2.3}$$

where $p_{\bar{h}^z,\sigma_\mathrm{n}}(h^z)$ is a function which reaches its maximum at $\bar{h}^z$ with the width $\sigma_\mathrm{n} \ll \sigma_\mathrm{h}$, and the normalization constant $Z = \sum_{h^z} M(h^z) p_{\bar{h}^z,\sigma_\mathrm{n}}(h^z)$. In the limit of perfect narrowing, one has $p_{\bar{h}^z,\sigma_\mathrm{n}}(h^z) = \delta_{\bar{h}^z,h^z}$. The density operator $\hat{\rho}_J(\bar{h}^z, \sigma_\mathrm{n})$ lacks the off-diagonal elements, which is a consequence of the realistic assumption that a series of measurements is performed on a time scale much larger than $\tau_\perp$, and the final result is derived from the that series as an average (see discussion in Sec. 1.3.3).

Provided no manipulations intended for the creation of correlations between the nuclear baths in the two QDs are performed, the states of the nuclear spin baths of QDs are uncorrelated, and the total initial density operator of the environment is

$$\hat{\rho}_J = \hat{\rho}^A_J(0) \otimes \hat{\rho}^B_J(0), \tag{2.4}$$

where the density matrices corresponding to nuclear bath states in QDs A and B are given either by Eq. (1.21) or Eq. (2.3). In a DQD system, it is also possible to create a narrowed distribution of Overhauser field difference between the QDs [159, 120, 122], which corresponds to a correlated state of the two nuclear spin environments with a diminished uncertainty of $\Delta h^z \coloneqq h^z_A - h^z_B$:

$$\begin{aligned}\hat{\rho}_{AB}(\Delta h^z, \sigma_\mathrm{n}) = \frac{1}{Z_{AB}} \sum_{h^z_A, h^z_B} & p_{AB}\big(h^z_A - h^z_B, \sigma_\mathrm{n}\big) \\ & \times \sum_{i,j} \big(|\chi_i(h^z_A)\rangle \langle\chi_i(h^z_A)|\big) \otimes \big(|\chi_j(h^z_B)\rangle \langle\chi_j(h^z_B)|\big),\end{aligned} \tag{2.5}$$

where p_{AB} has its maximum at Δh^z, while its width is $\sigma_{\mathrm{n}} \ll \sigma_{\mathrm{h}}$, and

$$Z_{AB} = \sum_{h_A^z, h_B^z} M_A(h_A^z) M_B(h_B^z) p_{AB}\big(h_A^z - h_B^z\big). \tag{2.6}$$

The above density operator can also be written as

$$\hat{\rho}_{AB}(\Delta h^z, \sigma_{\mathrm{n}}) = \sum_{h_A^z, h_B^z} w(h_A^z; \Delta h^z) \hat{\rho}_A(h_A^z) \otimes \hat{\rho}_B(h_B^z), \tag{2.7}$$

where $\hat{\rho}_Q(h_Q^z)$ is the perfectly narrowed state for dot Q and the weights

$$w(h_A^z; \Delta h^z) = p_{AB}\big(h_A^z - h_B^z, \sigma_{\mathrm{n}}\big) M_A(h_A^z) M_B(h_B^z = h_A^z + \Delta h^z)/Z_{AB}. \tag{2.8}$$

2.3 Time Evolution of Two-Qubit State in QDs

It is important to note explicitly the two assumptions which are used in the model. The first assumption is that at initial time there are no any correlations between the qubits' subsystem and their environments, i.e. $\hat{\rho}(0) \otimes \hat{\rho}_J(0)$, where $\hat{\rho}(0)$ is the initial density operator of the qubits. The second one is that there is no interaction between the two electron spins (because of the strong localization of electrons in their QDs, the overlap of the electrons' wave functions is negligible), and the two nuclear environments are well-separated (each nuclear spin interacts with only one electron). Hence, the total Hamiltonian of the system is of the separable form $\hat{H}_A \otimes \mathbb{1}_B + \mathbb{1}_A \otimes \hat{H}_B$, where $\hat{H}_Q$ is the Hamiltonian which describes the electron and the nuclear spins of dot Q.

2.3.1 Free evolution

The Hamiltonian $\hat{H}_Q$, containing of the hyperfine interaction part, Eq. (2.1), and the intrabath dipolar interaction part, Eq. (1.20), has a property that the z projection of the total spin is conserved in the system

$$\left[\hat{H}_Q, \hat{S}_Q^z + \sum_{k \in Q} \hat{J}_k^z\right] = 0. \tag{2.9}$$

To make use of that property, it is convenient to introduce projection operators $\Pi_{m,\sigma} \coloneqq \hat{P}_{\sigma\sigma} \hat{\Pi}_m$, where operator $\hat{P}_{\sigma\sigma'} \coloneqq |\sigma\rangle \langle\sigma'|$, with $\sigma = \sigma'$ here, projects on the subspace of a given electron spin $S^z = \sigma/2$ (where $\sigma = \pm 1$), and operator $\hat{\Pi}_m$ projects on the subspace of the fixed total z component of the nuclear spin, i.e. the subspace of states $|\chi(m)\rangle$, which fulfills the condition $\sum(k) \hat{J}_k^z |\chi(m)\rangle = m |\chi_m\rangle$. These projection operators allow to express an important feature of the evolution operator $\hat{U}_Q(t) \coloneqq \exp(-i\hat{H}_Q t)$ (note that it is assumed here $\hbar = 1$):

$$\Pi_{m,\sigma} \hat{U}_Q(t) \Pi_{m',\sigma'} = \delta_{m+\sigma/2, m'+\sigma'/2} \Pi_{m,\sigma} \hat{U}_Q(t) \Pi_{m',\sigma'}. \tag{2.10}$$

This means that during evolution the states in the $\{\sigma, m\}$ and $\{\bar{\sigma}, m + \sigma/2\}$ (where $\bar{\sigma} \equiv -\sigma$) subspaces are coupled, so the whole state space of the system consists of a number of decoupled subspaces which differ in their z projection of the total spin.

In general, the evolution of the two-qubit density operator can be expressed as

$$\rho_{\alpha\beta,\gamma\delta}(t) = \sum_{\alpha'\beta'\gamma'\delta'} R^{\alpha'\beta'\gamma'\delta'}_{\alpha\beta\gamma\delta}(t)\,\rho_{\alpha'\beta',\gamma'\delta'}(0), \tag{2.11}$$

where

$$R^{\alpha'\beta'\gamma'\delta'}_{\alpha\beta\gamma\delta}(t) \coloneqq \mathrm{Tr}_J\Big(\langle\alpha\beta|\,\hat{U}(t)\,|\alpha'\beta'\rangle\,\hat{\rho}_J(0)\,\langle\gamma'\delta'|\,\hat{U}^\dagger(t)\,|\gamma\delta\rangle\Big), \tag{2.12}$$

and $\hat{U}(t) \coloneqq \hat{U}_A(t)\otimes\hat{U}_B(t)$ is the evolution operator of the system ($|\alpha\beta\rangle \coloneqq |\alpha\rangle_A \otimes |\beta\rangle_B$ is the two-qubit state).

To begin with, a general density operator of the environment $\hat{\rho}_J$, Eq. (2.5), will be considered. For now, in that density operator $p(h^z_A - h^z_B)$ will be replaced by $p(h^z_A, h^z_B)$, to embrace a broad class of possibly correlated environmental states. Using Eq. (2.10) and taking into account the fact that $\Pi_{m_Q}\hat{\rho}_J\Pi_{n_Q} \propto \delta_{m_Q n_Q}$, one obtains

$$\begin{aligned} R^{\alpha'\beta'\gamma'\delta'}_{\alpha\beta\gamma\delta}(t) \equiv\ & \delta_{\alpha\alpha'}\delta_{\beta\beta'}\delta_{\gamma\gamma'}\delta_{\delta\delta'}R^{\alpha\beta\gamma\delta}_{\alpha\beta\gamma\delta}(t) \\ & + \delta_{\alpha\alpha'}\delta_{\bar{\beta}\beta'}\delta_{\gamma\gamma'}\delta_{\beta\delta}\delta_{\bar{\beta}\delta'}R^{\alpha\bar{\beta}\gamma\bar{\beta}}_{\alpha\beta\gamma\beta}(t) \\ & + \delta_{\bar{\alpha}\alpha'}\delta_{\beta\beta'}\delta_{\delta\delta'}\delta_{\alpha\gamma}\delta_{\bar{\alpha}\gamma'}R^{\bar{\alpha}\beta\bar{\alpha}\delta}_{\alpha\beta\alpha\delta}(t) \\ & + \delta_{\alpha\gamma}\delta_{\bar{\alpha}\alpha'}\delta_{\bar{\alpha}\gamma'}\delta_{\beta\delta}\delta_{\bar{\beta}\beta'}\delta_{\bar{\beta}\delta'}R^{\bar{\alpha}\bar{\beta}\bar{\alpha}\bar{\beta}}_{\alpha\beta\alpha\beta}(t). \end{aligned} \tag{2.13}$$

In that expression, one can explicitly see how the constraints on the nuclear density operator discussed in Sec. 2.2.2 and the conservation law Eq. (2.9) reduce the number of evolution functions R, which are necessary for the description of two-qubit dynamics.

If the baths are uncorrelated, then one can express the functions R defined in Eq. (2.12) using the functions which are derived for description of the evolution of a single qubit interacting with its bath [160, 161]. The evolution of qubit Q can be described as:

$$\begin{aligned} \rho^Q_{\sigma\sigma'}(t) &= \mathrm{Tr}_J\Big(\langle\sigma|\,\hat{U}_Q(t)\hat{\rho}^Q(0)\otimes\hat{\rho}^Q_J(0)\hat{U}^\dagger_Q(t)\,|\sigma'\rangle\Big), \\ &= \sum_{\xi,\xi'}\mathrm{Tr}_J\Big(\langle\sigma|\,\hat{U}_Q(t)\,|\xi\rangle\,\hat{\rho}^Q_J(0)\,\langle\xi'|\,\hat{U}^\dagger_Q(t)\,|\sigma'\rangle\Big)\,\rho^Q_{\xi\xi'}(0), \\ &=: \sum_{\xi,\xi'} K^Q_{\sigma\xi,\xi'\sigma'}(t)\,\rho^Q_{\xi\xi'}(0), \end{aligned} \tag{2.14}$$

where $K^Q_{\sigma\xi,\xi'\sigma'}(t)$ encapsulates the influence of the environment on the evolution of the reduced density operator of qubit Q. It is worth to notice that the above representation [160, 161, 162] is closely related to the operator-sum (Kraus) representation of evolution of $\hat{\rho}^Q$. The use of functions R it is much more convenient when the number of relevant Kraus operators is large (as in the present case). The K functions, in turn, consist of two terms:

$$K_{\sigma\xi,\xi'\sigma'} \equiv \delta_{\sigma\xi}\delta_{\sigma'\xi'}K_a^{\sigma\sigma'} + \delta_{\sigma\sigma'}\delta_{\sigma\bar{\xi}}\delta_{\sigma\bar{\xi}'}K_b^{\sigma}, \tag{2.15}$$

with

$$K_a^{\sigma\sigma'} \coloneqq \sum_m \mathrm{Tr}\Big(\hat{P}_{\sigma'\sigma}\Pi_m\hat{U}\Pi_m\hat{P}_{\sigma\sigma'}\rho_J\Pi_m\hat{U}^\dagger\Big), \tag{2.16}$$

$$K_b^{\sigma} \coloneqq \sum_m \mathrm{Tr}\Big(\hat{P}_{\sigma\sigma}\Pi_m\hat{U}\Pi_{m+\sigma/2}\hat{P}_{\bar{\sigma}\bar{\sigma}}\rho_J\Pi_{m+\sigma/2}\hat{U}^\dagger\Big), \tag{2.17}$$

where for shortness of notation the time dependence of $K_{a/b}(t)$ and $\hat{U}(t)$ has not been explicitly written. In terms of the K functions, elements of the single electron density operator are described as

$$\rho^Q_{\sigma\sigma}(t) = K_a^{Q,\sigma\sigma}(t)\,\rho^Q_{\sigma\sigma}(0) + K_b^{Q,\sigma}(t)\,\rho^Q_{\bar{\sigma}\bar{\sigma}}(0), \tag{2.18}$$
$$\rho^Q_{\sigma\bar{\sigma}}(t) = K_a^{Q,\sigma\bar{\sigma}}(t)\,\rho^Q_{\sigma\bar{\sigma}}(0), \tag{2.19}$$

where one can see that the dynamics of coherences ($\rho_{+-} = \rho^*_{-+}$) is not affected by the dynamics of the populations (ρ_{++} and ρ_{--}). This fact has been noted for the first time in Ref. [116]. Moreover, from the conservation of the total population, $\rho_{++} + \rho_{--} \equiv 1$, one has the relation $K_b^{Q,\sigma}(t) = 1 - K_a^{Q,\bar{\sigma}\bar{\sigma}}(t)$.

Similarly, one can derive the expression for time evolution of the two-qubit reduced density operator in the case of uncorrelated nuclear baths:

$$\rho_{\sigma_A\sigma_B,\sigma'_A\sigma'_B}(t) = \sum_{\xi_A,\xi_B,\xi'_A,\xi'_B} \rho_{\xi_A\xi_B,\xi'_A\xi'_B}(0) K^A_{\sigma_A\xi_A,\xi'_A\sigma'_A}(t) K^B_{\sigma_B\xi_B,\xi'_B\sigma'_B}(t), \tag{2.20}$$

and using Eq. (2.15) one obtains the specific form of R function, in which the four terms on the RHS of Eq. (2.13) are given by $K_a^{A,\alpha\gamma}K_a^{B,\beta\delta}$, $K_a^{A,\alpha\gamma}K_b^{B,\delta}$, $K_b^{A,\alpha}K_a^{B,\beta\delta}$, and $K_b^{A,\alpha}K_b^{B,\beta}$, respectively.

Finally, by employing the above formulas, one obtains the diagonal elements of the two-qubit density operator,

$$\begin{aligned}\rho_{\sigma\xi,\sigma\xi}(t) = {} & K_a^{A,\sigma\sigma}K_a^{B,\xi\xi}\rho_{\sigma\xi,\sigma\xi}(0) + K_a^{A,\sigma\sigma}K_b^{B,\xi}\rho_{\sigma\bar{\xi},\sigma\bar{\xi}}(0) \\ & + K_b^{A,\sigma}K_a^{B,\xi\xi}\rho_{\bar{\sigma}\xi,\bar{\sigma}\xi}(0) + K_b^{A,\sigma}K_b^{B,\xi}\rho_{\bar{\sigma}\bar{\xi},\bar{\sigma}\bar{\xi}}(0),\end{aligned} \tag{2.21}$$

where for shortness of notation the time-dependence of $K(t)$ functions has not been explicitly written.

It is important to notice that off-diagonal elements corresponding to the coherences between the states differing by a single spin-flip depend on themselves and their hermitian-conjugated partners

$$\begin{aligned}\rho_{\sigma\xi,\sigma\bar{\xi}}(t) &= K_a^{A,\sigma\sigma}K_a^{B,\xi\bar{\xi}}\rho_{\sigma\xi,\sigma\bar{\xi}}(0) + K_b^{A,\sigma}K_a^{B,\xi\bar{\xi}}\rho_{\bar{\sigma}\xi,\bar{\sigma}\xi}(0), \\ \rho_{\sigma\xi,\bar{\sigma}\xi}(t) &= K_a^{A,\sigma\bar{\sigma}}K_a^{B,\xi\xi}\rho_{\sigma\xi,\bar{\sigma}\xi}(0) + K_a^{A,\sigma\bar{\sigma}}K_b^{B,\xi}\rho_{\sigma\bar{\xi},\bar{\sigma}\bar{\xi}}(0),\end{aligned} \tag{2.22}$$

and the coherences between the states differing by two spin flips depend on themselves only

$$\rho_{\sigma\xi,\bar{\sigma}\bar{\xi}}(t) = K_a^{A,\sigma\bar{\sigma}}K_a^{B,\xi\bar{\xi}}\rho_{\sigma\xi,\bar{\sigma}\bar{\xi}}(0)\ . \tag{2.23}$$

The electron spin structure of Eqs. (2.21)–(2.23) remains the same also in the general case described by Eqs. (2.11) and (2.13), in which the interbath correlations are allowed. In connection to that, it is worth to make a remark on the initial states of the qubits described by a density operator diagonal in the basis of Bell states, which will be analyzed in detail below. In the product basis $|\sigma_A\sigma_B\rangle$, this matrix has nonzero populations, and nonzero coherences between the states differing by two spin flips (nonzero values are only on the diagonal and the antidiagonal, i.e. it is of the X form), and from the equations of motion Eqs. (2.21)–(2.23) it is clear that initial X form is preserved at all times.

Below the two-qubit density operator is presented, where in its upper half the elements which mix with each other during the evolution are marked with different

colors: populations ρ_{11}, ρ_{22}, ρ_{33}, ρ_{44} (black) constitute the group whose elements depend on all elements of the group, coherences ρ_{12}, ρ_{34} (red) and ρ_{13}, ρ_{24} (green) constitute similar groups, whereas coherences ρ_{14} and ρ_{23} are independent, i.e. they depend only on their initial values. The structure of the coherences in the lower part is analogous to that of the upper one (due to that fact, they are presented in gray in order to not encumber the picture).

$$\hat{\rho}_{\text{free ev.}} = \begin{array}{c} \begin{matrix} |{+}{+}\rangle & |{+}{-}\rangle & |{-}{+}\rangle & |{-}{-}\rangle \end{matrix} \\ \begin{pmatrix} \rho_{11} & \rho_{12} & \rho_{13} & \rho_{14} \\ \rho_{21} & \rho_{22} & \rho_{23} & \rho_{24} \\ \rho_{31} & \rho_{32} & \rho_{33} & \rho_{34} \\ \rho_{41} & \rho_{42} & \rho_{43} & \rho_{44} \end{pmatrix} \end{array} \begin{matrix} \langle{+}{+}| \\ \langle{+}{-}| \\ \langle{-}{+}| \\ \langle{-}{-}| \end{matrix}$$

2.3.2 Spin echo

The spin echo protocol, which rephases qubits and removes inhomogeneous broadening, does not help much in the case of narrowed bath states, so in this subsection only the thermal state of uncorrelated baths will be considered.

In the protocol, a π rotation of qubit state (assumed to be a perfect rotation by π around the x axis, for concreteness) is performed to each qubit at time τ, and the qubits' coherence is measured at time 2τ. The corresponding evolution operator $\hat{U}_Q$ in Eq. (2.14) reads

$$\hat{U}_Q^{\text{SE}}(2\tau) = \mathrm{e}^{-i\hat{H}_Q\tau}(-i\hat{\sigma}_x)\mathrm{e}^{-i\hat{H}_Q\tau}. \tag{2.24}$$

After application of spin echo procedure it is expected that maximal revival of the coherence will be observed at time 2τ. Using these functions, which are derived using the above evolution operator, one can obtain the 2τ-dependence (i.e. the dependence on the total duration of the echo sequence) of the two-qubit reduced density operator.

To see the dependence of the echo signal as a function of the durations of the free evolution periods τ_1 and τ_2, one can rewrite the evolution operator as

$$\hat{U}_Q^{\text{SE}}(\tau_1,\tau_2) = \mathrm{e}^{-i\hat{H}_Q\tau_2}(-i\hat{\sigma}_x)\mathrm{e}^{-i\hat{H}_Q\tau_1}, \tag{2.25}$$

The recovery of the signal is expected for $\tau_1 \approx \tau_2$.

Therefore, one can obtain $K_{\sigma\xi,\xi'\sigma'}$ functions with either a single argument of 2τ (the total duration of the sequence with π rotation at instant τ) or two arguments τ_1 and τ_2. The structure of the functions is identical in both cases, under the natural assumption that $\tau_2 > 0$, but it is richer than the structure of $K(t)$ functions derived for the case of free evolution. Now the K functions are of the form

$$\begin{aligned} K_{\sigma\xi,\xi'\sigma'} \equiv{}& \delta_{\sigma\bar{\xi}}\delta_{\sigma'\bar{\xi}'}K_a^{\sigma\sigma'} + \delta_{\sigma\sigma'}\delta_{\sigma\bar{\xi}}\delta_{\sigma\bar{\xi}'}K_b^{\sigma} \\ &+ \delta_{\sigma\sigma'}\delta_{\sigma\xi}\delta_{\sigma\xi'}K_c^{\sigma} + \delta_{\sigma\bar{\sigma}'}\delta_{\sigma\xi}\delta_{\sigma\bar{\xi}'}K_d^{\sigma}, \end{aligned} \tag{2.26}$$

where

$$K_a^{\sigma\sigma'} := \sum_m \mathrm{Tr}(\hat{P}_{\sigma'\sigma}\hat{U}_2^{m,m}\hat{P}_{\sigma\bar{\sigma}}\hat{U}_1^{m,m}\hat{P}_{\bar{\sigma}\bar{\sigma}'}\hat{\rho}_J(\hat{U}_1^\dagger)^{m,m}\hat{P}_{\bar{\sigma}'\sigma'}(\hat{U}_2^\dagger)^{m,m}), \tag{2.27}$$

$$K_b^{\sigma} := \sum_m \mathrm{Tr}(\hat{P}_{\sigma\sigma}\hat{U}_2^{m,m+\sigma}\hat{P}_{\bar{\sigma}\sigma}\hat{U}_1^{m+\sigma,m+2\sigma}\hat{P}_{\bar{\sigma}\bar{\sigma}}\hat{\rho}_J(\hat{U}_1^\dagger)^{m+2\sigma,m+\sigma}\hat{P}_{\sigma\bar{\sigma}}(\hat{U}_2^\dagger)^{m+\sigma,m}), \tag{2.28}$$

$$\begin{aligned} K_c^{\sigma} :=& \sum_m \mathrm{Tr}(\hat{P}_{\sigma\sigma}\hat{U}_2^{m,m}\hat{P}_{\sigma\bar{\sigma}}\hat{U}_1^{m,m-\sigma}\hat{P}_{\sigma\sigma}\hat{\rho}_J(\hat{U}_1^\dagger)^{m-\sigma,m}\hat{P}_{\bar{\sigma}\sigma}(\hat{U}_2^\dagger)^{m,m}) \\ &+ \sum_m \mathrm{Tr}(\hat{P}_{\sigma\sigma}\hat{U}_2^{m,m+\sigma}\hat{P}_{\bar{\sigma}\sigma}\hat{U}_1^{m+\sigma,m+\sigma}\hat{P}_{\sigma\sigma}\hat{\rho}_J(\hat{U}_1^\dagger)^{m+\sigma,m+\sigma}\hat{P}_{\sigma\bar{\sigma}}(\hat{U}_2^\dagger)^{m+\sigma,m}), \end{aligned} \tag{2.29}$$

$$\begin{aligned} K_d^{\sigma} :=& \sum_m \mathrm{Tr}(\hat{P}_{\bar{\sigma}\sigma}\hat{U}_2^{m,m}\hat{P}_{\sigma\bar{\sigma}}\hat{U}_1^{m,m-\sigma}\hat{P}_{\sigma\bar{\sigma}}\hat{\rho}_J(\hat{U}_1^\dagger)^{m-\sigma,m-\sigma}\hat{P}_{\bar{\sigma}\sigma}(\hat{U}_2^\dagger)^{m-\sigma,m}) \\ &+ \sum_m \mathrm{Tr}(\hat{P}_{\bar{\sigma}\sigma}\hat{U}_2^{m,m+\sigma}\hat{P}_{\bar{\sigma}\sigma}\hat{U}_1^{m+\sigma,m+\sigma}\hat{P}_{\sigma\bar{\sigma}}\hat{\rho}_J(\hat{U}_1^\dagger)^{m+\sigma,m}\hat{P}_{\sigma\bar{\sigma}}(\hat{U}_2^\dagger)^{m,m}), \end{aligned} \tag{2.30}$$

where the U operators are defined as $\hat{U}_{1/2}^{n,m} := \hat{\Pi}_n\hat{U}(\tau_{1/2})\hat{\Pi}_m$ and $(\hat{U}_{1/2}^\dagger)^{n,m} := \hat{\Pi}_n\hat{U}^\dagger(\tau_{1/2})\hat{\Pi}_m$.

The structure of $\hat{\rho}(2\tau)$ is now more complicated compared to that of the free evolution case. Each diagonal element $\rho_{\sigma\xi,\sigma\xi}(2\tau)$ still depends only on the initial values of all diagonal elements,

$$\begin{aligned} \rho_{\sigma\xi,\sigma\xi}(2\tau) =& K_b^{A,\sigma}K_b^{B,\xi}\rho_{\sigma\xi,\sigma\xi}(0) \\ &+ \left(K_b^{A,\sigma}K_a^{B,\xi\xi} + K_b^{A,\sigma}K_d^{B,\xi}\right)\rho_{\sigma\bar{\xi},\sigma\bar{\xi}}(0) \\ &+ \left(K_a^{A,\sigma\sigma}K_b^{B,\xi} + K_d^{A,\sigma}K_b^{B,\xi}\right)\rho_{\bar{\sigma}\xi,\bar{\sigma}\xi}(0) \\ &+ \Big(K_a^{A,\sigma\sigma}K_a^{B,\xi\xi} + K_a^{A,\sigma\sigma}K_d^{B,\xi} \\ &+ \ K_d^{A,\sigma}K_a^{B,\xi\xi} + K_d^{A\sigma}K_d^{B,\xi}\Big)\rho_{\bar{\sigma}\bar{\xi},\bar{\sigma}\bar{\xi}}(0), \end{aligned} \tag{2.31}$$

but the coherences behave differently compared to the case of free evolution.

Any off-diagonal element of the density operator with a single flip depends now on the initial values of all similar elements, and the same holds for the off-diagonal elements with two spin flips, but these two groups of coherences are still disjoint.

The decay of entanglement of Bell states is a consequence of dynamics of occupations and two-spin-flip coherence, so it is instructive to write out explicitly the formula for the latter:

$$\begin{aligned} \rho_{\sigma\xi,\bar{\sigma}\bar{\xi}}(2\tau) =& K_c^{A,\sigma}K_c^{B,\xi}\rho_{\sigma\xi,\bar{\sigma}\bar{\xi}}(0) + K_c^{A,\sigma}K_a^{B,\xi\bar{\xi}}\rho_{\sigma\bar{\xi},\bar{\sigma}\xi}(0) \\ &+ K_a^{A,\sigma\bar{\sigma}}K_c^{B,\xi}\rho_{\bar{\sigma}\xi,\sigma\bar{\xi}}(0) + K_a^{A,\sigma\bar{\sigma}}K_a^{B,\xi\bar{\xi}}\rho_{\bar{\sigma}\bar{\xi},\sigma\xi}(0). \end{aligned} \tag{2.32}$$

As can be seen from the above formulas Eqs. (2.26)–(2.32), the exact dynamics is more complicated than in the free evolution case, but a state initialized in an X form again retains this structure throughout the evolution.

Below the two-qubit density operator is presented, where the elements which mix during the evolution are marked with different colors: populations ρ_{11}, ρ_{22}, ρ_{33}, ρ_{44} (black) constitute the group whose elements depend on themselves only, coherences

ρ_{12}, ρ_{34}, ρ_{21}, ρ_{43} (red), ρ_{13}, ρ_{24}, ρ_{31}, ρ_{42} (green), and ρ_{14}, ρ_{23}, ρ_{32}, ρ_{41} (blue) constitute similar separated groups.

$$\hat{\rho}_{\text{echo}} = \begin{array}{c} \begin{matrix} |{+}{+}\rangle & |{+}{-}\rangle & |{-}{+}\rangle & |{-}{-}\rangle \end{matrix} \\ \begin{pmatrix} \rho_{11} & \rho_{12} & \rho_{13} & \rho_{14} \\ \rho_{21} & \rho_{22} & \rho_{23} & \rho_{24} \\ \rho_{31} & \rho_{32} & \rho_{33} & \rho_{34} \\ \rho_{41} & \rho_{42} & \rho_{43} & \rho_{44} \end{pmatrix} \end{array} \begin{matrix} \langle{+}{+}| \\ \langle{+}{-}| \\ \langle{-}{+}| \\ \langle{-}{-}| \end{matrix}$$

2.4 Approximation Schemes for the Model

One simple method which allows to account the impact of nuclear spin bath on the electron spin dynamics, namely QSBA, was discussed in the Introduction (Sec. 1.3.3). Here, I concentrate on the approximations that explicitly account for the hyperfine interaction with a nuclear spin bath.

2.4.1 Effective two-spin approximation

In moderate external magnetic field, the $\hat{V}_{\text{ff}}$ term plays an important role. At some Ω (corresponding to $B \approx 0.5$ T in GaAs QDs and in lower magnetic fields when spin echo decay is considered [140]) the influence of $\hat{h}_{\perp}$ becomes a dominant source of decoherence, and the dipolar-induced fluctuations of $\hat{h}^z$ are of minor importance. The purely hyperfine-induced decoherence of electron spin in the regime of moderate B fields has been studied using various approaches [116, 110, 123, 163, 164, 111, 124, 165, 166, 125, 126]. Here, I concentrate on such fields which cause the decay of NFID or echo signal on time scale $t \ll 1/A_{\max}$, where $A_{\max}$ is the maximal value of the hyperfine coupling A_k. In III-V QDs, for which there is a nuclear spin at every lattice site, and for which all the $\mathcal{A}_\alpha$ have similar values, one has $1/A_{\max} \approx N/\mathcal{A} \approx 10$ μs for $N = 10^6$. Using the time-energy uncertainty, one can infer that for $t \ll 1/A_{\max}$ the exact shape of A_k distribution is irrelevant, allowing us to take all the A_k couplings to be the same. When one considers a regime of $t \ll \min_{k,l}[1/(\omega_k - \omega_l)]$, where ω_k and ω_l are Zeeman splittings of distinct nuclei (this condition is also easier to fulfill at low B), the presence of multiple nuclear species can be neglected, and one may treat the nuclear spin bath as a large single spin $\hat{\mathbf{J}} = \sum_{k=1}^{N} \hat{\mathbf{J}}_k$. The advantage of these approximation is that such a uniform coupling (UC) model can be easily solved exactly both in the case of free evolution, including NFID [125], and in the case of spin echo [165] for practically any N, and for any value of Ω, including $\Omega = 0$. From the point of view of investigation of entanglement dynamics it is important that this method allows for calculation of all the components of $\hat{\rho}(t)$, since certain features of entanglement decay, for example the presence or absence of entanglement sudden death (ESD) [167, 168] when one of the Bell states is considered, can be captured only with a theoretical approach that accurately describes the changes of qubit's populations. On longer time scales, an approach that takes into account the presence of distinct nuclear species and/or the inhomogeneity of hyperfine couplings becomes necessary, e.g. the effective pure dephasing Hamiltonian approach [164, 111], which has been experimentally verified [140].

It is worth to mention that the same approximation has been used also for a similar Hamiltonian describing an electron bound on a defect in a crystal with

localized spin moments of ions [169].

2.4.1.1 Free evolution

To calculate the two-qubit density operator, one has to choose a method of approximate calculation of $K(t)$ functions (or $R(t)$ functions in the case of correlated baths). At low magnetic fields the uniform coupling (UC) model, in which all A_k couplings are assumed to be the same (all equal to $\mathcal{A}/N$), is suitable. Moreover, it is assumed here that all the nuclei have the same Zeeman splitting ω, so nuclear spins can be aggregated in a single nuclear macrospin $\hat{\mathbf{J}} = \sum_{k=1}^{N} \hat{\mathbf{J}}_k$. As discussed above in Sec. 2.4.1, this approximation is expected to be justified at low fields, at which the coherence decays on time scale $t \ll N/\mathcal{A}$, $\min_{k,l}[1/(\omega_k - \omega_l)]$.

After replacing the nuclear operators by a collective angular momentum operator $\hat{\mathbf{J}}$, one can use the basis of collective nuclear spin states $|\zeta, j, m\rangle$, for which $\hat{J}^2 |\zeta, j, m\rangle = j(j+1) |\zeta, j, m\rangle$ and $\hat{J}^z |\zeta, j, m\rangle = m |\zeta, j, m\rangle$, and where ζ is the quantum number accounting for the number of different possibilities to add N spins producing a total spin j. The single QD Hamiltonian

$$\hat{H}_{\mathrm{UC}} = \Omega \hat{S}^z + \omega \hat{J}^z + \frac{\mathcal{A}}{N} \hat{\mathbf{S}} \cdot \hat{\mathbf{J}} \tag{2.33}$$

couples states only in pairs:

$$\begin{aligned} \mathrm{e}^{-i\hat{H}_{\mathrm{UC}} t} |\sigma; \zeta, j, m\rangle \equiv\ & a_{jm\sigma}(t) |\sigma; \zeta, j, m\rangle \\ & + b_{jm\sigma}(t) |\bar{\sigma}; \zeta, j, m + \sigma/2\rangle , \end{aligned} \tag{2.34}$$

therefore, the subspaces of fixed j and ζ are decoupled of each other. As explained in Sec. 2.2.2, the nuclear density operator is diagonal in the basis of eigenstates of $\hat{J}^z$, so that it can be written as

$$\hat{\rho}_J = \frac{1}{Z} \sum_{j,m,\zeta} p_m |\zeta, j, m\rangle \langle \zeta, j, m| , \tag{2.35}$$

where p_m are the appropriate weights (i.e. $p_m = 1$ for the thermal state and $p_m = \delta_{mm_0}$ for narrowed state), and Z is the statistical sum. Recalling the fact that the Hamiltonian is diagonal in ζ quantum numbers, it is possible to perform the summation over them right away:

$$\hat{\rho}_J = \frac{1}{Z} \sum_{jm} n_j p_m |j, m\rangle \langle j, m| , \tag{2.36}$$

where n_j is the number of subspaces with given j (see Appendix (p. 119)).

With the above nuclear density operator, using Eq. (2.34) and the results given in Section 2.3, one can obtain the explicit form of K functions in the case of free evolution:

$$K_a^{Q,\sigma\sigma'}(t) = \frac{1}{Z} \sum_{jm} n_j a^Q_{jm\sigma}(t) \big(a^Q_{jm\sigma'}(t)\big)^* , \tag{2.37}$$

$$K_b^{Q,\sigma}(t) = \frac{1}{Z} \sum_{jm} n_j |b^Q_{jm\bar{\sigma}}(t)|^2 . \tag{2.38}$$

In the case of correlated baths described by a density operator from Eq. (2.5), within the UC approximation $h_Q^z = m_Q\mathcal{A}/N_Q$, one obtains

$$\begin{aligned} R^{\alpha'\beta'\gamma'\delta'}_{\alpha\beta\gamma\delta}(t) = \frac{1}{Z} \sum_{m_A - m_B = \Delta m} \sum_{j_A, j_B} n_{j_A} n_{j_B} \\ \times \Big(\quad a_{j_A m_A \alpha'} a_{j_B m_B \beta'} a^*_{j_A m_A \gamma'} a^*_{j_B m_B \delta'} \delta_{\alpha\alpha'}\delta_{\beta\beta'}\delta_{\gamma\gamma'}\delta_{\delta\delta'} \\ + a_{j_A m_A \alpha'} a^*_{j_A m_A \gamma'} |b_{j_B m_B \beta'}|^2 \delta_{\alpha\alpha'}\delta_{\bar\beta\beta'}\delta_{\gamma\gamma'}\delta_{\beta\delta}\delta_{\bar\beta\delta'} \\ + a_{j_B m_B \beta'} a^*_{j_B m_B \delta'} |b_{j_A m_A \alpha'}|^2 \delta_{\alpha\bar\alpha'}\delta_{\beta\beta'}\delta_{\delta\delta'}\delta_{\alpha\gamma}\delta_{\bar\alpha\gamma'} \\ + |b_{j_A m_A \alpha'}|^2 |b_{j_B m_B \beta'}|^2 \delta_{\alpha\gamma}\delta_{\bar\alpha\alpha'}\delta_{\bar\alpha\gamma'}\delta_{\beta\delta}\delta_{\bar\beta\beta'}\delta_{\bar\beta\delta'} \Big), \end{aligned} \tag{2.39}$$

where the time dependence of a and b functions, and the superscripts $Q = A, B$ have been suppressed for shortness of notation. It is worth to pay attention to the fact that the structure of Eq. (2.13) is reproduced here.

2.4.1.2 Spin echo

As already mentioned in Sec. 2.3.2, in the echo case only uncorrelated thermal baths are considered. The explicit expressions for the single-qubit evolution functions are:

$$K_a^{\sigma\sigma'}(\Delta t) = \sum_{jm} n_j \; a^{(1)}_{j,m,\bar\sigma} \; a^{(2)}_{j,m,\sigma} \; a^{(1)*}_{j,m,\bar\sigma'} \; a^{(2)*}_{j,m,\sigma'}, \tag{2.40}$$

$$K_b^{\sigma}(\Delta t) = \sum_{jm} n_j \Big(|a^{(1)}_{j,m,\sigma}|^2 \; |b^{(2)}_{j,m,\bar\sigma}|^2 + |b^{(1)}_{j,m,\sigma}|^2 \; |a^{(2)}_{j,m+\sigma,\sigma}|^2 \Big), \tag{2.41}$$

$$K_c^{\sigma}(\Delta t) = \sum_{jm} n_j \Big(a^{(1)}_{j,m,\sigma} \; b^{(2)}_{j,m,\bar\sigma} \; b^{(1)*}_{j,m,\bar\sigma} \; a^{(2)*}_{j,m+\bar\sigma,\bar\sigma} + b^{(1)}_{j,m,\sigma} \; a^{(2)}_{j,m+\sigma,\sigma} \; a^{(1)*}_{j,m,\bar\sigma} \; b^{(2)*}_{j,m,\sigma} \Big), \tag{2.42}$$

$$K_d^{\sigma}(\Delta t) = \sum_{jm} n_j \; |b^{(1)}_{j,m,\bar\sigma}|^2 \; |b^{(2)}_{j,m+\bar\sigma,\bar\sigma}|^2, \tag{2.43}$$

where $a^{(k)}_{j,m,\sigma} \coloneqq a_{j,m,\sigma}(\tau_k)$ and $b^{(k)}_{j,m,\sigma} \coloneqq b_{j,m,\sigma}(\tau_k)$ (with $k = 1, 2$), $\Delta t \coloneqq \tau_1 + \tau_2$. Maximum of the echo signal is obtained for $\tau_1 = \tau_2 = \Delta t/2$.

The full formulas for $a_{jm\sigma}$ and $b_{jm\sigma}$ functions can be found in Appendix (p. 119). For the qualitative discussion, here it should only be noted that for a qubit splitting $\Omega \ll \sigma_\mathrm{h}$ one has $|a_{jm\sigma}| \approx 1$ and $|b_{jm\sigma}| \propto \sigma_\mathrm{h}/\Omega$. Therefore, at large fields, all the K_i functions having at least one b function are diminished. This reflects the fact that at large Ω the nuclear spin bath induces to pure dephasing of the qubit: only the K_a^{+-} functions, which accounts for the decay of the initially present coherences, matter. The UC approximation confirms this fact directly.

2.4.2 Effective three-spin approximation[1]

In order to test the results obtained within the effective two-spin approximation, I have performed the same calculations of entanglement (concurrence) dynamics

[1] The results of subsection "Effective three-spin approximation" obtained in 2014 have not been published, but are documented as a report prepared during realization of NCN grant no. DEC-2012/07/B/ST3/03616.

using an effective three-spin approximation, which is based on the assumption that there are two groups of nuclear spins, each having the same hyperfine couplings. Such a model can be motivated as follows. The electron wave function is approximated by a piecewise constant function with two steps, which results in the emergence of two groups of nuclear spins with coupling constants $A_i = \mathcal{A}|\psi(\mathbf{r} \in \text{region } i)|^2$. In such a case, the Hamiltonian of the single QD reads:

$$\hat{H}_Q = \Omega\hat{S}^z + \omega\sum_{k_1=1}^{N_1}\hat{J}^z_{k_1} + A_1\sum_{k_1=1}^{N_1}\hat{\mathbf{S}}\cdot\hat{\mathbf{J}}_{k_1} + \omega\sum_{k_2=1}^{N_2}\hat{J}^z_{k_2} + A_2\sum_{k_2=1}^{N_2}\hat{\mathbf{S}}\cdot\hat{\mathbf{J}}_{k_2}.$$

Here it is assumed, as previously, that electron is confined in a QD and interacts with the homonuclear spin bath via hyperfine interaction.

The above Hamiltonian has a property that it conserves the z component of the total spin of the system (Eq. (2.9) holds for it as well). This implies that the state space of such a Hamiltonian is formed of the disjoint subspaces of a given value of z component of the total spin. I use as a basis of the state space the set of states of the form $|\xi\rangle\otimes|j_1m_1\rangle\otimes|j_2m_2\rangle = |\xi j_1m_1j_2m_2\rangle$, where ξ is z component of electron spin, $j_1,\ j_2$ are the magnitudes of the total spins of the first and the second group of nuclear spins, respectively, and $m_1,\ m_2$ are the z components of the total spins of the first and the second group of nuclear spins, respectively. The evolution of a state $|\xi j_1m_1j_2m_2\rangle$ will take place only in the subspace where z component of the total spin is constant and equals $\xi + m_1 + m_2$. All states of each subspace can be divided into two groups: $|\xi j_1m_1j_2m_2\rangle$, where $m_1 + m_2 = m_0$, and $|\bar{\xi}j_1m_1'j_1m_2'\rangle$, where $m_1' + m_2' = m_0 + 2\xi$.

This knowledge about the structure of the state space of the problem allows to simplify the calculations. There is no need to perform calculations with a Hamiltonian acting in the whole state space (of dimension $2^{1+N_1+N_2}$ for nuclear spins $\frac{1}{2}$) at the same time. Instead of it, one can consider $\left(\frac{N_1}{2}+1\right)\left(\frac{N_2}{2}+1\right)$ different (j_1,j_2)-pairs, for each of them calculate the evolution of each single state in the restricted subspace to which it belongs and sum up all the results at the end. It is worth noting that the dimension of the largest subspace of the constant z component of the total spin $\xi + m_1 + m_2$ will be for the $\left(j_1=\frac{N_1}{2}, j_2=\frac{N_2}{2}\right)$-pair and it is equal to $4j - 2m_0 + 1$ in the case of $j_1 = j_2 = j$. Using such an approach, one can perform the calculations for a larger number of nuclear spins in the bath (in comparison to the case of direct calculations, which can be done for less than 20 nuclear spins). Now the main difficulty one faces is to perform all the summations rather than to diagonalize the relevant part of the Hamiltonian.

The goal is then to calculate $K_{\sigma\xi\xi'\sigma'}(t)$ functions. Let us first define the initial density operator of the nuclear spin bath in a narrowed state:

$$\begin{aligned}\hat{\rho}_{\text{bath}}(0) &= \frac{1}{Z}\sum_{\substack{j_1,j_1,\alpha_1,\alpha_2,\\ A_1m_1+A_2m_2=h_0^z}} |j_1m_1\alpha_1j_1m_2\alpha_2\rangle\langle j_1m_1\alpha_1j_2m_2\alpha_2| \\ &= \frac{1}{Z}\sum_{\substack{j_1,j_1,\\ A_1m_1+A_2m_2=h_0^z}} \rho_{j_1m_1j_2m_2}|j_1m_1j_1m_2\rangle\langle j_1m_1j_2m_2|,\end{aligned}$$

where $\rho_{j_1m_1j_2m_2} = \rho_{j_1j_2} = n_{j_1}n_{j_2}$ and $n_{j_i} = \frac{N_i!}{\left(\frac{N_i}{2}-j_i\right)!\left(\frac{N_i}{2}+j_i\right)!}\frac{2j_i+1}{\frac{N_i}{2}+j_i+1}$ is the degeneracy of a state $|j_im_i\rangle$ with respect to quantum numbers j_i, m_i, (quantum number α_i

labels the ways how the individual spins were added in order to obtain a state with the total spin j_i), h_0^z is the magnitude of the z component of the Overhauser field, Z is a statistical sum,

$$Z = \sum_{\substack{j_1 j_2, \\ A_1 m_1 + A_2 m_2 = h_0^z}} \rho_{j_1 j_2}.$$

Having the explicit form of density operator of nuclear spin bath, one can calculate $K_{\sigma\xi\xi'}$ functions:

$$\begin{aligned}
K_{\sigma\xi\xi'\sigma'}(t) &= \mathrm{Tr}_{\mathrm{bath}} \left\{ \langle\sigma|\mathrm{e}^{-i\hat{H}_i t}|\xi\rangle \hat{\rho}_{\mathrm{bath}}(0) \langle\xi'|\mathrm{e}^{i\hat{H}_i t}|\sigma'\rangle \right\} \\
&= \mathrm{Tr}_{\mathrm{bath}} \left\{ \langle\sigma|\mathrm{e}^{-i\hat{H}_i t}|\xi\rangle\langle\xi'| \sum_{\substack{j_1, j_2, \\ A_1 m_1 + A_2 m_2 = h_0^z}} \rho_{j_1 m_1 j_2 m_2} |j_1 m_1 j_2 m_2\rangle\langle j_1 m_1 j_2 m_2|\mathrm{e}^{i\hat{H}_i t}|\sigma'\rangle \right\} \\
&= \sum_{\substack{j_1', m_1', j_2', m_2', \\ j_1, j_2, A_1 m_1 + A_2 m_2 = h_0^z}} \rho_{j_1 m_1 j_2 m_2} \langle\sigma j_1' m_1' j_2' m_2'|\mathrm{e}^{-i\hat{H}_i t}|\xi j_1 m_1 j_2 m_2\rangle \\
&\times \langle\xi' j_1 m_1 j_2 m_2|\mathrm{e}^{i\hat{H}_i t}|\sigma' j_1' m_1' j_2' m_2'\rangle \\
&= \sum_{\substack{j_1', m_1', j_2', m_2', \\ j_1, j_2, A_1 m_1 + A_2 m_2 = h_0^z}} \rho_{j_1 m_1 j_2 m_2} \langle\sigma j_1' m_1' j_2' m_2'|\mathrm{e}^{-i\hat{H}_i t}|\xi j_1 m_1 j_2 m_2\rangle \\
&\times \left(\langle\sigma' j_1' m_1' j_2' m_2'|\mathrm{e}^{-i\hat{H}_i t}|\xi' j_1 m_1 j_2 m_2\rangle \right)^{\dagger}.
\end{aligned}$$

The matrix elements have the property that

$$\begin{aligned}
\langle\sigma j_1' m_1' j_2' m_2'|\mathrm{e}^{-i\hat{H}_i t}|\xi j_1 m_1 j_2 m_2\rangle &= \delta_{\sigma + m_1' + m_2', \xi + m_1 + m_2} \delta_{j_1', j_1} \delta_{j_2', j_2} \\
&\times \langle\sigma j_1' m_1' j_2' m_2'|\mathrm{e}^{-i\hat{H}_i t}|\xi j_1 m_1 j_2 m_2\rangle.
\end{aligned}$$

This property allows to perform summations over j_1', j_2' analytically and to obtain the simplified expression for $K_{\sigma\xi\xi'\sigma'}(t)$

$$\begin{aligned}
K_{\sigma\xi\xi'\sigma'}(t) = \sum_{\substack{m_1', m_2', \\ j_1, j_2, A_1 m_1 + A_2 m_2 = h_0^z}} & \rho_{j_1 j_2} \, \delta_{\sigma + m_1' + m_2', \xi + m_1 + m_2} \, \delta_{\sigma' + m_1' + m_2', \xi' + m_1 + m_2} \\
&\times \langle\sigma j_1 m_1' j_2 m_2'|\mathrm{e}^{-i\hat{H}_i t}|\xi j_1 m_1 j_2 m_2\rangle \left(\langle\sigma' j_1 m_1' j_2 m_2'|\mathrm{e}^{-i\hat{H}_i t}|\xi' j_1 m_1 j_2 m_2\rangle \right)^{\dagger}.
\end{aligned}$$

There is no way to calculate these matrix elements analytically (because of the high dimension of a subspace in the general case). I have calculated them numerically using only the relevant part of the Hamiltonian in the calculations (i.e. the part which acts in a subspace z component of total spin for which is equal to $\xi + m_1 + m_2$). Complexity of computation of $K_{\sigma\xi\xi'\sigma'}(t)$ functions depends on the choice of state of nuclear bath: for narrowed nuclear bath state one should perform calculations using the above formula with all possible m_1 and m_2 which satisfy the condition $A_1 m_1 + A_2 m_2 = h_0^z$ (in the general case it will lead to a necessity to perform the calculations in a few subspaces with different m_0); for thermal nuclear bath state one should perform the calculations for all possible values of h_0^z, i.e. perform an additional summation over h_0^z. Here it is worth noting that in the case $A_1 = A_2$ the entire evolution will take place in a single subspace only ($A_1 m_1 + A_2 m_2 = A_1(m_1 + m_2) = h_0^z$,

$m_1 + m_2 = h_0^z/A_1 = m_0$) and one gets back the uniform coupling model (two-spin approximation).

To preserve the connection with previously introduced notation, it should be noted that $K_a^{\sigma\sigma'}(t)$ function corresponds to $K_{\sigma\xi\xi'\sigma\prime}(t)$ function with $\{\sigma,\xi,\xi',\sigma'\} = \{+,+,+,+\},\{-,-,-,-\},\{+,+,-,-\},\{-,-,+,+\}$, and K_b^{σ} function corresponds to $K_{\sigma\xi\xi'\sigma\prime}(t)$ function with $\{\sigma,\xi,\xi',\sigma'\} = \{+,-,-,+\}$, $\{-,+,+,-\}$, for other combinations of indices $K_{\sigma\xi\xi'\sigma\prime}(t) \equiv 0$.

As a unit of time it is instructive to use two-dot T_2^* which is defined as

$$\frac{1}{(T_2^*)^2} \coloneqq \frac{1}{\left(T_{2,A}^*\right)^2} + \frac{1}{\left(T_{2,B}^*\right)^2}, \tag{2.44}$$

where $T_{2,A}^*$, $T_{2,B}^*$ are the dephasing times for qubit A and B, respectively. Assuming that bath consists of nuclear spins of a single species and $J = \frac{1}{2}$, one has the exact relation between the dephasing time of a single QD, its size, and hyperfine coupling $T_{2,i}^* = \frac{\sqrt{2}}{\sigma} = \frac{\sqrt{8}}{\sqrt{\sum_{j=1}^{N_i} A_j^2}}$, where N_i is the number of nuclear spins in the ith QD, and A_j is the hyperfine coupling between the electron spin and the jth nuclear spin of that QD.

By using the relation $\sum_{j=1}^{N_i} A_j^2 = \frac{\mathcal{A}^2}{N_i}$ [108] and fixing $T_{2,q_A}^* = T_{2,q_B}^* = 1$, one can introduce a parameter $R \coloneqq \frac{A_2}{A1}$, which indicates how different the hyperfine couplings in the two different groups are. This parameter now sets the hyperfine couplings $A_1 = \sqrt{\frac{8}{N_1+N_2R^2}}$ and $A_2 = RA_1$. It should be noted that the case of $R = 1$ is equivalent to a uniform coupling model with $N = N_1 + N_2$, whereas the cases of $R = 0$ or $R \to \infty$ also correspond to a uniform coupling model, but with $N = N_1$ or $N = N_2$, respectively.

The numerical calculations of the reduced two-qubit density operator based on the effective two-spin approximation ($N = 200$) and these based on effective three-spin approximations ($N_1 = N_2 = 100$ with $R = 2,\ 5,\ 10$) show that in the case of high-temperature bath state the results are identical, whereas in the case of narrowed bath states on time scale up to several tens of T_2^* the differences are small (about 1%) and start to be noticeable at long times $t > 10T_2^*$. This convergence of the results, obtained in two different approximation approaches, confirms the validity of the two-spin approximation (uniform coupling model), especially at short times, and points out that UC model catches the essence of the decay of coherences and entanglement of two spin qubits.

The idea of approximation of the central spin Hamiltonian of a system, which has a large number of nuclear spins with all different hyperfine couplings (like an electron spin in QD), as interaction of the central spin with a small number of large composite spins have been systematically investigated in Ref. [170], where the way of construction of such consecutive approximations is presented.

2.5 The Results

2.5.1 Quantification of entanglement of two electron spins

To analyze the dynamics of entanglement it is necessary to discuss first the methods of its quantification. As initial states of two qubits I consider Bell states

$$|\Phi_{\pm}\rangle = \frac{1}{\sqrt{2}}(|{+}{+}\rangle \pm |{-}{-}\rangle),$$

$$|\Psi_{\pm}\rangle = \frac{1}{\sqrt{2}}(|{+}{-}\rangle \pm |{-}{+}\rangle),$$

and a Werner state:

$$\hat{\rho}_{\mathrm{W}} = \frac{1-p}{4}\mathbb{1} + p\,|\Psi_{-}\rangle\langle\Psi_{-}|\,, \tag{2.45}$$

where $p \in [0,1]$ can be interpreted as the probability that $\hat{\rho}_{\mathrm{W}}$ is in fact the entangled $|\Psi_{-}\rangle$ state.

The initially pure state of two qubits becomes mixed in course of time evolution due to interaction with the environment. The amount of entanglement in a mixed state of two qubits may be quantified using various measures [5, 7], from which the concurrence has been chosen, since it is one of the most popular measures for two-qubit states and, in addition, it is easy to calculate numerically.

For the initial Bell state at very high magnetic fields, at which qubits undergo pure dephasing, the concurrence $C(t) \approx 2|\rho_{ab}(t)|$, where $\rho_{ab}(t)$ is the initially nonzero coherence. In the case of uncoupled qubits, the amount of entanglement is given by multiplication of known high-field results for single-qubit decoherence. Below, mostly low and moderate magnetic fields, at which $C(t)$ shows new features not inherited from the single-qubit coherence decay, are considered.

Measuring the amount of entanglement in an experiment is a challenging task, since it requires performing a full tomographic reconstruction of $\hat{\rho}(t)$ (see e.g. Ref. [66] for an experimental example with DQDs, and Ref. [171] for a theoretical proposal of a tomography scheme for DQDs taking into account the limitations specific to experiments on gated QDs). To reconstruct a two-qubit state, one should gather data from at least 15 different measurement settings, so obviously any simpler method of entanglement quantification will be helpful, even if it will be able to detect entanglement of only a certain class of states. With such an intention, entanglement witnesses [154] have been constructed. They are defined as observables which have a negative expectation value only when the state is entangled. It is worth to stress that not every entangled state will be detected by a given witness. Usually one constructs an entanglement witness bearing in mind a certain form of a mixed entangled state which one aims to detect [153]. In the system of electrically gated DQD the projection on a singlet state, $\hat{P}_{\mathrm{S}}$, is a natural two-qubit measurement operator [47], so one immediately gets an entanglement witness $\hat{w}_{\mathrm{S}} \equiv 1/2 - \hat{P}_{\mathrm{S}}$. The measurements of $\langle \hat{P}_{\mathrm{S}}(t) \rangle$, which show the decay of an entangled two-spin singlet state in DQD, are routinely performed since the first coherent control of singlet-triplet qubit was demonstrated [58]. If one aims to detect the entanglement of any other Bell state, then it will require first to perform, in principle possible, conversion of that state into singlet state.

Another approach to entanglement quantification is measuring of the efficiency of execution of some task for which entanglement is crucial. For two qubits, quantum

teleportation is a task of such kind [155, 156, 157, 158]. With an entangled state $\hat{\rho}_{AB}$ of spins A and B (located in possibly distant QDs) established, and with the third dot C located nearby the dot A (in order to allow for two-qubit operations on A and C), a quantum state of spin C can be transferred to spin B with the use of two-qubit gate on A and C, and with single-qubit operations and projective measurements. At the beginning, a Bell state of spins A and B is initialized, and then at a later time t a pure state $|\phi_C\rangle$ is created in dot C. Next, the teleportation protocol is carried out on time scale negligible compared to the time scales of qubits' dynamics. Ideal realization of the teleportation procedure teleports the state of qubit C at instant t, fidelity of which compared to its initial state is

$$F_\phi(t) = \langle\phi_C| \operatorname{Tr}_{CA}\big(\hat{\rho}_{CAB}(t)\big) |\phi_C\rangle \,, \tag{2.46}$$

is determined by the density operator $\hat{\rho}_{AB}(t)$ at the moment of teleportation. It has been proven [12, 172] that the fidelity averaged over all $|\phi_C\rangle$ states, $\bar{F}(t)$, cannot exceed 2/3 for separable $\hat{\rho}_{AB}(t)$, and hence, the observation of $\bar{F} > 2/3$ proves the existence of entanglement of spins A and B. Fortunately for practical purposes, in order to obtain the average fidelity one can limit the number of measurements to these involving only six mutually unbiased basis states [158, 173], e.g. $|\pm X\rangle \equiv (|+\rangle \pm |-\rangle)\sqrt{2}$, $|\pm Y\rangle \equiv (|+\rangle \pm i\,|-\rangle)\sqrt{2}$, $|\pm Z\rangle \equiv \{|+\rangle\,, |-\rangle\}$, instead of the whole set of qubit states.

2.5.2 Entanglement dynamics due to coupling to thermal and partially narrowed baths

According to the discussion in Sec. 1.3.3 one can use QSBA to predict the free evolution of qubits, when states of nuclear spin baths are not artificially modified beforehand, i.e. electron spins interact with nuclear baths, which are in the thermal equilibrium (or partially narrowed) state. It is expected that the results obtained using this approach are correct on a time scale of the order of T_2^*. Therefore, it is reasonable to use the UC approach from Sec. 2.4.1. This model has been used for different physical systems and the UC solution for the free evolution of a spin interacting with a thermal nuclear bath is well known [134, 174]. The details of UC model are included in Appendix (p. 119), where closed expressions for $K_a^{\sigma\sigma'}$ and K_b^σ are given.

In high magnetic fields, $\Omega \gg \sigma_\mathrm{h}$, decoherence is nearly of pure dephasing type: as shown in Appendix (p. 119), for large bath (i.e. for large N) and at times $t \ll \Omega/\sigma_\mathrm{h}^2$ one has

$$K_a^{Q,\sigma\bar{\sigma}}(t) \approx \mathrm{e}^{-i\sigma\Omega_Q t} \exp\left(-\left(\frac{t}{T_{2,Q}^*}\right)^2\right), \tag{2.47}$$

where Q labels the A and B qubits. This result can be obtained by disregarding the $\hat{V}_\mathrm{ff}$ operator and calculating an average over static h^z fields with normal distribution (see Eq. (1.22)) [127]. On the other hand, the K_b^σ functions are strongly suppressed due to large Ω, and therefore, $K_a^{\sigma\sigma} = 1 - K_b^{\bar{\sigma}} \approx 1$.

The exact form of the transient dynamics of K_b^σ is of less importance for $\Omega \gg \sigma_\mathrm{h}$, but the attention should be paid that at $t > T_{2,Q}^*$ one has

$$K_b^{Q,\sigma}(t > T_{2,Q}^*) \approx \frac{\sigma_Q^2}{\Omega^2} = \frac{2}{(\Omega T_{2,Q}^*)^2} \equiv \frac{2}{\tilde{\Omega}_Q^2}, \tag{2.48}$$

where $\tilde{\Omega}_Q \coloneqq \Omega T^*_{2,Q}$ is the dimensionless Zeeman splitting of electron spin in dot Q, expressed in units of $\frac{\hbar}{T_2^*}$ (with a simplifying assumption $\hbar = 1$), see Appendix (p. 119) for derivation of this formula.

From the formula for the concurrence of X state, Eq. (1.5), one can clearly see that at high fields for Bell states $C(t) \approx 2|\rho_{ab}(t)|$ (where $\rho_{ab}(t)$ is the nonzero coherence present in a given Bell state) up to entanglement sudden death time t_D at which $|\rho_{ab}| = \sqrt{\rho_{cc}\rho_{dd}}$ (where all the indices a, b, c, d are distinct):

$$C(t < t_\mathrm{D}) \approx \exp\left(-\left(\frac{t}{T_2^*}\right)^2\right), \tag{2.49}$$

where the two-dot T_2^* time is defined in Eq. (2.44). To estimate quantitatively t_D, one has to look at the diagonal elements of $\hat{\rho}(t)$ which initially were equal to zero. In high fields, $\tilde{\Omega}_Q > 1$, for long times, $t > T_2^*$, using Eqs. (2.21) and (2.48) and assuming that the initial state was $|\Phi_\pm\rangle$ (analogous reasoning applies to any Bell state), one has

$$\begin{aligned}\rho_{22}(t) &= K_a^{A,++}K_b^{B,-}\rho_{11}(0) + K_b^{A,+}K_a^{B,--}\rho_{44}(0)\\ &= \frac{1}{2}\left(\left(1 - K_b^{A,-}\right)K_b^{B,-} + K_b^{A,+}\left(1 - K_b^{B,+}\right)\right),\\ &\approx \frac{1}{\tilde{\Omega}_A^2} + \frac{1}{\tilde{\Omega}_B^2}.\end{aligned} \tag{2.50}$$

The occupation $\rho_{33}(t)$ is described by the same equation. While solving the following equation for t_D $|\rho_{14}(t_\mathrm{D})| = \sqrt{\rho_{22}(t_\mathrm{D})\rho_{33}(t_\mathrm{D})}$, where for $\rho_{14}(t) = K_a^{A,+-}K_a^{B,+-}$ the high-field approximation was used, Eq. (2.47), and assuming $\Omega_A = \Omega_B = \Omega$ one obtains

$$t_\mathrm{D} = T_2^*\sqrt{\sqrt{2}\ln \Omega T_2^*}. \tag{2.51}$$

After the introduction of dimensionless qubit splitting $\tilde{\Omega} \coloneqq \Omega T_2^*$, and dimensionless time $\tilde{t} \coloneqq t/T_2^*$, the expressions for both the concurrence and the ESD time take concise forms

$$C(t < t_\mathrm{D}) \approx \mathrm{e}^{-\tilde{t}^2}, \tag{2.52}$$

$$\tilde{t}_\mathrm{D} = \sqrt{\sqrt{2}\ln\tilde{\Omega}}\,. \tag{2.53}$$

The above reasoning suggests that this universality is expected at $\tilde{\Omega} \gg 1$, but the numerical predictions obtained using the UC model show that it holds at all magnetic fields, with $N \gg 1$ being the only requirement. In Fig. 2.1 the results for $C(\tilde{t})$ at $\tilde{\Omega} = 0$, 5, and ∞ (actually, a value so large that any further increase of it does not change the result in a visible manner) are shown. It should be noted that in this graph the results calculated for symmetric ($N_A = N_B$) QD and for strongly asymmetric ($N_A = 2N_B$) QD are presented. From these plots one can draw two conclusions: only the high magnetic field result is in quantitative agreement with Eq. (2.52) (as expected), and, more importantly, $C(\tilde{t})$ depends only on $\tilde{\Omega}$. As shown in Fig. 2.1, in low and moderate magnetic fields, $\tilde{\Omega} \approx 1$, the concurrence has an oscillatory component, that originates from oscillations of K_b^σ functions with frequency $\propto\tilde{\Omega}$, which have higher amplitudes at low fields, so they lead to oscillations

of the diagonal elements of the two-qubit density operator. It is also worth noting that at lower fields the sudden death of entanglement is clearly visible (at time t_{D} concurrence becomes equal to 0 exactly, $C(t_{\mathrm{D}}) = 0$). The dependence of $\tilde{t}_{\mathrm{D}}$ on $\tilde{\Omega}$ is shown in the inset of Fig. 2.1. The same results for concurrence $C(t)$ and entanglement sudden death time $t_{\mathrm{D}}(\Omega)$ for two electron spin qubits interacting with baths in the thermal states were obtained in Ref. [162], where the authors propose to sense low magnetic fields by measuring of t_{D}. In Refs. [175] and [176] the possible significance of entanglement dynamics for the operation of chemical magnetometers is discussed. Here it has been shown that $\tilde{t}_{\mathrm{D}} \coloneqq t_{\mathrm{D}}/T_2^*$ is a function of $\tilde{\Omega} \coloneqq \Omega T_2^*$ only. This knowledge makes possible practical use of any pair of QDs (even two dots of very different sizes) for such a magnetometry scheme. The universality of the entanglement decay expressed in units of T_2^* can be first used for a calibration of a device, since high-field decay can be fitted using the simple formula Eq. (2.52). After obtaining in that way the value of T_2^*, the universal dependence $\tilde{t}_{\mathrm{D}}$ (shown in the inset of Fig. 2.1) or the approximation to it (Eq. (2.51)) may next be used.

In some experiments on DQDs [65], in order to separately address each of the qubits (i.e. perform the single-qubit unitary operations using a.c. magnetic field), the qubits were exposed to a magnetic field of different strength in each QD, i.e. Ω_A was slightly different from Ω_B. Below, the resulting correction to the entanglement sudden death time is presented using a parameter η which accounts for the relative difference of magnetic field $\Omega_A = \Omega$ and $\Omega_B = (1+\eta)\Omega$, with $\eta \ll 1$. The first-order correction to formula (2.53) is obtained by repeating the same derivation as previously: $\tilde{t}_{\mathrm{D}} \approx \tilde{t}_0 + \delta\tilde{t}$ with

$$\delta\tilde{t} = -\eta \frac{(T_{2,B}^*)^2}{(T_{2,A}^*)^2 + (T_{2,B}^*)^2} \frac{1}{\tilde{t}_0}, \tag{2.54}$$

where $\tilde{t}_0$ corresponds to $\tilde{t}_D$ for $\Omega_A = \Omega_B$, i.e. to the value from Eq. (2.51).

Qubits initially being in the Werner state from Eq. (2.45) shows a qualitatively different behavior of $\tilde{t}_{\mathrm{D}}$. Using Eq. (2.21) one can obtain (retaining only terms of leading order in $1/\tilde{\Omega}^2$) the $\tilde{t} > 1$ values of $\rho_{11} = \rho_{44} \approx (1-p)/4 + p^2/\tilde{\Omega}^2$, which together with $|\rho_{23}| \approx \frac{p}{2}\mathrm{e}^{-\tilde{t}^2}$ result in

$$\tilde{t}_{\mathrm{D,W}} = \sqrt{\ln\left[\left(\frac{1-p}{2p} + \frac{2}{\tilde{\Omega}^2}\right)^{-1}\right]}, \tag{2.55}$$

which at high fields, $\tilde{\Omega} \gg 2\sqrt{p/(1-p)}$, gives an $\tilde{\Omega}$-independent result, $\tilde{t}_{\mathrm{D,W}} \approx \sqrt{\ln(2p/(1-p))}$, shown in the inset of Fig. 2.1.

Summarizing the results of this subsection, it is worth to note the basic features of the mixed $\hat{\rho}(t)$ state. The leading effect of the nuclear spin baths is the dephasing of qubits' coherences, and the secondary effect at a finite magnetic field is a partial redistribution of populations. The initial Bell state of qubits evolves into a state $\hat{\rho}(t)$ with initially zero populations increased to some level ($\propto \frac{1}{\tilde{\Omega}}$) and with reduced coherences, i.e. it becomes a Werner-like state. This type of evolution of two-qubit density operator induced by hyperfine interaction holds also in the cases of narrowed and correlated nuclear baths discussed in the following sections.

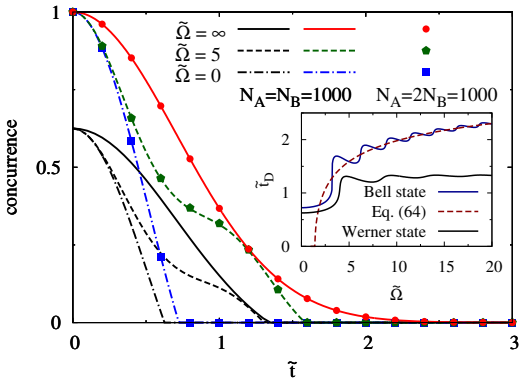

Figure 2.1: Concurrence decay for two electron spins interacting with uncorrelated thermal baths. The electron spins are initially in one of the Bell states, and the dynamics of their reduced density operator is calculated using the UC approach. Time is in units of two-dot T_2^* defined in Eq. (2.44), and the dimensionless Zeeman splitting is $\tilde{\Omega} := \Omega T_2^*$. The result for $\tilde{\Omega} = \infty$ (which in fact is a value large enough for the changes in $C(\tilde{t})$ upon increasing it to be invisible in the Figure) is the same as the result of calculation using the pure dephasing approximation from Eq. (2.47). Lines and symbols correspond to two distinct sets of N_A and N_B. The agreement of the results corresponding to the same values of $\tilde{\Omega}$ illustrates the universal character of the $C(\tilde{t})$ behavior. Black lines show results for the initial Werner state with $p = 3/4$. In the inset we show the dependence of the ESD time $\tilde{t}_D := t_D/T_2^*$ on $\tilde{\Omega}$: blue solid line is the exact result for Bell states, dashed line is the approximate large-field result from Eq. (2.53), and black solid line is the exact result for Werner state with $p = 3/4$. The figure is reproduced from Ref. [1].

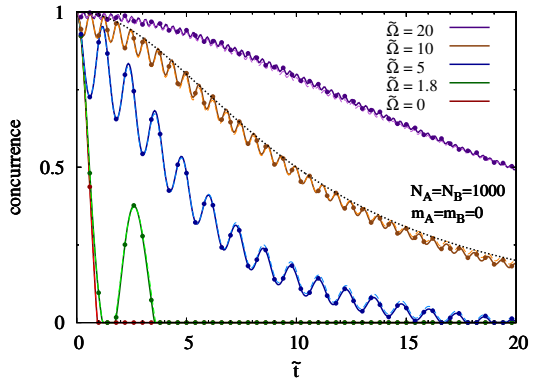

Figure 2.2: Concurrence decay for two electron spins initialized in one of the Bell states interacting with two separate uncorrelated nuclear baths in narrowed states (each bath has $h_Q^z = 0$). The calculations are performed using the UC approach (so that $h_Q^z = 0$ corresponds to $m_Q = 0$). Time is in units of two-dot T_2^* defined in Eq. (2.44), and the dimensionless Zeeman splitting is $\tilde{\Omega} := \Omega T_2^*$. Solid lines correspond to the case of two identical QDs ($N_A = N_B = 1000$), dashed lines correspond to the case of two strongly asymmetric QDs ($N_A = 2N_B = 1000$), symbols correspond to the case of two identical QDs consisting of realistic number of nuclear spins ($N_A = N_B = 10^6$), and the dotted line is the calculation in the pure dephasing approximation using Eq. (2.56) for $\tilde{\Omega} = 10$. Note that symbols are in full agreement with solid lines, i.e. the results for two identical QDs are independent of the sizes of these QDs in the domain of applicability of the UC approach. Dashed lines are very close to the solid ones (the difference between the two is most visible for $\tilde{\Omega} = 5$) showing that results obtained for QDs of different sizes, are very similar one to another when expressed in the dimensionless units used here. The figure is reproduced from Ref. [1].

2.5.3 Entanglement dynamics due to coupling to nuclear spin baths in a strongly narrowed state

In this subsection, nuclear spin baths in a strongly narrowed state described either by Eqs. (2.3) and (2.4) for uncorrelated baths, or by Eq. (2.5) for correlated baths in DQD are considered. They are discussed in subsections 2.5.3.1 and 2.5.3.2, respectively. Here it is assumed that the fluctuations of h_Q^z are constrained to such a degree that the dephasing due to averaging over a quasistatic spread of $h_{A,B}^z$ becomes irrelevant, and other processes (related to averaging over the transverse components of Overhauser fields) have to be taken into account. Thus, $\sigma_{\rm n}$ (the width of relevant distribution of h_Q^z or $\Delta h^z \coloneqq h_A^z - h_B^z$) is so small that the timescale of coherence decay due to it, $\approx 1/\sigma_{\rm n}$, is much longer than the time scale of entanglement decay, that is discussed below.

2.5.3.1 Each bath narrowed separately

The free evolution for the narrowed bath state can be calculated in the same way as for high-temperature bath state (presented in the previous section) with the only difference that now the $K_{a/b}(t)$ evolution functions are obtained assuming a narrowed state in each of the QDs (see Appendix (p. 119)). It is convenient to analyze the main features of the entanglement decay using approximate expressions, valid for $\Omega_Q \gg \sigma_Q$, where $\Omega_Q = \Omega + h_Q^z$ is the total spin splitting in the dot Q (note that spin splitting due to the external magnetic field B is again assumed to be the same in both QDs). For $\Omega_Q \gg \sigma_{\rm h}$ on time scales discussed in Appendix (p. 119), for $h_Q^z = 0$ one can obtain a smooth coherence decay

$$K_{a,p=0}^{Q,+-}(t) \approx \frac{{\rm e}^{-i\Omega_Q t}}{1+it/\tau_Q} = {\rm e}^{-i\Omega_Q t}\frac{{\rm e}^{-i\arctan t/\tau_Q}}{\sqrt{1+(t/\tau_Q)^2}}, \tag{2.56}$$

where

$$\tau_Q = \frac{4N_Q\Omega_Q}{\mathcal{A}^2} = \frac{1}{2}\Omega_Q (T_{2,Q}^*)^2. \tag{2.57}$$

The characteristic decay time τ_Q becomes a function of Ω_Q, since the influence of transverse Overhauser fields diminishes with increasing qubit splitting Ω_Q. It is important to note here that the same results have also been obtained using the ring diagram theory (RDT) [164, 111], and they can also be derived by performing a classical average over the transverse components of the Overhauser field [108, 177]. The derivation of this approximate formula from the exact UC solution is presented in Ref. [125].

On a time scale $t \ll N_Q/\mathcal{A}$ for finite bath polarization one has [126]

$$K_{a,p}^{Q,+-}(t) \approx {\rm e}^{-i\Omega_Q t}\frac{p_Q}{p_Q\cos\left(\frac{2Jpt}{\tau_Q}\right) + ip_{Q,\perp}^2\sin\left(\frac{2Jpt}{\tau_Q}\right)}, \tag{2.58}$$

where J is the nuclear spin (with all the nuclei assumed to have the same J), $p_Q \in [0,1]$ is the nuclear polarization, and $p_{Q,\perp}^2 = J + 1 - \langle (J^z)^2\rangle/J$. Note that for unpolarized bath $p_Q = 0$ the transverse component $p_\perp^2 = J(J+1)/3$, and the $p_Q \to 0$ limit of Eq. (2.58) gives Eq. (2.56).

The above functions derived within the UC model are modulated by oscillations (with frequency $\approx \tilde{\Omega}_Q$) of amplitude $\approx 8/\tilde{\Omega}_Q^2$, which vanish only for $t \gg \tau_Q$ (see

Appendix (p. 119)). In low magnetic fields, $\tilde{\Omega}_Q$, the evolution of diagonal elements of the reduced density operator is determined by $K^{\sigma}_{b,Q}$ functions. These functions also oscillate with amplitude $\approx 4/\tilde{\Omega}_Q^2$, but at times at times $t \gg \tau_Q$ their oscillations dephase and the functions stabilize, $K^{\sigma}_{b,Q} \approx 2/\tilde{\Omega}_Q^2$. In Fig. 2.2, the results for the concurrence decay of initially Bell states at zero bath polarization are shown. The oscillations of K functions cause the oscillations of concurrence: at low magnetic fields their relatively large amplitude leads to pronounced effects of entanglement death and revival – see the result for $\tilde{\Omega} = 1.8$ for most prominent demonstration. At higher fields they cause only a saw-tooth pattern of $\tilde{\Omega}$ dependence of the final ESD time (shown in Fig. 2.3). Like in the previous section, one can also derive approximate analytical formulas for ESD time at large magnetic fields. Since the expressions in the narrowed bath state case are more involved, for sake of clarity, it is better to note only the asymptotic behaviour of sudden death time t_{D}: when initial two-qubit state is one of Bell state, $t_{\mathrm{D}} \propto B^2$, whereas for a Werner state it grows slowly, $t_{\mathrm{D}} \propto B\sqrt{p/(1-p)}$. The calculated numerically results, which agree with the estimates, are shown in Fig. 2.3. Lastly, the use of the "universal" units of $\tilde{\Omega}$ and $\tilde{t}$ introduced in the previous section should be justified. It does not follow from the formulas for $K_a^{\sigma\bar{\sigma}}$ given above that in the fully narrowed case one can expect the results for all pairs of dots (e.g. having $N_A \neq N_B$) to collapse on the same curve when using these units. Nevertheless, it is instructive to use them in order to make an easy comparison with the results shown previously (and in order to underline the coherence-enhancing effect brought by nuclear bath narrowing). Additionally, when $\tilde{\Omega}_A = \tilde{\Omega}_B$ one can show that for short times (when $C(\tilde{t}) \approx 1$), decay of concurrence is quadratic in time $C(\tilde{t}) \approx 1 - 2\tilde{t}^2/\tilde{\Omega}^2$. For long times no universal result for QDs with $T^*_{2,A} \neq T^*_{2,B}$ exist, but numerical results shown in Fig 2.2, which are obtained for QDs of different sizes (solid and dashed lines correspond to $N_A = N_B$ and $N_A = 2N_B$, respectively), are almost indistinguishable.

2.5.3.2 Narrowing of the Overhauser field gradient – the case of correlated baths

In the case of correlated state of nuclear spin baths described by Eq. (2.5), the first thing to notice is the major difference in decoherence of $|\Phi_\pm\rangle$ and $|\Psi_\pm\rangle$ states. The coherence of $|\Phi_\pm\rangle$ states averaged over quasistatic values of h^z_A and h^z_B (denoted by $\langle..\rangle_z$) gives

$$\rho_{++,--}(t) \propto \langle \exp\bigl(-i(h^z_A + h^z_B)t\bigr)\rangle_z \propto \exp\Bigl(-(t/T^*_2)^2\Bigr), \tag{2.59}$$

where T^*_2 is given by Eq. (2.44). Despite the fact that the difference of h^z_A and h^z_B has diminished fluctuations, the distribution of each of $h^z_{A,B}$ is still the same as for the high-temperature state (with the only exception of the case of maximal Δh^z corresponding to two baths fully polarized in opposite directions). On the contrary, the $|\Psi_\pm\rangle$ states are unaffected by inhomogeneous broadening, because under averaging over $h^z_{A,B}$ the coherence is affected only by fluctuations of the transverse components of the Overhauser fields $\rho_{+-,-+}(t) \propto \langle \exp(-i\Delta h^z t)\rangle_z = \exp(-i\Delta h^z t)$. It can be stated in other words that the $|\Psi_\pm\rangle$ states form a decoherence-free subspace [178, 179, 180] with respect to correlated pure-dephasing noise. This effect is demonstrated in Fig. 2.4, where concurrence was obtained in the UC approach

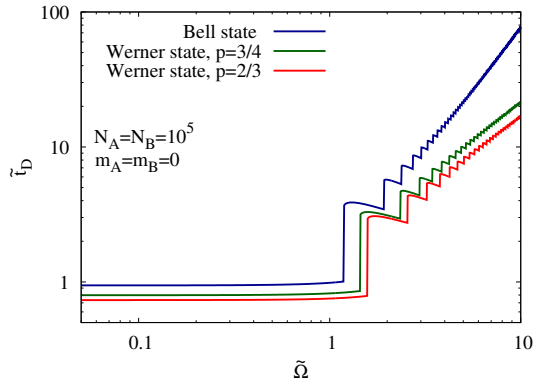

Figure 2.3: Time of final entanglement death for Bell states (the results are the same for all the states) and Werner states (see Eq. (2.45)) with $p=2/3$ and $3/4$. The nuclear baths for the two dots are uncorrelated, and each is narrowed to the state of $h^z = 0$. Calculation is done within the UC model with $N_A = N_B = 10^5$. Time is in units of two-dot T_2^* defined in Eq. (2.44), and the dimensionless Zeeman splitting is $\tilde{\Omega} := \Omega T_2^*$. The figure is reproduced from Ref. [1].

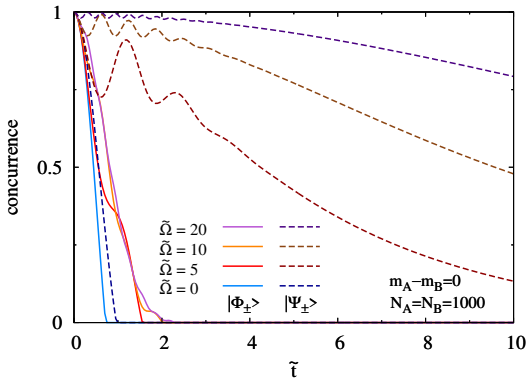

Figure 2.4: Decay of concurrence of $|\Phi_\pm\rangle$ and $|\Psi_\pm\rangle$ Bell states interacting with correlated nuclear baths in a state of strongly narrowed distribution of $\Delta h^z := h_A^z - h_B^z$ (taken to be $\Delta h^z = 0$ here). Calculations are performed using the UC approach. The $|\Phi_\pm\rangle$ states (solid lines) decay just like in the thermal bath case (compare with Fig. 2.1), while the decay of $|\Psi_\pm\rangle$ states (dashed lines) is very similar to the decay observed in the case of separate narrowing of each of the nuclear baths (compare with Fig. 2.2), only the fast oscillations of $C(t)$ are absent for $t \gtrsim T_2^*$. Time is in units of two-spin T_2^* defined in Eq. (2.44), and the dimensionless Zeeman splitting is $\tilde{\Omega} := \Omega T_2^*$. The figure is reproduced from Ref. [1].

using Eqs. (2.11) and (2.39) for all the Bell states are shown for $\Delta h^z = 0$. The entanglement of $|\Phi_\pm\rangle$ states decays basically in the same way as in Fig. 2.1, whereas the shape of $C(\tilde{t})$ dependence for $|\Psi_\pm\rangle$ states resembles that from Fig. 2.2.

The relationship between the entanglement evolution in the case of the correlated bath and that of uncorrelated baths can be easily seen at high magnetic fields, $\Omega \gg \sigma_\mathrm{h}$. The concurrence of Bell states is approximately proportional to the relevant coherence, which can be related to functions $K_{a,p_Q}^{Q,\sigma\bar{\sigma}}$ (where $p_Q \in [-1,1]$ is the polarization of the dot Q) describing single-spin coherence decay. For example, for $|\Psi_\pm\rangle$ states, using Eq. (2.7), and defining $\Delta p := p_A - p_B = \Delta h^z / \mathcal{A}J$, one can obtain

$$\frac{\rho_{+-,-+}(t)}{\rho_{+-,-+}(0)} = \sum_{p_A} w(p_A;\Delta p) K_{a,p_A}^{A,+-}(t) K_{a,p_B=p_A-\Delta p}^{B,-+}(t), \tag{2.60}$$

where the $K_{a,p_Q}^{Q,\sigma\bar{\sigma}}$ are the single-dot dephasing functions, i.e. the relevant two-spin coherence is an appropriately weighted average over results of calculations assuming uncorrelated baths. The UC approximation allows to get easily the expression for the distribution of weights. Using the notation from Eqs. (2.5) and (2.7) one has

$M_Q(p_Q) = \sum_{j_Q \geq |JN_Q p_Q|} n_{j_Q}$ and

$$w(p_A; \Delta p) = \frac{M_A(p_A) M_B(p_B = p_A - \Delta p)}{\sum_{p_A} M_A(p_A) M_B(p_B = p_A - \Delta p)}. \tag{2.61}$$

The behavior of the expression Eq. (2.60) originates from the fact that according to an approximate formula Eq. (5.11) the degeneracy factors $n_{j_Q} \sim j_Q \exp(-2j_Q^2/N)$ decrease rapidly with j_Q for $j_Q \gg \sqrt{N_Q/2}$. So, the weights from Eq. (2.61) are maximized when $p_A = \Delta p N_B/(N_A + N_B) =: \bar{p}_A$ (to which $p_B = -\Delta p N_A/(N_A + N_B) =: \bar{p}_B$ corresponds). This is shown in Figs. 2.5, 2.6, where $w(m_A; \Delta m)$ with $m_A = p_A N_A J$ is plotted. In other words, the sum of Eq. (2.60) is dominated by the narrowed bath states corresponding to these $\bar{p}_Q$. After performing the summation, the fast oscillations of the NFID coherence signal are averaged out at times $t > T_2^*$. Therefore, the coherence (and hence, entanglement) decay can be approximated as

$$\frac{\rho_{+-,-+}(t)}{\rho_{+-,-+}(0)} \approx K^{A,+-}_{a,\bar{p}_A}(t) K^{B,-+}_{a,\bar{p}_B}(t), \tag{2.62}$$

where $K^{Q,\sigma\bar{\sigma}}_{a,\bar{p}_Q}$ are the oscillation-free functions from Eq. (2.58). This derivation relied on assuming that the relevant $m_Q \gg \sqrt{N_Q/2}$, but when $\Delta p = 0$ Eq. (2.60) is dominated by $m_Q \lesssim \sqrt{N_Q}$, and the decay can be approximated by a product of two zero-polarization single-dot $K_a^{\sigma\bar{\sigma}}$ functions from Eq. (2.56). The shape of the distribution of weights $w(m_A; \Delta m)$ (namely, the fact that the highest weights are distributed in close vicinity of corresponding maximal value) and the obtained approximations explain the similarity of the entanglement decay between Fig. 2.2 and Fig. 2.4, illustrated in Fig. 2.7, where the entanglement decay for correlated baths calculated using UC model (with $\Delta h^z = 0$) is plotted with the corresponding results for uncorrelated baths (each narrowed to $h_Q^z = 0$), which are also calculated using UC model.

2.5.4 Entanglement echo

Because of the quasistatic origin of electron spin dephasing caused by a thermal nuclear spin bath, execution of the spin echo procedure restores efficiently single-qubit coherence [58, 181, 140]. Here it is important to make a note about features of echo signal: for electron spins in gated QDs, at low magnetic fields (when the time scale $t < N/\mathcal{A}$ is of interest) the dynamics of the echo signal is caused by nuclear Larmor precession, and the presence of distinct nuclear species with $\omega_\alpha \neq \omega_\beta$ [164, 111, 165, 140, 166] manifests at long times, specifically for times larger than $1/\omega_{\alpha\beta}$ (where $\omega_{\alpha\beta} := \omega_\alpha - \omega_\beta$).

Thus, the spin echo procedure applied to two electron spin qubits is expected to be efficient, especially in high magnetic fields, $\Omega \gg \sigma_\mathrm{h}$, when nuclear spin baths cause pure dephasing of qubits. When dealing with a single spin, the echo refocuses the coherence of superposition of $\hat{S}^z$ by application of π_x or π_y pulse ($-i\hat{\sigma}_x$ or $-i\hat{\sigma}_y$ operator, respectively), which amounts to exchange of amplitudes between $|+\rangle$ and $|-\rangle$ states. Any two-qubit state can also be subjected to simultaneous application of $\pi_{x/y}$ pulses [66, 67, 182] in order to recover its coherence. This procedure acts in the same way as the single qubit echo: for every Bell state, the π pulses interchange the amplitudes of the two relevant basis states. So, here the procedure of two-qubit

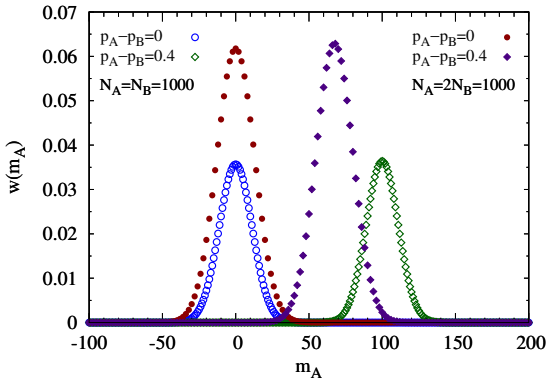

Figure 2.5: Typical distributions of normalized weights for individual (m_A, m_B)-pairs for two nuclear spin baths in correlated state $\Delta h^z := h_A^z - h_B^z \Leftrightarrow \Delta p := p_A - p_B = \frac{\Delta h^z}{\mathcal{A}J} \Rightarrow m_B = (m_A/N_A J - \Delta p) N_B J$ in the case of two identical QDs (open symbols) and in the case of two strongly asymmetric QDs (filled symbols). According to the formula discussed in Sec. 2.5.3.2, the maximum of the distribution occurs at $\bar{m}_A = \Delta p N_A N_B J/(N_A + N_B)$, which for $\Delta p = 0.4$ gives 100 ($66\frac{2}{3} \approx 67$) for symmetric (asymmetric) QDs and parameters used here. The normalization is $\sum_{m_A} w(m_A; \Delta m) = 1$. The figure is reproduced from Ref. [1].

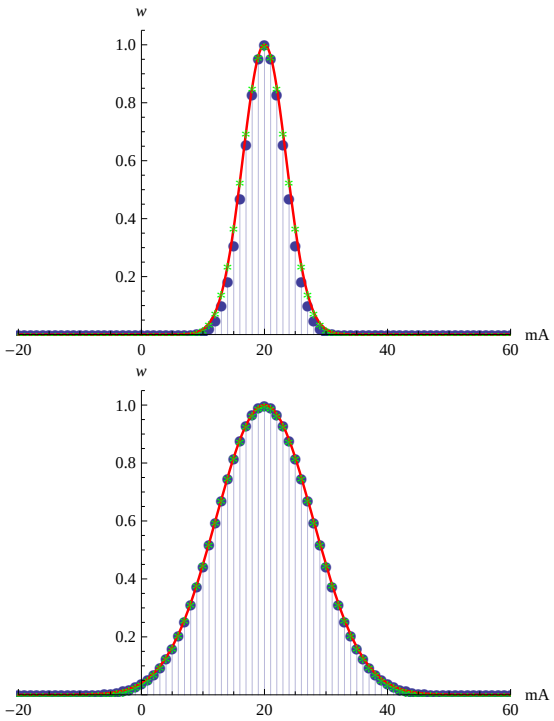

Figure 2.6: Distributions of weights for (m_A, m_B)-pairs for two nuclear spin baths of spins $\frac{1}{2}$ (upper panel) and $\frac{3}{2}$ (lower panel) in correlated state $\Delta h^z := h_A^z - h_B^z \Leftrightarrow \Delta p := p_A - p_B = \frac{\Delta h^z}{\mathcal{A}J} \Rightarrow m_B = (m_A/N_A J - \Delta p) N_B J$ in the case of two identical QDs ($N_A = N_B = 100$). Blue dots represent weights $w(m_A, m_B)$ calculated exactly for $\Delta m = 40$ which gives bath polarization $\Delta p = \frac{\Delta m}{NJ} = 0.8$ for spins $\frac{1}{2}$ and ≈ 0.27 for spins $\frac{3}{2}$. Green asterisks represent weights $w(m_A, m_B)$ calculated exactly (and shifted by 20 to the right) for $\Delta m = 0$ which gives bath polarization 0 for spins $\frac{1}{2}$ and $\frac{3}{2}$. The solid red line represents the approximated formula for weights $w(m_A; \Delta m) = \mathrm{e}^{-\frac{\left(m - \frac{\Delta m}{2}\right)^2}{2\sigma^2}}$, where $\sigma = \sqrt{\frac{1}{6} NJ(J+1)}$.

echo, which is realized by application of synchronized single-qubit π rotations, is considered. In low magnetic fields, $\Omega_Q \lesssim \sigma_\mathrm{h}$, on the time scale of $t \ll 1/\omega_{\alpha\beta}$ (when one can disregard the existence of distinct ω_α splittings of various nuclear species on that time scale) one can rely on the single-species UC approach to spin echo signal from Secs. 2.3.2 and 2.4.1.2 . In Fig. 2.9 the time-dependence of concurrence in a "real-time" version of the echo protocol is shown. For $t < \tau_1 = 4T_2^*$ the free evolution decay of entanglement is plotted, and for later times lines in this figure

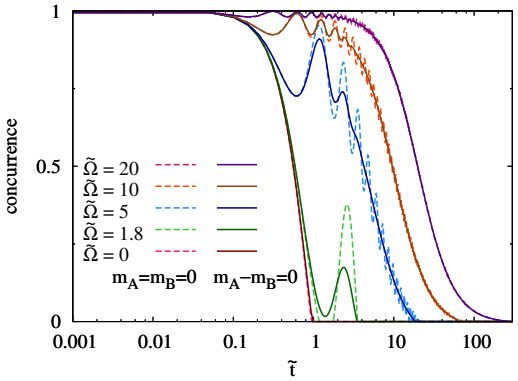

Figure 2.7: Concurrence decay for two electron spins interacting with two uncorrelated and correlated nuclear baths in narrowed states. The spins are initially in $|\Psi_+\rangle$ or $|\Psi_-\rangle$ Bell state and the dynamics of their reduced density operator is calculated using the UC approach. Dashed lines correspond to the case of separately narrowed baths (calculated for bath sizes $N_A = N_B = 10^5$), while solid lines correspond to the case of correlated state of the baths (calculated for bath sizes $N_A = N_B = 1000$) with $\Delta h^z = 0$. Time is in units of two-dot T_2^* defined in Eq. (2.44), and the dimensionless Zeeman splitting is $\tilde{\Omega} := \Omega T_2^*$. The figure is reproduced from Ref. [1].

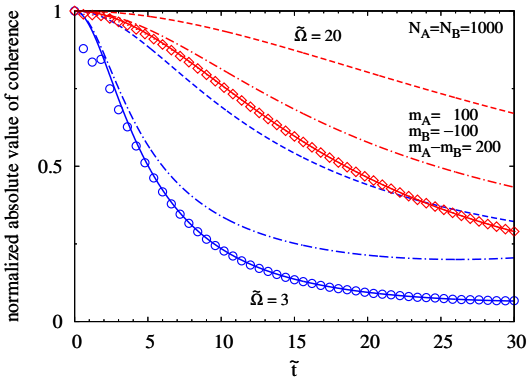

Figure 2.8: Normalized absolute values of single-qubit and two-qubit coherences (for initial $|\Psi_\pm\rangle$ state) calculated for two dots with $N_A = N_B = 1000$ in fields $\tilde{\Omega} = 3$ (in blue) and $\tilde{\Omega} = 20$ (in red). Dashed and dot-dashed lines correspond to coherences of qubits A and B, respectively, calculated using Eq. (2.58) assuming $p_A = 0.2$ and $p_B = -0.2$. Since h_Q^z is enhancing (suppressing) the total qubit splitting for dot A (B), the decays of these coherences are visibly distinct, especially for lower value of external field. Solid lines correspond to the absolute value of $K_{+-,-+}(t) = K_a^{A,+-}(t)\, K_a^{B,-+}(t)$ function from Eq. (2.62), i.e. the two-qubit coherence $\rho_{+-,-+}(t)$ calculated assuming uncorrelated narrowed baths. Symbols correspond to the absolute value of $\rho_{+-,-+}(t)$ calculated with the UC approach for correlated baths narrowed to $\Delta p = 0.4$. The agreement of the latter with the solid lines is very good for $\tilde{t} \gtrsim 1$ (at shorter times the UC solution exhibits oscillations, see solid lines in Fig. 2.7). The figure is reproduced from Ref. [1].

show the evolution of $C(t = \tau_1 + \tau_2)$ after application of π pulses at τ_1. In high enough magnetic fields, at $\tau_2 \approx \tau_1$ a partial entanglement recovery is observed. It is worth stressing that the two-qubit coherence is always partially recovered at the echo time (see the inset of Fig. 2.9), but the entanglement is regained only when magnetic field is above a certain value, i.e. $\tilde{\Omega} > 1$. This effect can easily be understood: in low magnetic fields, for $\tilde{\Omega} < 1$, the diagonal elements of the two-qubit density operator are strongly perturbed, and partial recovery of coherence is not sufficient for entanglement revival to occur, as follows from Eq. (1.5). For such a revival to occur

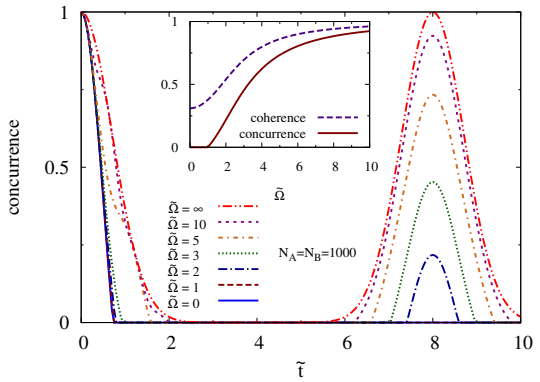

Figure 2.9: Concurrence as a function of time in the presence of echo π pulse at $\tilde{t}=4$ for different values of magnetic field, calculated for an initial Bell state. The calculation is performed within the UC model assuming a single nuclear species, on time scale of $t \ll \omega_\alpha$ (so that the values of ω_α are irrelevant and in the calculation they are assumed to be zero). Note that for $\tilde{\Omega}=0$ and 1 the entanglement does not revive at the echo time of $\tilde{t}=8$. For larger $\tilde{\Omega}$ the entanglement is indeed revived by the echo procedure and its maximal value grows with increasing $\tilde{\Omega}$. Inset: absolute value of normalized two-qubit coherence vs. entanglement at the time of maximum of the echo signal as a function of $\tilde{\Omega}$. At lowest magnetic fields, the amount of recovered coherence is not large enough to lead to a recovery of entanglement. The figure is reproduced from Ref. [1].

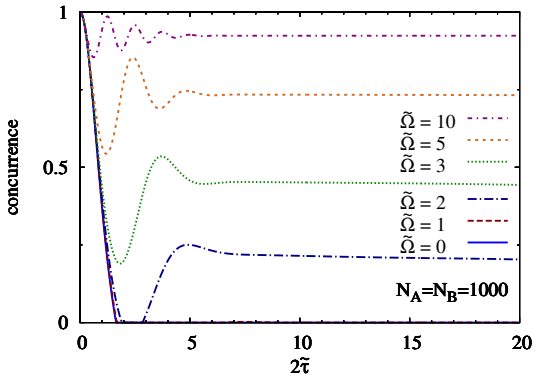

Figure 2.10: Concurrence at the maximum of echo-induced revival as a function of total echo sequence time for various magnetic fields calculated using the UC approach. The electron spins are initially in one of the Bell states and interact with two separate baths consisting of a single nuclear species. The figure is reproduced from Ref. [1].

the echoed coherence must fulfill the relation $|\rho_{ab}| > \sqrt{\rho_{cc}\rho_{dd}}$, where ρ_{cc} and ρ_{dd} are the occupations created by bath-induced qubit dynamics). In Fig. 2.10, dependence of echo peak amplitude on the total sequence time $2\tilde{\tau}$ is shown. In higher magnetic fields, $\tilde{\Omega} \gg 1$, the entanglement of the system of homonuclear spins quickly, on time scale of $2\tilde{\tau} \approx 1$, reduces by an amount $\propto 1/\tilde{\Omega}^2$ and then it stays nearly constant. This effect was discussed in Refs. [110, 165] where it has been shown that the echo procedure removes almost perfectly the influence of transverse Overhauser fields on electron spin coherence. It was shown in Ref. [165] that at longer times single-spin echo signal of such a homonuclear system has a small-amplitude oscillation of $C(t)$ with frequency ω, therefore the echoed entanglement of two spin qubits will also oscillate in the same manner. Finally, at much longer times the entanglement would decay completely due to dephasing caused by intrabath dynamics induced by dipolar interaction between nuclear spins [183, 184, 110, 185].

2.5.5 Projection on a singlet and averaged teleportation fidelity as witnesses of decaying entanglement

Lastly, I show that other methods of proving the existence and quantifying the amount of entanglement in the system of two electron spin qubits can be as useful as the measure of entanglement (e.g. concurrence). In this subsection, the methods introduced in Sec. 2.5.1 are analyzed, i.e. the measurement of an entanglement witness related to the projection on one of the Bell states (say, singlet $|\Psi_-\rangle$) and the measurement of the averaged quantum teleportation fidelity. These methods are reasonable to use only when one has some prior knowledge of the character of the mixed entangled state $\hat{\rho}(t)$, to which they will be applied. So, summing up the above consideration of the time evolution of state of two electron spins initially being in one of Bell states, one can state that:

- the X form of the two-qubit state is preserved during the whole evolution;
- only the initially nonzero coherence remains finite when free evolution is considered (in the case of spin echo this statement is only approximately true, since the second coherence is in fact generated during the evolution, but its magnitude is of the order of $1/\tilde{\Omega}^2$ in high magnetic fields);
- initially zero occupations become finite (in high magnetic fields, of magnitude of the order of $1/\tilde{\Omega}^2$), and their values are approximately equal;
- initially nonzero coherence decays due to the dominantly pure-dephasing influence of the bath.

Therefore, the state $\hat{\rho}(t)$ is a Werner-like state with diminished coherence,

$$\hat{\rho}(t) \approx \begin{pmatrix} \frac{1-p(t)}{4} & 0 & 0 & 0 \\ 0 & \frac{1+p(t)}{4} & -|\rho_{23}(t)|\mathrm{e}^{-i\gamma(t)} & 0 \\ 0 & -|\rho_{23}(t)|\mathrm{e}^{i\gamma(t)} & \frac{1+p(t)}{4} & 0 \\ 0 & 0 & 0 & \frac{1-p(t)}{4} \end{pmatrix}, \tag{2.63}$$

where it is assumed that the initial state was $|\Psi_-\rangle$, $p(t) \approx 1 - 2\big(K_b^A(t) + K_b^B(t)\big)$ (for a free evolution and assuming $K_b^{Q,+} \approx K_b^{Q,-}$), and $\gamma(t)$ is a possibly non-trivial phase.

It should be stressed that the entanglement of these states depends only on the modulus of $\rho_{23}(t)$. In the above density operator, in the case of free evolution and high-temperature nuclear spin bath state, one has $\gamma(t) = (\Omega_A - \Omega_B)t$, so a non-trivial phase appears when external magnetic field is non-uniform and there is a magnetic field gradient between the QDs. Nuclear spin baths in narrowed states, apart from direct change of Ω_Q by a value corresponding to h_Q^z, give rise to another effect. In the simplest configuration when $h_Q^z = 0$ and magnetic field gradient is off, due to the presence of the phase term in Eq. (2.56), one has $\gamma(t) = \arctan(t/\tau_A) - \arctan(t/\tau_B)$, where τ_Q given in Eq. (2.57) depends on the bath size N_Q. This results in non-trivial phase dynamics in the case of non-identical QDs. Similar reasoning applies for initial $|\Phi_\pm\rangle$ state, for which one obtains $\gamma(t) = (\Omega_A + \Omega_B)t$ in the thermal bath case, so these states will always have a fast phase dynamics at finite magnetic field. But when two-spin echo procedure is applied, $\gamma = 0$.

In the case $\gamma=0$, the witness proposed in Sec. 2.5.1, $\hat{w}_{\rm S}=1-\hat{P}_{\rm S}$ is an optimal one [153], since it always detects entanglement when it is actually present in the system. This fact for the maximally mixed bath case was previously discussed in Ref. [162].

It is easy to see that $\langle\hat{w}_{\rm S}\rangle=-\frac{1}{2}C(t)$. Below, the expectation value $P_{\rm S}(t)=\mathrm{Tr}\big(\hat{\rho}(t)\hat{P}_{\rm S}\big)$ will be shown. Analyzing that quantity, one should remember that $P_{\rm S}(t)>1/2$ confirms entanglement (and also estimates its amount quantitatively). However, for $\gamma(t)\neq0$, values below the threshold $P_{\rm S}(t)<1/2$ do not certify that the state is necessarily separable. The projection onto the singlet state can be expressed in terms of density operator elements: $P_{\rm S}(t)=|\rho_{23}(t)|\cos\gamma(t)+(p(t)+1)/4$, while $C(t)=\max[2|\rho_{23}(t)|-(1-p(t))/2,0]$.

The averaged quantum teleportation fidelity, used as an entanglement witness, shows similar behavior. For concreteness, let us suppose that two qubits are initialized in the state $|\Psi_-\rangle$. The teleportation protocol based on this assumption works perfectly when two-qubit state $\hat{\rho}(t)$ corresponds to a pure state $|\Psi_-\rangle$.

If two-qubit state $\hat{\rho}_{\rm AB}(t)$ is of the X form, then the initial state $|\psi_{\rm C}\rangle=\alpha|+\rangle+\beta|-\rangle$ of qubit C transforms after teleportation (using protocol for singlet $|\Psi_-\rangle$) in a state of qubit B:

$$\hat{\rho_{\rm B}}(t)=\begin{pmatrix}|\alpha|^2(\rho_{22}+\rho_{33})+|\beta|^2(\rho_{11}+\rho_{44}) & -2(\alpha^*\beta\mathrm{Re}\rho_{14}+\alpha\beta^*\mathrm{Re}\rho_{23})\\ -2(\alpha\beta^*\mathrm{Re}\rho_{14}+\alpha^*\beta\mathrm{Re}\rho_{23}) & |\alpha|^2(\rho_{11}+\rho_{44})+|\beta|^2(\rho_{22}+\rho_{33})\end{pmatrix}, \tag{2.64}$$

and the fidelity of teleportation of qubit C in state $|\psi_{\rm C}\rangle$ is

$$\begin{aligned}F_{\alpha,\beta}=&\,2|\alpha|^2|\beta|^2(\rho_{11}-\rho_{22}-\rho_{33}+\rho_{44})-4|\alpha|^2|\beta|^2\mathrm{Re}\rho_{23}\\&+\rho_{22}+\rho_{33}-4\mathrm{Re}\Big((\alpha\beta^*)^2\Big)\mathrm{Re}\rho_{14}.\end{aligned} \tag{2.65}$$

By substituting the explicit form of density operator $\hat{\rho}(t)$ from Eq. (2.63) of qubits A and B one obtains

$$F_{\alpha,\beta}(t)=-2p(t)|\alpha\beta|^2+4|\alpha\beta|^2|\rho_{23}(t)|\cos\gamma(t)+\frac{1+p(t)}{2}. \tag{2.66}$$

Characteristically, the fidelity of teleportation of basis states (the only states with no coherence, by definition), $|+\rangle$ and $|-\rangle$, does not require any coherence and is determined by population function $p(t)$ (it is equal to $(1+p)/2$). Hence, measuring the teleportation fidelity of a basis state instantly after the initialization the two-qubit state in a Werner state gives the value of p. The teleportation fidelity averaged over the teleported states is

$$\bar{F}(t)=\frac{2}{3}|\rho_{23}(t)|\cos\gamma(t)+\frac{1}{2}+\frac{p(t)}{6}. \tag{2.67}$$

When $\gamma=0$, one has $\bar{F}(t)=C(t)/3+2/3$, therefore, when $\bar{F}=2/3$ the corresponding $\hat{\rho}(t)$ state is separable. The nonzero $\gamma(t)$ forces the averaged fidelity to oscillate between 1/3 and 1. It is worth to note that if $\bar{F}<1/2$ then it means that the teleported state is anticorrelated with the desired state, and it is a pronounced sign of using the wrong assumption about the two-qubit state $\hat{\rho}(t)$ (i.e. using a wrong teleportation protocol). Projection onto the singlet state $P_S(\tilde{t})$ and averaged teleportation fidelity $\bar{F}(\tilde{t})$ in the case of $\gamma=0$ are shown for thermal and narrowed bath states in Figs. 2.11 and 2.13, respectively.

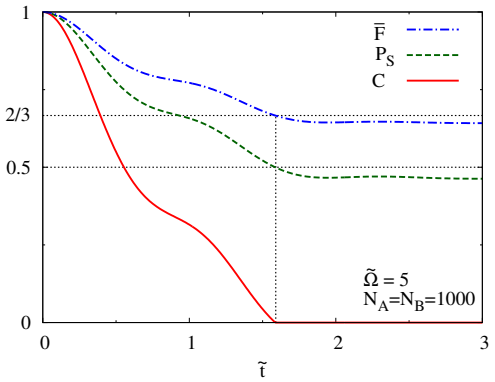

Figure 2.11: Concurrence $C(\tilde{t})$, projection on singlet $P_{\mathrm{S}}(\tilde{t})$, and averaged fidelity of teleportation $\bar{F}(\tilde{t})$ for two electron spins initially being in a singlet state $|\Psi_-\rangle$ for the case of interaction with two separate nuclear spin baths in high-temperature states calculated using the UC approach at $\tilde{\Omega} = 5$. The vertical dotted line marks the time at which the state becomes disentangled, while the horizontal dotted lines at 0.5 and 2/3 correspond to values at which $P_{\mathrm{S}}(\tilde{t})$ and $\bar{F}(\tilde{t})$, respectively, cease to indicate the presence of entanglement. Time is in units of two-dot T_2^* defined in Eq. (2.44), and the dimensionless Zeeman splitting is $\tilde{\Omega} := \Omega T_2^*$. The figure is reproduced from Ref. [1].

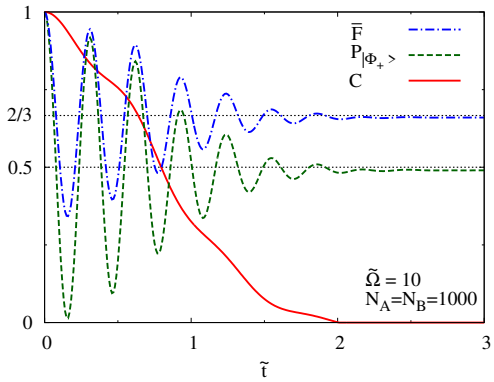

Figure 2.12: Concurrence $C(\tilde{t})$, projection on $|\Phi_+\rangle$ Bell state $P_{|\Phi_+\rangle}(\tilde{t})$, and averaged fidelity of teleportation $\bar{F}(\tilde{t})$ for two electron spins initially being in $|\Phi_+\rangle$ state for the case of interaction with two separate nuclear spin baths in thermal states calculated using the UC approach for $\tilde{\Omega} = 10$. The figure is reproduced from Ref. [1].

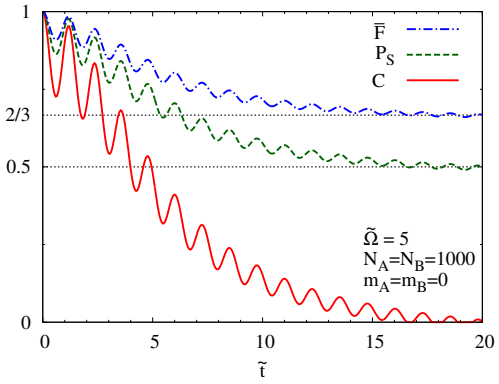

Figure 2.13: The same as above, only for narrowed state of A and B baths (each having $h_Q^z = 0$). The figure is reproduced from Ref. [1].

From these figures, it is clear that the presented quantities contain the same information about two-qubit entanglement as the concurrence does. The result for $P_{\mathrm{S}}(\tilde{t})$ from Fig. 2.11 corresponds to moderate magnetic field ($\tilde{\Omega} = 5$), and it fills

the gap between limiting cases of $\tilde{\Omega} \ll 1$ and $\tilde{\Omega} \gg 1$ which have been investigated experimentally and theoretically in Ref. [58].

The effect of $\gamma(t) \neq 0$ is shown in Fig. 2.12, where the entanglement decay of $|\Phi_+\rangle$ state is presented. The projection $P_{|\Phi_+\rangle}(t)$ and averaged teleportation fidelity $\bar{F}(t)$ have been calculated assuming that $|\Phi_+\rangle$ state is used during execution of corresponding procedures as the resource of entanglement. The results show strong oscillatory behavior, but their envelopes are analogous to the results for $|\Psi_-\rangle$ state (Fig. 2.11), and also contain information about the amount of two-qubit entanglement. Finally, it is worth noticing that if phase dependence $\gamma(t)$ is known, one can employ an experimental procedure which results in projection onto (or teleportation with) a "proper" state. On the other hand, if one knows $\gamma(t)$, then one can perform post-processing of experimental data in order to obtain the smooth decay curves.

2.6 Conclusions

In this chapter, the dynamics of the entanglement of two electron spin qubits interacting with their nuclear spin baths was considered. Specifically, the influence of various states of the nuclear spin bath (e.g. high-temperature state, narrowed states, correlated states) on the entanglement decay during free evolution and two-spin echo procedure was investigated.

It has been shown that hyperfine interaction of two electron spins initially being in a Bell state with the nuclear spin baths leads to forming of a Werner-like two-qubit state: in moderate and high magnetic fields initial coherence reduces due to pure dephasing, and initially absent populations get nonzero value $\propto 1/B^2$. The dynamically generated admixture $\propto \mathbb{1}$ manifests in appearance of entanglement sudden death at finite time, when coherence is still present in the system. In moderate magnetic fields, varying in time populations of electron spins interacting with nuclear baths in narrowed states may cause a revival of entanglement after its sudden death. Using the quantum information terms, one can say that the entanglement decay induced by the hyperfine interaction of electron spin qubits with nuclear spin environment can be viewed as a non-Markovian phase damping quantum channel with an admixture of generalized amplitude dumping corresponding to the infinite-temperature environment. It has been shown that the entanglement dynamics of two qubits interacting with nuclear spin baths in a correlated narrowed state can be reproduced assuming uncorrelated states of the two baths with certain polarizations, values of which correspond to the maximums in the weight distributions of polarization pairs associated with a given correlated state.

It has been shown that the entanglement can be recovered by application of the two-spin echo procedure. Local manipulations (π pulses) performed with qubits allow to rephase two-qubit coherence and to revive their entanglement. This procedure, however, is efficient only in high enough external magnetic fields. There exist the lowest strength of magnetic field (which equals approximately the typical Overhauser field of QD), below which the procedure gives no effect at all.

Finally, it has been shown that considered decay of entanglement of two electron spin qubits, initially being in a Bell state, can be detected and, what is more important, quantified without experimentally demanding tomography of two-qubit state. The level of two-qubit entanglement (e.g. concurrence) can be faithfully inferred from measurement of entanglement witness (projection of the current two-qubit

state on the initial, maximally entangled, one) or from measurement of the averaged fidelity of state of the third qubit, which was teleported spending two-qubit entanglement during execution of that operation. The entanglement of Werner-like states generated from the initial Bell state during free evolution due to the hyperfine interaction of electron spins with nuclear spin baths is uniquely connected with the results of the above-mentioned measurements, hence, in this particular system these measurements detect the two-qubit entanglement and quantify it identically as concurrence does.

Chapter 3

Retardation of Entanglement Decay of Two Spin Qubits by Quantum Measurements

In this chapter, I study a system of two electron spins, each interacting with its small nuclear spin environment. Such a system can be viewed as a prototype system of two qubits that are based on the spins of electrons localized in two quantum dots. I propose a way to counteract the decay of entanglement of such qubits by performing some manipulations on them (which are within reach of experimentalists), e.g. repeatable quantum projective measurements of these qubits. Unlike in the quantum Zeno's effect, the goal of the proposed manipulations is not to freeze two qubits in their initial state and to preclude any time evolution of the state by infinitely frequent quantum measurements. Instead of that, performing a few cycles of free evolution of the system for some time τ followed by a quantum measurement of qubits subsystem with subsequent postselection of two-qubit state (the same as the initial one) produces quantum correlations in the environments and also restores the quantum correlations of qubits. By numerical calculation of the system evolution (the full density operator $\hat{\rho}(t)$), I show that, in contrast to the fast decay of two-qubit entanglement which occurs in case of free evolution, application of the proposed manipulation sequence gradually builds up coherences in the entire system, and further decay of quantum correlations of two qubits may be significantly slowed down for specific combinations of cycle durations τ and numbers of performed cycles. The results contained in this chapter have been presented at a few conferences (see List of Conference Presentations on p. 129) and are publicly available as a preprint [186].

3.1 Introduction

Spin of an electron localized on a QD in a semiconductor nanostructure is a promising physical realization of qubit as it can be reliably initialized, manipulated, and read out [47, 48, 55]. To be a useful element of a quantum computer, such a qubit must fulfill, among others, the criterion of long decoherence times [73, 187]. Providing no manipulations aimed at mitigation of the influence exerted by the environment on the spin qubits have been applied, coherences as well as quantum correlations of electron spin QD qubits decay on a nanosecond time scale [47, 48, 108]. The main factor of such a fast decay is the Fermi contact hyperfine interaction of electron spin with nuclear spins of atoms from which the nanostructure is built [162, 1].

There have already been proposed and implemented in experiment a few strategies to enhance the decoherence times of electron spin, such as: dynamical decoupling of spin qubits from their environments [140]; preparing an artificial state of environment (so-called narrowed state of nuclear spin bath) [120]; or simply making use of materials which are made of atoms with spinless nuclei, e.g. isotopically-purified ^{28}Si [188]. All these strategies can be summarized as: avoiding as much as possible any interaction of the qubits with their environments.

In this chapter I propose another strategy to counteract the decoherence and, as a consequence, to inhibit the decay of quantum correlations of two electron spin qubits. I explore the process of transfer of coherences and quantum correlations from a pair of entangled electron spin qubits to the environment, combined with quantum measurements of the qubits' subsystem. Provided that the evolution of the system is non-Markovian, i.e. it preserves some memory of past interactions, it turns out that the environment, being in a quantum state obtained after a period of free evolution of the system, can dephase the qubits with a lower rate. Using a simple model of a system of two electron spin QD qubits, presented in Sec. 3.2, I investigate the effect of application of the manipulation procedure described in Sec. 3.3 on dynamics of entanglement decay. Results are discussed in Sec. 3.4, where it is shown that both parts of the procedure, namely, free evolution of the system and quantum measurement of the qubits' subsystem with subsequent postselection of the two-qubit quantum state, are equally important, and that only for specific combinations of durations τ of free evolution periods and number n of cycles, significant retardation of entanglement decay can be achieved.

I would like to stress that the proposed manipulation procedure is not a realization of the quantum Zeno's effect [189]. Here, the goal is not to freeze qubits in their initial state and to preclude any time evolution of the state by infinitely frequent quantum measurements. Instead of that, we let qubits interact with their environments and transfer to them some coherences and quantum correlations during the evolution of the joint system.

3.2 The Model of Electron Spin Quantum Dot Qubits

To begin with, I describe the model of electron spin QD qubits, which will be used to illustrate the proposed manipulation sequence. I consider a system of two semiconductor QDs (e.g. gated QDs created in AlGaAs/GaAs nanostructure or self-assembled InGaAs QDs), each of which has a localized electron. Since such systems are usually operated at low temperatures, I suppose that electrons are in their

ground orbitals. In such a case, one can exclude from further consideration the spatial part of the electron's wave functions and focus only on the spin part of the wave functions.

3.2.1 Two non-interacting quantum dots

For the sake of clarity, I first assume that during periods of free evolution of the system there is no interdot interaction, which could create some entanglement between the two QDs and, especially, between electron spins (e.g. electrons are strongly localized in QDs because of a high enough inter-QD potential barrier or relatively long distance between the QDs and the electron wave functions hardly overlap, so no interaction between the two electron spins occurs). It is worth mentioning that we will be analyzing the behavior of entanglement on the timescale from 0 to a few T_2^* (see Eq. (3.21) for the definition of T_2^*). For such short times no part of the interaction Hamiltonian, apart from the Fermi contact hyperfine interaction of electron spin with nuclear spins from its environment, is essential, because it does not manifest at short times (e.g. the energies of dipolar or quadrupolar interaction of nuclear spins are orders of magnitude lower than energy of hyperfine interaction), whereas the Fermi contact hyperfine interaction leads to the fast complete decay of entanglement initially present in the electron spins subsystem in any finite (including zero) magnetic field, as shown in the previous Chapter (see Fig. 2.1).

Thus, the Hamiltonian of the DQD system has the form:

$$\hat{H}_{\mathrm{DQD}} = \hat{H}^{(1)}_{\mathrm{QD}} \otimes \mathbb{1} + \mathbb{1} \otimes \hat{H}^{(2)}_{\mathrm{QD}}. \tag{3.1}$$

The Hamiltonian $\hat{H}^{(i)}_{\mathrm{QD}}$ of a single QD contains the following terms:

$$\hat{H}^{(i)}_{\mathrm{QD}} = \hat{H}^{(i)}_{\mathrm{el.}} + \hat{H}^{(i)}_{\mathrm{nucl.\ env.}} + \hat{H}^{(i)}_{\mathrm{int.}}. \tag{3.2}$$

The first and the second terms of $\hat{H}^{(i)}_{\mathrm{QD}}$ are the Zeeman energies of electron spin and its nuclear spin environment (NSE), respectively:

$$\hat{H}_{\mathrm{el.}} = \Omega \hat{S}_z \otimes \mathbb{1}^{\otimes N}, \tag{3.3}$$

where $\Omega = g_{\mathrm{eff.}} \mu_{\mathrm{B}} B_z$ is the Zeeman splitting of electron spin, $g_{\mathrm{eff.}}$ is the effective g-factor of electron spin, μ_{B} is the Bohr magneton, B_z is z component of external magnetic field, $\hat{S}_z$ is the operator of the z-component of electron spin, N is the number of nuclear spins interacting with the electron spin. For the sake of simplicity, I have also adopted the assumption that all the nuclear spins are of the same type J, so the identity operator $\mathbb{1}$ used above is of dimension $2J+1$.

$$\hat{H}_{\mathrm{nucl.\ env.}} = \mathbb{1}_{\mathrm{el.}} \otimes \sum_{n=1}^{N} \omega^{(n)} \mathbb{1}^{\otimes(n-1)} \otimes \hat{J}_z^{(n)} \otimes \mathbb{1}^{\otimes(N-n)}, \tag{3.4}$$

where $\omega^{(n)} = g^{(n)} \mu_{\mathrm{N}} B_z$ is the Zeeman splitting of nth nuclear spin, $g^{(n)}$ in the nuclear g-factor of nth nuclear spin, μ_{N} is the nuclear magneton, and $\mathbb{1}_{\mathrm{el.}}$ is the identity operator of the electron spin subspace.

The last term of the Hamiltonian $\hat{H}^{(i)}_{\mathrm{QD}}$ is the hyperfine interaction between electron spin and nuclear spins:

$$\hat{H}_{\mathrm{int.}} = \sum_{n=1}^{N} A_n \hat{\mathbf{S}} \otimes \mathbb{1}^{\otimes(n-1)} \otimes \hat{\mathbf{J}}^{(n)} \otimes \mathbb{1}^{\otimes(N-n)}, \tag{3.5}$$

where $\hat{\mathbf{S}} = \left(\hat{S}_x, \hat{S}_y, \hat{S}_z\right)$ is the electron spin operator, $\hat{\mathbf{J}}^{(n)} = \left(\hat{J}_x^{(n)}, \hat{J}_y^{(n)}, \hat{J}_z^{(n)}\right)$ is the spin operator of nth nucleus and A_n is the hyperfine coupling between electron spin and the nth nuclear spin.

3.2.2 Two quantum dots with coupled electron spins

When electrons are close enough to each other their wave functions noticeably overlap, which leads to appearance of two more terms of spin interactions: on one hand, the Hamiltonian of the system will acquire a term describing exchange interaction of electron spins, on the other hand, in such a system configuration each electron spin will interact with at least a few nuclear spins belonging to another QD, and thus electron spins become coupled indirectly through their common environment. Now, the Hamiltonian of the DQD system has the following terms:

$$\begin{aligned}\hat{H}_{\mathrm{DQD}}^{\mathrm{full}} = \hat{H}_{\mathrm{el.1}} + \hat{H}_{\mathrm{el.2}} + \hat{H}_{\mathrm{nucl.env.}} \\ + \hat{H}_{\mathrm{el.1-nucl.env.int.}} + \hat{H}_{\mathrm{el.2-nucl.env.int.}} \\ + \hat{H}_{\mathrm{el.1-el.2\,int.}}.\end{aligned} \tag{3.6}$$

All terms of the Hamiltonian, apart from the last term, which is a new one, have almost the same forms as previously (cf. Eqs. (3.2), (3.3), (3.4), (3.5)), with change of meaning of parameter N, which denotes now the number of all nuclear spins in the system, $N = N_1 + N_2$, where N_i is the number of nuclear spins in the ith QD:

$$\hat{H}_{\mathrm{el.1}} = \Omega^{(1)} \hat{S}_z^{(1)} \otimes \mathbb{1}_{\mathrm{el.}} \otimes \mathbb{1}^{\otimes N}, \tag{3.7}$$

$$\hat{H}_{\mathrm{el.2}} = \Omega^{(2)} \mathbb{1}_{\mathrm{el.}} \otimes \hat{S}_z^{(2)} \otimes \mathbb{1}^{\otimes N}, \tag{3.8}$$

$$\hat{H}_{\mathrm{nucl.\ env.}} = \mathbb{1}_{\mathrm{el.}}^{\otimes 2} \otimes \sum_{n=1}^{N} \omega^{(n)} \mathbb{1}^{\otimes(n-1)} \otimes \hat{J}_z^{(n)} \otimes \mathbb{1}^{\otimes(N-n)}, \tag{3.9}$$

$$\hat{H}_{\mathrm{el.1-nucl.env.int.}} = \sum_{n=1}^{N} A_n^{(1)} \hat{\mathbf{S}}^{(1)} \otimes \mathbb{1}_{\mathrm{el.}} \otimes \mathbb{1}^{\otimes(n-1)} \otimes \hat{\mathbf{J}}^{(n)} \otimes \mathbb{1}^{\otimes(N-n)}, \tag{3.10}$$

$$\hat{H}_{\mathrm{el.2-nucl.env.int.}} = \sum_{n=1}^{N} A_n^{(2)} \mathbb{1}_{\mathrm{el}} \otimes \hat{\mathbf{S}}^{(2)} \otimes \mathbb{1}^{\otimes(n-1)} \otimes \hat{\mathbf{J}}^{(n)} \otimes \mathbb{1}^{\otimes(N-n)}. \tag{3.11}$$

It is reasonable to assume that interaction between two electron spins in the considered system is of the form of Heisenberg exchange Hamiltonian with an isotropic constant coupling A_0 [73]:

$$\hat{H}_{\mathrm{el.1-el.2\,int.}} = A_0\, \hat{\mathbf{S}}^{(1)} \otimes \hat{\mathbf{S}}^{(2)} \otimes \mathbb{1}^{\otimes N}. \tag{3.12}$$

It is worth noting here the obvious fact about the Hamiltonian $\hat{H}_{\mathrm{DQD}}^{\mathrm{full}}$ (Eq. (3.6)) that when the coupling A_0 between electron spins is greater than the energy of

interaction of these electron spins with their nuclear environments ($A_0 > \mathcal{A}_1, \mathcal{A}_2$ where $\mathcal{A}_i := \sum_{n=1}^{N} A_n^{(i)}$ is the total energy of hyperfine interaction), the exchange interaction between electron spins helps to preserve initially present entanglement between electron spins. In the extreme case, when $\hat{H}_{\mathrm{el.1-el.2\,int.}}$ (Eq. (3.12)) is the leading interaction term of the Hamiltonian $\hat{H}_{\mathrm{DQD}}^{\mathrm{full}}$ (Eq. (3.6)), two electron spins initially being in singlet or unpolarized triplet state do not lose their coherence much during the evolution and remain in a state that is close to the initial one, because singlet and triplet states of electron spins turn out to be close to the eigenstates of the Hamiltonian $\hat{H}_{\mathrm{DQD}}^{\mathrm{full}}$ (Eq. (3.6)). Therefore, the level of two-qubit entanglement stays quite high and does not decay significantly during the evolution of the system, so any manipulation aimed at inhibition of the decay of entanglement is hardly needed in that case.

3.3 Manipulation Procedure with Quantum Measurements and Postselection of Two-Qubit State

Motivated by experimentalists' capabilities to initialize localized in QDs electrons in singlet state and to perform projective measurements onto singlet state [47, 48, 190], I consider a quantum measurement of two electron spins subsystem (hereinafter referred to as TESS or, simply, two qubits), specifically, the measurement answering whether TESS is in a certain two-qubit state or not. In general, such a quantum measurement can be described by the measurement operators $\hat{M}_1$ ("yes" result) and $\hat{M}_2$ ("no" result):

$$\hat{M}_1 = \sqrt{k}\,\hat{\Pi}_{2\mathrm{q}} \otimes \mathbb{1}_{2\mathrm{env}} + \sqrt{1-k}\,\left(\mathbb{1} - \hat{\Pi}_{2\mathrm{q}} \otimes \mathbb{1}_{2\mathrm{env}}\right), \tag{3.13}$$

$$\hat{M}_2 = \sqrt{1-k}\,\hat{\Pi}_{2\mathrm{q}} \otimes \mathbb{1}_{2\mathrm{env}} + \sqrt{k}\,\left(\mathbb{1} - \hat{\Pi}_{2\mathrm{q}} \otimes \mathbb{1}_{2\mathrm{env}}\right). \tag{3.14}$$

where $\hat{\Pi}_{2\mathrm{q}}$ is a projector in two-qubit subspace onto a chosen two-qubit state, parameter $k \in [\frac{1}{2}, 1]$ is a strength of the measurement, $\mathbb{1}$ is the identity operator of dimension of the system's state space, and $\mathbb{1}_{2\mathrm{env}}$ is the identity operator of dimension of the environment (two NSEs) subsystem's state space. The extreme values of the quantum measurement strength have clear physical meanings: $k = 1$ corresponds to the case of measurement of the highest strength, i.e. the projective measurement,

$$\hat{M}_1 = \hat{\Pi}_{2\mathrm{q}} \otimes \mathbb{1}_{2\mathrm{env}}, \tag{3.15}$$

$$\hat{M}_2 = \mathbb{1} - \hat{\Pi}_{2\mathrm{q}} \otimes \mathbb{1}_{2\mathrm{env}}, \tag{3.16}$$

and $k = \frac{1}{2}$ corresponds to the case of completely ineffective measurement,

$$\hat{M}_1 = \hat{M}_2 = \frac{1}{\sqrt{2}}\mathbb{1}. \tag{3.17}$$

The intermediate values of strength k correspond to such quantum measurements that give the outcomes which are the probabilistic mixture of the outcomes of projective operators $\hat{\Pi}_{2\mathrm{q}} \otimes \mathbb{1}_{2\mathrm{env}}$ and $\mathbb{1} - \hat{\Pi}_{2\mathrm{q}} \otimes \mathbb{1}_{2\mathrm{env}}$, i.e. the fidelity of the outcomes, compared with that of projective measurement, is determined by the measurement strength and is equal to k. By construction, the measurement operators $\hat{M}_1$, $\hat{M}_2$ fulfill the completeness relation $\sum_{i=1}^{2} \hat{M}_i^\dagger \hat{M}_i \equiv \mathbb{1}$ for any k from its range.

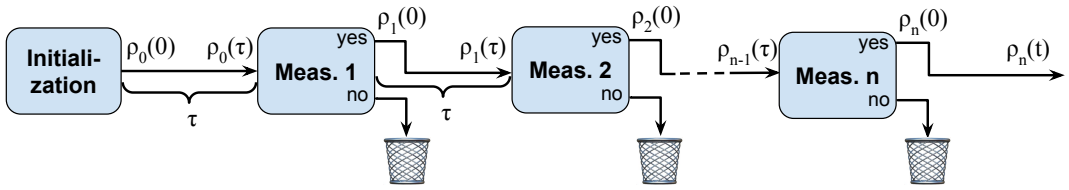

Figure 3.1: Schematic representation of the proposed manipulation sequence with quantum measurements and postselection of the two-qubit state. The procedure begins from initialization of the system in the state $\hat{\rho}_0(0)$, which contains maximally entangled two-qubit state. Next, free evolution is allowed for a time period τ, at the end of which the state $\hat{\rho}_0(\tau)$ is obtained. System being in that state is measured (specifically, the projection of the actual two-qubit state on the initial one is performed), that produces one of two possible outcomes. The "yes" outcome, referred to as $\hat{\rho}_1(0)$ state, is a useful state for possible further repetition of the described manipulation cycle of free evolution followed by the measurement or for immediate use as a quantum resource. When "no" result is obtained, i.e. the run of the procedure has not delivered the desired quantum state, the run is interrupted.

The manipulation procedure consists of initialization of the system in its initial state and a few manipulation cycles. The manipulation cycle, in turn, has two parts: free evolution of the system for a period τ and execution of quantum measurement with subsequent postselection of two-qubit state. The idea of the manipulation procedure is shown in Fig. 3.1. First, the system is initialized in a state $\hat{\rho}_{\text{ini}} = \hat{\rho}_{2\text{q}}(0) \otimes \hat{\rho}_{2\text{env}}(0) =: \hat{\rho}_0(0)$. The initial two-qubit state, $\hat{\rho}_{2\text{q}}(0)$, is supposed to be a maximally entangled state, whereas NSEs usually are in a high-temperature state [108], which has no coherences at all (if no manipulations have been performed on them beforehand). Such a choice of NSE initial state is physically motivated: even low temperatures of the order of a few tens mK, at which experiments with QDs are routinely performed, are already sufficiently high for nuclear spins due to the smallness of their Zeeman energies or dipolar interaction compared to $k_{\text{B}}T$ in typical experimental conditions. Thus, the initial state of NSEs has the form $\hat{\rho}_{2\text{env}}(0) = \hat{\rho}_{\text{env}_1}(0) \otimes \hat{\rho}_{\text{env}_2}(0)$, where $\hat{\rho}_{\text{env}_i}(0) = \frac{1}{Z_i}\mathbb{1}$, $Z_i = (2J+1)^{N_i}$, $i = 1, 2$.

After initialization, we let the system freely evolve for some period τ obtaining the state $\hat{\rho}_0(\tau) = \hat{U}(\tau)\hat{\rho}_0(0)\hat{U}^\dagger(\tau)$, where $\hat{U}(\tau) := \exp\left(-\frac{i}{\hbar}\hat{H}\tau\right)$. Next, the quantum measurement of TESS is performed producing, according to the measurement postulate of quantum mechanics [3], in an indeterministic way, one of two possible states

$$\hat{\rho}_1^{\text{yes}}(0) := \frac{\hat{M}_1\hat{\rho}_0(\tau)\hat{M}_1^\dagger}{\text{Tr}\left(\hat{M}_1\hat{\rho}_0(\tau)\hat{M}_1^\dagger\right)} \tag{3.18}$$

or

$$\hat{\rho}_1^{\text{no}}(0) := \frac{\hat{M}_2\hat{\rho}_0(\tau)\hat{M}_2^\dagger}{\text{Tr}\left(\hat{M}_2\hat{\rho}_0(\tau)\hat{M}_2^\dagger\right)} \tag{3.19}$$

with probabilities calculated according to the Born's rule $p^{\text{yes}} = \text{Tr}\left(\hat{M}_1\hat{\rho}_0(\tau)\hat{M}_1^\dagger\right)$ and $p^{\text{no}} = \text{Tr}\left(\hat{M}_2\hat{\rho}_0(\tau)\hat{M}_2^\dagger\right)$, respectively.

The state $\hat{\rho}_1^{\rm yes}(0)$, which corresponds to the operator $\hat{M}_1$, is postselected for further manipulations. If the outcome of the measurement happens to be the state $\hat{\rho}_1^{\rm no}(0)$, then it is rejected and execution of the manipulation procedure is interrupted. After successful execution of the nth manipulation cycle, the state

$$\hat{\rho}_n(0) \coloneqq \frac{\hat{\rho}_n^{\hat{M}_1}(0)}{\mathrm{Tr}\left(\hat{\rho}_n^{\hat{M}_1}(0)\right)}, \tag{3.20}$$

where $\hat{\rho}_n^{\hat{M}_1}(0) \coloneqq \hat{M}_1\hat{\rho}_{n-1}(\tau)\hat{M}_1^\dagger$, is obtained, for which I study the dynamics of its two-qubit entanglement.

3.4 Results and Discussion

I would like to note that it is crucial in the simulations to keep the density operator of the whole system, $\hat{\rho}_n(t)$, and not to reduce it to the two-qubit density operator $\hat{\rho}_{2\rm q}(t)$ by tracing out NSEs. Having at hand the full density operator, one can investigate the transfer of coherences and quantum correlations in the system to the greatest degree. As the dimension of the system state space grows exponentially with the number of nuclear spins, our capabilities to simulate application of the proposed manipulation procedure are limited to small systems, so I present here the results obtained for the system of two QDs with homonuclear ($J = \frac{1}{2}$) NSEs of the same size $N_1 = N_2 = 5$.

In the simulations, as an initial two-qubit state I have used singlet state, $\hat{\rho}_{2\rm q}(0) = |\psi_-\rangle\langle\psi_-|$, where $|\psi_-\rangle = \frac{1}{\sqrt{2}}\left(|\uparrow\downarrow\rangle - |\downarrow\uparrow\rangle\right)$, which is the easiest for initialization two-qubit state of two electron spins in a DQD. The projector operator $\hat{\Pi}_{2\rm q}$ has also been chosen to be the projector onto singlet state, $\hat{\Pi}_{2\rm q} = |\psi_-\rangle\langle\psi_-|$.

To quantify the amount of entanglement of two-qubit state $\hat{\rho}_{2\rm q}$, I use concurrence [21]. I also use negativity [23] to estimate the level of entanglement between two parts of the system. I show below that of particular interest is the negativity between TESS and NSEs.

While considering the quantum correlation dynamics, it is convenient for further analysis to express time in units of two-qubit T_2^* defined as follows (see Eq. (2.44))

$$\frac{1}{\left(T_2^*\right)^2} = \frac{1}{\left(T_2^{*(1)}\right)^2} + \frac{1}{\left(T_2^{*(2)}\right)^2}, \tag{3.21}$$

where $T_2^{*(i)}$ is the single-qubit dephasing time, for nuclear spin environment consisting of spins $J = \frac{1}{2}$ the single-qubit dephasing time is given by $T_2^{*(i)} = \sqrt{8}\hbar/\sqrt{\sum_{n=1}^{N_i}\left(A_n^{(i)}\right)^2}$. The decay of entanglement of two electron spin qubits plotted using time unit of T_2^* is independent of the system size and the magnitude of the hyperfine interaction (see Chapter 2).

The results of simulations, which are shown in figures 3.2–3.5, have been obtained for the system being in moderate magnetic field, $\Omega = 5\left[\frac{\hbar}{T_2^*}\right]$. In Fig. 3.2 the time dependencies of concurrence of two-qubit state (top panel) and negativity (bottom panel) are shown for a few different numbers n of performed cycles. As can be seen

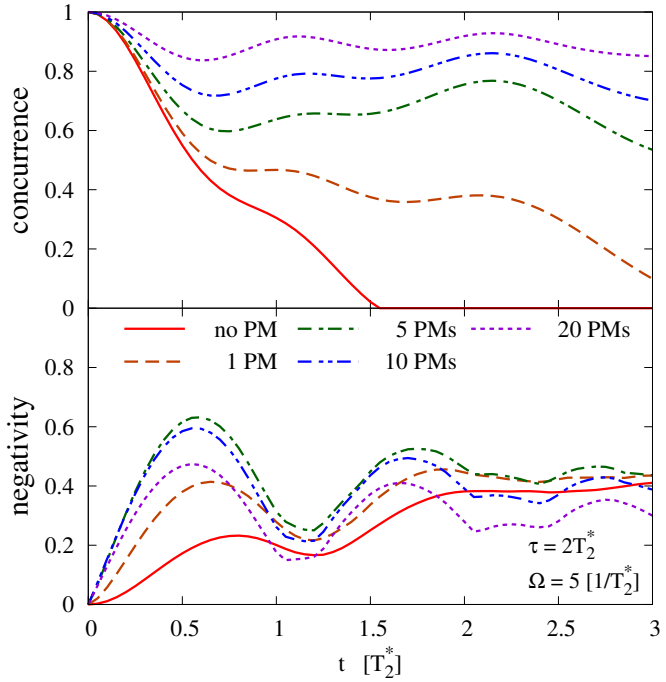

Figure 3.2: Concurrence of two-qubit state $\hat{\rho}_{2q}(t)$ and negativity calculated for the system state $\hat{\rho}_n(t)$ divided into two parts, TESS and NSEs, as functions of time t after the last projective measurement (PM). NSEs consist of $N_1 = N_2 = 5$ uniformly coupled spins $\frac{1}{2}$. The system is in moderate magnetic field, $\Omega = 5\left[\frac{\hbar}{T_2^*}\right]$. The projective measurements are performed after the period of system evolution $\tau = 2T_2^*$.

from the top panel of Fig. 3.2, normally entanglement is completely lost at time $t \approx 1.5T_2^*$, but application of just a single manipulation cycle causes a significant rise of the entanglement level at all times in the presented range and noticeably retards its decay. With increasing number n of performed cycles, the level of entanglement systematically grows, reaching almost its maximal value. Along with the decay of entanglement in TESS, one can see the appearance of entanglement between initially uncorrelated parts of the system, namely, between TESS and their NSEs (see bottom panel of Fig. 3.2).

In order to estimate the effect of retardation of entanglement decay produced by application of the manipulation procedure, I monitor the level of concurrence calculated for $t = 2T_2^*$, which is shown in Fig. 3.3, as a function of number n of performed projective measurements and period τ between them. Using this map, one can find the optimal values of the parameters n and τ, which maximize the retardation of entanglement decay. On one hand, increasing the number of manipulation cycles almost always enhances the effect, on the other hand, it turns out that there exists the optimal duration τ of the free evolution periods, which is $\tau_{\text{opt.}} \approx 2T_2^*$ for the simulated system.

The probability to obtain the desired state $\hat{\rho}_n(0)$, which is shown in left panel of Fig. 3.4, decreases monotonically with number n of performed cycles due to the fact that in each cycle the probability to obtain the postselected two-qubit state which is the same as the initial one is strongly less than one. It is also worth noting

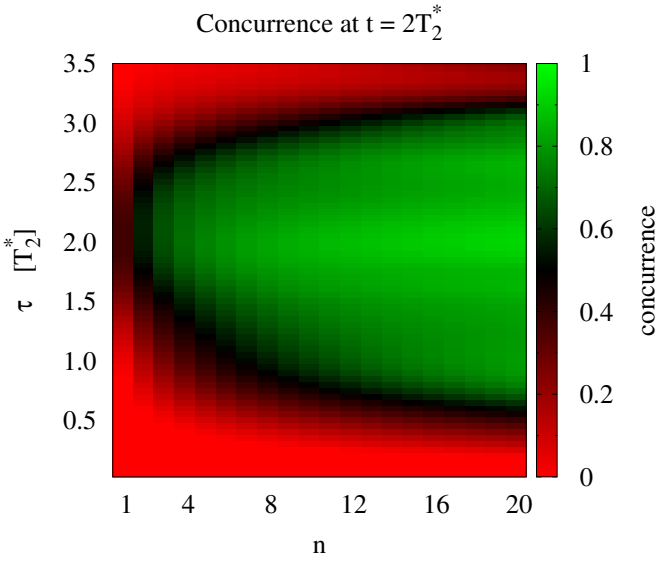

Figure 3.3: Concurrence calculated for $\hat{\rho}_{2q}(t = 2T_2^*)$ as a function of number n of performed projective measurements and period τ between them. NSEs consist of $N_1 = N_2 = 5$ uniformly coupled spins $\frac{1}{2}$. The system is in moderate magnetic field, $\Omega = 5\left[\frac{\hbar}{T_2^*}\right]$.

that probability of $\hat{\rho}_n(0)$ decreases sub-exponentially with increasing n, so it drops relatively slowly and it is at the level of a few percent after execution of about $n = 20$ cycles.

In the right panel of Fig. 3.4, it can be seen that, after a fast decrease, for longer cycle durations $\tau > T_2^*$ the probability of $\hat{\rho}_n(0)$ becomes a weakly dependent function of τ for a fixed parameter n and slightly oscillates around the corresponding mean value.

For practical purposes, one should choose an optimal combination of procedure parameters n and τ such that maximizes simultaneously the effect of retardation of entanglement decay (see Fig. 3.3) and the probability to obtain such a state (see map in Fig. 3.4).

In Fig. 3.5 the dependence of intensity of the effect on strength k of quantum measurement used in the manipulation procedure is shown. It turns out that with increasing parameter n concurrence of two-qubit state, as a function of k, gradually develops a plateau at nearly maximal level possible for a given value of n. The plateau is situated between $k = 1$ and some lower value of k, and for increasing parameter n, it progressively reaches surprisingly low values of k. Thus, long sequences of manipulation cycles lower requirement for the strength k of quantum measurement with practically no loss in the end effect. From a practical point of view, when dealing with a concrete experimental realization of the physical system, in which the strength k of quantum measurements is limited by a certain constant value, this value sets the minimal number n of quantum measurements that will produce a noticeable effect of retardation of the entanglement decay. As can be seen from the map in Fig. 3.5, for $k = 1$ the significant effect is already obtained for manipulation sequence with $n = 3$, whereas low values of k require to be compensated by large number n of cycles of the procedure (e.g. when $k \approx 0.6$ the effect starts to be noticeable after application of the manipulation procedure with $n = 20$).

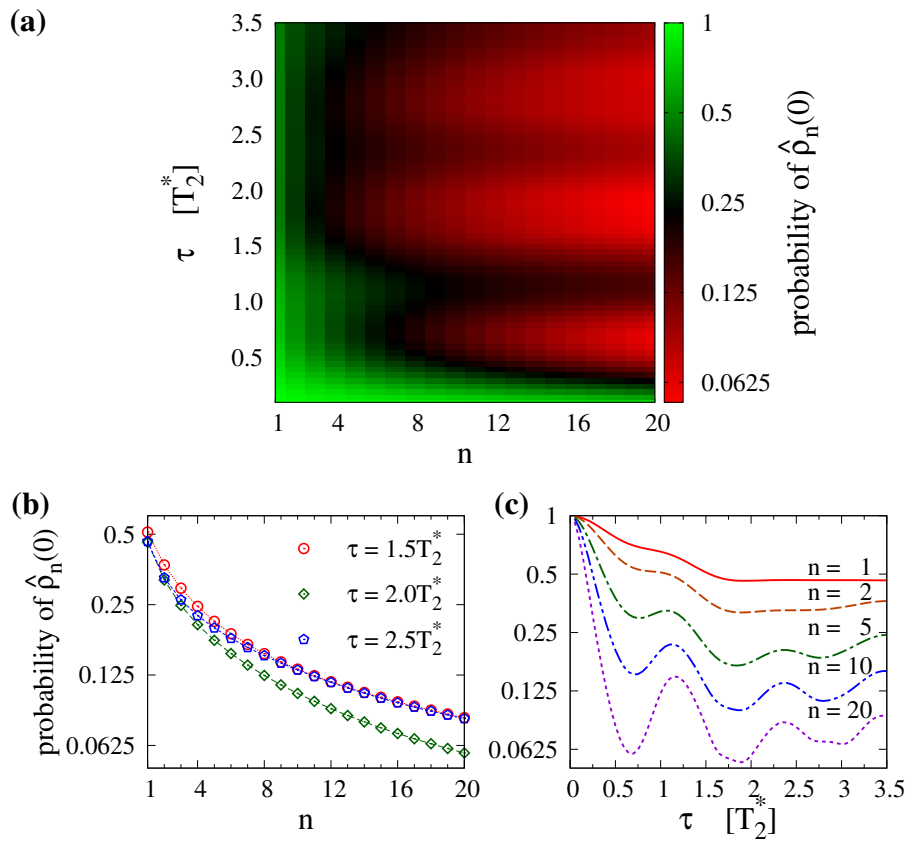

Figure 3.4: (a) Probability to obtain the state $\hat{\rho}_n(0)$ as a function of number n of performed projective measurements and period τ between them.
(b), (c) Cross-sections of the map (a): Probability to obtain the state $\hat{\rho}_n(0)$ as a function of number n of performed projective measurements (b) and as a function of period τ between projective measurements (c). NSEs consist of $N_1 = N_2 = 5$ uniformly coupled spins $\frac{1}{2}$. The system is in moderate magnetic field, $\Omega = 5\left[\frac{\hbar}{T_2^*}\right]$.

The possibility to significantly retard entanglement decay by performing the manipulations with quantum measurements originates from the non-Markovian dynamics of the system [116, 191]. During free evolution, electron spins, initially being in an entangled state, transfer through the hyperfine interaction some of their quantum correlations to the nuclear spin environments. Execution of the quantum measurement of two-electron spin subsystem with subsequent postselection of two-electron spin state restores its quantum correlations. The state of nuclear spin subsystems, conditioned on past dynamics, in turn, preserves the quantum correlations previously obtained from the electron spins, and thus, the flow rate of quantum correlations from the electron spins to nuclear spin environments in following instants of the system evolution may be reduced, which is manifested as the retardation of electron spin entanglement decay.

Possible overlap of the electrons' wave functions, which makes electrons coupled directly as well as indirectly through the common nuclear spin environment, does not rule out the effect of retardation of two-qubit entanglement decay of the proposed procedure (see Fig. 3.6), it causes minor deviations of the level of entanglement compared to the case of non-interacting electrons. It is worth to stress that if

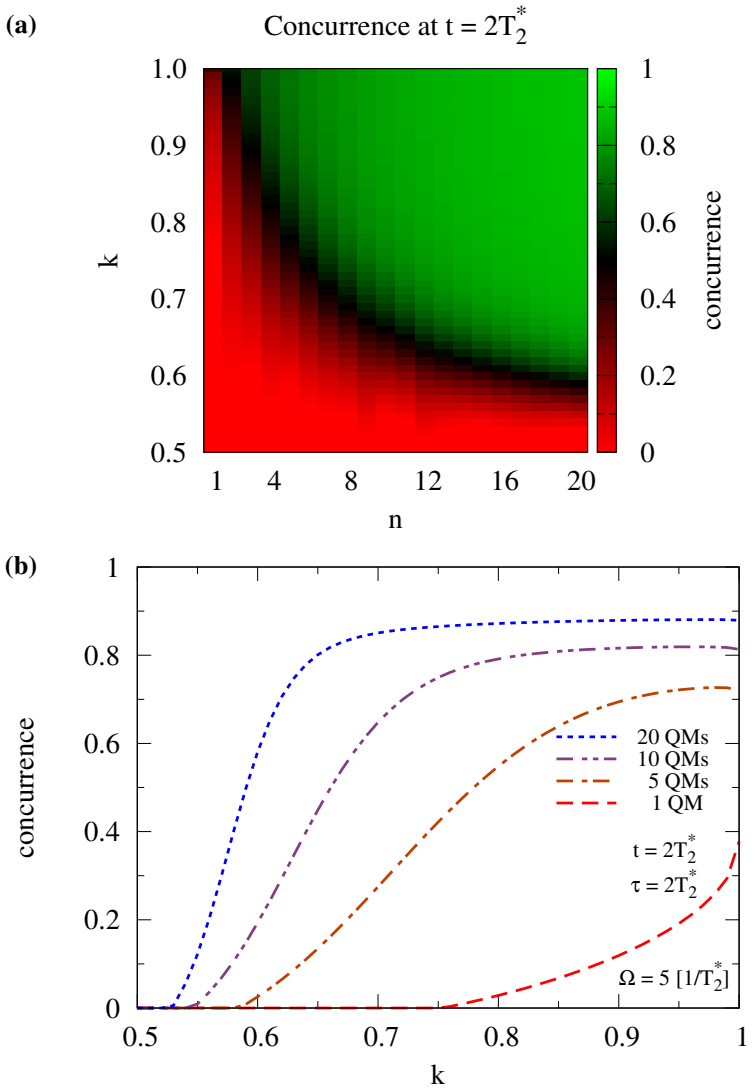

Figure 3.5: (a) Concurrence of the two-qubit state $\hat{\rho}_{2q}(t)$ calculated at $t = 2T_2^*$ as a function of number n of quantum measurements (QM) performed with period $\tau = 2T_2^*$ and their strength k.
(b) Cross-section of the map (a): Concurrence of the two-qubit state $\hat{\rho}_{2q}(t)$ calculated at $t = 2T_2^*$ as a function of strength k of quantum measurements performed with period $\tau = 2T_2^*$. NSEs consist of $N_1 = N_2 = 5$ spins $\frac{1}{2}$. The system is in moderate magnetic field, $\Omega = 5\left[\frac{\hbar}{T_2^*}\right]$.

the overlap of the electrons' wave functions is high, then one cannot consider such electrons as individual qubits as they will tend to transit to a state close to an eigenstate of their interaction Hamiltonian. So, starting initially from the singlet state qubits will indeed maintain entanglement between each other at high level (even without application of the procedure) but at the same time strong coupling will significantly disturb fidelity of single-qubit operations, which one unavoidably needs in order to perform any quantum computations. For that reason, when one is going to use single electron spins as qubits, after their initialization (e.g. in pairs in singlet state) electrons need to be kept well-separated from each other, whereas two-qubit interaction will be switched on only for specific periods to perform intended

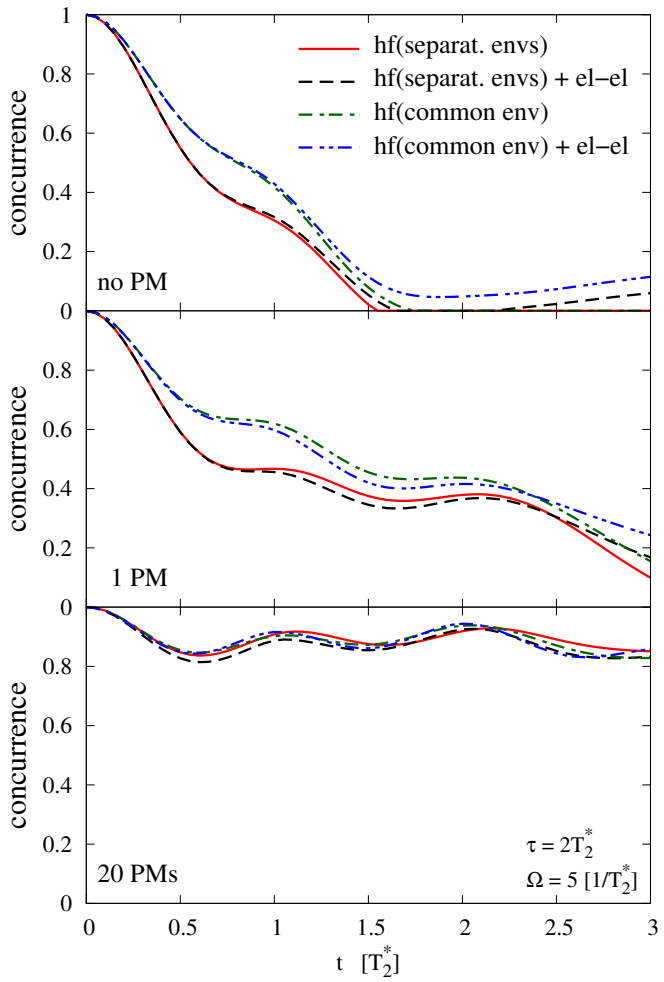

Figure 3.6: Concurrence of the two-qubit state $\hat{\rho}_{2q}(t)$ as a function of time t after the last projective measurement (PM): top panel – no PM, middle panel – 1 PM, bottom panel – 20 PMs. Solid and dashed lines correspond to system evolutions under the hyperfine Hamiltonian with separate nuclear spin environments, whereas dash dotted and dash double-dotted lines correspond to the system evolutions when each electron spin is also coupled to the nuclear spin environment of the another electron spin at the level of 10% of the coupling to nuclear spins from its own QD. Dashed and dash double-dotted lines shows the concurrence of the system in which the direct interaction between electron spins is present $\left(\text{at the level of 10\% of the total coupling between the electron spin and the nuclear spins, } A_0 = 0.1\sum_{i=1}^{N} A_i^{(1)} = 0.1\sum_{i=1}^{N} A_i^{(2)}\right)$. NSEs consist of $N_1 = N_2 = 5$ spins $\frac{1}{2}$. The system is in moderate magnetic field, $\Omega = 5\left[\frac{\hbar}{T_2^*}\right]$. The projective measurements are performed after the period of system evolution $\tau = 2T_2^*$.

two-qubit operations. Therefore, the approximation of non-interacting electron spin qubits considered in Sec. 3.2.1 is the basic scenario. On the other hand, simulations indicate that presence of either kind of interdot interactions increases the success rate of the proposed procedure, e.g. for the system described in Fig. 3.6 the success rate of the procedure consisting of 20 cycles with $\tau = 2T_2^*$ with projective measurement

is about 6% when no interdot interaction is present, and raises to about 7% for the system with direct electron–electron interaction, or about 9% for the system with common nuclear spin environment, and about 10% when both kinds of interactions take place in the system.

3.5 Conclusions

In contrast to the fast decay of two-qubit entanglement on a time scale of the order of T_2^* (shown in Fig. 1 of Ref. [162] or here in Fig. 2.1 [1] and Figs. 3.2, 3.6), performing a few cycles of evolution of initially entangled two electron spin qubits interacting with their nuclear spin environments, followed by quantum measurement performed on two-qubit subsystem, gradually builds up coherences in the entire system, and further decay of quantum correlations of two qubits may be significantly slowed down for specific cycle durations τ and numbers n of the performed cycles.

The effect shown here differs significantly from the quantum Zeno's effect, as the desired inhibition of quantum correlation decay maximizes only for some cycle durations $\tau > 0$ and is absent in the limit of continuous monitoring of two-qubit state, $\tau = 0$, since the described mechanism is based on the transfer of quantum correlation initially contained in two-qubit subsystem to its environment. This process needs some time to occur, and it is blocked in the limit of continuous monitoring of two-qubit state ($\tau = 0$).

The disadvantage of such a way of counteracting the decoherence is the necessity to postselect the proper two-qubit state after each quantum measurement and the associated with that decreasing overall probability of success. On the other hand, the probability to obtain the desired state $\hat{\rho}_n(t)$ decreases sub-exponentially with n.

The strong (projective) measurements produce maximal effect of retardation of entanglement decay, but the effect can be also achieved in the case of weak measurements. The more cycles have been performed (the larger n), the weaker quantum measurements can be used to achieve a nearly maximal effect.

Since the proposed procedure of retardation of entanglement decay requires only execution of the quantum measurements of two-electron subsystem, its practical realization seems to be much easier than execution of dynamical decoupling of qubits from their environments or preparation of a narrowed nuclear spin bath state, but due to the indeterminacy involved in the manipulation procedure, only a fraction of executed runs will give the desired state $\hat{\rho}_n(0)$, and, therefore, it is not the most convenient way to counteract the decoherence. On the other hand, simulations show that when one applies the manipulation procedure with number of cycles $n \geqslant 10$, the quantum measurement need not be of projective type ($k = 1$) anymore, it can be of moderate strength ($k \approx 0.8$), and the probability to obtain the desired state $\hat{\rho}_n(0)$, which will exhibit a slower decay of entanglement, is pretty large (about 10%). Thus, it may be viewed of fundamental interest to implement such a manipulation procedure in currently existing systems of electron spin QD qubits in order to check experimentally whether predicted effect of retardation of entanglement decay is achievable in real systems.

Chapter 4

Dynamical Generation of Entanglement of Two Singlet-Triplet Qubits

In this chapter, I analyze in detail a procedure of entangling of two singlet-triplet (S-T_0) qubits operated in a regime when energy associated with the magnetic field gradient, ΔB_z, is an order of magnitude smaller than the exchange energy, J, between singlet and triplet states [66]. I have studied theoretically a single S-T_0 qubit in free induction (FID) and spin echo (SE) experiments. I have obtained analytical expressions for time dependence of components of its Bloch vector for quasistatical fluctuations of ΔB_z and quasistatical or dynamical $1/f^\beta$-type fluctuations of J. I have then considered the impact of fluctuations of these parameters on the efficiency of the entangling procedure which uses an Ising-type coupling between two S-T_0 qubits. In particular, I have obtained the analytical expression for the evolution of two qubits affected by $1/f^\beta$-type fluctuations of J. This expression indicates the maximal level of entanglement that can be generated by performing the entangling procedure. This results deliver also an evidence that in the above-mentioned experiment S-T_0 qubits were affected by uncorrelated $1/f^\beta$ charge noises. The results contained in this chapter have been presented at a few conferences (see List of Conference Presentations on p. 129).

4.1 Introduction

Spin qubits based on gated quantum dots [47, 192, 48] can be initialized, coherently controlled, and read out. Qubits based on a spin of a single electron [73] localized in a QD can be controlled with electron-spin resonance techniques [77, 193, 194], while two-qubit gates can be performed with the help of exchange interaction [73, 78, 195], which is controlled electrically [58, 65, 196, 197, 84, 198, 199]. Implementation of single-spin control with ac electric [193, 194, 200] and magnetic [77, 65] fields is nevertheless experimentally challenging, especially in GaAs based QDs, in which interaction with nuclei [201, 108, 202, 144] leads to significant broadening of electron spin resonance lines (this is in contrast to experimental situation in Si-based single-electron QDs [203, 204, 50], for which nuclear noise can be removed by isotopic purification [50, 205]). Research on all-electrical control (possibly without ac fields) is an active field. Such a control is possible for spin qubits based on a few electrons localized in multiple quantum dots [192]. In a double quantum dot (DQD) containing two electrons one can easily initialize and partially control a qubit, whose logical states correspond to singlet S and unpolarized triplet T_0 formed by the two electrons [58] (note that one can as well use two QDs with larger odd number of electrons per dot [206]), and all-electrical ac control is also possible in a variety of other designs based on two [207], three [208, 209, 210] and four [211] electrons. I focus here on the DQD-based two-electron singlet-triplet (S-T_0) qubit, for which full electrical control over the state of the qubit is possible when the spin splittings of electrons localized in the two dots are distinct. This can be achieved with creation of a gradient of nuclear spin polarization [120, 159] in nuclear spin rich material such as GaAs or with the help of micromagnets creating a gradient of magnetic field [65].

Creation of entanglement [6, 7] of two spin-based qubits is the next necessary step in development of a QD spin qubit platform for quantum information processing. For two single-spin qubits, exchange interaction leads to creation of entangled two-qubit states [65, 64, 198, 196], while in the case of S-T_0 qubits it is the electric dipole-dipole (capacitive) interaction [212] that has been most commonly used for interqubit coupling [61, 66] (although exchange coupling could be used too [213, 214, 215]). Our focus in the this chapter is on creation of entanglement and its evolution due to capacitive interqubit interaction, as it was demonstrated experimentally for two S-T_0 qubits in Ref. [66].

Interaction of qubits with their environments that fluctuate in an uncontrolled manner leads to decoherence [20] of their quantum states. In this process, the entanglement, which requires existence of a coherent superposition of at least two product states of the two qubits, is also destroyed [7]. For single electron spins in QDs, the dominant cause of entanglement decay is their hyperfine interaction with the nuclear baths [162, 1]. Decoherence of S-T_0 qubits, on the other hand, can be dominated by the nuclear bath at low singlet-triplet splitting [140], but for large splittings it is mostly caused by charge noise [216, 217, 151], with the nuclear-induced decay [218, 177] possibly playing a role when the fluctuations of S-T_0 splitting are suppressed [86]. Influence of quasistatic charge and nuclear noises on the simplest protocol of generation of entanglement of two capacitively coupled S-T_0 qubits was considered in Ref. [219]. In this chapter I consider a more involved protocol from Ref. [66] under the influence of dynamical charge noise.

In the experiment [66], the two S-T_0 qubits were initialized in a separable state,

and subsequently they were evolving in the presence of a finite singlet-triplet splitting J. With both qubits having nonzero J, dipolar interaction between them leads to the appearance of an Ising-type interaction, which in the decoherence-free case would lead to periodic creation of maximal two-qubit entanglement. In the experiment, only one period of such entanglement oscillation (with entanglement reaching only a fraction of its maximal possible value) is visible. Furthermore, for the entanglement to be nonzero the two qubits have to be subjected to a spin echo refocusing pulse that removes the influence of the slowest environmental fluctuations on their evolution. The strong decoherence is significantly affecting the entanglement generation and evolution. The goal of this study is to understand processes originated from nuclear polarization fluctuations and charge noise affecting the singlet-triplet splittings which limit the ability to generate entangled two-qubit states for experimental protocol performed in Ref. [66]. The main conclusion of this study is that the spin echo protocol removes most of the influence of the nuclear polarization fluctuations, and the observed decoherence is caused by charge noise. The experimental data from Ref. [66] is consistent with the assumption that each qubit is subjected to $1/f^{\beta}$ charge noise with $\beta \lesssim 1$ (as seen for a single S-T_0 qubit [151]), and the noises affecting the two qubits are independent. I also discuss the qualitative difference in the character of the dominant decoherence process between the cases of small $\beta \lesssim 1$ and large $\beta > 1$ – in the former case the imperfectly echoed-out single-qubit noise has dominant influence, while in the latter case of very low frequency noise the fluctuations of two-qubit coupling are the main reason for imperfect entanglement.

The chapter is organized as follows. In Sec. 4.2 I give an overview of the physics of a single S-T_0 qubit, and discuss the influence of fluctuating external magnetic or electric fields on the decoherence of such qubit seen in the free induction decay (FID) as well as spin echo (SE) experiments. In Sec. 4.3 I recall a procedure that has been designed for entangling two S-T_0 qubits [66]. I briefly discuss ways of entanglement quantification that have been applied to the system of two qubits in Sec. 4.4. In Sec. 4.5 I then analyze the influence of the above-mentioned factors that lead to decoherence on the efficiency of the procedure of entangling of two S-T_0 qubits. I show there that a dynamically fluctuating electric field affecting qubits' exchange splittings may limit the maximal level of two-qubit state entanglement by destroying two-qubit entangling gate or simply by dephasing of individual qubits. Finally, Sec. 4.6 closes the chapter with a discussion of conclusions on the nature of charge noise in the system studied in Ref. [66] that one can draw by comparing the results of present calculation to the observations described there. In the appendices (p. 122) I present explicit expressions that describe the averaged values of S-T_0 qubit components as functions of the duration of free induction decay and spin echo experiments as well as attenuation factors originated from $1/f^{\beta}$ dynamical noise of exchange splittings of the qubits.

4.2 The Physics of a Singlet-Triplet Qubit

4.2.1 The Hamiltonian and control over the qubit

In a singlet-triplet qubit, the quantum state is stored in the joint spin state of two electrons in a DQD, with one electron localized in each of the two dots, the left (L) and the right (R) one [212, 58, 159, 151]. The logical states of the qubit are the singlet

$|S\rangle = \frac{1}{\sqrt{2}}(|\uparrow_L\downarrow_R\rangle - |\downarrow_L\uparrow_R\rangle)$ and the spin unpolarized triplet $|T_0\rangle = \frac{1}{\sqrt{2}}(|\uparrow_L\downarrow_R\rangle + |\downarrow_L\uparrow_R\rangle)$. The remaining two states, spin polarized triplets, $|\uparrow_L\uparrow_R\rangle$ and $|\downarrow_L\downarrow_R\rangle$, are split off by the constant magnetic field applied in the plane of the structure. In this chapter, I adopt the convention that the Bloch sphere of S-T_0 qubit is defined in such a way that state $|S\rangle$ ($|T_0\rangle$) coincides with north (south) pole of the sphere and the axis connecting these two points is the z axis.

It was demonstrated in Ref. [58] that it is possible to reliably initialize the two electron spins in singlet state $|S\rangle$, perform rotations around z axis of the Bloch sphere, as well as a read out in a form of projective measurements onto $|S\rangle$. All these operations can be realized utilizing the fast control of the exchange interaction that is achieved by applying proper voltage pulses to the metallic gates on the surface of the device. The states $|S\rangle$ and $|T_0\rangle$ are naturally split by energy J due to the exchange interaction between electrons in the DQD [78, 195]. This energy difference can be influenced by controlling either the energy difference between the ground single-electron states of the two dots (the so-called detuning ϵ) [58, 220], or the height of the interdot barrier [73, 84]. According to Ref. [66], the value of J can be varied from much less than 1 μeV to a few μeV on a time scale of a nanosecond. We have then the following time-dependent and externally controlled term in the Hamiltonian of the qubit (in units of $\hbar$):

$$\hat{H}_J(t) = J(t)\frac{\hat{\sigma}_z}{2} \ . \tag{4.1}$$

Rotations about the x axis of the Bloch sphere (or equivalently, the rotations between $|S\rangle$ and $|T_0\rangle$ states) present a greater challenge. In Ref. [159] it was realized with the help of an interdot gradient of electron spin splitting ΔB_z caused by difference of nuclear polarizations in the two dots. If the local fields (either nuclear Overhauser fields, or magnetic fields from external magnets) in both dots were identical, $|S\rangle$ and $|T_0\rangle$, states would not experience any dynamics, since the phase acquired by spin-down state $|\downarrow_L\rangle$ (spin-up state $|\uparrow_L\rangle$) of the electron in the L dot would be cancelled by the spin-up state $|\uparrow_R\rangle$ (spin down state $|\downarrow_R\rangle$) of the electron in the R dot. The field gradient breaks this symmetry, which can be seen in the following example, where we allow $|S\rangle$ to evolve for time t

$$\begin{aligned} |S\rangle &= \frac{1}{\sqrt{2}}\left(|\uparrow_L\downarrow_R\rangle - |\downarrow_L\uparrow_R\rangle\right) \\ &\xrightarrow{t} \frac{1}{\sqrt{2}}\left(|\uparrow_L\downarrow_R\rangle - \mathrm{e}^{it\Delta B_z}|\downarrow_L\uparrow_R\rangle\right) \ . \end{aligned} \tag{4.2}$$

We can see that the initial state transforms back-and-forth between singlet and the unpolarized triplet, as the phase factor oscillates between 1 and -1 with frequency set by ΔB_z. The field gradient ΔB_z contributes the following term to the qubit's Hamiltonian:

$$\hat{H}_{\Delta B_z} = \Delta B_z\frac{\hat{\sigma}_x}{2} \ , \tag{4.3}$$

where $\hat{\sigma}_x = |S\rangle\langle T_0| + |T_0\rangle\langle S|$.

The difficulty in the realization of precise singlet-to-triplet transitions lies in the fact that the necessary field gradient, in most cases, is generated by the slowly fluctuating Overhauser field established by the nuclear spins of the atoms comprising the sample [113]. Therefore, ΔB_z must be treated as given (in fact, it must be

measured beforehand, and value of ΔB_z varies in different repetitions of the experiment), hence, it would induce an ongoing transition between $|S\rangle$ and $|T_0\rangle$, which is undesirable in the context of the entangling procedure. Instead, such a procedure requires precise state transformations on demand. For example, if one desires to execute a rotations from $|S\rangle$ to $|T_0\rangle$ at a given moment t' it would be ideal if ΔB_z could be turned on only for a interval $[t', t' + \pi/\Delta B_z]$, so that phase in Eq. (4.2) is $\mathrm{e}^{i\Delta B_z \cdot (t' + \frac{\pi}{\Delta B_z} - t')} = \mathrm{e}^{i\pi} = -1$. Since there is no practical way to change the value of ΔB_z during a single realization of the procedure, one cannot simply turn off the gradient and stop the transition. Nevertheless, the transition can be effectively blocked by overshadowing ΔB_z with strong enough splitting J, which can be controlled with relative ease, and it can be switched on and off at will. In order to realize the idealized scenario such as the one described above, the time scale on which J is manipulated must be the shortest time scale in the problem. In particular, this time scale must be much shorter than the period of rotations around x axis $1/\Delta B_z$ as well as the period of z rotations set by the maximal value of singlet-triplet splitting $1/J_{\max}$. Note that pulse-shaping techniques for gate error mitigation were derived for S-T_0 qubits [221, 222, 223], but their implementation has proven to be challenging so far, and I focus here on the simplest control scheme used in experiment on creation of entanglement in Ref. [66]. Let us also note that entanglement of two S-T_0 qubits in the situation in which ΔB_z is always larger than J was generated using a scheme involving ac control of J [224], which is distinct from the one used in Ref. [66] and analyzed here.

4.2.2 Decoherence of a single S-T_0 qubit

4.2.2.1 The nature of noisy terms in the Hamiltonian

A qubit evolving with nominally constant ΔB_z and J is undergoing decoherence due to uncontrolled fluctuations of these parameters. When the magnetic field gradient ΔB_z is due to the difference of the z components of nuclear Overhauser fields in the two dots (which is the case on which I focus here), the main mechanism responsible for its fluctuations is the spin diffusion process [113, 225] caused by dipolar interactions between the nuclear spins. Note that I focus here on $J \gg \Delta B_z$ regime, in which only the large-amplitude classical fluctuations of the Overhauser fields can affect the qubit. This is in contrast to $J \ll \Delta B_z$ case, in which a quantum treatment of nuclear fluctuations is necessary [110, 185, 226]. The large-amplitude fluctuations have a characteristic decorrelation time scale of about one second [113, 225], which is much longer than the time scale of a single run of the experiment, i.e. a single repetition of qubit's initialization – evolution – measurement cycle. Therefore, $\Delta B_z(t)$ can be treated as quasistatic [132, 108, 177], i.e. it is considered as a constant (i.e. time independent) random variable with certain probability distribution $p(\Delta B_z)$. For a large number of nuclei, this distribution is normal [127], with the average value $\overline{\Delta B_z}$ and the dispersion (standard deviation) $\sigma_{\Delta B_z} = \sqrt{\overline{\Delta B_z^2} - (\overline{\Delta B_z})^2}$. Within this approximation, the result of the experiments are interpreted as follows. Given the initial density operator of the qubit, $\hat{\rho}(0) = \hat{\rho}_{\mathrm{ini}}$, its evolution during the experiment run number n, is described by the qubit Hamiltonian $\hat{H}_q(t) = \hat{H}_J(t) + \hat{H}_{\Delta B_z}$ with an

unknown, but constant, value of $\Delta B_z = \Delta B_z^n$ drawn from the distribution $p(\Delta B_z)$,

$$\hat{\rho}(t|\Delta B_z^n) = \mathrm{e}^{-it(J\hat{\sigma}_z+\Delta B_z\hat{\sigma}_x)/2}\hat{\rho}_{\mathrm{ini}}\mathrm{e}^{it(J\hat{\sigma}_z+\Delta B_z\hat{\sigma}_x)/2}\Big|_{\Delta B_z=\Delta B_z^n}. \tag{4.4}$$

The final results are derived from the whole series of N experiment repetitions with the same initial state. Therefore, the expectation values of the measured quantities are calculated with the help of the averaged density operator according to

$$\begin{aligned}\hat{\rho}_{\mathrm{fin}}(t) &= \frac{1}{N}\sum_{n=1}^{N}\hat{\rho}(t|\Delta B_z^n) \\ &\xrightarrow{N\to\infty} \int_{-\infty}^{\infty} d(\Delta B_z)p(\Delta B_z)\hat{\rho}(t|\Delta B_z) = \overline{\hat{\rho}(t|\Delta B_z)}\,.\end{aligned} \tag{4.5}$$

On the other hand, the exchange splitting $J(t)$ changes due to fluctuations of local electric fields, i.e. due to charge noise, which is ubiquitous in semiconductor nanostructures. The charge noise typically has its spectral weight concentrated at low frequencies. Contributions of noise at frequencies corresponding to the inverse of typical qubit coherence time are typically negligible when considering free evolution of the qubit (hence the noise can be treated then as quasistatic), but they have to be taken into account when modeling the spin echo experiment [151], in which the influence of the lowest-frequency noise is removed, and coherence times are longer. In order to model the experimental data, one has to average the qubit's evolution over many realizations of the stochastic process $J(t)$. If the noise statistics is assumed to be Gaussian (which is natural for the noise consisting of many independent contributions), and if the evolution can be treated in the pure dephasing approximation (i.e. neglecting $\Delta B_z\hat{\sigma}_x$ term when $\Delta B_z \ll J(t)$), the averaging can be done analytically. In the case of non-Gaussian noise and when keeping the general form of the Hamiltonian, one has to resort to numerical simulations [227, 228].

It was shown [151] that the GaAs/AlGaAs S-T_0 qubit is affected by noise having power spectral density of $1/f^\beta$ form with $\beta \approx 0.7$ in the range of frequencies relevant for correct description of spin echo signal. It is unclear if this value of β is specific to this material or only to the device used in that experiment.

4.2.2.2 Decoherence during free evolution of the qubit

I now assume that the initial state of a qubit is $|-y\rangle = \frac{1}{\sqrt{2}}(|S\rangle - i|T_0\rangle)$. This choice is connected with the entangling procedure used in Ref. [66], in which this single-qubit state is used as the initial one for both qubits. In a free induction decay (FID) experiment, the qubit undergoes evolution without any manipulations between its initialization and the coherence readout at time τ. With fixed values of J and ΔB_z, the expectation values of qubit observables $\langle\hat{\sigma}_i^{\mathrm{FID}}(\tau)\rangle = \langle -y|\hat{\sigma}_i(\tau)|-y\rangle$ are given by

$$\langle\hat{\sigma}_x^{\mathrm{FID}}(\tau)\rangle = \frac{J}{\sqrt{\Delta B_z^2 + J^2}}\sin\left(\sqrt{\Delta B_z^2 + J^2}\tau\right), \tag{4.6}$$

$$\langle\hat{\sigma}_y^{\mathrm{FID}}(\tau)\rangle = -\cos\left(\sqrt{\Delta B_z^2 + J^2}\tau\right), \tag{4.7}$$

$$\langle\hat{\sigma}_z^{\mathrm{FID}}(\tau)\rangle = -\frac{\Delta B_z}{\sqrt{\Delta B_z^2 + J^2}}\sin\left(\sqrt{\Delta B_z^2 + J^2}\tau\right). \tag{4.8}$$

The qubit evolves under the influence of $J \gg \Delta B_z$, so to the lowest order in $\Delta B_z/J$ the initial amplitude of x and y signals is ≈ 1, while the z signal has amplitude $\approx \Delta B_z/J$. In the presence of fluctuations of both J and ΔB_z all these signals will average to zero at long times, at which the arguments of the oscillatory functions taken from an appropriate distribution will have relative phases randomly distributed between 0 and 2π.

One can average the above expressions over ΔB_z and J assuming Gaussian and quasistatic fluctuations of either of these parameters. I focus on the largest observable, $\langle \hat{\sigma}_y^{\rm FID}(\tau)\rangle$, and I approximate $\sqrt{\Delta B_z^2 + J^2}\tau \approx J\tau + \Delta B_z^2 \tau/2J$, which is valid for $J \gg \Delta B_z$ and for short durations $\tau \ll 8J^3/\Delta B_z^4$. For J noise one gets then a simple Gaussian decay:

$$\left\langle \langle \hat{\sigma}_y^{\rm FID}(\tau)\rangle \right\rangle_J \approx -\frac{1}{2}\exp\Big[-(\tau/T_{2,J}^*)^2\Big]\cos(\bar{J}\tau)\ , \tag{4.9}$$

where $\bar{J}$ is the average value of J and the decay time scale is

$$T_{2,J}^* = \frac{\sqrt{2}}{\sigma_J}\ , \tag{4.10}$$

where σ_J is the standard deviation of J.

Averaging over ΔB_z gives

$$\begin{aligned}\left\langle \langle \hat{\sigma}_y^{\rm FID}(\tau)\rangle \right\rangle_{\Delta B_z} \approx &-\exp\left(-\frac{\tau^2 \overline{\Delta B_z}^2 \sigma_{\Delta B_z}^2}{2\left(J^2 + (\sigma_{\Delta B_z}^2\tau)^2\right)}\right) \\ &\times \frac{1}{\left(1+(\sigma_{\Delta B_z}^2\tau/J)^2\right)^{1/4}}\cos\Big(r(\tau)+s(\tau)\Big),\end{aligned} \tag{4.11}$$

where $r(\tau) = \frac{1}{2}\arctan\big(\sigma_{\Delta B_z}^2\tau/J\big)$, and $s(\tau) = J\tau\big(\overline{\Delta B_z}^2 + 2J^2 + 2(\sigma_{\Delta B_z}^2\tau)^2\big)/2\big(J^2 + (\sigma_{\Delta B_z}^2\tau)^2\big)\big)$. The decay envelope is then a product of two factors. The first one dominates the decay when $\overline{\Delta B_z} \gg \sigma_{\Delta B_z}$, i.e. in the situation in which a finite ΔB_z is used for coherent control of the qubit. Then at long τ this factor saturates at $\exp\big(-\overline{\Delta B_z}^2/2\sigma_{\Delta B_z}^2\big) \ll 1$, and the qubit loses most of its coherence at time scale $\tau \ll J/\sigma_{\Delta B_z}^2$, at which the factor can be approximated as $\exp\Big(-(\tau/T_{2,\Delta B_z}^*)^2\Big)$, where

$$T_{2,\Delta B_z}^* = \frac{\sqrt{2}}{\sigma_{\Delta B_z}} \cdot \frac{J}{\overline{\Delta B_z}}\ . \tag{4.12}$$

On the other hand, when $\overline{\Delta B_z} \ll \sigma_{\Delta B_z}$, the second factor dominates, and the signal envelope decays in power law fashion $\propto \sqrt{\tau_{\Delta B_z}/\tau}$, where the characteristic time $\tau_{\Delta B_z} = J/\sigma_{\Delta B_z}^2$.

It is important to note now that in the regime of $\bar{J} \gg \overline{\Delta B_z}$ and $\overline{\Delta B_z} \gg \sigma_{\Delta B_z}$ (that is relevant for experiments of interest in this chapter), one typically has $\sigma_J \gg \sigma_{\Delta B_z}$. This is due to the observed relation between J and detuning ϵ: $J \approx J_0 \exp(\epsilon/\epsilon_0)$, and the fact that the noise in J comes mostly from fluctuations of ϵ. One has thus $\delta J/J \sim \delta\epsilon/\epsilon_0$, so for constant level of detuning noise the standard deviation σ_J increases with J [151]. It is then a reasonable assumption to neglect the effect of fluctuations of ΔB_z in the calculation of decoherence. Furthermore, for $\bar{J} \gg \overline{\Delta B_z}$ the main effect of $\overline{\Delta B_z}\hat{\sigma}_x$ term is a slight tilt in xOz plane of the axis about which

the qubit's Bloch vector is precessing. Neglecting this effect, one arrives at the pure dephasing approximation to the qubit's Hamiltonian:

$$\hat{H}(t) \approx \left(\bar{J} + \delta J(t)\right) \frac{\hat{\sigma}_z}{2} \ , \tag{4.13}$$

where I have now included the time dependence of J noise. The off-diagonal element of the qubit's density operator is given by

$$\rho_{ST_0}(\tau) = \rho_{ST_0}(0)\, \mathrm{e}^{-i\bar{J}\tau} \left\langle \exp\left(-i \int_0^\infty f_{\mathrm{FID}}(t;\tau)\delta J(t)\mathrm{d}t \right) \right\rangle_{\delta J} \ , \tag{4.14}$$

where $\langle ... \rangle_{\delta J}$ denotes averaging over different realizations of $\delta J(t)$ noise, and $f_{\mathrm{FID}}(t;\tau) = \theta(t)\theta(\tau - t)$ is the FID time-domain filter function, where $\theta(t)$ is Heaviside step function. The transverse components of the qubit state are given by $\left\langle \langle \hat{\sigma}_x^{\mathrm{FID}}(\tau) \rangle \right\rangle = 2\mathrm{Re}\rho_{ST_0}(\tau)$ and $\left\langle \langle \hat{\sigma}_y^{\mathrm{FID}}(\tau) \rangle \right\rangle = 2\mathrm{Im}\rho_{ST_0}(\tau)$. For Gaussian $\delta J(t)$ noise only the second cumulant of the random phase is nonzero [229, 230, 149], and one has a closed formula for coherence:

$$\rho_{ST_0}(\tau) = \rho_{ST_0}(0)\, \mathrm{e}^{-i\bar{J}\tau}\, \mathrm{e}^{-\chi_{\mathrm{FID}}(\tau)} \ , \tag{4.15}$$

in which the attenuation factor χ_{FID} is defined in the following way

$$\begin{aligned} \chi_{\mathrm{FID}} &= \int_0^\infty \mathrm{d}t_1 \int_0^\infty \mathrm{d}t_2 f_{\mathrm{FID}}(t_1) f_{\mathrm{FID}}(t_2) \left\langle \delta J(t_1)\delta J(t_2) \right\rangle_{\delta J} \\ &= \int_0^\infty S(\omega) |\tilde{f}_{\mathrm{FID}}(\omega)|^2 \frac{\mathrm{d}\omega}{\pi} \ , \end{aligned} \tag{4.16}$$

where in the second line it has been assumed that the noise is stationary, so that its autocorrelation function is $C(t_1 - t_2) = \langle \delta J(t_1)\delta J(t_2) \rangle_{\delta J}$. The spectral density of the noise is $S(\omega) = \int_{-\infty}^{\infty} C(t)\mathrm{e}^{i\omega t}\mathrm{d}t$ and the frequency domain filter function [229, 230] is

$$\tilde{f}_{\mathrm{FID}}(\omega) = \int_{-\infty}^{\infty} f_{\mathrm{FID}}(t;\tau)\mathrm{e}^{i\omega t}\mathrm{d}t = 2\sin^2\left(\frac{\omega\tau}{2}\right)\frac{1}{\omega^2} \ . \tag{4.17}$$

In the case of $S(\omega) \sim \frac{1}{f^\beta}$ with $\beta = 0.7$, the attenuation factor defined in Eq. (4.16) depends on τ as a power function: $\chi_{\mathrm{FID}} \propto \tau^{1.7}$ (see Appendix (p. 123) for a detailed calculation).

Note that for $\beta \geq 1$ the integral in Eq. (4.16) diverges. However, in a real experimental setting, the total time of data acquisition, T_M, involving many repetitions of cycles of qubit initialization, evolution for time τ, and measurement, sets the low-frequency cutoff, $\omega_{\min} \sim 1/T_M$, for frequencies of the noise that actually affect the qubit [149, 151, 205]. Consequently, the lower limit of the integral in Eq. (4.16) should be $\omega_{\min} > 0$ instead of zero, making the attenuation factor finite. In this study I have set $\omega_{\min}/2\pi = 1$ mHz, corresponding to T_M in a perfectly realistic range of tens of minutes.

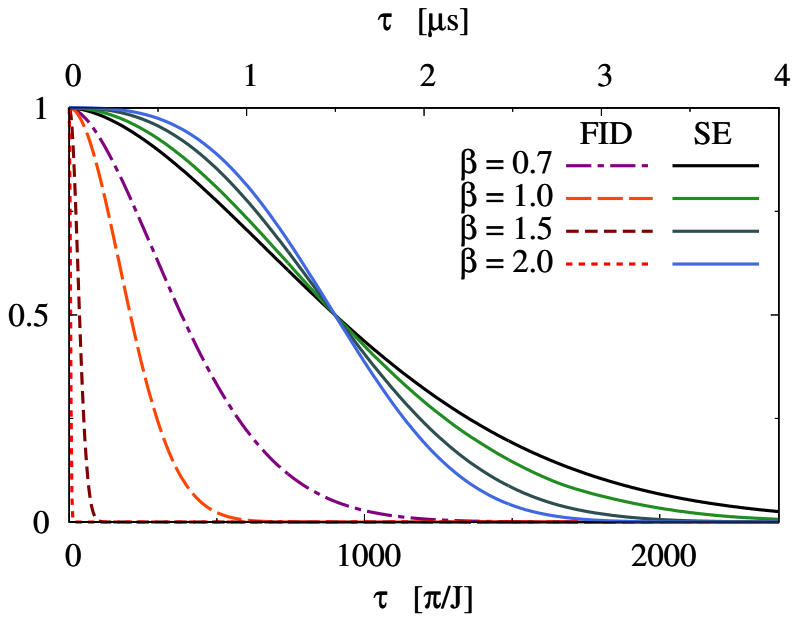

Figure 4.1: FID and SE signals of a single S-T_0 qubit for the case of $1/f^\beta$ noise in exchange splitting J, with fluctuations in ΔB_z neglected. The power of the noise was chosen to be such that ensures decay of SE signal as observed in the experiment [151] (such a noise power that leads to half-decay of SE signal in 1.5 μs for $J \approx 1$ μeV). Note that the improvement in coherence time due to echo relative to FID is larger when β is larger, i.e. when there is more noise power at the lowest frequencies.

4.2.2.3 Decoherence in spin echo protocol

The influence of very low frequency noise on qubit dephasing can be removed by employing a spin echo protocol [229], in which a qubit is subjected to a π rotation about an axis perpendicular to the axis along which the noise is coupled (here I focus on π rotations about the x axis) at time $t = \frac{\tau}{2}$, and the coherence is read out at the final time $t = \tau$.

Within the pure dephasing approximation introduced above, and for perfect short (δ function like) pulses, the calculation of echoed coherence signal as a function of duration τ of the echo procedure amounts to replacing the $f_{\rm FID}(t)$ function in Eq. (4.14) by a $f_{\rm SE}(t)$ function which is nonzero for $t \in [0, \tau]$ and changes its value from 1 to -1 at $t = \tau/2$, see e.g. Ref. [229, 149]. The coherence at the final readout time is given by a formula analogous to Eq. (4.15), only with $\chi_{\rm FID}(\tau)$ replaced by $\chi_{\rm SE}(\tau)$ in which $\tilde{f}_{\rm SE}(\omega) = 4\sin^4\frac{\omega\tau}{4}/\omega^2$ appears. The latter filter function strongly suppressed very low ω contribution (precisely from $\omega \ll 4\tau$ range) to the attenuation factor $\chi_{\rm SE}(\tau)$. For quasistatic charge noise one has $S(\omega) \approx \sigma_J \delta(\omega)$, and the echo protocol leads to a complete recovery of the initial coherence.

For J noise with nontrivial spectrum, but with a lot of noise power at low frequencies, the echo decay time is expected to be much longer than the FID decay time, see Fig. 4.1 for illustration. Recall that our justification for neglection of quasistatic ΔB_z fluctuations was the fact that in experimentally relevant parameter regime they lead to much slower FID decay than the J fluctuations. Echo-induced suppression of J noise effects could be suspected of leading to breakdown of that assumption. This is not the case: the echo protocol is also strongly suppressing

the effects of quasistatic transverse noise, provided that the effective transverse field ΔB_z is much smaller that the typical longitudinal field. For given values of J and ΔB_z one has

$$\begin{aligned}\langle\hat{\sigma}_y^{\mathrm{SE}}(\tau)\rangle &= \langle -y|\mathrm{e}^{i\hat{H}\frac{\tau}{2}}(i\hat{\sigma}_x)\mathrm{e}^{i\hat{H}\frac{\tau}{2}}\hat{\sigma}_y\mathrm{e}^{-i\hat{H}\frac{\tau}{2}}(-i\hat{\sigma}_x)\mathrm{e}^{-i\hat{H}\frac{\tau}{2}}|-y\rangle \\ &= \frac{1}{\Delta B_z^2+J^2}\left(J^2+\Delta B_z^2\cos\left(\sqrt{\Delta B_z^2+J^2}\tau\right)\right) . \end{aligned} \tag{4.18}$$

As before, this expression can be analytically averaged over ΔB_z for short durations $\tau \ll 8J^3/\Delta B_z^4$. The full result is more complicated than Eq. (4.11) (see Appendix (p. 122) for the full expression), but for $\sigma_{\Delta B_z}^2\tau/J \gg (\Delta B_z/\sigma_{\Delta B_z})^2$ one can arrive at

$$\left\langle\langle\hat{\sigma}_y^{\mathrm{SE}}(\tau)\rangle\right\rangle_{\Delta B_z} \approx \frac{J^2}{J^2+\overline{\Delta B_z}^2} + \frac{\sigma_{\Delta B_z}^2}{2\left(J^2+\overline{\Delta B_z}^2\right)}\left(\frac{J}{\sigma_{\Delta B_z}^2\tau}\right)^{3/2}\cos\left(\bar{J}\tau\right) , \tag{4.19}$$

where we see that at long times the only effect of quasistatic transverse noise is decrease of the coherence signal by factor $\approx (\overline{\Delta B_z}/\bar{J})^2 \ll 1$ of its initial value.

The echo signal averaged over quasistatic fluctuations of J looks similarly

$$\langle\langle\sigma_y^{\mathrm{SE}}(\tau)\rangle\rangle_J \approx \frac{\bar{J}^2+\sigma_J^2}{\bar{J}^2+\Delta B_z^2} + \frac{\Delta B_z^2}{\bar{J}^2+\Delta B_z^2}\exp\left(-\frac{\sigma_J^2\tau^2}{2}\right)\cos\left(\bar{J}\tau\right) . \tag{4.20}$$

For long times signal $\langle\langle\sigma_y^{\mathrm{SE}}(\tau)\rangle\rangle_J$ remains close to its initial value $(\bar{J}^2+\sigma_J^2)/(\bar{J}^2+\Delta B_z^2) \approx 1$.

4.3 The Procedure for Entangling Two S-T_0 Qubits

Now I proceed with the description of the procedure designed in Ref. [66] aimed to create maximally entangled two-qubit states out of an initial product state. Here, let us focus on an idealized setting in which both J and ΔB_z are piecewise-constant and fully controlled, so no averaging over their values is performed. Of course, in reality only J is controlled, and it furthermore fluctuates – and the consequences of this will be the main subject of subsequent sections.

Entanglement generation requires some kind of qubit-qubit interaction, and in the case of S-T_0 qubits one utilizes the coupling between electric dipoles induced by state-dependent charge distributions in each DQD [212]. Only if both qubits are in state $|S\rangle$, and their exchange splittings are finite, the charge distributions are asymmetric (due to mixing of the singlet state relevant here with a singlet state of two electrons localized in a single dot), and hence, each DQD possesses a nonzero electric dipole moment. Therefore, the effective Hamiltonian of this interaction is given by (in units of $\hbar$)

$$\hat{H}_{\mathrm{int}} = \frac{1}{4}J_{12}\left|SS\right\rangle\left\langle SS\right| = \frac{1}{4}J_{12}(\hat{\sigma}_z+\hat{\mathbb{1}})\otimes(\hat{\sigma}_z+\hat{\mathbb{1}}) . \tag{4.21}$$

It was established empirically in Ref. [66] that for values of splittings J_i used there the strength of the interaction is given by

$$J_{12} = \frac{J_1J_2}{K} , \tag{4.22}$$

where parameter K is a constant. Thus, the control over the exchange splittings (described in the previous section) simultaneously allows to modify the value of the coupling J_{12}. Note that the fact that $J_{12} \propto J_1 J_2$ exposes single-qubit gates to crosstalk when nearby S-T_0 qubits have finite J_i splittings, and methods for dealing with this issue have been discussed [231]. Furthermore, configuration interaction calculations have suggested the existence of parameter regions for two capacitively coupled S-T_0 qubits in which the relation between J_{12} and J_i is more complicated, leading e.g. to predictions of "sweet spots" at which charge-noise induced fluctuations of J_i and/or J_{12} are suppressed [232, 233]. Here, I focus on noisy behavior of J_i measured in Ref. [151] and the resulting noisy behavior of J_{12} following from Eq. (4.22).

The procedure consists of the following steps. Before each run the value of the gradients of magnetic field $\Delta B_{z,i}$ in each DQD is established (e.g. by a measurement or even setting the value with a dedicated procedure). Then each S-T_0 qubit is independently initialized in $|S\rangle$ state, yielding a separable two-qubit state

$$|\psi(t=0)\rangle = |S\rangle \otimes |S\rangle =: |SS\rangle \ . \tag{4.23}$$

For each qubit, the exchange splitting is turned off for a time interval corresponding to $\frac{\pi}{2}$ rotation around x axis due to magnetic gradients. Generally $\Delta B_{z,1} \neq \Delta B_{z,2}$ (for concreteness, suppose that $\Delta B_{z,1} \geqslant \Delta B_{z,2}$) so that each splitting has to be kept turned off for different time interval $t_i = \frac{\pi}{2\Delta B_{z,i}}$. After time t_1 one obtains

$$\begin{aligned} |\psi(t_1)\rangle &= \mathrm{e}^{-\frac{i}{2}\frac{\pi}{2}\hat{\sigma}_x} \otimes \mathrm{e}^{-\frac{i}{2}\Delta B_{z,2} t_1 \hat{\sigma}_x} |SS\rangle \\ &= \frac{1}{\sqrt{2}}\Big(|S\rangle - i\,|T_0\rangle \Big) \otimes \mathrm{e}^{\frac{i}{2}\frac{\pi}{2}\frac{\Delta B_{z,2}}{\Delta B_{z,1}}\hat{\sigma}_x} |S\rangle \ . \end{aligned} \tag{4.24}$$

Then, the splitting J_1 is raised to suppress the rotation of qubit 1 about x axis, while the rotation of qubit 2 is being completed in time $\delta t = t_2 - t_1$:

$$\begin{aligned} |\psi(t_1 + \delta t = t_2)\rangle &= \mathrm{e}^{-\frac{i}{2}J_1 \delta t \hat{\sigma}_z} \otimes \mathrm{e}^{-\frac{i}{2}\Delta B_{z,2}\delta t \hat{\sigma}_x} |\psi(t_1)\rangle \\ &= \frac{1}{\sqrt{2}}\Big(\mathrm{e}^{-i\frac{J_1\delta t}{4}} |S\rangle - i\mathrm{e}^{+i\frac{J_1\delta t}{4}} |T_0\rangle \Big) \\ &\otimes \frac{1}{\sqrt{2}}\Big(|S\rangle - i\,|T_0\rangle \Big) \, . \end{aligned} \tag{4.25}$$

In order to remove the phases imprinted on qubits due to finite $\Delta B_{z,i}$, the spin echo sequences are carried out on each qubit. (Of course, in the more realistic setting in which J fluctuates, the need to remove the influence of slowest of these fluctuations on the final two-qubit state is a much stronger motivation to employ spin echo.) The SE sequence consists of three steps: the evolution with splitting J_i over a chosen time interval, π rotation of a state about x axis (i.e. $2t_i$ interval when the splitting J_i is turned off), which is followed by the evolution for the same time interval. In this case, the durations of SE on each qubit are chosen so that both sequences terminate at the same instant τ. Since $t_1 \neq t_2$ this requirement implies that each SE starts at different time, and they last for unequal durations. Simultaneously during the evolution intervals excluding the periods of evolution corresponding to the π rotations both splittings are on, and hence the two-qubit coupling $\hat{H}_{\mathrm{int}}$ is on as well, thus allowing for qubits to entangle. Figure 4.2 showcases the time dependence of

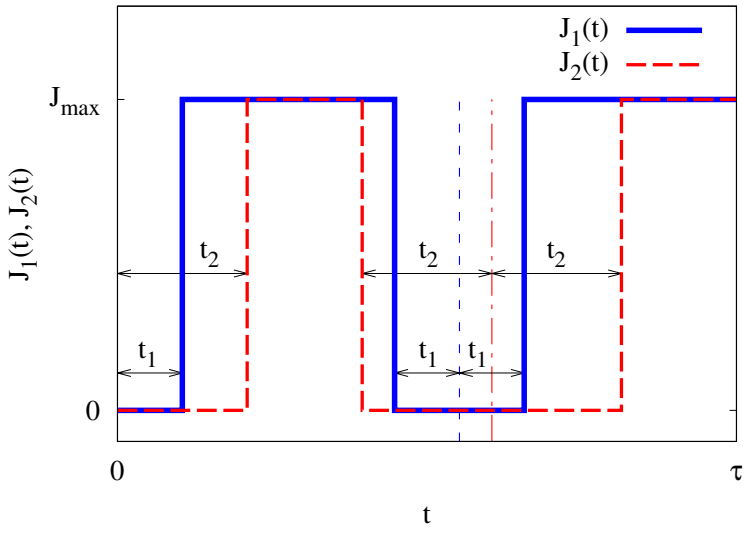

Figure 4.2: The temporal control of the exchange splittings $J_1(t)$, $J_2(t)$ during execution of the entangling procedure when the magnetic field gradients $\Delta B_{z,1} \neq \Delta B_{z,2}$. Thin vertical blue dashed and red dash-dotted lines are positioned at the middle of the durations of π pulses for qubit 1 and 2, respectively.

splittings J_1 and J_2 for the entirety of the entangling procedure. At the end of the procedure, the following state is produced:

$$\begin{aligned} |\tau\rangle \equiv |\psi(\tau)\rangle = & \frac{1}{2}\mathrm{e}^{-\frac{1}{2}iJ_{12}(\tau-3t_2)}\,|SS\rangle \\ & + \frac{i}{2}\,|ST_0\rangle + \frac{i}{2}\,|T_0S\rangle \\ & - \frac{1}{2}\mathrm{e}^{-\frac{1}{2}iJ_{12}(\tau-3t_2)}\,|T_0T_0\rangle\ . \end{aligned} \tag{4.26}$$

Recall that $t_2 > t_1$ because it was assumed that $\Delta B_{z,1} \geqslant \Delta B_{z,2}$ without loss of generality (if $\Delta B_{z,2} > \Delta B_{z,1}$ simply relabel the qubits to obtain the same result). Note that in the currently considered case of fixed J and ΔB_z the latter drops out from the final state $|\tau\rangle$.

It should be noted that for the discrete set of durations $\tau = \tau_{\mathrm{ent}}^{(a)} = (2a-1)\frac{\pi}{J_{12}} + 3t_2$, where a is a natural number, the state $|\tau\rangle$ is maximally entangled, specifically, for odd or even a the entangling procedure generates the state

$$|\psi_{\mathrm{o}}\rangle = \frac{i}{2}\left(-|SS\rangle + |ST_0\rangle + |T_0S\rangle + |T_0T_0\rangle\right) \tag{4.27}$$

or

$$|\psi_{\mathrm{e}}\rangle = \frac{i}{2}\left(|SS\rangle + |ST_0\rangle + |T_0S\rangle - |T_0T_0\rangle\right), \tag{4.28}$$

respectively. One can easily notice that the entangling procedure realizes a CPHASE gate: $-\mathrm{e}^{-iJ_{12}\frac{\tau-3t_2}{2}}|SS\rangle\langle T_0T_0| - |ST_0\rangle\langle T_0S| - |T_0S\rangle\langle ST_0| - \mathrm{e}^{-iJ_{12}\frac{\tau-3t_2}{2}}|T_0T_0\rangle\langle SS|$.

4.4 The Quantification of Two-Qubit Entanglement

The next step is to quantify the level of entanglement possessed by the two-qubit state $|\tau\rangle$ produced at the end of the entangling procedure. For two-qubit states de-

scribed by the density operator $\hat{\rho}$ the most commonly used measure of entanglement is the concurrence [21].

For the family of output states $\hat{\rho}(\tau) = |\tau\rangle\langle\tau|$ the concurrence is given by

$$C\left(\hat{\rho}(\tau)\right) = \left|\sin\left[\frac{1}{2}J_{12}(\tau - 3t_2)\right]\right| . \tag{4.29}$$

One can make use of an alternative strategy to check to what degree the resulting state is entangled: high level (greater than 1/2) of fidelity calculated between the actual state $|\tau\rangle$ and the expected entangled state $|\psi_{\rm o}\rangle$ or $|\psi_{\rm e}\rangle$, defined as $F(|\tau\rangle, |\psi_{\rm o}\rangle) = |\langle\tau|\psi_{\rm o}\rangle|^2$, confirms the entanglement [66]. In general, for mixed states, fidelity is defined as $F(\hat{\rho}(\tau), \hat{\rho}_{\rm o}) = {\rm Tr}\{\hat{\rho}(\tau)\hat{\rho}_{\rm o}\}$. If one of the states is pure, as we will be having below, fidelity is given by $F(\hat{\rho}(\tau), |\psi_{\rm o}\rangle) = \langle\psi_{\rm o}|\hat{\rho}(\tau)|\psi_{\rm o}\rangle$.

In Fig. 4.3 I show the results of numerical calculation of concurrence of the final two-qubit state as a function of the procedure duration τ in a model less idealized than in the previous section. While I am still assuming that J_i and $\Delta B_{z,i}$ do not experience any fluctuations, I now keep $\Delta B_{z,i}$ fixed during the evolution (as it is the case in experiment), so that the evolution with finite J_i does not amount to phase evolution in the computational basis of S/T_0 states of two qubits, thus numerical evaluation of the entanglement measure is necessary.

Although the impact of always-on $\Delta B_{z,i}$ terms amounts to a small drop of level of entanglement of the resulting state compared to that from the idealized scenario described in the previous section (see Fig. 4.3), it reveals also another delicate effect: level of entanglement of the resulting state $|\tau\rangle$ starts to oscillate with frequency of precession of single qubit states $\omega_i = \sqrt{\Delta B_{z,i}^2 + J_i^2}$ due to the fact that in such conditions the qubits' states rotate around the axis which does not coincide with z axis exactly, but is tilted in xz plane because of presence ΔB_z. Characteristically, the oscillations of entanglement of the state $\hat{\rho}(\tau)$ gradually increase their amplitude with increasing durations for $0 < \tau \lesssim 2\frac{\pi}{J_{12}}$ and reach their maximum amplitude at $\tau \approx 2\frac{\pi}{J_{12}}$. Then the amplitude of oscillations decreases for $2\frac{\pi}{J_{12}} \lesssim \tau \lesssim 4\frac{\pi}{J_{12}}$. The observed pattern of the fast oscillations of two-qubit entanglement is periodic in the duration τ of the entangling procedure, with a period of about $4\frac{\pi}{J_{12}}$. Such a pattern of oscillation amplitude τ-dependence is a consequence of the entangling procedure design: at $\tau = 2\frac{\pi}{J_{12}}$ the ideal resulting state $|\tau\rangle = -\frac{1}{2}\left(|S\rangle - i|T_0\rangle\right)^{\otimes 2}$ is unentangled due to a very specific combination of phases generated before and after the π rotations of qubits' states. The two-qubit state that is produced in the middle of the idealized realization of the entangling procedure (just before the step of π rotations) is fully entangled. However, when the axes around which qubit states precess are tilted from z direction, the initial superposition states do not rotate in the equatorial plane (as intended) but in a slightly tilted plane. After the π rotation around x axes those states land on the plane which is tilted off of the z axis in the opposite direction, and subsequently the phases which qubits' states acquire during the second half of the procedure are no longer in a perfect correspondence to the previously obtained phases and now they do not counterbalance each other, so the final two-qubit state manifests unexpected entanglement. One can also notice that in the presence of constant $\Delta B_{z,i}$ the period of slow entanglement oscillations is slightly longer compared to the idealized case (see Fig. 4.3). This fact cannot be illustrated with the help of Bloch sphere as it originates from a two-qubit interaction, but it is evident from the numerical diagonalization of the full two-qubit Hamiltonian: when $\Delta B_{z,i}$ are present,

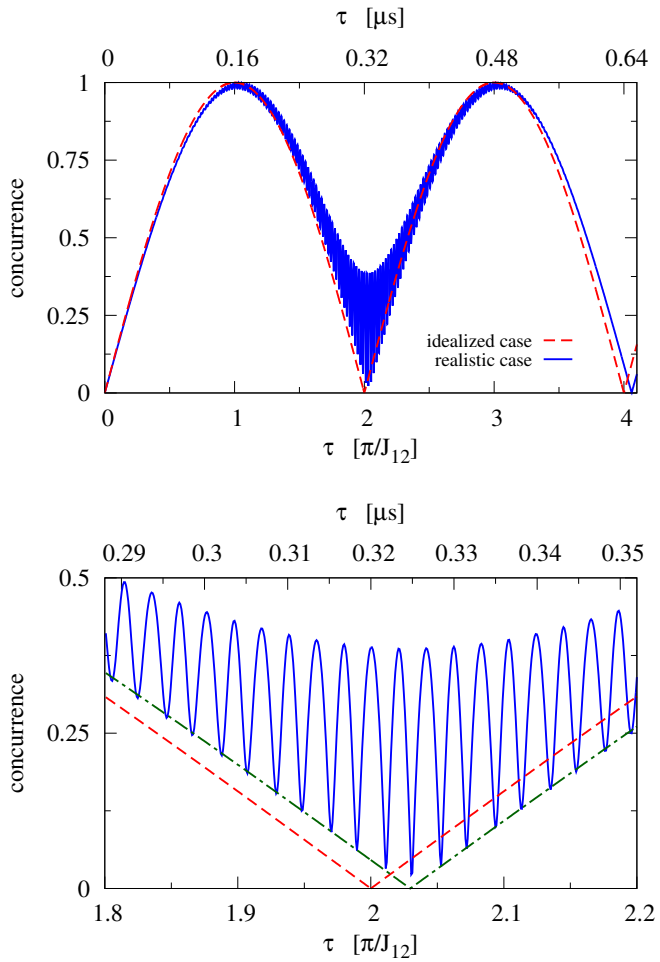

Figure 4.3: Top panel: Concurrence of the two-qubit state generated in the idealized realization of the entangling procedure described in Sec. 4.3 ($\Delta B_{z,i}$ are on during the qubit rotations only, the rotations assumed to be perfect) plotted as red dashed line, and the same for a more realistic procedure considered in Sec. 4.4 ($\Delta B_{z,i}$ are always on, albeit none of the parameters of the Hamiltonian are fluctuating) plotted as a solid blue line. The parameters are close to those from experiment [66]: $J_1 = J_2 = 1.2$ μeV (with corresponding frequency $J_i/h = 300$ MHz), $J_{12} = 1.29 \cdot 10^{-2}$ μeV, $\Delta B_{z,1} = \Delta B_{z,2} = 0.12$ μeV. Bottom panel: zoomed in region of the top panel in the vicinity of $\tau \approx 2\frac{\pi}{J_{12}}$, red dotted line is the concurrence obtained in the idealized case, blue solid line is the concurrence obtained in a more realistic case with constant parameters J_i, J_{12}, $\Delta B_{z,i}$, and blue green dash-dotted line is the concurrence obtained in the idealized case, but with value of J_{12} from the latter case.

the rate of acquisition of the desired two-qubit phase is slower than that of the ideal case (CPHASE gate is rotated from the basis of $\{|SS\rangle,\ |ST_0\rangle,\ |T_0S\rangle,\ |T_0T_0\rangle\}$ to the basis of eigenvectors of the full Hamiltonian, and as a result the rate of two-qubit phase acquisition becomes lower).

4.5 Entangling Procedure in the Presence of Decoherence

In the experiment [66] it turned out that the two-qubit states obtained as outcome of the procedure were indeed entangled, but only for short durations τ of the procedure. Furthermore, the maximal level of entanglement of the generated states was decreased compared to that of the expected ones. I consider below possible factors that preclude from obtaining the maximally entangled two-qubit states.

4.5.1 Influence of fluctuations of magnetic field gradients on efficiency of the entangling procedure

The magnetic field gradients between the QDs, which are the sources of finite $\Delta B_{z,i}$ (with $i = 1, 2$), are often produced by the polarized in an appropriate way nuclear spins of the atoms from which the sample is built [159, 66]. The spin bath is dynamically polarized before each iteration of the experiment of entangling of qubits. Due to the slowness of the intrinsic dynamics of the nuclear spin bath one does not expect any fluctuation on the time scale of a single run of the experiment (~ 1 μs). However, possible variations of the values of $\Delta B_{z,i}$ from one run of the experiment to another is the factor which can preclude from obtaining the maximally entangled states. This effect is mainly caused by imprecise rotations of qubits' states around x axis, which are performed just after the initializations of the qubits in $|SS\rangle$ state ($\frac{\pi}{2}$ rotations) and in the middle of the entangling procedure (π rotations). Such systematical errors lead to forming unequal superposition states of $|S\rangle$ and $|T_0\rangle$. The influence of quasistatic fluctuations of $\Delta B_{z,i}$ on the efficiency of the entangling procedure results in a decrease of the overall efficiency independently of τ, i.e. the fluctuating quasistatically $\Delta B_{z,i}$ influences in a similar way the outcomes for all duration τ of the entangling procedure.

This effect can be easily seen when one considers the idealized realization of the procedure: for simplicity, let us assume that only the first rotation was not exactly $\frac{\pi}{2}$ around x axis (errors of rotations $\hat{R}_x(\frac{\pi}{2})$ and $\hat{R}_x(\pi)$ will accumulate – there is no possibility that the next rotation cancels the error of the previous one). In such a case, the procedure will produce the state $|\tau(\theta_1,\theta_2)\rangle = |SS\rangle(-i)\sin\frac{\theta_1}{2}\sin\frac{\theta_2}{2}\exp(-i\frac{\tau}{2}J_{12}) + |ST_0\rangle(-i)\sin\frac{\theta_1}{2}\cos\frac{\theta_2}{2} + |T_0S\rangle(-i)\cos\frac{\theta_1}{2}\sin\frac{\theta_2}{2} + |T_0T_0\rangle\cos\frac{\theta_1}{2}\cos\frac{\theta_2}{2}\exp(-i\frac{\tau}{2})$, where θ_i is the actual angle of rotation of the state of ith qubit around x axis. This state $|\tau(\theta_1,\theta_2)\rangle$ is maximally entangled when superpositions of $|S\rangle$ and $|T_0\rangle$, created in each qubit from the separable two-qubit state $|SS\rangle$ after $\hat{R}_x(\frac{\pi}{2})$ rotation, are equal (i.e. all components have the same amplitudes): at $\tau = \pi/J_{12}$ the state $|\tau(\theta_1,\theta_2)\rangle$ should become $|\psi_o\rangle$, which is maximally entangled, so one can estimate entanglement of $|\tau(\theta_1,\theta_2)\rangle$ by calculating fidelity $F(|\tau(\theta_1,\theta_2)\rangle, |\psi_o\rangle) = |\langle\tau(\theta_1,\theta_2)|\psi_o\rangle|^2 = \frac{1}{4}|\sin\frac{\theta_1}{2}\sin\frac{\theta_2}{2} + \sin\frac{\theta_1}{2}\cos\frac{\theta_2}{2} + \cos\frac{\theta_1}{2}\sin\frac{\theta_2}{2} + \cos\frac{\theta_1}{2}\cos\frac{\theta_2}{2}|^2$, which has its maximum $F = 1$ when $\theta_1 = \theta_2 = \frac{\pi}{2}$. Any deviation of $\theta_1, \theta_2 \in [0, \pi]$ will reduce the degree of entanglement of the state $|\tau(\theta_1,\theta_2)\rangle$. On the other hand, having a pure state $|\tau(\theta_1,\theta_2)\rangle$ it is possible to calculate analytically its concurrence $C(|\tau(\theta_1,\theta_2)\rangle) = |\langle\tau(\theta_1,\theta_2)|\hat{\sigma}_y \otimes \hat{\sigma}_y|\tau^*(\theta_1,\theta_2)\rangle| = 4\sin\frac{\theta_1}{2}\cos\frac{\theta_1}{2}\sin\frac{\theta_2}{2}\cos\frac{\theta_2}{2}\sin(\frac{\tau}{2}J_{12})$, which, when $\tau = \pi/J_{12}$, varies from $C = 1$ for $\theta_1 = \theta_2 = \frac{\pi}{2}$ to $C = 0$ when $\theta_1, \theta_2 \to 0$ or π. Hence, the impact of quasistatical fluctuations of magnetic field gradients $\Delta B_{z,i}$ amounts to a loss of the

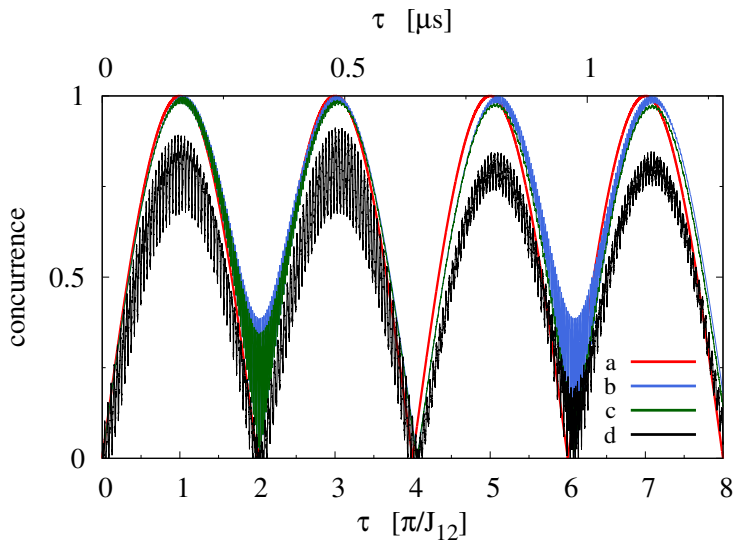

Figure 4.4: Concurrence of the two-qubit state $|\tau\rangle$ obtained in (a) idealized realization of entangling procedure (the same as red dashed line in Fig. 4.3), (b) entangling procedure with always-on constant $\Delta B_{z,i}$ (the same as blue solid line in Fig. 4.3), (c) entangling procedure in which magnetic field gradients $\Delta B_{z,i}$ are constant during a single run of entangling procedure but fluctuate quasistatically from one run to another (average over 10,000 realizations, $\Delta B_{z,i} \sim \mathcal{N}(\overline{\Delta B_{z,i}}, \sigma_{\Delta B_{z,i}})$, $\sigma_{\Delta B_{z,i}} = 15\%\,\overline{\Delta B_{z,i}}$), here rotations around x axis artificially kept perfect (i.e. precisely $\frac{\pi}{2}$ at the beginning and π in the middle of the procedure), (d) the same as (c) but with imprecise rotations around x axis which arise as a result of mismatch of the rotation time and the actual value of $\Delta B_{z,i}$. All results are obtained under the assumption that S-T_0 splittings J_i do not fluctuate and are switched on when needed (as shown in Fig. 4.2). Values of parameters are the same as in Fig. 4.3.

maximal level of produced entanglement (see Fig. 4.4). This effect is independent of the duration τ of the procedure and does not lead to a complete inability to yield some entanglement when fluctuations of $\Delta B_{z,i}$ are moderate or small. Another important observation which comes from Fig. 4.4 is that the presence of quasistatically fluctuating magnetic gradients $\Delta B_{z,i}$ during the entire entangling procedure, does not degrade the efficiency of the procedure by a significant amount while rotations of qubit states around x axis are accurate (cf. line c, which is very close to line b, with line d in Fig. 4.4).

Consequently, in the rest of the chapter, where I will focus on influence of fluctuations of J_i that will lead to complete decay of entanglement, I will neglect all the above-discussed effects of quasistatic fluctuations of $\Delta B_{z,i}$ and rotation errors caused by $\Delta B_{z,i}$ being finite, albeit small in comparison to J_i.

4.5.2 Influence of fluctuations of exchange splittings on efficiency of the entangling procedure

4.5.2.1 Quasistatic fluctuations of exchange splittings

To begin with, I consider the influence of quasistatic fluctuations of exchange splittings J_i on the entanglement generation. The influence of quasistatically fluctuat-

ing exchange splittings $J_1,\ J_2$ can be estimated by disregarding off-diagonal terms of the Hamiltonian (but the qubit rotations involved in the entangling procedure are assumed to be perfect) and performing the averaging of the density operator Eq. (4.30) over the distributions of $J_1,\ J_2$. I assume that $J_1,\ J_2$ fluctuate according to the normal distributions with mean values $\bar{J}_1,\ \bar{J}_2$ and standard deviations σ_{J_1}, σ_{J_2}, respectively.

The idealized entangling procedure generates states which are described by the following density operator:

$$\begin{aligned}\hat{\rho}(\tau) &= |\psi(\tau)\rangle\langle\psi(\tau)| \\ &= \frac{1}{4}\begin{pmatrix} 1 & -i\phi(\tau) & -i\phi(\tau) & -1 \\ i\phi^*(\tau) & 1 & 1 & -i\phi^*(\tau) \\ i\phi^*(\tau) & 1 & 1 & -i\phi^*(\tau) \\ -1 & i\phi(\tau) & i\phi(\tau) & 1 \end{pmatrix},\end{aligned} \tag{4.30}$$

where $\phi(\tau) = \exp\left(-i\frac{\tau}{2}J_{12}\right)$. After averaging over quasistatic fluctuations of $J_1,\ J_2$ one obtains the density operator

$$\langle\hat{\rho}(\tau)\rangle = \frac{1}{4}\begin{pmatrix} 1 & -i\langle\phi(\tau)\rangle & -i\langle\phi(\tau)\rangle & -1 \\ i\langle\phi^*(\tau)\rangle & 1 & 1 & -i\langle\phi^*(\tau)\rangle \\ i\langle\phi^*(\tau)\rangle & 1 & 1 & -i\langle\phi^*(\tau)\rangle \\ -1 & i\langle\phi(\tau)\rangle & i\langle\phi(\tau)\rangle & 1 \end{pmatrix}, \tag{4.31}$$

where

$$\begin{aligned}\langle\phi(\tau)\rangle = &\frac{2K}{\sqrt{4K^2+\sigma_{J_1}^2\sigma_{J_2}^2\tau^2}}\exp\left(-i\frac{4\bar{J}_1\bar{J}_2K\tau}{8K^2+2\sigma_{J_1}^2\sigma_{J_2}^2\tau^2}\right) \\ &\times\exp\left(-\frac{(\bar{J}_1^2\sigma_{J_2}^2+\bar{J}_2^2\sigma_{J_1}^2)\tau^2}{8K^2+2\sigma_{J_1}^2\sigma_{J_2}^2\tau^2}\right),\end{aligned} \tag{4.32}$$

where constant $K = \bar{J}_1\bar{J}_2/\bar{J}_{12}$, and $\bar{J}_{12} = \frac{\pi}{\tau_{\rm ent}}$. In the experiment [66], the values of parameters were as follows: $\bar{J}_1 = 1.16\ \mu$eV, $\bar{J}_2 = 1.32\ \mu$eV, $\bar{J}_{12} = 1.29\cdot 10^{-2}\ \mu$eV, $\overline{\Delta B_{z,1}} = \overline{\Delta B_{z,2}} = 0.12\ \mu$eV (so $t_2 = 0$ in the Eq. (4.29)). Note that I am using J_{12} twice larger than the value reported in Ref. [66]. However, with this value one obtains the period of oscillations of concurrence in agreement with experimental data, i.e. the first maximum of entanglement occurs at $\tau = \pi/J_{12} \approx 160$ ns.

Entanglement of Eq. (4.31) as a function of duration τ is shown in the top panel of Fig. 4.5 for J_i drawn from normal distribution with standard deviations $\sigma_i = 15\%\bar{J}_i$. Due to quasistatic fluctuations of J_i the overall efficiency of the entangling procedure decreases with increase of its duration τ. Although the direct impact of the quasistatic fluctuations of $J_1,\ J_2$ on the resulting two-qubit state is completely removed by utilizing simultaneous Hahn echo sequence on each qubit, the entangling interaction between qubits, which is determined by two-qubit interaction energy $J_{12} \propto J_1J_2$, remains sensitive to the fluctuations, and this causes decay of the entangling procedure efficiency with increasing duration τ.

4.5.2.2 Dynamical fluctuations of exchange splittings

In the experiment [66], the procedure of entangling two S-T_0 qubits was based on the SE procedure. While the SE perfectly cancels the impact of quasistatic single-qubit

noises on the end state, in the case of dynamical fluctuations it helps to refocus the state of the qubits only partially. Moreover, the two-qubit interaction part of the evolution operator that describes the entangling procedure (which is responsible for the entanglement generation) is not affected by the SE procedure, and consequently it is susceptible to noisy electric fields (leading to noise in J_i and J_{12}) in the same way as in FID experiment. As a result, the overall efficiency of the entangling procedure decays with increasing its duration τ.

In order to estimate analytically the influence of dynamical fluctuations of exchange splittings, I approximate the Hamiltonian of the system by its diagonal neglecting the off-diagonal terms associated with magnetic field gradients $\Delta B_{z,i}$, which were an order of magnitude smaller than exchange splittings J_i in the experiment [66]:

$$\begin{aligned}\hat{H}_{2\mathrm{q}} \approx \hat{H}_{2\mathrm{q}}^{\mathrm{diag}} = \frac{1}{2}\Big(&J_1(t)\sigma_z \otimes \mathbb{1} + J_2(t)\mathbb{1} \otimes \sigma_z \\ &+ \frac{1}{2}J_{12}(t)(\sigma_z + \mathbb{1}) \otimes (\sigma_z + \mathbb{1})\Big).\end{aligned} \tag{4.33}$$

Assuming perfect rotations of qubits' states, averaged density operator elements of the resulting two-qubit state after performing the entangling procedure are

$$\begin{aligned}&\langle \rho_{ab,cd}(\tau)\rangle = \langle\langle ab|\hat{\rho}(\tau)|cd\rangle\rangle \\ &= \langle\langle ab|\hat{U}_{\mathrm{SE}}(\tau)\hat{\rho}^{\mathrm{initial}}\hat{U}_{\mathrm{SE}}^{\dagger}(\tau)|cd\rangle\rangle \\ &= \langle\langle ab|\hat{U}_{\mathrm{FID}}\Big(\frac{\tau}{2},\tau\Big)\Big((-i\sigma_x)\otimes(-i\sigma_x)\Big)\hat{U}_{\mathrm{FID}}\Big(0,\frac{\tau}{2}\Big) \\ &\times \sum_{kl,mn}\rho_{kl,mn}^{\mathrm{initial}}|kl\rangle\langle mn| \\ &\times \hat{U}_{\mathrm{FID}}^{\dagger}\Big(0,\frac{\tau}{2}\Big)\Big((i\sigma_x)\otimes(i\sigma_x)\Big)\hat{U}_{\mathrm{FID}}^{\dagger}\Big(\frac{\tau}{2},\tau\Big)|cd\rangle\rangle,\end{aligned} \tag{4.34}$$

where evolution operator $\hat{U}_{\mathrm{FID}}(t_1,t_2) = \exp\left(-i\int_{t_1}^{t_2}\hat{H}_{2\mathrm{q}}(t)\mathrm{d}t\right) \approx \exp\left(-i\int_{t_1}^{t_2}\hat{H}_{2\mathrm{q}}^{\mathrm{diag}}(t)\mathrm{d}t\right)$.

Analyzing the two-qubit system, I consider two distinct possibilities of dynamical fluctuations: splitting energies J_1, J_2 could fluctuate independently, i.e. $J_i(t) = \bar{J}_i + \delta J_i(t)$, or their fluctuations may have a common source $J_i(t) = \bar{J}_i + s_i\delta J(t)$, where $s_i \in [0,1]$ is a coupling of ith qubit to the noise. Note that correlations of low-frequency charge noises affecting two quantum dots separated by ~ 100 nm distance have been observed in experiments [234, 235]. Correspondingly, the two-qubit coupling in the former case reads

$$\begin{aligned}J_{12}(t) = \frac{J_1(t)J_2(t)}{K} &= \frac{1}{K}\left[\bar{J}_1 + \delta J_1(t)\right]\left[\bar{J}_2 + \delta J_2(t)\right] \\ &\approx \frac{1}{K}\left[\bar{J}_1\bar{J}_2 + \bar{J}_2\delta J_1(t) + \bar{J}_1\delta J_2(t)\right],\end{aligned} \tag{4.35}$$

and in the latter case

$$\begin{aligned}J_{12}(t) = \frac{J_1(t)J_2(t)}{K} &= \frac{1}{K}\left[\bar{J}_1 + s_1\delta J(t)\right]\left[\bar{J}_2 + s_2\delta J(t)\right] \\ &\approx \frac{1}{K}\left[\bar{J}_1\bar{J}_2 + \left(s_1\bar{J}_1 + s_2\bar{J}_2\right)\delta J(t)\right].\end{aligned} \tag{4.36}$$

Note that I neglect here the quadratic in noises small terms $\propto \delta J_1(t)\delta J_2(t)$ and $\propto (\delta J(t))^2$.

For the case of independent (completely uncorrelated) charge noises that affect $J_1(t)$ and $J_2(t)$, the average density operator elements of the generated state are

$$\begin{aligned}
&\langle \rho_{ab,cd}(\tau)\rangle = \langle\langle ab|\hat{\rho}(\tau)|cd\rangle\rangle \\
&= \rho^{\text{initial}}_{-a-b,-c-d} \mathrm{e}^{-i\frac{\bar{J}_1\bar{J}_2}{4K}(ab-cd)\tau} \\
&\times \left\langle \exp\Big[-\frac{i}{2}\Big(\frac{\bar{J}_2}{2K}(ab-cd)\int_0^\tau \mathrm{d}t\, \delta J_1(t) f_{\text{FID}}(t) \right. \\
&\left. +\big(c-a+\frac{\bar{J}_2}{2K}(c+d-a-b)\big)\int_0^\tau \mathrm{d}t\, \delta J_1(t) f_{\text{SE}}(t)\Big)\Big] \right\rangle \\
&\times \left\langle \exp\Big[-\frac{i}{2}\Big(\frac{\bar{J}_1}{2K}(ab-cd)\int_0^\tau \mathrm{d}t\, \delta J_2(t) f_{\text{FID}}(t) \right. \\
&\left. +\big(d-b+\frac{\bar{J}_1}{2K}(c+d-a-b)\big)\int_0^\tau \mathrm{d}t\, \delta J_2(t) f_{\text{SE}}(t)\Big)\Big] \right\rangle \qquad (4.37) \\
&= \rho^{\text{initial}}_{-a-b,-c-d} \mathrm{e}^{-i\frac{\bar{J}_1\bar{J}_2}{4K}(ab-cd)\tau} \\
&\times \exp\Big[-\frac{1}{2}\Big\{ \Big(\frac{\bar{J}_2}{4K}(ab-cd)\Big)^2 \chi_{\text{FID},J_1}(\tau) \\
&+ \Big(\frac{1}{2}\big(c-a+\frac{\bar{J}_2}{2K}(c+d-a-b)\big)\Big)^2 \chi_{\text{SE},J_1}(\tau)\Big\}\Big] \\
&\times \exp\Big[-\frac{1}{2}\Big\{ \Big(\frac{\bar{J}_1}{4K}(ab-cd)\Big)^2 \chi_{\text{FID},J_2}(\tau) \\
&+ \Big(\frac{1}{2}\big(d-b+\frac{\bar{J}_1}{2K}(c+d-a-b)\big)\Big)^2 \chi_{\text{SE},J_2}(\tau)\Big\}\Big], \qquad (4.38)
\end{aligned}$$

where a, b, c, $d \in \{1,-1\}$ (these parameters code the basis $\{|SS\rangle, |ST_0\rangle, |T_0S\rangle, |T_0T_0\rangle\}$ as $\{11, 1\,{-1}, {-11}, {-1}\,{-1}\}$ in indices of density operator elements), and $\chi_{\text{FID},J_i}(\tau)$, $\chi_{\text{SE},J_i}(\tau)$ are the attenuation factors that describe the influence of dynamical noise of $J_i(t)$ in the case of FID (with constant time domain filter function $f_{\text{FID}}(t)$) or SE (with time domain filter function with a single sign inversion $f_{\text{SE}}(t)$). For noise spectrum of the form $S(\omega)=A/\omega^\beta$ they are given by

$$\chi_{\text{FID}}(\tau) = \frac{4A}{\pi}\int_0^\infty \frac{\mathrm{d}\omega}{\omega^{2+\beta}} \sin^2\frac{\omega\tau}{2}\ , \qquad (4.39)$$

$$\chi_{\text{SE}}(\tau) = \frac{16A}{\pi}\int_0^\infty \frac{\mathrm{d}\omega}{\omega^{2+\beta}} \sin^4\frac{\omega\tau}{4}\ , \qquad (4.40)$$

see Appendix (p. 123) for the details of derivation and simple analytical approximations in considered here cases of $\beta=0.7$ and 2.

Owing to the fact that the approximated Hamiltonian is diagonal, the density operator undergoes the decoherence of pure dephasing type. There are two essentially distinct types of the off-diagonal elements of two-qubit density operator. The density operator elements with a single spin flip: $\langle\rho_{11,1-1}(\tau)\rangle$, $\langle\rho_{11,-11}(\tau)\rangle$, $\langle\rho_{1-1,-1-1}(\tau)\rangle$, $\langle\rho_{-11,-1-1}(\tau)\rangle$ and their Hermitian conjugated partners diminish mainly due to decrease of single-qubits' signals $\propto \exp\big(-\frac{1}{2}\chi_{\text{SE}}(\tau)\big)$, whereas elements with two spin flips: $\langle\rho_{11,-1-1}(\tau)\rangle$, $\langle\rho_{1-1,-11}(\tau)\rangle$ and their Hermitian conjugated partners decay two times faster as both qubits make their contribution to the

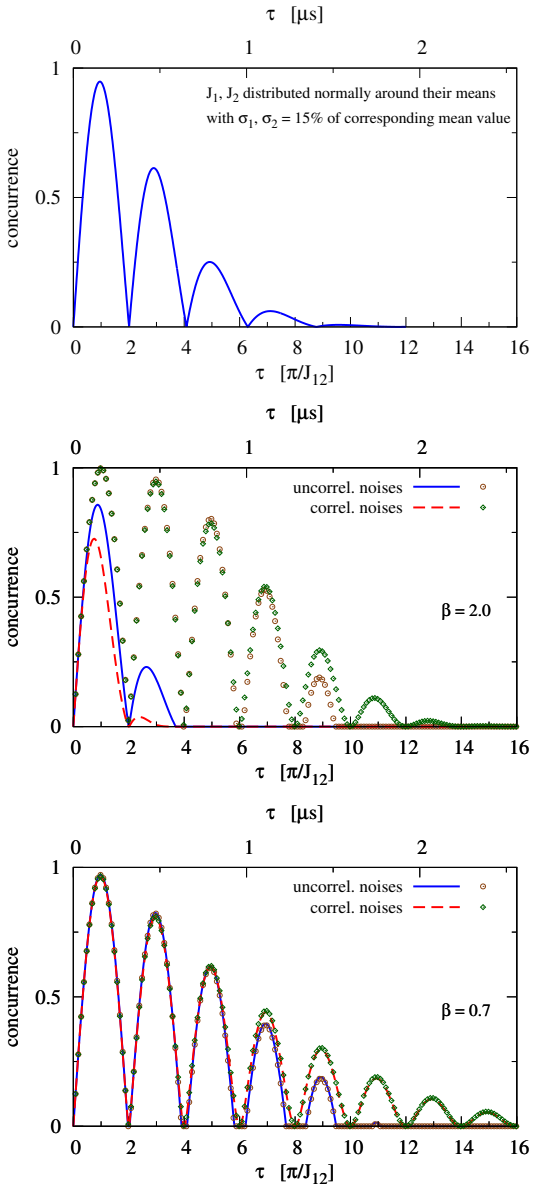

Figure 4.5: Concurrence of the two-qubit state $\langle\hat{\rho}(\tau)\rangle$ as a function of the duration τ of the entanglement generation procedure. Lines are results for the case in which fluctuations of J_i and J_{12} are taken into account, while results in which the fluctuations of J_{12} were artificially turned off are shown with open symbols. Top panel: The case of quasistatically fluctuating J_1, J_2 with standard deviations $\sigma_i = 0.15\bar{J}_i$ (Eq. (4.31)). Middle and bottom panels: The cases of dynamically fluctuating J_1, J_2, and hence J_{12}, due to $1/f^{\beta}$ noise that is uncorrelated (blue solid line) or perfectly correlated (red dashed lines) for the two qubits. The power of the noise affecting each qubit was chosen to be such that ensures the time scale of decay of single-qubit SE signal like in the experiment [151]: S-T_0 qubit having $J = 1.16$ μeV shows $T_{\rm SE} \approx 1.6$ μs, S-T_0 qubit having $J = 1.32$ μeV shows $T_{\rm SE} \approx 1.4$ μs.

decay $\propto \exp\left(-\chi_{\rm SE}(\tau)\right)$. Hence, the scale on which one can expect the generation of entangled state is limited from above by the single-qubit SE decay time.

In the case of correlated noises, $J_i(t) = \bar{J}_i + s_i\delta J(t)$, the averaged density operator

elements are of the following form:

$$\begin{aligned}
&\langle \rho_{ab,cd}(\tau)\rangle = \langle\langle ab|\hat{\rho}(\tau)|cd\rangle\rangle \\
&= \rho^{\text{initial}}_{-a-b,-c-d} \mathrm{e}^{-i\frac{\bar{J}_1\bar{J}_2}{4K}(ab-cd)\tau} \\
&\times \Big\langle \exp\Big[-\frac{i}{2}\Big\{\frac{s_1\bar{J}_2+s_2\bar{J}_1}{2K}(ab-cd) \\
&\times \int_0^\tau \mathrm{d}t\, \delta J(t) f_{\text{FID}}(t) \\
&+ \Big(s_1\big(c-a+\frac{\bar{J}_2}{2K}(c+d-a-b)\big) \\
&+ s_2\big(d-b+\frac{\bar{J}_1}{2K}(c+d-a-b)\big)\Big) \\
&\times \int_0^\tau \mathrm{d}t\, \delta J(t) f_{\text{SE}}(t)\Big\}\Big]\Big\rangle \qquad (4.41) \\
&= \rho^{\text{initial}}_{-a-b,-c-d} \mathrm{e}^{-i\frac{\bar{J}_1\bar{J}_2}{4K}(ab-cd)\tau} \\
&\times \exp\Big[-\frac{1}{2}\Big\{\Big(\frac{s_1\bar{J}_2+s_2\bar{J}_1}{4K}(ab-cd)\Big)^2 \chi_{\text{FID}}(\tau) \\
&+ \Bigg(\frac{1}{2}\Big(s_1\big(c-a+\frac{\bar{J}_2}{2K}(c+d-a-b)\big) \\
&+ s_2\big(d-b+\frac{\bar{J}_1}{2K}(c+d-a-b)\big)\Big)\Bigg)^2 \chi_{\text{SE}}(\tau)\Big\}\Big]. \qquad (4.42)
\end{aligned}$$

The key qualitative feature of Eqs. (4.38) and (4.42) is the presence of terms proportional to χ_{SE}, in which the low-frequency noise is suppressed by the echo procedure, and of terms proportional to χ_{FID}, related to fluctuations of interqubit interactions, in which the low-frequency noise spectrum fully contributes to dephasing.

In Fig. 4.5 the amount of entanglement is presented in the case of uncorrelated noises for two exponents characterizing $1/f^\beta$ noise, $\beta = 2.0$ and 0.7 (middle and bottom panels, respectively). As can be seen in the bottom panel of Fig. 4.5, for $\beta<1$ the decay of the overall efficiency of the entangling procedure is mainly caused by influence of fluctuations of splittings of individual qubits (which also fully determines the decay of the fidelity of single-qubit coherence). On the other hand, for $\beta > 1$, (e.g. $\beta = 2.0$, the middle panel of Fig. 4.5), the decay of the overall entanglement generation efficiency is mostly due to the infidelity of the entangling gate, which is realized by dynamically fluctuating two-qubit term. This is due to the fact that for noise that is very strongly concentrated at lowest frequencies, single-qubit noise is very efficiently suppressed by the echo procedure, and the non-echoed fluctuations of two-qubit interaction, which are the sources of terms $\propto \chi_{\text{FID}}/K$ in the above expressions for two-qubit coherences, are dominating the dephasing of the final state. Thus, the effect of dynamical noise of J_i with high value of β on the final state is qualitatively the same to that of quasistatic fluctuations of splittings J_i, where single-qubit terms cancel out perfectly (thanks to applying Hahn echo on each qubit) and the fidelity of two-qubit entangling gate, which is susceptible to fluctuations as in FID experiment, is diminishing when the duration τ of the procedure becomes longer.

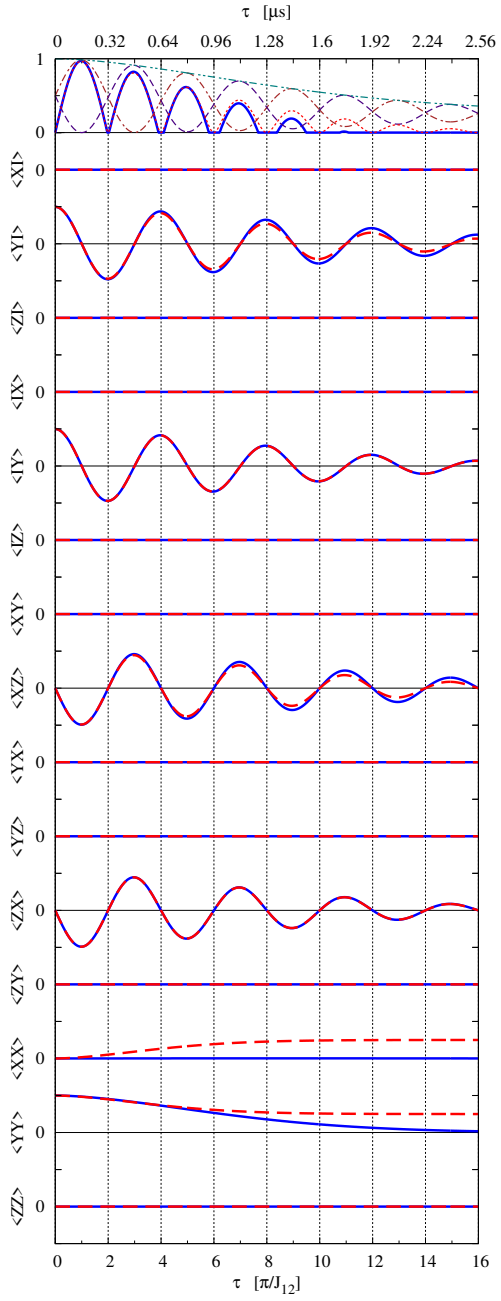

Figure 4.6: Pauli set for the case of $1/f^{0.7}$ noise. Blue lines show calculated Pauli set for two independent noises of $J_1(t), J_2(t)$, whereas red lines show calculated Pauli set for correlated noises $J_1(t) = J_2(t)$. In the top panel, for the case of independent noises the following measures are shown: blue solid line is concurrence of $\langle\hat{\rho}(\tau)\rangle$, brown dashed line is fidelity $\langle\psi_o|\langle\hat{\rho}(\tau)\rangle|\psi_o\rangle$ (see Eq. (4.27)), purple dash-dotted line is fidelity $\langle\psi_e|\langle\hat{\rho}(\tau)\rangle|\psi_e\rangle$ (see Eq. (4.28)), turquoise dotted line is fidelity $\langle\psi(\tau)|\langle\hat{\rho}(\tau)\rangle|\psi(\tau)\rangle$ (see Eq. (4.26); and red dotted line is concurrence calculated for correlated noises $J_1(t) = J_2(t)$. The power of the noise affecting each qubit was chosen to be such that ensures the time scale of decay of single-qubit SE signal like in the experiment [151]: S-T_0 qubit having $J = 1.16$ μeV shows $T_{\rm SE} \approx 1.6$ μs, S-T_0 qubit having $J = 1.32$ μeV shows $T_{\rm SE} \approx 1.4$ μs. In the case of fully correlated noises $J_1(t) = J_2(t)$, the higher power of the noise has been chosen for both qubits.

In Fig. 4.6 the two Pauli sets for two-qubit states created in the entangling procedure are presented for the case of two uncorrelated $1/f^{0.7}$ noises (blue lines) and for the case of two fully correlated $1/f^{0.7}$ noises (red lines). In noise-free experiment, one expects that the only nonzero two-qubit correlations $\langle \hat{\sigma}_i \otimes \hat{\sigma}_j \rangle = \mathrm{Tr}\{(\hat{\sigma}_i \otimes \hat{\sigma}_j)\, \hat{\rho}(\tau)\}$ are

$$\langle \sigma_x \otimes \sigma_z \rangle = \langle \sigma_z \otimes \sigma_x \rangle = -\sin J_{12} \frac{\tau}{2}, \tag{4.43}$$

$$\langle \sigma_z \otimes \mathbb{1} \rangle = \langle \mathbb{1} \otimes \sigma_y \rangle = \cos J_{12} \frac{\tau}{2}, \tag{4.44}$$

$$\langle \sigma_y \otimes \sigma_y \rangle = 1. \tag{4.45}$$

Dynamical fluctuations of splittings J_i destroy these correlations and diminish their amplitude with increasing duration τ. It is important to notice that fully correlated noises always lead to decreased but non-zero value of $\langle \sigma_y \otimes \sigma_y \rangle \overset{\tau\to\infty}{=} 2\,\mathrm{Re}\,\rho^{\mathrm{initial}}_{1-1,-11} = \frac{1}{2}$, and at the same time new two-qubit correlation $\langle \sigma_x \otimes \sigma_x \rangle \overset{\tau\to\infty}{=} 2\,\mathrm{Re}\,\rho^{\mathrm{initial}}_{1-1,-11} = \frac{1}{2}$ is generated. Therefore, the spatial correlations of noises can have a visible impact on the evolution of resulting state $\hat{\rho}(\tau)$ and components of the Pauli set. Hence, one can make use of this fact to estimate to what degree the noises were correlated in the experiment. By comparison of experimental data (Fig. 3 in Ref. [66]) with simulated results (Fig. 4.6) one may deduce that in the experiment [66] noises of splittings J_1 and J_2 were uncorrelated.

4.6 Conclusions

I have theoretically analyzed the creation and evolution of entanglement of two double quantum dot-based S-T_0 qubits measured in Ref. [66] while taking into account realistic charge and nuclear noise affecting the qubits. I have confirmed that it is possible to have nearly maximal coherence signal of a single S-T_0 qubit in the presence of quasistatic fluctuations of either exchange splitting J or magnetic-field gradient ΔB_z by performing spin echo procedure on the qubit. Then, I have shown that in the system of two S-T_0 qubits quasistatic fluctuations of $\Delta B_{z,i}$ lead only to partial decrease of overall efficiency of the entangling procedure due to imprecise rotations of the qubits' states.

Both quasistatic or dynamical fluctuations of exchange splittings J_1, J_2, and two-qubit coupling $J_{12} \propto J_1 J_2$ lead to decay of overall efficiency of the entangling procedure with increasing its duration τ. The level of correlation of charge noises, as well as their exact functional form (i.e. value of parameter β characterizing the $1/f^{\beta}$ noise affecting J) translates in a distinctive manner into the shape of decay of two-qubit entanglement as a function of procedure duration τ. Decay of the overall efficiency of entangling procedure may arise as a result of the infidelity of single qubit operations (due to dynamical fluctuations of splittings J_1, J_2) or may be caused by infidelity of the entangling gate (due to fluctuations of two-qubit coupling J_{12}).

Comparison of experimental data from Ref. [66] with calculations presented in this chapter shows that the charge noises in the system of two S-T_0 qubit investigated there were uncorrelated. The main reason of the decreased level of entanglement of the resulting two-qubit state is infidelity of single-qubit operations (as I have obtained for $1/f^{\beta}$ noise with $\beta = 0.7$ consistent with the noise observed in other experiments [151] on the samples similar to those used in Ref. [66]), whereas con-

tribution of the non-ideal two-qubit gate is negligible in the considered entangling procedure in the regime $\Delta B_{z,i} \ll J_i$. I predict that for J noises of more prominently low-frequency character (i.e. $1/f^{\beta}$ with β closer to 2 than 1), the fluctuations of the two-qubit interactions, which are not echoed by π pulses applied to the two qubits separately, will become the main factor suppressing the maximal entanglement achievable in the considered procedure. I have also identified qualitative features of long-time behavior of two-qubit observables from the Pauli set that should be visible when the exchange splitting noises for the two qubits are correlated.

Chapter 5

Concluding Part

5.1 Summary

In this dissertation, the entanglement dynamics of two electron spin QD qubits has been studied. The system of two qubits based on single electron spins localized in semiconductor (III-V) QDs was considered in Chapters 2 and 3. In the former chapter, the theoretical model of the system was presented as well as approximations to it, which allow to calculate and investigate the time evolution of two-qubit entanglement for the case of free evolution as well as for the case of two-qubit spin echo experiments. The equivalence of the quantum entanglement measure and the quantum entanglement witnesses for the two qubits in the considered system has been indicated. In the latter chapter, the way to retard the decay of two-qubit entanglement in that system was presented. Surprisingly enough, it has been found that even a small number n of successive quantum measurements performed on two-qubit subsystem separated by a time period τ may significantly inhibit the entanglement decay. In addition, fortunately, the strength of quantum measurement can be progressively weaker as the number n of performed measurements grows, without causing a noticeable reduction of the effect. In Chapter 4 the dynamical production of the quantum entanglement of two S-T_0 qubits was considered. The influence of fluctuations (quasistatic or dynamical due to $1/f^\beta$ noise) of qubit Hamiltonian parameters on the efficiency of the entangling procedure was analyzed. The estimates for time evolution of a single qubit components as well as for two-qubit state have been obtained. The impact of possible correlation of dynamical noises affecting the qubits' energy splittings has also been discussed.

The essentially new knowledge that has been established in this dissertation is summarized in the conclusions of each chapter (pp. 74, 89, 113), and for convenience of the reader, is also formulated below in the form of concise statements to be defended.

5.2 Statements to Be Defended

From the analysis presented in the main chapters 3–5 one can draw several statements that, to my best knowledge, are original and have brought a value to the literature of entanglement studies.

In Chapter 2 it has been shown that the decay of entanglement of two spin QD qubits plotted as a function of time using units of two-dot T_2^* has a universal form,

i.e. it does not depend on exact values of hyperfine interaction couplings, exact number of nuclear spins in QDs, and is the same even for nonequal QDs. At first sight, this finding looks like a purely technical observation, but it is extremely useful while comparing, for example, the results obtained for systems of different sizes. One should remember that it is not possible to compute precisely the dynamics of two electron spins taking into account the real number of nuclear spins without making any approximation. However, by using units of two-dot T_2^* it is possible to directly confront results obtained within different approaches and for different parameters of the system, or to compare them with results of direct numerical computations of the time evolution of small systems (with a few nuclear spins in a QD).

While considering various possible states of the nuclear spin bath, it has been shown that in the case of narrowed and correlated nuclear bath states, entanglement decays in a similar manner, i.e. the level of entanglement (locally averaged over fast oscillations) obtained for a narrowed state overlaps with that for the corresponding correlated state. Hence, the calculation of entanglement decay for narrowed nuclear state, which requires less numeric computations, gives, in principle, enough information about the entanglement dynamics of two electron spins.

It has been demonstrated that there exists a minimal nonzero value of the strength of magnetic field which is necessary to perform successfully the two-spin echo procedure in order to rephase the qubits back and to regain some entanglement. This limit is approximately of the value of the typical Overhauser field of a QD. It is worth to pay attention here to the fact that it is highly instructive to express the strength of the external magnetic field in inverse units of two-dot T_2^*. By doing so, it becomes clear what strength of magnetic field is low (such that corresponds to $\tilde{\Omega} < 1$) or moderate (when Ω is about a few inverse T_2^*).

It has been demonstrated that entanglement of two electron spins interacting with nuclear spin baths can be detected and quantified faithfully by measuring an entanglement witness (specifically, projection on the initial entangled state) or by performing a quantum teleportation protocol (by average fidelity of that procedure). In that system, the level of entanglement turns out to be related uniquely with the above-mentioned quantities, which are a lot handy to measure compared to the full tomography of a two-qubit state.

In Chapter 3 it has been pointed out that a manipulation procedure consisting of free evolution part and quantum measurement with postselection of two-qubit state may retard the decay of two-qubit entanglement for specific combinations of its parameters, namely, the duration τ of free evolution, the number n of performed quantum measurements and their strength k. It has been shown that, despite the indeterminacy involved in the procedure (i.e. not each run of the procedure will produce the desired state $\hat{\rho}_n(t)$), the estimated probability of success may be pretty large (about 10%) for relatively long sequences ($n \approx 10$). It has been also demonstrated that application of long sequences gives a twofold profit: on one hand, the larger n, the more pronounce effect of retardation, and on the other hand, the larger n, the weaker quantum measurement (the lower k) can be used in the manipulation procedure to produce a nearly maximal effect.

In Chapter 4 it has been shown that in the system of two S-T_0 qubits, operated in a regime when energy associated with the magnetic field gradient ΔB_z is an order of magnitude smaller than the exchange energy J between singlet and triplet states, the efficiency of the entangling procedure decreases with increasing its duration τ due

to either quasistatic or dynamical fluctuations of exchange splittings J_1, J_2 and two-qubit coupling J_{12}. In the case of dynamical fluctuations due to charge noise of $1/f^{\beta}$ type, the leading factor of decay switches from infidelities of single-qubit operations (originated from fluctuating J_1, J_2) when $\beta < 1$ to infidelity of the entangling gate (originated from fluctuations of J_{12}) when $\beta > 1$. It has also been demonstrated that the level of correlation of the charge noises which affect the qubits is reflected in the time evolution of two-qubit correlations, and hence, it may be deduced from the corresponding experimental data whether the charge noise originates from a common source for both qubits or qubits are affected by their local charge noises. The analytical expression of the two-qubit density operator calculated taking into account the $1/f^{\beta}$ noise of exchange splittings J_1, J_2 allows to establish a limit from above on the possible level of entanglement of two-qubit state produced by execution of the entangling procedure.

Appendix

Uniform-Coupling Approximation to the Central Spin Problem

The uniform-coupling model allows to calculate the time evolution of the central spin due to the fact that the dynamics occur in the uncoupled subspaces spanned by two states, $|\sigma, j, m\rangle$ and $|\bar{\sigma}, j, m+\sigma\rangle$ (where $\sigma = \pm 1$ is the $\hat{\sigma}_z$ eigenvalue for the electron spin) [1]:

$$\mathrm{e}^{-i\hat{H}t}\,|\sigma, j, m\rangle \equiv a_{jm\sigma}(t)\,|\sigma, j, m\rangle + b_{jm\sigma}(t)\,|\bar{\sigma}, j, m+\sigma\rangle\,. \tag{5.1}$$

The time-dependent coefficients $a_{jm\sigma}(t)$ and $b_{jm\sigma}(t)$ read as follows [125]:

$$a_{jm\sigma}(t) = \mathrm{e}^{-iE_{m\sigma}t}\left(\cos v_{jm\sigma}t/2 - i\frac{z_{m\sigma}}{v_{jm\sigma}}\sin v_{jm\sigma}t/2\right), \tag{5.2}$$

$$b_{jm\sigma}(t) = -i\mathrm{e}^{-iE_{m\sigma}t}\frac{x_{jm\sigma}}{v_{jm\sigma}}\sin v_{jm\sigma}t/2. \tag{5.3}$$

where several auxiliary quantities were used

$$E_{m\sigma} \coloneqq \frac{1}{2}\big((2m+\sigma)\omega - \mathcal{A}/2N\big), \tag{5.4}$$

$$x_{jm\sigma} \coloneqq \mathcal{A}\sqrt{j(j+1) - m(m+\sigma)}/N, \tag{5.5}$$

$$z_{m\sigma} \coloneqq \sigma\big(\Omega - \omega + \mathcal{A}(m+\sigma/2)/N\big), \tag{5.6}$$

$$v_{jm\sigma} \coloneqq \sqrt{x_{jm\sigma}^2 + z_{m\sigma}^2}, \tag{5.7}$$

The evolution of an electron spin coupled to the nuclear spins is then described by the functions $K_a^{\sigma\sigma'}(t)$ and $K_b^{\sigma}(t)$ defined in Sec. 2.3:

$$K_a^{\sigma\sigma'}(t) = \frac{1}{Z}\sum_{jm} n_j p_m a_{jm\sigma}(t) a^*_{jm\sigma'}(t), \tag{5.8}$$

$$K_b^{\sigma}(t) = \frac{1}{Z}\sum_{jm} n_j p_m |b_{jm\bar{\sigma}}(t)|^2, \tag{5.9}$$

where Z is the normalization factor, p_m are the appropriate weights, and n_j are the degeneracies of subspaces with given j. When the nuclear spin J is in a high-temperature state one has $Z = (2J+1)^N$ and $p_m = 1$, whereas for fully narrowed nuclear state with $h^z = m_0\mathcal{A}/N$ one has $p_m = \delta_{mm_0}$ and $Z = \sum_{j\geq|m_0|} n_j$.

The degeneracy factor n_j is given for nuclear bath consisting of N spins $\frac{1}{2}$ by [236]

$$n_j = \frac{N!}{(N/2-j)!)(N/2+j)!}\frac{2j+1}{N/2+j+1} \tag{5.10}$$

$$\approx 2^N \frac{4(2j+1)}{\sqrt{2\pi}N^{3/2}}\mathrm{e}^{-2j^2/N}, \tag{5.11}$$

where in the second expression it is assumed $N \gg 1$ and $j \ll N/2$. In high magnetic fields, $\Omega \gg \sigma_\mathrm{h} \sim \mathcal{A}/\sqrt{N}$, with nuclear spin bath in a high-temperature state one has

$$\frac{z_{jm\sigma}}{v_{jm\sigma}} \approx \sigma\left(1 - \frac{\sigma_\mathrm{h}^2}{2\Omega_{m\sigma}^2}\right), \tag{5.12}$$

where $\Omega_{m\sigma} \coloneqq \Omega - \omega + \mathcal{A}(m+\sigma/2)/N \approx \Omega$. The approximation of Zeeman splitting $\Omega_{m\sigma}$ is based on the observation that according to Eq. (5.11) the sum in Eqs. (5.8-5.9) is dominated by terms with $j \lesssim \sqrt{N}$, which also limits the relevant values of m. The quantity $v_{jm\sigma}$ can be also approximated as

$$v_{jm\sigma} \approx \Omega_{m\sigma} + \frac{\mathcal{A}^2}{2N\Omega_{m\sigma}}, \tag{5.13}$$

where the second term can be dropped on time scale $t \ll \Omega/\sigma_\mathrm{h}^2$. Finally, combining altogether one obtains

$$K_a^{\sigma\bar{\sigma}}(t) \approx \frac{\mathrm{e}^{-i\sigma\Omega t}}{2^N}\sum_{jm} n_j \mathrm{e}^{-i\sigma\mathcal{A}mt/N} \approx \mathrm{e}^{-i\sigma\Omega t}\mathrm{e}^{-(t/T_{2,Q}^*)^2}, \tag{5.14}$$

where the sum over j and m values is approximated [127] by an integral $\int P(m)\mathrm{d}m$ with $P(m) \propto \exp(-m^2/2\sigma_\mathrm{h}^2)$ where σ_h is given in Eq. (1.23), and the resulting single-dot $T_{2,Q}^*$ time is given by $\sqrt{2}/\sigma_\mathrm{h}$. It should be noted that a partial narrowing of the nuclear distribution (i.e. elimination of certain values of m values the sums), resulting in a diminished value of σ_h, leads to the above formula for $K_a^{\sigma\bar{\sigma}}(t)$, only with increased $T_{2,Q}^*$, as long as the time scale of interest $t \lesssim T_{2,Q}^* \ll \Omega/\sigma_\mathrm{h}^2$.

In such a case, an approximation for $K_b^\sigma(t)$ can be obtained by using the following substitution

$$\frac{x_{jm\sigma}^2}{v_{jm\sigma}^2} \approx \frac{\mathcal{A}^2}{N^2\Omega^2}\big(j(j+1) - m(m+\sigma)\big), \tag{5.15}$$

in Eq. (5.3), which is accurate in the leading order of σ^2/Ω^2. By that means one obtains

$$K_b^\sigma(t) \approx \frac{1}{2^N}\sum_{j,m} n_j \frac{\mathcal{A}^2}{N^2\Omega^2}\big(j(j+1) - m(m+\sigma)\big)\sin^2 v_{jm\sigma}t/2. \tag{5.16}$$

Using $v_{jm\sigma} \approx \Omega_{m\sigma}$ (valid at $t \ll T_2^*\Omega/\sigma$) it is clear that the oscillatory terms in the above equation average out to $1/2$ for $t \gg T_2^*$. At these long times, using the relation [125]

$$\frac{1}{2^N}\sum_{j,m} n_j\big(j(j+1) - m(m+\sigma)\big) = N/2, \tag{5.17}$$

one obtains

$$K_b^\sigma(t \gg T_{2,Q}^*) \approx \frac{\mathcal{A}^2}{4N\Omega^2} = \frac{2}{\tilde{\Omega}_Q^2}, \tag{5.18}$$

where $\tilde{\Omega}_Q \coloneqq \Omega T^*_{2,Q}$.

An analogous analytical analysis is applicable for the case of fully narrowed nuclear spin bath. Introducing Zeeman spitting dependent on m, $\Omega_m \coloneqq \Omega - \omega + \mathcal{A}m/N$ one has the following approximate relations:

$$z_{m\sigma} \approx \sigma\Omega_m, \tag{5.19}$$

$$\frac{z_{m\sigma}}{v_{jm\sigma}} \approx \mathrm{sgn}(\Omega_m)\left(1 - \frac{x^2_{jm\sigma}}{2\Omega^2_m}\right), \tag{5.20}$$

$$\frac{x_{jm\sigma}}{v_{jm\sigma}} \approx \frac{x_{jm\sigma}}{|\Omega_m|}, \tag{5.21}$$

which lead to

$$K^{\sigma\bar{\sigma}}_a(t) \approx \frac{\mathrm{e}^{-i\sigma\omega t}}{Z_m}\sum_{j\geq|m|} n_j \mathrm{e}^{-\frac{i}{2}\mathrm{sgn}(z_{m\sigma})(v_{jm\sigma}+v_{jm\bar{\sigma}})t} \times \prod_{\sigma=\pm}\left(1 + \frac{x^2_{jm\sigma}}{4\Omega^2_m}(\mathrm{e}^{i\mathrm{sgn}(z_{m\sigma})v_{jm\sigma}t} - 1)\right). \tag{5.22}$$

In the above formula, the terms in the second line are responsible for the fast oscillations visible in the entanglement decay in Fig. 2.2 (note that the concurrence of a decohered Bell state, when not being very small, is proportional to one of the two-qubit coherences, given by the product of two $K^{\sigma\bar{\sigma}}_a(t)$ functions). The estimate of the amplitude of these oscillations shows that it is $\approx 8/\tilde{\Omega}^2$, where $\tilde{\Omega} \coloneqq \Omega T^*_2$, and the two-dot T^*_2 time is defined in Eq. (2.44).

The first term in Eq. (5.22) gives the envelope of the decay. Noticing that $v_{jm\sigma} \approx |\Omega_m| + x^2_{jm\sigma}/2|\Omega_m|$, one obtains the following approximation for $K\sigma\bar{\sigma}_a(t)$ functions

$$K^{\sigma\bar{\sigma}}_a(t) \approx \mathrm{e}^{-i\sigma(\Omega+\mathcal{A}m/N)t}\frac{1}{Z_m}\sum_{j\geq|m|} n_j \times \exp\left(-i\sigma\frac{\mathcal{A}^2}{2N^2\Omega_m}\big(j(j+1) - m^2\big)t\right). \tag{5.23}$$

In Ref. [125] it was shown how Eq. (2.56) follows from the above formula when $m = 0$. It should be stressed that with the above approximation for $v_{jm\sigma}$, the time scale of validity of this result is $t \ll 4|\Omega_m|^3/x^4_{jm\sigma} \approx 4(N/\mathcal{A})\cdot(\Omega_m/\mathcal{A})\cdot\delta_m^{-2}$, where $\delta_m \coloneqq \mathcal{A}/\sqrt{N}\Omega_m$, and $\delta_m \ll 1$ is the necessary condition [111, 165] for applicability of the effective Hamiltonian approximation leading to Eq. (2.56). This time scale exceeds $N/\mathcal{A}$ (the time on which the uniform coupling model is expected to be applicable at all) when $\delta_m \ll (2/N)^{1/6}$, which coincides with $\delta_m \ll 1$ when $N \geq 10^6$. Lastly, it is worth to note that an approximate expression for $K^{\sigma}_b(t)$ can be derived analogously to the one from Eq. (5.16). Because of the lack of summation over m the oscillations in $K^{\sigma}_b(t)$ cancel out at longer times, for $t \gg \tau_Q$ where τ_Q is the characteristic decay time scale of $K^{\sigma\bar{\sigma}}_a(t)$ given in Eq. (2.57). The value at which $K^{\sigma}_b(t)$ stabilizes is also given by Eq. (5.18), only with Ω replaced by Ω_m.

Components of Single S-T_0 Qubit as Functions of Duration τ

In the ideal case, FID signals (i.e. average $\langle\hat{\sigma}_i^{\mathrm{FID}}(\tau)\rangle$ components of S-T_0 qubit) evolve as follows.

$$\begin{aligned}
&\langle\hat{\sigma}_x^{\mathrm{FID}}(\tau)\rangle \coloneqq \langle -y|\mathrm{e}^{i\hat{H}\tau}\hat{\sigma}_x\mathrm{e}^{-i\hat{H}\tau}|-y\rangle \\
&= \langle -y|\Bigg(\cos\Big(\frac{\tau}{2}\sqrt{\Delta B_z^2+J^2}\Big)\mathbb{1} \\
&+ i\sin\Big(\frac{\tau}{2}\sqrt{\Delta B_z^2+J^2}\Big)\frac{\Delta B_z}{\sqrt{\Delta B_z^2+J^2}}\hat{\sigma}_x \\
&+ i\sin\Big(\frac{\tau}{2}\sqrt{\Delta B_z^2+J^2}\Big)\frac{J}{\sqrt{\Delta B_z^2+J^2}}\hat{\sigma}_z\Bigg) \\
&\times\hat{\sigma}_x\Bigg(\cos\Big(\frac{\tau}{2}\sqrt{\Delta B_z^2+J^2}\Big)\mathbb{1} \\
&- i\sin\Big(\frac{\tau}{2}\sqrt{\Delta B_z^2+J^2}\Big)\frac{\Delta B_z}{\sqrt{\Delta B_z^2+J^2}}\hat{\sigma}_x \\
&- i\sin\Big(\frac{\tau}{2}\sqrt{\Delta B_z^2+J^2}\Big)\frac{J}{\sqrt{\Delta B_z^2+J^2}}\hat{\sigma}_z\Bigg)|-y\rangle \\
&= \frac{J}{\sqrt{\Delta B_z^2+J^2}}\sin\Big(\sqrt{\Delta B_z^2+J^2}\tau\Big).
\end{aligned}$$

$$\begin{aligned}
\langle\hat{\sigma}_y^{\mathrm{FID}}(\tau)\rangle &= -\cos\Big[\sqrt{\Delta B_z^2+J^2}\tau\Big] \\
&\approx -\cos\Big[\Big(J+\frac{\Delta B_z^2}{2J}\Big)\tau\Big],
\end{aligned}$$

the approximation is good for $\tau \ll \frac{8J^3}{\Delta B_z^4}$.

$$\langle\hat{\sigma}_z^{\mathrm{FID}}(\tau)\rangle = -\frac{\Delta B_z}{\sqrt{\Delta B_z^2+J^2}}\sin\Big(\sqrt{\Delta B_z^2+J^2}\tau\Big).$$

In the ideal case, SE signals (i.e. average $\langle\hat{\sigma}_i^{\mathrm{SE}}(\tau)\rangle$ components of S-T_0 qubit) evolve as follows.

$$\begin{aligned}
\langle\hat{\sigma}_x^{\mathrm{SE}}(\tau)\rangle &= \langle -y|\mathrm{e}^{i\hat{H}\frac{\tau}{2}}(i\hat{\sigma}_x)\mathrm{e}^{i\hat{H}\frac{\tau}{2}}\hat{\sigma}_x\mathrm{e}^{-i\hat{H}\frac{\tau}{2}}(-i\hat{\sigma}_x)\mathrm{e}^{-i\hat{H}\frac{\tau}{2}}|-y\rangle \\
&= \frac{8\Delta B_z^2 J}{(\Delta B_z^2+J^2)^{3/2}}\cos\Big(\frac{1}{4}\sqrt{\Delta B_z^2+J^2}\tau\Big) \\
&\times\sin^2\Big(\frac{1}{4}\sqrt{\Delta B_z^2+J^2}\tau\Big).
\end{aligned}$$

$$\langle\hat{\sigma}_y^{\mathrm{SE}}(\tau)\rangle = \frac{1}{\Delta B_z^2+J^2}\Big(J^2+\Delta B_z^2\cos\Big(\sqrt{\Delta B_z^2+J^2}\tau\Big)\Big).$$

$$\langle\hat{\sigma}_z^{\mathrm{SE}}(\tau)\rangle = \frac{\Delta B_z}{(\Delta B_z^2 + J^2)^{3/2}}\left[2J^2\sin^2\left(\frac{1}{2}\sqrt{\Delta B_z^2 + J^2}\tau\right)\right.$$
$$\left. + \Delta B_z^2\sin\left(\sqrt{\Delta B_z^2 + J^2}\tau\right)\right].$$

Assuming that $\bar{J} \gg \overline{\Delta B_z}$, σ_J, after averaging over quasistatic fluctuations of the parameter ΔB_z or J one obtains the following approximate expressions for y qubit component during SE.

$$\langle\langle\sigma_y^{\mathrm{SE}}(\tau)\rangle\rangle_{\Delta B_z} \approx \frac{J^2}{J^2 + \overline{\Delta B_z}^2}$$
$$+ \frac{1}{J^2 + \overline{\Delta B_z}^2}\exp\left(-\frac{\overline{\Delta B_z}^2\sigma_{\Delta B_z}^2\tau^2}{2(J^2 + (\sigma_{\Delta B_z}^2\tau)^2)}\right)$$
$$\times\left[\frac{J^{3/2}(J(\overline{\Delta B_z}^2 + \sigma_{\Delta B_z}^2) + i\sigma_{\Delta B_z}^4\tau)}{2(J + i\sigma_{\Delta B_z}^2\tau)^{5/2}}\right.$$
$$\left.\times\exp\left(-iJ\tau\frac{\overline{\Delta B_z}^2 + 2J^2 + 2(\sigma_{\Delta B_z}^2\tau)^2}{2(J^2 + (\sigma_{\Delta B_z}^2\tau)^2)}\right) + \mathrm{c.c.}\right].$$

$$\langle\langle\sigma_y^{\mathrm{SE}}(\tau)\rangle\rangle_J \approx \frac{\bar{J}^2 + \sigma_J^2}{\bar{J}^2 + \Delta B_z^2} + \frac{\Delta B_z^2}{\bar{J}^2 + \Delta B_z^2}\exp\left(-\frac{\sigma_J^2\tau^2}{2}\right)\cos\left(\bar{J}\tau\right).$$

S-T_0 Qubit Attenuation Factors Derived for Dynamically Fluctuating Splitting

I present here the calculation of the attenuation factors $\chi_{\mathrm{FID}}(\tau)$ and $\chi_{\mathrm{SE}}(\tau)$ that account for the effect of dynamically fluctuating splittings J_1, J_2.

The attenuation factor $\chi_{\mathrm{FID}}(\tau)$ is calculated as follows.

$$\begin{aligned}
\chi_{\mathrm{FID}}(\tau) &= \int_0^\tau \mathrm{d}t_1 \int_0^\tau \mathrm{d}t_2 \langle \delta J(t_1)\delta J(t_2)\rangle f_{\mathrm{FID}}(t_1) f_{\mathrm{FID}}(t_2) \\
&= \int_{-\infty}^{\infty} \mathrm{d}t_1 \int_{-\infty}^{\infty} \mathrm{d}t_2 \int_{-\infty}^{\infty} \frac{\mathrm{d}\omega}{2\pi} \mathrm{e}^{-i\omega(t_1-t_2)} S(\omega) \\
&\times \int_{-\infty}^{\infty} \frac{\mathrm{d}\omega_1}{2\pi} \tilde{f}_{\mathrm{FID}}(\omega_1)\mathrm{e}^{-i\omega_1 t_1} \int_{-\infty}^{\infty} \frac{\mathrm{d}\omega_2}{2\pi} \tilde{f}_{\mathrm{FID}}(\omega_2)\mathrm{e}^{-i\omega_2 t_2} \\
&= \int_{-\infty}^{\infty} \mathrm{d}\omega_1 \int_{-\infty}^{\infty} \mathrm{d}\omega_2 \int_{-\infty}^{\infty} \frac{\mathrm{d}\omega}{2\pi} \delta(\omega+\omega_1)\delta(\omega-\omega_2) \\
&\times \tilde{f}_{\mathrm{FID}}(\omega_1)\tilde{f}_{\mathrm{FID}}(\omega_2) S(\omega) \\
&= \int_{-\infty}^{\infty} \frac{\mathrm{d}\omega}{2\pi} \tilde{f}_{\mathrm{FID}}(-\omega)\tilde{f}_{\mathrm{FID}}(\omega) S(\omega) = \int_{-\infty}^{\infty} \frac{\mathrm{d}\omega}{2\pi} \left|\tilde{f}_{\mathrm{FID}}(\omega)\right|^2 S(\omega) \\
&= \int_{-\infty}^{\infty} \frac{\mathrm{d}\omega}{2\pi} \frac{2F_{\mathrm{FID}}(\omega\tau)}{\omega^2} S(\omega) = 2\int_0^{\infty} \frac{\mathrm{d}\omega}{\pi} \frac{F_{\mathrm{FID}}(\omega\tau)}{\omega^2} S(\omega).
\end{aligned}$$

Using the explicit analytical expressions for the filter function, $F_{\mathrm{FID}}(\omega\tau) = 2\sin^2\frac{\omega\tau}{2}$, and the spectral density of noise, $S(\omega) = \frac{A}{\omega^\beta}$, where A is a constant corresponding to the power of the noise, one obtains the following expression for the attenuation factor

$$\chi_{\mathrm{FID}}(\tau) = \frac{4A}{\pi} \int_0^{\infty} \mathrm{d}\omega \sin^2\frac{\omega\tau}{2} \frac{1}{\omega^{2+\beta}},$$

which for $\beta = 0.7$ can be evaluated giving finally:

$$\chi_{\mathrm{FID}}(\tau) = \frac{2A}{\pi} \cos\left(\frac{3\pi}{20}\right) \Gamma(-1.7)\, \tau^{1.7} \approx 2.24\, \frac{2A}{\pi} \tau^{1.7},$$

as the definite integral can be calculated analytically

$$\int_0^{\infty} \mathrm{d}\omega \sin^2\frac{\omega\tau}{2} \frac{1}{\omega^{2+0.7}} = \frac{1}{2} \cos\left(\frac{3\pi}{20}\right) \Gamma(-1.7)\, \tau^{1.7},$$

where $\Gamma(x)$ is the gamma function.

Similarly, the attenuation factor $\chi_{\mathrm{SE}}(\tau)$ reads as follows.

$$\begin{aligned}
\chi_{\mathrm{SE}}(\tau) &= \int_0^\tau \mathrm{d}t_1 \int_0^\tau \mathrm{d}t_2 \langle \delta J(t_1)\delta J(t_2)\rangle f_{SE}(t_1) f_{SE}(t_2) \\
&= 2\int_0^{\infty} \frac{\mathrm{d}\omega}{\pi} \frac{F_{\mathrm{SE}}(\omega\tau)}{\omega^2} S(\omega).
\end{aligned}$$

Using the explicit analytical expressions for the filter function, $F_{\mathrm{SE}}(\omega\tau) = 8\sin^4\frac{\omega\tau}{4}$, and the spectral density of noise, $S(\omega) = \frac{A}{\omega^\beta}$, one obtains the following expression for the attenuation factor

$$\chi_{\mathrm{SE}}(\tau) = \frac{16A}{\pi}\int_0^\infty \mathrm{d}\omega \sin^4\frac{\omega\tau}{4}\frac{1}{\omega^{2+\beta}},$$

which for $\beta = 0.7$ can be evaluated giving finally:

$$\chi_{\mathrm{SE}}(\tau) = \frac{2A}{\pi}\left(2^{0.3}-1\right)\cos\left(\frac{3\pi}{20}\right)\Gamma\left(-1.7\right)\tau^{1.7} \approx 0.52\,\frac{2A}{\pi}\tau^{1.7},$$

as the definite integral can be calculated analytically

$$\int_0^\infty \mathrm{d}\omega \sin^4\frac{\omega\tau}{4}\frac{1}{\omega^{2+0.7}} = \frac{1}{8}\left(2^{0.3}-1\right)\cos\left(\frac{3\pi}{20}\right)\Gamma\left(-1.7\right)\tau^{1.7}.$$

The attenuation factor $\chi_{\mathrm{SE}}(\tau)$ for the noise with $\beta = 2.0$ is $\chi_{\mathrm{SE}}(\tau) = \frac{A}{12}\tau^3$ as the following definite integral can be calculated analytically $\int_0^\infty \mathrm{d}\omega \sin^4\frac{\omega\tau}{4}\frac{1}{\omega^{2+2.0}} = \frac{\pi}{192}\tau^3$.

List of Seminar Presentations

Part of the results contained in Chapter 4 of the dissertation has been presented on the seminar "Coherence-Correlations-Complexity" at Wrocław University of Science and Technology, Department of Theoretical Physics, title of the presentation: *Dynamics of entanglement of two singlet-triplet qubits: role of nuclear spin baths and charge noise*, December 9th, 2015.

List of Conference Presentations

Part of the results contained in the dissertation has been presented on the following scientific conferences and workshops:

- Igor Bragar and Łukasz Cywiński, *Decay of entanglement of two electron spins coupled to a nuclear spin bath* (poster presentation), **42nd "Jaszowiec" International School and Conference on the Physics of Semiconductors**, June 22nd–27th, 2013, Wisła, Poland;

- Igor Bragar and Łukasz Cywiński, *Dynamika splątania dwóch spinów elektronów oddziałujących ze spinami jądrowymi*, ang. *Dynamics of entanglement of two electron spins interacting with nuclear spins*, (oral presentation), **XIX Workshop "Spin in Semiconductors – New Materials for Spintronics"**, April 12th, 2014, Obory, Poland;

- Igor Bragar and Łukasz Cywiński, *Dynamics of entanglement of two electron spins interacting with nuclear spin baths* (poster presentation), **43rd "Jaszowiec" International School and Conference on the Physics of Semiconductors**, June 7th–12th, 2014, Wisła, Poland;

- Igor Bragar and Łukasz Cywiński, *Dynamics of entanglement of two electron spins interacting with nuclear spin baths* (poster presentation), **2nd School and conference on Spin-based quantum information processing**, August 18th–22nd, 2014, Konstanz, Germany;

- Igor Bragar and Łukasz Cywiński, *Dynamika splątania dwóch singletowo-trypletowych kubitów w strukturze GaAs-AlGaAs*, ang. *Dynamics of entanglement of two singlet-triplet qubits in GaAs-AlGaAs structure*, (oral presentation), **XX Workshop "Spin in Semiconductors – New Materials for Spintronics"**, April 18th, 2015, Obory, Poland;

- Igor Bragar, *Dynamics of entanglement of two electron spins interacting with nuclear spin baths in quantum dots* (oral presentation), **PhD Student Symposium of Institute of Physics of the Polish Academy of Sciences**, May 25th–27th, 2015, Kazimerz Dolny, Poland;

- Igor Bragar and Łukasz Cywiński, *Dynamics of entanglement of two singlet-tripet qubits in GaAs-AlGaAs heterostructure* (poster presentation), **44th "Jaszowiec" International School and Conference on the Physics of Semiconductors**, June 20th–25th, 2015, Wisła, Poland;

- Igor Bragar and Łukasz Cywiński, *Dynamics of entanglement between two singlet-triplet qubits: role of nuclear spin baths and charge noise* (poster presentation), **SpinTech VIII International School & Conference on Spintronics and Quantum Information Technology**, August 10th–13th, 2015, Basel, Switzerland;

- Igor Bragar and Łukasz Cywiński, *Dynamics of entanglement between two singlet-triplet qubits: role of nuclear spin baths and charge noise* (poster presentation), **4th International Workshop on the Optical Properties of Nanostructures**, February 17th–19th, 2016, Wrocław, Poland;

- Igor Bragar, *Retardation of Quantum Correlation Decay of Two Spin Qubits by Quantum Measurements* (poster presentation), **YOUNG MULTIS – Multiscale Phenomena in Condensed Matter**, July 5th–7th, 2021, Kraków, Poland, `https://indico.ifj.edu.pl/event/497/overview`;

- Igor Bragar and Łukasz Cywiński, *Limitations on Maximal Level of Entanglement of Two Singlet-Triplet Qubit States in GaAs Gated Quantum Dots* (poster presentation), **49th "Jaszowiec" International School and Conference on the Physics of Semiconductors**, September 1st–10th, 2021, Warszawa, Poland, `https://www.jaszowiec.edu.pl`;

- Igor Bragar, *Retardation of Quantum Correlation Decay of Two Spin Qubits by Quantum Measurements* (poster presentation), **49th "Jaszowiec" International School and Conference on the Physics of Semiconductors**, September 1st–10th, 2021, Warszawa, Poland, `https://www.jaszowiec.edu.pl`;

- Igor Bragar, *Retardation of Entanglement Decay of Two Spin Qubits by Quantum Measurements* (poster presentation), **20th International Conference on Modulated Semiconductor Structures**, October 31st–November 5th, 2021, Toyama, Japan, `https://ep2ds24mss20.org`.

List of Publications

Part of the results contained in Chapter 2 of the dissertation has been published in the paper:

- Igor Bragar and Łukasz Cywiński, *Dynamics of entanglement of two electron spins interacting with nuclear spin baths in quantum dots*,
  Phys. Rev. B 91, 155310 (2015) [1].

The results presented in Chapters 3 and 4 will be published soon. The results of Chapter 3 are publicly available as a preprint [186].

References

[1] Igor Bragar and Łukasz Cywiński. Dynamics of entanglement of two electron spins interacting with nuclear spin baths in quantum dots. *Phys. Rev. B*, 91:155310, Apr 2015. doi:10.1103/PhysRevB.91.155310.

[2] H.-P. Breuer and F. Petruccione. *The Theory of Open Quantum System*. Oxford University Press, New York, 2007. doi:10.1093/acprof:oso/9780199213900.001.0001.

[3] Michael A. Nielsen and Isaac L. Chuang. *Quantum Computation and Quantum Information: 10th Anniversary Edition*. Cambridge University Press, Cambridge, 10th edition, 2011. doi:https://doi.org/10.1017/CBO9780511976667.

[4] Reinhard F. Werner. Quantum states with einstein-podolsky-rosen correlations admitting a hidden-variable model. *Phys. Rev. A*, 40:4277–4281, Oct 1989. doi:10.1103/PhysRevA.40.4277.

[5] Martin B. Plenio and Shashank Virmani. An introduction to entanglement measures. *Quant. Info. Comput.*, 7:1, Jan 2007. doi:https://doi.org/10.26421/QIC7.1-2-1.

[6] Ryszard Horodecki, Paweł Horodecki, Michał Horodecki, and Karol Horodecki. Quantum entanglement. *Rev. Mod. Phys.*, 81:865–942, Jun 2009. doi:10.1103/RevModPhys.81.865.

[7] Leandro Aolita, Fernando de Melo, and Luiz Davidovich. Open-system dynamics of entanglement. *Rep. Prog. Phys.*, 78(4):042001, Mar 2015. doi:10.1088/0034-4885/78/4/042001.

[8] Benjamin Schumacher. Quantum coding. *Phys. Rev. A*, 51:2738–2747, Apr 1995. doi:10.1103/PhysRevA.51.2738.

[9] John Preskill. Lecture Notes for Physics 229: Quantum Information and Computation. chapter 4. URL: http://theory.caltech.edu/~preskill/ph229/.

[10] David P. DiVincenzo. Two-bit gates are universal for quantum computation. *Phys. Rev. A*, 51:1015–1022, Feb 1995. doi:10.1103/PhysRevA.51.1015.

[11] Michał Horodecki and Paweł Horodecki. Reduction criterion of separability and limits for a class of distillation protocols. *Phys. Rev. A*, 59:4206–4216, Jun 1999. doi:10.1103/PhysRevA.59.4206.

[12] Sandu Popescu. Bell's inequalities versus teleportation: What is nonlocality? *Phys. Rev. Lett.*, 72:797–799, Feb 1994. doi:10.1103/PhysRevLett.72.797.

[13] A. Einstein, B. Podolsky, and N. Rosen. Can quantum-mechanical description of physical reality be considered complete? *Phys. Rev.*, 47:777–780, May 1935. doi:10.1103/PhysRev.47.777.

[14] E. Schrödinger. Die gegenwärtige Situation in der Quantenmechanik. *Die Naturzkissenschafte*, 23:807–812, Nov 1935. doi:10.1007/BF01491891.

[15] E. Schrödinger. Die gegenwärtige Situation in der Quantenmechanik. *Die Naturzkissenschafte*, 23:823–828, Dec 1935. doi:10.1007/BF01491914.

[16] E. Schrödinger. Die gegenwärtige Situation in der Quantenmechanik. *Die Naturzkissenschafte*, 23:844–849, Dec 1935. doi:10.1007/BF01491987.

[17] John D. Trimmer. The present situation in quantum mechanics: A translation of Schrödinger's 'Cat Paradox' Paper. *Proceedings of the American Philosophical Society*, 124:323–338, Oct 1980. URL: http://www.jstor.org/stable/986572.

[18] Archak Purkayastha, Giacomo Guarnieri, Mark T. Mitchison, Radim Filip, and John Goold. Tunable phonon-induced steady-state coherence in a double-quantum-dot charge qubit. *npj Quantum Inf*, 6:27, Mar 2020. doi:10.1038/s41534-020-0256-6.

[19] Wojciech Hubert Zurek. Decoherence, einselection, and the quantum origins of the classical. *Rev. Mod. Phys.*, 75:715–775, May 2003. doi:10.1103/RevModPhys.75.715.

[20] K. Hornberger. Introduction to decoherence theory. In Andreas Buchleitner, Carlos Viviescas, and Markus Tiersch, editors, *Entanglement and Decoherence*, volume 768 of *Lecture Notes in Physics*, chapter 5, pages 221–276. Springer, Berlin, Heidelberg, 2009. doi:10.1007/978-3-540-88169-8_5.

[21] William K. Wootters. Entanglement of formation of an arbitrary state of two qubits. *Phys. Rev. Lett.*, 80:2245–2248, Mar 1998. doi:10.1103/PhysRevLett.80.2245.

[22] Ting Yu and J. H. Eberly. Evolution from entanglement to decoherence. *Quant. Info. Comp.*, 7:459–468, Jul 2007. doi:https://doi.org/10.26421/QIC7.5-6-3.

[23] G. Vidal and R. F. Werner. Computable measure of entanglement. *Phys. Rev. A*, 65:032314, Feb 2002. doi:10.1103/PhysRevA.65.032314.

[24] Asher Peres. Separability criterion for density matrices. *Phys. Rev. Lett.*, 77:1413–1415, Aug 1996. doi:10.1103/PhysRevLett.77.1413.

[25] Michał Horodecki, Paweł Horodecki, and Ryszard Horodecki. Separability of mixed states: necessary and sufficient conditions. *Physics Letters A*, 223(1):1–8, Nov 1996. doi:https://doi.org/10.1016/S0375-9601(96)00706-2.

[26] Johann von Neumann. *Mathematische Grundlagen der Quantenmechanik*. Verlag von Julius Springer, Berlin, 1932. pp. 13–15. URL: https://gdz.sub.uni-goettingen.de/id/PPN379400774.

[27] Max Born. Zur quantenmechanik der stoßvorgänge. *Zeitschrift für Physik*, 37:863–867, Dec 1926. doi:10.1007/BF01397477.

[28] N. Bohr. Can quantum-mechanical description of physical reality be considered complete? *Phys. Rev.*, 48:696–702, Oct 1935. doi:10.1103/PhysRev.48.696.

[29] J. S. Bell. On the Einstein Podolsky Rozen paradox. *Physics Physique Fizika*, 1:195–200, Nov 1964. doi:10.1103/PhysicsPhysiqueFizika.1.195.

[30] A. S. Holevo. Bounds for the quantity of information transmitted by a quantum communication channel (in Russian). *Probl. Peredachi Inf. (Problems Inform. Transmission)*, 9:3–11/177–183, 1973. URL: https://www.mathnet.ru/eng/ppi903.

[31] Yu. I. Manin. *Vychislimoe i nevychislimoe [Computable and Noncomputable] (in Russian)*. Sovetskoe Radio, Moscow, 1980. pp. 13–15.

[32] Richard P. Feynman. Simulating physics with computers. *Int J Theor Phys*, 21:467–488, Jun 1982. doi:10.1007/BF02650179.

[33] Charles H. Bennett and Stephen J. Wiesner. Communication via one- and two-particle operators on Einstein-Podolsky-Rosen states. *Phys. Rev. Lett.*, 69:2881–2884, Nov 1992. doi:10.1103/PhysRevLett.69.2881.

[34] Charles H. Bennett, Gilles Brassard, Claude Crépeau, Richard Jozsa, Asher Peres, and William K. Wootters. Teleporting an unknown quantum state via dual classical and Einstein-Podolsky-Rosen channels. *Phys. Rev. Lett.*, 70:1895–1899, Mar 1993. doi:10.1103/PhysRevLett.70.1895.

[35] Peter W. Shor. Polynomial-time algorithms for prime factorization and discrete logarithms on a quantum computer. *SIAM J. Comput.*, 26:1484–1509, Oct 1997. doi:10.1137/S0097539795293172.

[36] Lov K. Grover. From Schrödinger's equation to the quantum search algorithm. *Am. J. Phys.*, 69:769–777, Jul 2001. doi:10.1119/1.1359518.

[37] D. Dieks. Communication by EPR devices. *Physics Letters A*, 92(6):271–272, Nov 1982. doi:https://doi.org/10.1016/0375-9601(82)90084-6.

[38] P.W. Milonni and M.L. Hardies. Photons cannot always be replicated. *Physics Letters A*, 92(7):321–322, Nov 1982. doi:https://doi.org/10.1016/0375-9601(82)90899-4.

[39] W. K. Wootters and W. H. Zurek. A single quantum cannot be cloned. *Nature*, 299(5886):802–803, Oct 1982. doi:10.1038/299802a0.

[40] L. Mandel. Is a photon amplifier always polarization dependent? *Nature*, 304(5922):188, Jul 1983. doi:10.1038/304188a0.

[41] Arun Kumar Pati and Samuel L. Braunstein. Impossibility of deleting an unknown quantum state. *Nature*, 404(6774):164–165, Mar 2000. doi:10.1038/404130b0.

[42] Howard Barnum, Carlton M. Caves, Christopher A. Fuchs, Richard Jozsa, and Benjamin Schumacher. Noncommuting mixed states cannot be broadcast. *Phys. Rev. Lett.*, 76:2818–2821, Apr 1996. doi:10.1103/PhysRevLett.76.2818.

[43] Samuel L. Braunstein and Arun K. Pati. Quantum information cannot be completely hidden in correlations: Implications for the black-hole information paradox. *Phys. Rev. Lett.*, 98:080502, Feb 2007. doi:10.1103/PhysRevLett.98.080502.

[44] Jozef Gruska and Hiroshi Imai. Power, Puzzles and Properties of Entanglement. In M. Margenstern and Y. Rogozhin, editors, *Machines, Computations, and Universality*, pages 25–68. Springer, Berlin Heidelberg New York, 2001. URL: https://link.springer.com/chapter/10.1007/3-540-45132-3_3.

[45] Asher Peres and Daniel R. Terno. Quantum information and relativity theory. *Rev. Mod. Phys.*, 76:93–123, Jan 2004. doi:10.1103/RevModPhys.76.93.

[46] M. A. Nielsen and Isaac L. Chuang. Programmable quantum gate arrays. *Phys. Rev. Lett.*, 79:321–324, Jul 1997. doi:10.1103/PhysRevLett.79.321.

[47] R. Hanson, L. P. Kouwenhoven, J. R. Petta, S. Tarucha, and L. M. K. Vandersypen. Spins in few-electron quantum dots. *Rev. Mod. Phys.*, 79:1217–1265, Oct 2007. doi:10.1103/RevModPhys.79.1217.

[48] Guido Burkard, Thaddeus D. Ladd, John M. Nichol, Andrew Pan, and Jason R. Petta. Semiconductor spin qubits. *arXiv.org*, 2112.08863, Dec 2021. doi:10.48550/ARXIV.2112.08863.

[49] Shannon P. Harvey. Quantum dots/spin qubits, Feb 2022. doi:10.1093/acrefore/9780190871994.013.83.

[50] Jun Yoneda, Kenta Takeda, Tomohiro Otsuka, Takashi Nakajima, Matthieu R. Delbecq, Giles Allison, Takumu Honda, Tetsuo Kodera, Shunri Oda, Yusuke Hoshi, Noritaka Usami, Kohei M. Itoh, and Seigo Tarucha. A quantum-dot spin qubit with coherence limited by charge noise and fidelity higher than 99.9%. *Nature Nanotech*, 13(2):102–106, Feb 2018. doi:10.1038/s41565-017-0014-x.

[51] Akito Noiri, Kenta Takeda, Takashi Nakajima, Takashi Kobayashi, Amir Sammak, Giordano Scappucci, and Seigo Tarucha. Fast universal quantum gate above the fault-tolerance threshold in silicon. *Nature*, 601(7893):338–342, Jan 2022. doi:10.1038/s41586-021-04182-y.

[52] Adam R. Mills, Charles R. Guinn, Michael J. Gullans, Anthony J. Sigillito, Mayer M. Feldman, Erik Nielsen, and Jason R. Petta. Two-qubit silicon quantum processor with operation fidelity exceeding 99%. *Science Advances*, 8(14):eabn5130, Apr 2022. doi:10.1126/sciadv.abn5130.

[53] Xiao Xue, Maximilian Russ, Nodar Samkharadze, Brennan Undseth, Amir Sammak, Giordano Scappucci, and Lieven M. K. Vandersypen. Quantum logic with spin qubits crossing the surface code threshold. *Nature*, 601(7893):343–347, Jan 2022. doi:10.1038/s41586-021-04273-w.

[54] Ren-Bao Liu, Wang Yao, and L. J. Sham. Quantum computing by optical control of electron spins. *Adv. Phys.*, 59(5):703–802, Aug 2010. doi:10.1080/00018732.2010.505452.

[55] Kristiaan De Greve, David Press, Peter L. McMahon, and Yoshihisa Yamamoto. Ultrafast optical control of individual quantum dot spin qubits. *Rep. Prog. Phys.*, 76(9):092501, Sep 2013. doi:10.1088/0034-4885/76/9/092501.

[56] V. V. Dobrovitski, G. D. Fuchs, A. L. Falk, C. Santori, and D. D. Awschalom. Quantum control over single spins in diamond. *Ann. Rev. Cond. Mat. Phys.*, 4(1):23–50, Apr 2013. doi:10.1146/annurev-conmatphys-030212-184238.

[57] Floris A. Zwanenburg, Andrew S. Dzurak, Andrea Morello, Michelle Y. Simmons, Lloyd C. L. Hollenberg, Gerhard Klimeck, Sven Rogge, Susan N. Coppersmith, and Mark A. Eriksson. Silicon quantum electronics. *Rev. Mod. Phys.*, 85:961–1019, Jul 2013. doi:10.1103/RevModPhys.85.961.

[58] J. R. Petta, A. C. Johnson, J. M. Taylor, E. A. Laird, A. Yacoby, M. D. Lukin, C. M. Marcus, M. P. Hanson, and A. C. Gossard. Coherent manipulation of coupled electron spins in semiconductor quantum dots. *Science*, 309(5744):2180–2184, Sep 2005. doi:10.1126/science.1116955.

[59] Lucio Robledo, Jeroen Elzerman, Gregor Jundt, Mete Atatüre, Alexander Högele, Stefan Fält, and Atac Imamoglu. Conditional dynamics of interacting quantum dots. *Science*, 320(5877):772–775, May 2008. doi:10.1126/science.1155374.

[60] P. Neumann, R. Kolesov, B. Naydenov, J. Beck, F. Rempp, M. Steiner, V. Jacques, G. Balasubramanian, M. L. Markham, D. J. Twitchen, S. Pezzagna, J. Meijer, J. Twamley, F. Jelezko, and J.Wrachtrup. Quantum register based on coupled electron spins in a room-temperature solid. *Nature Phys*, 6:249–253, Apr 2010. doi:10.1038/nphys1536.

[61] I. van Weperen, B. D. Armstrong, E. A. Laird, J. Medford, C. M. Marcus, M. P. Hanson, and A. C. Gossard. Charge-state conditional operation of a spin qubit. *Phys. Rev. Lett.*, 107:030506, Jul 2011. doi:10.1103/PhysRevLett.107.030506.

[62] Danny Kim, Samuel G. Carter, Alex Greilich, Allan S. Bracker, and Daniel Gammon. Ultrafast optical control of entanglement between two quantum-dot spins. *Nature Phys*, 7:223–229, Mar 2011. doi:10.1038/nphys1863.

[63] Alex Greilich, Samuel G. Carter, Danny Kim, Allan S. Bracker, and Daniel Gammon. Optical control of one and two hole spins in interacting quantum

dots. *Nature Photon*, 5:702–708, Nov 2011. doi:10.1038/nphoton.2011.237.

[64] K. C. Nowack, M. Shafiei, M. Laforest, G. E. D. K. Prawiroatmodjo, L. R. Schreiber, C. Reichl, W. Wegscheider, and L. M. K. Vandersypen. Single-shot correlations and two-qubit gate of solid-state spins. *Science*, 333:1269–1272, Aug 2011. doi:10.1126/science.1209524.

[65] R. Brunner, Y.-S. Shin, T. Obata, M. Pioro-Ladrière, T. Kubo, K. Yoshida, T. Taniyama, Y. Tokura, and S. Tarucha. Two-qubit gate of combined single-spin rotation and interdot spin exchange in a double quantum dot. *Phys. Rev. Lett.*, 107:146801, Sep 2011. doi:10.1103/PhysRevLett.107.146801.

[66] M. D. Shulman, O. E. Dial, S. P. Harvey, H. Bluhm, V. Umansky, and A. Yacoby. Demonstration of entanglement of electrostatically coupled singlet-triplet qubits. *Science*, 336:202–205, Apr 2012. doi:10.1126/science.1217692.

[67] F. Dolde, I. Jakobi, B. Naydenov, N. Zhao, S. Pezzagna, C. Trautmann, J. Meijer, P. Neumann, F. Jelezko, and J.Wrachtrup. Room-temperature entanglement between single defect spins in diamond. *Nature Phys*, 9:139–143, Mar 2013. doi:10.1038/nphys2545.

[68] M. Ciorga, A. S. Sachrajda, P. Hawrylak, C. Gould, P. Zawadzki, S. Jullian, Y. Feng, and Z. Wasilewski. Addition spectrum of a lateral dot from coulomb and spin-blockade spectroscopy. *Phys. Rev. B*, 61:R16315–R16318, Jun 2000. doi:10.1103/PhysRevB.61.R16315.

[69] A.J. Hill and P.H. Ladbrooke. *Electronics Letters*, 22:218–220, Feb 1986. doi:10.1049/el:19860152.

[70] K. Lee, M. S. Shur, T. J. Drummond, and H. Morkoç. Low field mobility of 2-d electron gas in modulation doped $Al_xGa_{1-x}As$/GaAs layers. *J. of Appl. Phys.*, 54(11):6432–6438, Nov 1983. doi:10.1063/1.331922.

[71] Frank Stern. Self-consistent results for n-type Si inversion layers. *Phys. Rev. B*, 5:4891–4899, Jun 1972. doi:10.1103/PhysRevB.5.4891.

[72] Peter J. Price. Electron transport in polar heterolayers. *Surface Science*, 113(1):199–210, Jan 1982. doi:https://doi.org/10.1016/0039-6028(82)90586-6.

[73] Daniel Loss and David P. DiVincenzo. Quantum computation with quantum dots. *Phys. Rev. A*, 57:120–126, Jan 1998. doi:10.1103/PhysRevA.57.120.

[74] S. Amasha, K. MacLean, Iuliana P. Radu, D. M. Zumbühl, M. A. Kastner, M. P. Hanson, and A. C. Gossard. Electrical control of spin relaxation in a quantum dot. *Phys. Rev. Lett.*, 100:046803, Jan 2008. doi:10.1103/PhysRevLett.100.046803.

[75] Hans-Andreas Engel and Daniel Loss. Detection of single spin decoherence in a quantum dot via charge currents. *Phys. Rev. Lett.*, 86:4648–4651, May 2001. doi:10.1103/PhysRevLett.86.4648.

[76] Hans-Andreas Engel and Daniel Loss. Single-spin dynamics and decoherence in a quantum dot via charge transport. *Phys. Rev. B*, 65:195321, May 2002. doi:10.1103/PhysRevB.65.195321.

[77] F. H. L. Koppens, C. Buizert, K. J. Tielrooij, I. T. Vink, K. C. Nowack, T. Meunier, L. P. Kouwenhoven, and L. M. K. Vandersypen. Driven coherent oscillations of a single electron spin in a quantum dot. *Nature*, 442(7104):766–771, Aug 2006. doi:10.1038/nature05065.

[78] Guido Burkard, Daniel Loss, and David P. DiVincenzo. Coupled quantum dots as quantum gates. *Phys. Rev. B*, 59:2070–2078, Jan 1999. doi:10.1103/PhysRevB.59.2070.

[79] Heng Fan, Vwani Roychowdhury, and Thomas Szkopek. Optimal two-qubit quantum circuits using exchange interactions. *Phys. Rev. A*, 72:052323, Nov 2005. doi:10.1103/PhysRevA.72.052323.

[80] J. M. Elzerman, R. Hanson, L. H. Willems van Bereven, B. Witkamp, L. M. K. Vandersypen, and L. P. Kouwenhoven. Single-shot read-out of an individual electron spin in a quantum dot. *Nature*, 430:431–435, Jul 2004. doi:10.1038/nature02693.

[81] L. P. Kouwenhoven, D. G. Austing, and Tarucha S. Few-electron quantum dots. *Rep. Prog. Phys.*, 64(6):701–736, Jun 2001. doi:10.1088/0034-4885/64/6/201.

[82] William A. Coish and Daniel Loss. Quantum computing with spins in solids. In H. Kronmüller, S. Parkin, and D.D. Awschalom, editors, *Handbook of Magnetism and Advanced Magnetic Materials*, chapter *Spintronics and Magnetoelectronics: Semiconductor Spintronics*. John Wiley & Sons, Ltd, 2007. doi:https://doi.org/10.1002/9780470022184.hmm512.

[83] J. M. Elzerman, R. Hanson, J. S. Greidanus, L. H. Willems van Beveren, S. De Franceschi, L. M. K. Vandersypen, S. Tarucha, and L. P. Kouwenhoven. Few-electron quantum dot circuit with integrated charge read out. *Phys. Rev. B*, 67:161308, Apr 2003. doi:10.1103/PhysRevB.67.161308.

[84] Frederico Martins, Filip K. Malinowski, Peter D. Nissen, Edwin Barnes, Saeed Fallahi, Geoffrey C. Gardner, Michael J. Manfra, Charles M. Marcus, and Ferdinand Kuemmeth. Noise suppression using symmetric exchange gates in spin qubits. *Phys. Rev. Lett.*, 116:116801, Mar 2016. doi:10.1103/PhysRevLett.116.116801.

[85] Hugo Ribeiro, J. R. Petta, and Guido Burkard. Harnessing the GaAs quantum dot nuclear spin bath for quantum control. *Phys. Rev. B*, 82:115445, Sep 2010. doi:10.1103/PhysRevB.82.115445.

[86] K. M. Weiss, J. M. Elzerman, Y. L. Delley, J. Miguel-Sanchez, and A. Imamoğlu. Coherent two-electron spin qubits in an optically active pair of coupled InGaAs quantum dots. *Phys. Rev. Lett.*, 109:107401, Sep 2012. doi:10.1103/PhysRevLett.109.107401.

[87] David Press, Thaddeus D. Ladd, Bingyang Zhang, and Yoshihisa Yamamoto. Complete quantum control of a single quantum dot spin using ultrafast optical pulses. *Nature*, 456(7219):218–221, Nov 2008. doi:10.1038/nature07530.

[88] F. Bloch. Nuclear induction. *Phys. Rev.*, 70:460–474, Oct 1946. doi:10.1103/PhysRev.70.460.

[89] A.G. Redfield. The theory of relaxation processes. In John S. Waugh, editor, *Advances in Magnetic Resonance*, volume 1 of *Advances in Magnetic and Optical Resonance*, pages 1–32. Academic Press, 1965. doi:https://doi.org/10.1016/B978-1-4832-3114-3.50007-6.

[90] Luca Chirolli and Guido Burkard. Decoherence in solid-state qubits. *Advances in Physics*, 57(3):225–285, May 2008. doi:10.1080/00018730802218067.

[91] Ulrich Weiss. *Quantum Dissipative Systems (Fourth Edition)*, chapter *Part I. General Theory of Open Quantum Systems*, pages 8–10. World Scientific, Singapore, 2012. doi:10.1142/9789814503556_0002.

[92] Vittorio Gorini, Andrzej Kossakowski, and E. C. G. Sudarshan. Completely positive dynamical semigroups of N-level systems. *J. Math. Phys.*, 17(5):821–825, May 1976. doi:10.1063/1.522979.

[93] G. Lindblad. On the generators of quantum dynamical semigroups. *Commun.Math. Phys.*, 48(2):119–130, Jun 1976. doi:10.1007/BF01608499.

[94] Toshimasa Fujisawa, David Guy Austing, Yasuhiro Tokura, Yoshiro Hirayama, and Seigo Tarucha. Allowed and forbidden transitions in artificial hydrogen and helium atoms. *Nature*, 419(6904):278–281, Sep 2002. doi:10.1038/nature00976.

[95] G. Dresselhaus. Spin-orbit coupling effects in zinc blende structures. *Phys. Rev.*, 100:580–586, Oct 1955. doi:10.1103/PhysRev.100.580.

[96] Roland Winkler. *Spin—Orbit Coupling Effects in Two-Dimensional Electron and Hole Systems*, chapter *Inversion-Asymmetry-Induced Spin Splitting*, pages 69–129. Springer Berlin Heidelberg, Berlin, Heidelberg, 2003. doi:10.1007/978-3-540-36616-4_6.

[97] Igor Žutić, Jaroslav Fabian, and S. Das Sarma. Spintronics: Fundamentals and applications. *Rev. Mod. Phys.*, 76:323–410, Apr 2004. doi:10.1103/RevModPhys.76.323.

[98] E.I. Rashba. Properties of semiconductors with an extremum loop. I. Cyclotron and combinational resonance in a magnetic field perpendicular to the plane of the loop. *Soviet Physics, Solid State*, 2:1109–1122, 1960.

[99] Yu. A. Bychkov and E.I. Rashba. Properties of 2D electron gas with lifted spectral degeneracy. *JETP Lett.*, 39:78–81, Jan 1984. URL: http://jetpletters.ru/ps/1264/article_19121.shtml.

[100] P. Pfeffer. Effect of inversion asymmetry on the conduction subbands in GaAs – $Ga_{1-x}Al_xAs$ heterostructures. *Phys. Rev. B*, 59:15902–15909, Jun 1999. doi:10.1103/PhysRevB.59.15902.

[101] Alexander V. Khaetskii and Yuli V. Nazarov. Spin-flip transitions between Zeeman sublevels in semiconductor quantum dots. *Phys. Rev. B*, 64:125316, Sep 2001. doi:10.1103/PhysRevB.64.125316.

[102] Vitaly N. Golovach, Alexander Khaetskii, and Daniel Loss. Phonon-induced decay of the electron spin in quantum dots. *Phys. Rev. Lett.*, 93:016601, Jun 2004. doi:10.1103/PhysRevLett.93.016601.

[103] M. M. Glazov. *Electron and Nuclear Spin Dynamics in Semiconductor Nanostructures*, chapter *4 Hyperfine Interaction of Electron and Nuclear Spins*. Oxford University Press, Sep 2018. doi:10.1093/oso/9780198807308.001.0001.

[104] A. Abragam. *The Principles of Nuclear Magnetism*, chapter *VI. Electron-Nucleus Interactions* (section *II. Magnetic Interactions*). Oxford University Press, Oxford, 1961.

[105] W. Pauli. Zur quantenmechanik des magnetischen elektrons. *Zeitschrift für Physik*, 43(9):601–623, Sep 1927. doi:10.1007/BF01397326.

[106] L. D. Landau and E. M. Lifshitz. *The classical theory of fields*, chapter *V Constant Electromagnetic Fields* (*§ 36 Coulomb's law*). Pergamon Press, Oxford, 1971.

[107] David J. Griffiths. *Introduction to Electrodynamics*, chapter *1. Vector Analysis* (*1.5.3 The Three-Dimensional Delta Function*). Prentice-Hall, Upper Saddle River, New Jersey, Sep 1999.

[108] Ł. Cywiński. Dephasing of electron spin qubits due to their interaction with nuclei in quantum dots. *Acta. Phys. Pol. A*, 119, May 2011. doi:10.12693/APhysPolA.119.576.

[109] E. A. Chekhovich, A. Ulhaq, E. Zallo, F. Ding, O. G. Schmidt, and M. S. Skolnick. Measurement of the spin temperature of optically cooled nuclei and GaAs hyperfine constants in GaAs/AlGaAs quantum dots. *Nature Mater*, 16(10):982–986, Oct 2017. doi:10.1038/nmat4959.

[110] Wang Yao, Ren-Bao Liu, and L. J. Sham. Theory of electron spin decoherence by interacting nuclear spins in a quantum dot. *Phys. Rev. B*, 74:195301, Nov 2006. doi:10.1103/PhysRevB.74.195301.

[111] Łukasz Cywiński, Wayne M. Witzel, and S. Das Sarma. Pure quantum dephasing of a solid-state electron spin qubit in a large nuclear spin bath coupled by long-range hyperfine-mediated interaction. *Phys. Rev. B*, 79:245314, Jun 2009. doi:10.1103/PhysRevB.79.245314.

[112] Changxue Deng and Xuedong Hu. Nuclear spin diffusion in quantum dots: Effects of inhomogeneous hyperfine interaction. *Phys. Rev. B*, 72:165333, Oct 2005. doi:10.1103/PhysRevB.72.165333.

[113] D. J. Reilly, J. M. Taylor, E. A. Laird, J. R. Petta, C. M. Marcus, M. P. Hanson, and A. C. Gossard. Measurement of temporal correlations of the overhauser field in a double quantum dot. *Phys. Rev. Lett.*, 101:236803, Dec 2008. doi:10.1103/PhysRevLett.101.236803.

[114] Filip K. Malinowski, Frederico Martins, Łukasz Cywiński, Mark S. Rudner, Peter D. Nissen, Saeed Fallahi, Geoffrey C. Gardner, Michael J. Manfra, Charles M. Marcus, and Ferdinand Kuemmeth. Spectrum of the nuclear environment for gaas spin qubits. *Phys. Rev. Lett.*, 118:177702, 2017. doi:10.1103/PhysRevLett.118.177702.

[115] C. Barthel, D. J. Reilly, C. M. Marcus, M. P. Hanson, and A. C. Gossard. Rapid single-shot measurement of a singlet-triplet qubit. *Phys. Rev. Lett.*, 103:160503, Oct 2009. doi:10.1103/PhysRevLett.103.160503.

[116] W. A. Coish and Daniel Loss. Hyperfine interaction in a quantum dot: Non-Markovian electron spin dynamics. *Phys. Rev. B*, 70:195340, Nov 2004. doi:10.1103/PhysRevB.70.195340.

[117] D. Klauser, W. A. Coish, and Daniel Loss. Nuclear spin state narrowing via gate-controlled Rabi oscillations in a double quantum dot. *Phys. Rev. B*, 73:205302, May 2006. doi:10.1103/PhysRevB.73.205302.

[118] Dimitrije Stepanenko, Guido Burkard, Geza Giedke, and Atac Imamoğlu. Enhancement of electron spin coherence by optical preparation of nuclear spins. *Phys. Rev. Lett.*, 96:136401, Apr 2006. doi:10.1103/PhysRevLett.96.136401.

[119] G. Giedke, J. M. Taylor, D. D'Alessandro, M. D. Lukin, and A. Imamoğlu. Quantum measurement of a mesoscopic spin ensemble. *Phys. Rev. A*, 74:032316, Sep 2006. doi:10.1103/PhysRevA.74.032316.

[120] Hendrik Bluhm, Sandra Foletti, Diana Mahalu, Vladimir Umansky, and Amir Yacoby. Enhancing the coherence of a spin qubit by operating it as a feedback loop that controls its nuclear spin bath. *Phys. Rev. Lett.*, 105:216803, Nov 2010. doi:10.1103/PhysRevLett.105.216803.

[121] A. Greilich, D. R. Yakovlev, A. Shabaev, A. L. Efros, I. A. Yugova, R. Oulton, V. Stavarache, D. Reuter, A. Wieck, and M. Bayer. Mode locking of electron spin coherences in singly charged quantum dots. *Science*, 313:341–345, Jul 2006. doi:10.1126/science.1128215.

[122] M. D. Shulman, S. P. Harvey, J. M. Nichol, S. D. Bartlett, A. C. Doherty, V. Umansky, , and A. Yacoby. Suppressing qubit dephasing using real-time Hamiltonian estimation. *Nat Commun*, 5:5156, Oct 2014. doi:10.1038/ncomms6156.

[123] W. A. Coish, Jan Fischer, and Daniel Loss. Exponential decay in a spin bath. *Phys. Rev. B*, 77:125329, Mar 2008. doi:10.1103/PhysRevB.77.125329.

[124] W. A. Coish, Jan Fischer, and Daniel Loss. Free-induction decay and envelope modulations in a narrowed nuclear spin bath. *Phys. Rev. B*, 81(16):165315, Apr 2010. doi:10.1103/PhysRevB.81.165315.

[125] Edwin Barnes, Łukasz Cywiński, and S. Das Sarma. Master equation approach to the central spin decoherence problem: Uniform coupling model and role of projection operators. *Phys. Rev. B*, 84:155315, Oct 2011. doi:10.1103/PhysRevB.84.155315.

[126] Edwin Barnes, Łukasz Cywiński, and S. Das Sarma. Nonperturbative master equation solution of central spin dephasing dynamics. *Phys. Rev. Lett.*, 109:140403, Oct 2012. doi:10.1103/PhysRevLett.109.140403.

[127] I. A. Merkulov, Al. L. Efros, and M. Rosen. Electron spin relaxation by nuclei in semiconductor quantum dots. *Phys. Rev. B*, 65:205309, Apr 2002. doi:10.1103/PhysRevB.65.205309.

[128] A. C. Johnson, J. R. Petta, J. M. Taylor, A. Yacoby, M. D. Lukin, C. M. Marcus, M. P. Hanson, and A. C. Gossard. Triplet-singlet spin relaxation via nuclei in a double quantum dot. *Nature*, 435:925–928, Jun 2005. doi:10.1038/nature03815.

[129] F. H. L. Koppens, J. A. Folk, J. M. Elzerman, R. Hanson, L. H. Willems van Beveren, I. T. Vink, H. P. Tranitz, W. Wegscheider, L. P. Kouwenhoven, and L. M. K. Vandersypen. Control and detection of singlet-triplet mixing in a random nuclear field. *Science*, 309(5739):1346–1350, Aug 2005. doi:10.1126/science.1113719.

[130] M. V. Gurudev Dutt, Jun Cheng, Bo Li, Xiaodong Xu, Xiaoqin Li, P. R. Berman, D. G. Steel, A. S. Bracker, D. Gammon, Sophia E. Economou, Ren-Bao Liu, and L. J. Sham. Stimulated and spontaneous optical generation of electron spin coherence in charged GaAs quantum dots. *Phys. Rev. Lett.*, 94:227403, Jun 2005. doi:10.1103/PhysRevLett.94.227403.

[131] P.-F. Braun, X. Marie, L. Lombez, B. Urbaszek, T. Amand, P. Renucci, V. K. Kalevich, K. V. Kavokin, O. Krebs, P. Voisin, and Y. Masumoto. Direct observation of the electron spin relaxation induced by nuclei in quantum dots. *Phys. Rev. Lett.*, 94:116601, Mar 2005. doi:10.1103/PhysRevLett.94.116601.

[132] J. M. Taylor and M. D. Lukin. Dephasing of quantum bits by a quasi-static mesoscopic environment. *Quantum Inf Process*, 5:503–536, Dec 2006. doi:10.1007/s11128-006-0036-z.

[133] F. M. Cucchietti, J. P. Paz, and W. H. Zurek. Decoherence from spin environments. *Phys. Rev. A*, 72:052113, Nov 2005. doi:10.1103/PhysRevA.72.052113.

[134] Wenxian Zhang, V. V. Dobrovitski, K. A. Al-Hassanieh, E. Dagotto, and B. N. Harmon. Hyperfine interaction induced decoherence of electron spins in quantum dots. *Phys. Rev. B*, 74:205313, Nov 2006. doi:10.1103/PhysRevB.74.205313.

[135] Gang Chen, Doron L. Bergman, and Leon Balents. Semiclassical dynamics and long-time asymptotics of the central-spin problem in a quantum dot. *Phys. Rev. B*, 76(4):045312, Jul 2007. doi:10.1103/PhysRevB.76.045312.

[136] Alexandre Faribault and Dirk Schuricht. Spin decoherence due to a randomly fluctuating spin bath. *Phys. Rev. B*, 88:085323, Aug 2013. doi:10.1103/PhysRevB.88.085323.

[137] Daniel Stanek, Carsten Raas, and Götz S. Uhrig. Dynamics and decoherence in the central spin model in the low-field limit. *Phys. Rev. B*, 88:155305, Oct 2013. doi:10.1103/PhysRevB.88.155305.

[138] Johannes Hackmann and Frithjof B. Anders. Spin noise in the anisotropic central spin model. *Phys. Rev. B*, 89:045317, Jan 2014. doi:10.1103/PhysRevB.89.045317.

[139] W. M. Witzel and S. Das Sarma. Multiple-pulse coherence enhancement of solid state spin qubits. *Phys. Rev. Lett.*, 98:077601, Feb 2007. doi:10.1103/PhysRevLett.98.077601.

[140] Hendrik Bluhm, Sandra Foletti, Izhar Neder, Mark Rudner, Diana Mahalu, Vladimir Umansky, and Amir Yacoby. Dephasing time of GaAs electron-spin qubits coupled to a nuclear bath exceeding 200 μs. *Nature Phys*, 7:109–113, Feb 2011. doi:10.1038/nphys1856.

[141] Alexander V. Khaetskii, Daniel Loss, and Leonid Glazman. Electron spin decoherence in quantum dots due to interaction with nuclei. *Phys. Rev. Lett.*, 88(18):186802, 2002. doi:10.1103/PhysRevLett.88.186802.

[142] Alexander Khaetskii, Daniel Loss, and Leonid Glazman. Electron spin evolution induced by interaction with nuclei in a quantum dot. *Phys. Rev. B*, 67(19):195329, May 2003. doi:10.1103/PhysRevB.67.195329.

[143] John Schliemann, Alexander V. Khaetskii, and Daniel Loss. Spin decay and quantum parallelism. *Phys. Rev. B*, 66(24):245303, Dec 2002. doi:10.1103/PhysRevB.66.245303.

[144] Wen Yang, Wen-Long Ma, and Ren-Bao Liu. Quantum many-body theory for electron spin decoherence in nanoscale nuclear spin baths. *Rep. Prog. Phys.*, 80(1):016001, Nov 2017. doi:10.1088/0034-4885/80/1/016001.

[145] E. Paladino, Y. M. Galperin, G. Falci, and B. L. Altshuler. $1/f$ noise: Implications for solid-state quantum information. *Rev. Mod. Phys.*, 86:361–418, Apr 2014. doi:10.1103/RevModPhys.86.361.

[146] Ulrich Weiss. *Quantum Dissipative Systems (Fourth Edition)*, chapter *Part IV. Dissipative Two-State System*, pages 414–416. World Scientific, Singapore, 2012. doi:10.1142/9789814503556_0005.

[147] Y. M. Galperin, B. L. Altshuler, J. Bergli, and D. V. Shantsev. Non-Gaussian low-frequency noise as a source of qubit decoherence. *Phys. Rev. Lett.*, 96:097009, Mar 2006. doi:10.1103/PhysRevLett.96.097009.

[148] Josef Schriefl, Yuriy Makhlin, Alexander Shnirman, and Gerd Schön. Decoherence from ensembles of two-level fluctuators. *New J. Phys.*, 8(1):1, Jan 2006. doi:10.1088/1367-2630/8/1/001.

[149] P. Szańkowski, G. Ramon, J. Krzywda, D. Kwiatkowski, and Ł. Cywiński. Environmental noise spectroscopy with qubits subjected to dynamical decoupling. *J. Phys.: Condens. Matter*, 29(33):333001, Jul 2017. doi:10.1088/1361-648X/aa7648.

[150] Y. M. Galperin, B. L. Altshuler, J. Bergli, and D. V. Shantsev. Non-Gaussian low-frequency noise as a source of qubit decoherence. *Phys. Rev. Lett.*, 96:097009, Mar 2006. doi:10.1103/PhysRevLett.96.097009.

[151] O. E. Dial, M. D. Shulman, S. P. Harvey, H. Bluhm, V. Umansky, and A. Yacoby. Charge noise spectroscopy using coherent exchange oscillations in a singlet-triplet qubit. *Phys. Rev. Lett.*, 110:146804, Apr 2013. doi:10.1103/PhysRevLett.110.146804.

[152] John Preskill. Quantum computing and the entanglement frontier. *arXiv.org*, 1203.5813, Mar 2012. doi:10.48550/ARXIV.1203.5813.

[153] O. Gühne, P. Hyllus, D. Bruß, A. Ekert, M. Lewenstein, C. Macchiavello, and A. Sanpera. Detection of entanglement with few local measurements. *Phys. Rev. A*, 66:062305, Dec 2002. doi:10.1103/PhysRevA.66.062305.

[154] Otfried Gühne and Géza Tóth. Entanglement detection. *Phys. Rep.*, 474:1–75, Apr 2009. doi:10.1016/j.physrep.2009.02.004.

[155] Charles H. Bennett, Gilles Brassard, Claude Crépeau, Richard Jozsa, Asher Peres, and William K. Wootters. Teleporting an unknown quantum state via dual classical and Einstein-Podolsky-Rosen channels. *Phys. Rev. Lett.*, 70:1895–1899, Mar 1993. doi:10.1103/PhysRevLett.70.1895.

[156] Michał Horodecki, Paweł Horodecki, and Ryszard Horodecki. General teleportation channel, singlet fraction, and quasidistillation. *Phys. Rev. A*, 60:1888–1898, Sep 1999. doi:10.1103/PhysRevA.60.1888.

[157] Frank Verstraete and Henri Verschelde. Optimal teleportation with a mixed state of two qubits. *Phys. Rev. Lett.*, 90:097901, Mar 2003. doi:10.1103/PhysRevLett.90.097901.

[158] S. J. van Enk, N. Lütkenhaus, and H. J. Kimble. Experimental procedures for entanglement verification. *Phys. Rev. A*, 75:052318, May 2007. doi:10.1103/PhysRevA.75.052318.

[159] Sandra Foletti, Hendrik Bluhm, Diana Mahalu, Vladimir Umansky, and Amir Yacoby. Universal quantum control of two-electron spin quantum bits using dynamic nuclear polarization. *Nature Phys*, 5:903–908, Dec 2009. doi:10.1038/nphys1424.

[160] B. Bellomo, R. Lo Franco, and G. Compagno. Non-Markovian effects on the dynamics of entanglement. *Phys. Rev. Lett.*, 99:160502, Oct 2007. doi:10.1103/PhysRevLett.99.160502.

[161] B. Bellomo, R. Lo Franco, and G. Compagno. Entanglement dynamics of two independent qubits in environments with and without memory. *Phys. Rev. A*, 77:032342, Mar 2008. doi:10.1103/PhysRevA.77.032342.

[162] Paweł Mazurek, Katarzyna Roszak, Ravindra W. Chhajlany, and Paweł Horodecki. Sensitivity of entanglement decay of quantum-dot spin qubits to the external magnetic field. *Phys. Rev. A*, 89:062318, Jun 2014. doi:10.1103/PhysRevA.89.062318.

[163] Changxue Deng and Xuedong Hu. Electron-spin dephasing via hyperfine interaction in a quantum dot: An equation-of-motion calculation of electron-spin correlation functions. *Phys. Rev. B*, 78:245301, Dec 2008. doi:10.1103/PhysRevB.78.245301.

[164] Łukasz Cywiński, Wayne M. Witzel, and S. Das Sarma. Electron spin dephasing due to hyperfine interactions with a nuclear spin bath. *Phys. Rev. Lett.*, 102:057601, Feb 2009. doi:10.1103/PhysRevLett.102.057601.

[165] Łukasz Cywiński, V. V. Dobrovitski, and S. Das Sarma. Spin echo decay at low magnetic fields in a nuclear spin bath. *Phys. Rev. B*, 82:035315, Jul 2010. doi:10.1103/PhysRevB.82.035315.

[166] Izhar Neder, Mark S. Rudner, Hendrik Bluhm, Sandra Foletti, Bertrand I. Halperin, and Amir Yacoby. Semiclassical model for the dephasing of a two-electron spin qubit coupled to a coherently evolving nuclear spin bath. *Phys. Rev. B*, 84:035441, Jul 2011. doi:10.1103/PhysRevB.84.035441.

[167] Karol Życzkowski, Paweł Horodecki, Michał Horodecki, and Ryszard Horodecki. Dynamics of quantum entanglement. *Phys. Rev. A*, 65:012101, Dec 2001. doi:10.1103/PhysRevA.65.012101.

[168] Ting Yu and J. H. Eberly. Finite-time disentanglement via spontaneous emission. *Phys. Rev. Lett.*, 93:140404, Sep 2004. doi:10.1103/PhysRevLett.93.140404.

[169] S.M. Ryabchenko and Yu. G. Semenov. Spin-correlation effects for a large-radius electron center in a magnetically mixed semiconductor. *Journal of Experimental and Theoretical Physics*, 57:825–832, Apr 1983. URL: http://www.jetp.ras.ru/cgi-bin/e/index/e/57/4/p825?a=list.

[170] Lachlan P. Lindoy and David E. Manolopoulos. Simple and accurate method for central spin problems. *Phys. Rev. Lett.*, 120:220604, Jun 2018. doi:10.1103/PhysRevLett.120.220604.

[171] Niklas Rohling and Guido Burkard. Tomography scheme for two spin-$\frac{1}{2}$ qubits in a double quantum dot. *Phys. Rev. B*, 88:085402, Aug 2013. doi:10.1103/PhysRevB.88.085402.

[172] S. Massar and S. Popescu. Optimal extraction of information from finite quantum ensembles. *Phys. Rev. Lett.*, 74:1259–1263, Feb 1995. doi:10.1103/PhysRevLett.74.1259.

[173] W. Pfaff, B. J. Hensen, H. Bernien, S. B. van Dam, M. S. Blok, T. H. Taminiau, M. J. Tiggelman, R. N. Schouten, M. Markham, D. J. Twitchen, and R. Hanson. Unconditional quantum teleportation between distant solid-state quantum bits. *Science*, 345:532–535, May 2014. doi:10.1126/science.1253512.

[174] W. A. Coish, Daniel Loss, E. A. Yuzbashyan, and B. L. Altshuler. Quantum versus classical hyperfine-induced dynamics in a quantum dot. *J. Appl. Phys.*, 101(8):081715, Apr 2007. doi:10.1063/1.2722783.

[175] Jianming Cai, Gian Giacomo Guerreschi, and Hans J. Briegel. Quantum control and entanglement in a chemical compass. *Phys. Rev. Lett.*, 104:220502, Jun 2010. doi:10.1103/PhysRevLett.104.220502.

[176] M. Tiersch, G. G. Guerreschi, J. Clausen, and H. J. Briegel. Quantum control and entanglement in a chemical compass. *J. Phys. Chem. A*, 118:13–20, Jan 2014. doi:10.1021/jp408569d.

[177] Jo-Tzu Hung, Łukasz Cywiński, Xuedong Hu, and S. Das Sarma. Hyperfine interaction induced dephasing of coupled spin qubits in semiconductor double quantum dots. *Phys. Rev. B*, 88:085314, Aug 2013. doi:10.1103/PhysRevB.88.085314.

[178] G. M. Palma, K.-A. Suominen, and A. K. Ekert. Quantum computers and dissipation. *Proc. R. Soc. Lond. A*, 452:567–584, Mar 1996. doi:10.1098/rspa.1996.0029.

[179] Daniel A. Lidar. Review of decoherence-free subspaces, noiseless subsystems, and dynamical decoupling. In Sabre Kais, editor, *Quantum Information and Computation for Chemistry*, pages 295–354. John Wiley & Sons, Ltd, 2014. doi:https://doi.org/10.1002/9781118742631.ch11.

[180] Piotr Szańkowski, Marek Trippenbach, Łukasz Cywiński, and Yehuda B. Band. The dynamics of two entangled qubits exposed to classical noise: role of spatial and temporal noise correlations. *Quantum Inf Process*, 14:3367–3397, Sep 2015. doi:10.1007/s11128-015-1044-7.

[181] F. H. L. Koppens, K. C. Nowack, and L. M. K. Vandersypen. Spin echo of a single electron spin in a quantum dot. *Phys. Rev. Lett.*, 100:236802, Jun 2008. doi:10.1103/PhysRevLett.100.236802.

[182] R. Lo Franco, A. D'Arrigo, G. Falci, G. Compagno, and E. Paladino. Preserving entanglement and nonlocality in solid-state qubits by dynamical decoupling. *Phys. Rev. B*, 90:054304, Aug 2014. doi:10.1103/PhysRevB.90.054304.

[183] Rogerio de Sousa and S. Das Sarma. Theory of nuclear-induced spectral diffusion: Spin decoherence of phosphorus donors in Si and GaAs quantum dots. *Phys. Rev. B*, 68:115322, Sep 2003. doi:10.1103/PhysRevB.68.115322.

[184] W. M. Witzel, Rogerio de Sousa, and S. Das Sarma. Quantum theory of spectral-diffusion-induced electron spin decoherence. *Phys. Rev. B*, 72:161306, Oct 2005. doi:10.1103/PhysRevB.72.161306.

[185] W. M. Witzel and S. Das Sarma. Quantum theory for electron spin decoherence induced by nuclear spin dynamics in semiconductor quantum computer architectures: Spectral diffusion of localized electron spins in the nuclear solid-state environment. *Phys. Rev. B*, 74:035322, Jul 2006. doi:10.1103/PhysRevB.74.035322.

[186] Igor Bragar. Retardation of entanglement decay of two spin qubits by quantum measurements. *arXiv.org*, 2110.13826, Oct 2021. doi:10.48550/arXiv.2110.13826.

[187] David P. DiVincenzo. The physical implementation of quantum computation. *Fortschr. Phys.*, 48(9-11):771–783, Oct 2000. doi:https://doi.org/10.1002/1521-3978(200009)48:9/11<771::AID-PROP771>3.0.CO;2-E.

[188] Alexei M. Tyryshkin, Shinichi Tojo, John J. L. Morton, Helge Riemann, Nikolai V. Abrosimov, Peter Becker, Hans-Joachim Pohl, Thomas Schenkel, Michael L. W. Thewalt, Kohei M. Itoh, and S. A. Lyon. Electron spin coherence exceeding seconds in high-purity silicon. *Nature Mater*, 11:143–147, Feb 2012. doi:10.1038/nmat3182.

[189] B. Misra and E. C. G. Sudarshan. The Zeno's paradox in quantum theory. *J. Math. Phys.*, 18(4):756–763, Apr 1977. doi:10.1063/1.523304.

[190] Danny Kim, Samuel G. Carter, Alex Greilich, Allan S. Bracker, and Daniel Gammon. Ultrafast optical control of entanglement between two quantum-dot spins. *Nature Phys*, 7(3):223–229, Mar 2011. doi:10.1038/nphys1863.

[191] E. Ferraro, H.-P. Breuer, A. Napoli, M. A. Jivulescu, and A. Messina. Non-Markovian dynamics of a single electron spin coupled to a nuclear spin bath. *Phys. Rev. B*, 78:064309, Aug 2008. doi:10.1103/PhysRevB.78.064309.

[192] Anasua Chatterjee, Paul Stevenson, Silvano De Franceschi, Andrea Morello, Nathalie P. de Leon, and Ferdinand Kuemmeth. Semiconductor qubits in practice. *Nat Rev Phys*, 3(3):157–177, Mar 2021. doi:10.1038/s42254-021-00283-9.

[193] K. C. Nowack, F. H. L. Koppens, Yu. V. Nazarov, and L. M. K. Vandersypen. Coherent control of a single electron spin with electric fields. *Science*, 318:1430–1433, Nov 2007. doi:10.1126/science.1148092.

[194] M. Pioro-Ladrière, T. Obata, Y. Tokura1, Y. -S. Shin, T. Kubo, K. Yoshida, T. Taniyama, and S. Tarucha. Electrically driven single-electron spin resonance in a slanting Zeeman field. *Nature Phys*, 4:776–779, Oct 2008. doi:10.1038/nphys1053.

[195] Qiuzi Li, Łukasz Cywiński, Dimitrie Culcer, Xuedong Hu, and S. Das Sarma. Exchange coupling in silicon quantum dots: Theoretical considerations for quantum computation. *Phys. Rev. B*, 81:085313, Feb 2010. doi:10.1103/PhysRevB.81.085313.

[196] M. Veldhorst, C. H. Yang, J. C. C. Hwang, W. Huang, J. P. Dehollain, J. T. Muhonen, S. Simmons, A. Laucht, F. E. Hudson, K. M. Itoh, A. Morello, and A. S. Dzurak. A two-qubit logic gate in silicon. *Nature*, 526(7573):410–414, Oct 2015. doi:10.1038/nature15263.

[197] M. D. Reed, B. M. Maune, R. W. Andrews, M. G. Borselli, K. Eng, M. P. Jura, A. A. Kiselev, T. D. Ladd, S. T. Merkel, I. Milosavljevic, E. J. Pritchett, M. T. Rakher, R. S. Ross, A. E. Schmitz, A. Smith, J. A. Wright, M. F.

Gyure, and A. T. Hunter. Reduced sensitivity to charge noise in semiconductor spin qubits via symmetric operation. *Phys. Rev. Lett.*, 116:110402, Mar 2016. doi:10.1103/PhysRevLett.116.110402.

[198] T. F. Watson, S. G. J. Philips, E. Kawakami, D. R. Ward, P. Scarlino, M. Veldhorst, D. E. Savage, M. G. Lagally, Mark Friesen, S. N. Coppersmith, M. A. Eriksson, and L. M. K. Vandersypen. A programmable two-qubit quantum processor in silicon. *Nature*, 555(7698):633–637, Mar 2018. doi:10.1038/nature25766.

[199] W. Huang, C. H. Yang, K. W. Chan, T. Tanttu, B. Hensen, R. C. C. Leon, M. A. Fogarty, J. C. C. Hwang, F. E. Hudson, K. M. Itoh, A. Morello, A. Laucht, and A. S. Dzurak. Fidelity benchmarks for two-qubit gates in silicon. *Nature*, 569(7757):532–536, May 2019. doi:10.1038/s41586-019-1197-0.

[200] E. A. Laird, C. Barthel, E. I. Rashba, C. M. Marcus, M. P. Hanson, and A. C. Gossard. Hyperfine-mediated gate-driven electron spin resonance. *Phys. Rev. Lett.*, 99:246601, Dec 2007. doi:10.1103/PhysRevLett.99.246601.

[201] W. A. Coish and J. Baugh. Nuclear spins in nanostructures. *Phys. Status Solidi B*, 246(10):2203–2215, Sep 2009. doi:10.1002/pssb.200945229.

[202] E. A. Chekhovich, M. N. Makhonin, A. I. Tartakovskii, A. Yacoby, H. Bluhm, K. C. Nowack, and L. M. K. Vandersypen. Nuclear spin effects in semiconductor quantum dots. *Nature Mater*, 12:494–504, May 2013. doi:10.1038/nmat3652.

[203] Erika Kawakami, Thibaut Jullien, Pasquale Scarlino, Daniel R. Ward, Donald E. Savage, Max G. Lagally, Viatcheslav V. Dobrovitski, Mark Friesen, Susan N. Coppersmith, Mark A. Eriksson, and Lieven M. K. Vandersypen. Gate fidelity and coherence of an electron spin in an Si/SiGe quantum dot with micromagnet. *PNAS*, 113(42):11738–11743, Oct 2016. doi:10.1073/pnas.1603251113.

[204] M. Veldhorst, J. C. C. Hwang, C. H. Yang, A. W. Leenstra, B. de Ronde, J. P. Dehollain, J. T. Muhonen, F. E. Hudson, K. M. Itoh, A. Morello, and A. S. Dzurak. An addressable quantum dot qubit with fault-tolerant control-fidelity. *Nature Nanotech*, 9(12):981–985, Dec 2014. doi:10.1038/NNANO.2014.216.

[205] Tom Struck, Arne Hollmann, Floyd Schauer, Olexiy Fedorets, Andreas Schmidbauer, Kentarou Sawano, Helge Riemann, Nikolay V. Abrosimov, Łukasz Cywiński, and Dominique Bougeard. Low-frequency spin qubit energy splitting noise in highly purified ^{28}Si/SiGe. *npj Quantum Inf*, 6:40, May 2020. doi:10.1038/s41534-020-0276-2.

[206] A. P. Higginbotham, F. Kuemmeth, M. P. Hanson, A. C. Gossard, and C. M. Marcus. Coherent operations and screening in multielectron spin qubits. *Phys. Rev. Lett.*, 112:026801, Jan 2014. doi:10.1103/PhysRevLett.112.026801.

[207] Dohun Kim, Zhan Shi, C. B. Simmons, D. R. Ward, J. R. Prance, Teck Seng Koh, John King Gamble, D. E. Savage, M. G. Lagally, Mark Friesen, S. N. Coppersmith, and Mark A. Eriksson. Quantum control and process tomography of a semiconductor quantum dot hybrid qubit. *Nature*, 511(7507):70–74, Jul 2014. doi:10.1038/nature13407.

[208] J. Medford, J. Beil, J. M. Taylor, S. D. Bartlett, A. C. Doherty, E. I. Rashba, D. P. DiVincenzo, H. Lu, A. C. Gossard, and C. M. Marcus. Self-consistent measurement and state tomography of an exchange-only spin qubit. *Nature Nanotech*, 8:654–659, Sep 2013. doi:10.1038/nnano.2013.168.

[209] J. Medford, J. Beil, J. M. Taylor, E. I. Rashba, H. Lu, A. C. Gossard, and C. M. Marcus. Quantum-dot-based resonant exchange qubit. *Phys. Rev. Lett.*, 111:050501, Jul 2013. doi:10.1103/PhysRevLett.111.050501.

[210] Maximilian Russ, J. R. Petta, and Guido Burkard. Quadrupolar exchange-only spin qubit. *Phys. Rev. Lett.*, 121:177701, Oct 2018. doi:10.1103/PhysRevLett.121.177701.

[211] Arnau Sala and Jeroen Danon. Exchange-only singlet-only spin qubit. *Phys. Rev. B*, 95:241303, Jun 2017. doi:10.1103/PhysRevB.95.241303.

[212] J .M. Taylor, H. A. Engel, W. Dur, A. Yacoby, C. M. Marcus, P. Zoller, and M. D. Lukin. Fault-tolerant architecture for quantum computation using electrically controlled semiconductor spins. *Nature Phys*, 1(3):177–183, Dec 2005. doi:10.1038/nphys174.

[213] Rui Li, Xuedong Hu, and J. Q. You. Controllable exchange coupling between two singlet-triplet qubits. *Phys. Rev. B*, 86:205306, Nov 2012. doi:10.1103/PhysRevB.86.205306.

[214] Matthew P. Wardrop and Andrew C. Doherty. Exchange-based two-qubit gate for singlet-triplet qubits. *Phys. Rev. B*, 90:045418, Jul 2014. doi:10.1103/PhysRevB.90.045418.

[215] Pascal Cerfontaine, René Otten, M. A. Wolfe, Patrick Bethke, and Hendrik Bluhm. High-fidelity gate set for exchange-coupled singlet-triplet qubits. *Phys. Rev. B*, 101:155311, Apr 2020. doi:10.1103/PhysRevB.101.155311.

[216] W. A. Coish and Daniel Loss. Singlet-triplet decoherence due to nuclear spins in a double quantum dot. *Phys. Rev. B*, 72:125337, Sep 2005. doi:10.1103/PhysRevB.72.125337.

[217] Xuedong Hu and S. Das Sarma. Charge-fluctuation-induced dephasing of exchange-coupled spin qubits. *Phys. Rev. Lett.*, 96:100501, Mar 2006. doi:10.1103/PhysRevLett.96.100501.

[218] W. Yang and R. B. Liu. Decoherence of coupled electron spins via nuclear spin dynamics in quantum dots. *Phys. Rev. B*, 77:085302, Feb 2008. doi:10.1103/PhysRevB.77.085302.

[219] Yang-Le Wu and S. Das Sarma. Decoherence of two coupled singlet-triplet spin qubits. *Phys. Rev. B*, 96:165301, Oct 2017. doi:10.1103/PhysRevB.96.165301.

[220] J. M. Taylor, J. R. Petta, A. C. Johnson, A. Yacoby, C. M. Marcus, and M. D. Lukin. Relaxation, dephasing, and quantum control of electron spins in double quantum dots. *Phys. Rev. B*, 76:035315, Jul 2007. doi:10.1103/PhysRevB.76.035315.

[221] Xin Wang, Lev S. Bishop, J. P. Kestner, Edwin Barnes, Kai Sun, and S. Das Sarma. Composite pulses for robust universal control of singlet-triplet qubits. *Nat Commun*, 3(1):997, Aug 2012. doi:10.1038/ncomms2003.

[222] J. P. Kestner, Xin Wang, Lev S. Bishop, Edwin Barnes, and S. Das Sarma. Noise-resistant control for a spin qubit array. *Phys. Rev. Lett.*, 110:140502, Apr 2013. doi:10.1103/PhysRevLett.110.140502.

[223] Xin Wang, Lev S. Bishop, Edwin Barnes, J. P. Kestner, and S. Das Sarma. Robust quantum gates for singlet-triplet spin qubits using composite pulses. *Phys. Rev. A*, 89:022310, Feb 2014. doi:10.1103/PhysRevA.89.022310.

[224] John M. Nichol, Lucas A. Orona, Shannon P. Harvey, Saeed Fallahi, Geoffrey C. Gardner, Michael J. Manfra, and Amir Yacoby. High-fidelity entangling gate for double-quantum-dot spin qubits. *npj Quantum Inf*, 3(1):3, Jan 2017. doi:10.1038/s41534-016-0003-1.

[225] D. J. Reilly, J. M. Taylor, J. R. Petta, C. M. Marcus, M. P. Hanson, and A. C. Gossard. Exchange control of nuclear spin diffusion in a double quantum dot. *Phys. Rev. Lett.*, 104:236802, Jun 2010. doi:10.1103/PhysRevLett.104.236802.

[226] W. M. Witzel and S. Das Sarma. Wavefunction considerations for the central spin decoherence problem in a nuclear spin bath. *Phys. Rev. B*, 77:165319, Apr 2008. doi:10.1103/PhysRevB.77.165319.

[227] Guy Ramon. Dynamical decoupling of a singlet-triplet qubit afflicted by a charge fluctuator. *Phys. Rev. B*, 86:125317, Sep 2012. doi:10.1103/PhysRevB.86.125317.

[228] Guy Ramon. Non-Gaussian signatures and collective effects in charge noise affecting a dynamically decoupled qubit. *Phys. Rev. B*, 92:155422, Oct 2015. doi:10.1103/PhysRevB.92.155422.

[229] Rogerio de Sousa. Electron spin as a spectrometer of nuclear-spin noise and other fluctuations. In Marco Fanciulli, editor, *Electron Spin Resonance and Related Phenomena in Low-Dimensional Structures*, pages 183–220. Springer Berlin Heidelberg, Berlin, Heidelberg, 2009. doi:10.1007/978-3-540-79365-6_10.

[230] Łukasz Cywiński, Roman M. Lutchyn, Cody P. Nave, and S. Das Sarma. How to enhance dephasing time in superconducting qubits. *Phys. Rev. B*, 77:174509, May 2008. doi:10.1103/PhysRevB.77.174509.

[231] Donovan Buterakos, Robert E. Throckmorton, and S. Das Sarma. Crosstalk error correction through dynamical decoupling of single-qubit gates in capacitively coupled singlet-triplet semiconductor spin qubits. *Phys. Rev. B*, 97:045431, Jan 2018. doi:10.1103/PhysRevB.97.045431.

[232] Erik Nielsen, Richard P. Muller, and Malcolm S. Carroll. Configuration interaction calculations of the controlled phase gate in double quantum dot qubits. *Phys. Rev. B*, 85:035319, Jan 2012. doi:10.1103/PhysRevB.85.035319.

[233] Guo Xuan Chan, J. P. Kestner, and Xin Wang. Charge noise suppression in capacitively coupled singlet-triplet spin qubits under magnetic field. *Phys. Rev. B*, 103:L161409, Apr 2021. doi:10.1103/PhysRevB.103.L161409.

[234] Jelmer M. Boter, Xiao Xue, Tobias Krähenmann, Thomas F. Watson, Vickram N. Premakumar, Daniel R. Ward, Donald E. Savage, Max G. Lagally, Mark Friesen, Susan N. Coppersmith, Mark A. Eriksson, Robert Joynt, and Lieven M. K. Vandersypen. Spatial noise correlations in a Si/SiGe two-qubit device from Bell state coherences. *Phys. Rev. B*, 101:235133, Jun 2020. doi:10.1103/PhysRevB.101.235133.

[235] J. Yoneda, J. S. Rojas-Arias, P. Stano, K. Takeda, A. Noiri, T. Nakajima, D. Loss, and S. Tarucha. Noise-correlation spectrum for a pair of spin qubits in silicon. *arXiv:2208.14150*, Aug 2022. URL: http://arxiv.org/abs/2208.14150, doi:10.48550/ARXIV.2208.14150.

[236] A. Melikidze, V. V. Dobrovitski, H. A. De Raedt, M. I. Katsnelson, and B. N. Harmon. Parity effects in spin decoherence. *Phys. Rev. B*, 70:014435, Jul 2004. doi:10.1103/PhysRevB.70.014435.

List of Figures